Understanding moisture buffering effects in the indoor environment

Cascione, Valeria

Award date:
2021

Awarding institution:
University of Bath

Understanding moisture buffering effects in the indoor environment

submitted by

Valeria Cascione

for the degree of for the Degree of Doctor of Philosophy

of the

University of Bath

Department of Architecture and Civil Engineering

February 2021

Signed on behalf of the Faculty of Engineering and Design .....

Acknowledgements

My first thanks go to Dan Maskell, Andy Shea and Pete Walker for their supervision, guidance and huge support during this journey. In particular, thanks to Dan for being always present in the best and worst times, and for his guidance in my professional and academic development. Thanks also to the other academic staff for their friendliness and availability in different moments of the PhD.

I would like to immensely thank Neil Price for his patience and support in helping me with my crazy requests. Also thanks to Will Bazeley, David Surgenor, Murrie Frank and Craig Brakes for their hard work and for helping me to make a huge part of my PhD work possible. Also thanks to Olivier Camus, Martin Naidu and Miles Chamber together with the other technical staff for their support in the laboratory.

Thanks to Andrew Chapman for his support for the statistical analysis in my thesis and everyone else on campus that helped me in different aspects of my journey. Thanks to all researchers and PhD students, in particular Valentina, that made this time in Bath special.

I would like also to thank Monto Mani and Venkatarama Reddy from the Indian Institute of Science in Bangalore, for inviting and supervising me during my visit in India, and the UKIERI project for giving me the chance to live this wonderful experience. Huge thanks to their families and PhD students for their welcoming and friendliness.

Thanks to my Italian high school teacher, who thought I was incapable to write (or to do anything). I am really proud to prove to her that my writing is actually good and appreciated. At least in English.

Last but not least, thanks to my parents, my sister, my family and friends that are my best fans and they always pushed me to be and do better, even though they think I live in London and they still don't know what a PhD is. Thanks to Martyn, who has been next to me in this challenging years and helped me every time he could with my "wet plaster" research.

Abbi il coraggio di conoscere,
ma accetta di non sapere mai

Abstract

High or low indoor relative humidity (RH) levels may have negative effects on people's health and well-being. To regulate the humidity, air conditioning systems can be used, requiring energy and increasing the environmental emissions. However, some materials, like clay and gypsum, which are described as hygroscopic, can passively regulate the indoor climate, reducing peaks of internal relative humidity, when applied on exposed surfaces to the room air. Their capacity to moderate indoor humidity fluctuations is due to their ability to adsorb and desorb moisture, a process referred to as moisture buffering. This property is evaluated through the Moisture Buffering Value (MBV), which allows for a simplistic calculation of the potential of materials by considering the material properties and humidity regulation. Due to the simplified interpretation of moisture buffering, the testing methods are not representative of the material behaviour in a real building. Furthermore, moisture buffering can be measured, following various standards that are not directly comparable. Alternative experimental studies have attempted to investigate the actual performance of materials in real buildings, but there is no standard methodology yet and no established relationship between moisture buffering and building performances.

This PhD aimed to understand the moisture buffering effects in the indoor environment, by establishing a method to measure this property in full-scale experimentation and laboratory testing. The research was initially developed, by considering three independent approaches: laboratory testing, field work and simulations. In the laboratory testing, clay, gypsum, lime and plasterboard's hygrothermal properties were tested, to observe and compare their moisture buffering behaviour and investigate the correlation between material properties and moisture buffering potential. Successively, the testing protocol boundary conditions and test protocol were investigated. The effect of temperature, RH fluctuation and air velocity on moisture buffering capacity of plasters was investigated.

Field work aimed to study the response of real size rooms to humidity fluctuations, to evaluate the impact of moisture buffering, when buildings are exposed to external climate variations, ventilation and indoor temperature variations. Two hygroscopic rooms were compared to a reference room (non-hygroscopic). The testing methodology and equipment were designed to observe the moisture exchange through ventilation, building infiltration and wall moisture buffering capacity. The investigation showed the important impact of hygroscopic materials on the regulation

of the indoor moisture content. When the humidity increases, the walls store moisture from the indoor reducing the amount of moisture removed through ventilation. When the absolute humidity is low, the cold air that moves into the building through ventilation constantly replaces the indoor moist air. Therefore, the outdoor air over-dries the indoor environment. In this case walls release moisture in the room to counterbalance the moisture removed by ventilation.

Based on the rooms tested in field work, simulations were used to analyse the contribution of sub-layers and wall design on the moisture buffering performance of plasters. Materials in direct contact with the environment are responsible for the regulation of the indoor moisture. Materials exposed to the indoor stored and released most of the moisture and depending on the humidity level and moisture load, those materials regulate the amount of moisture that moves into the sub-layers.

The culmination of this investigation converged the three research approaches in order to compare and investigate the behaviour of indoor materials in laboratory and in a real building. By merging the three approaches, significant differences between simulations and experimental in-situ testing were found. In simulations, walls buffer more moisture than in the experimental cells. On the other hand, simulations showed a good agreement with the experimental laboratory testing that demonstrates numerical models are based on laboratory measured properties, which are not always representative of the real moisture buffering behaviour of a material when applied to a building.

The ability to test the moisture buffering performance of buildings is the key for material performance assessment. This thesis provides guidelines that reduce uncertainty to assess moisture buffering. It investigated and introduced different approaches to evaluate the materials performances from the material development to their application on buildings. The impact of this research is to push the development of new moisture control materials at a laboratory scale, with new confidence in their larger scale performance. This will result in an indoor environment that is healthier and more comfortable, by maintaining of the optimal indoor RH level, whilst reducing the risk of condensation and decay of construction materials.

Contents

List of Figures

List of Tables

List of Symbols

α Time factor [-]

β Correction factor [-]

Δw_{max} Average humidity ratio increase $[g/kg]$

δ_p Water Vapour Permeability $[kg/m \cdot s \cdot Pa]$

$\dot{g}$ Moisture production per hour [kg/h]

$\dot{M}_{diff}$ Water vapour diffusion through walls per hour [kg/h]

$\dot{M}_{HVAC}$ Water vapour removed/gained by HVAC per hour $[kg/h]$

$\dot{M}_{Vent}$ Water vapour removed/gained by ventilation per hour $[kg/h]$

Φ porosity [%]

ϕ Relative Humidity [−]

ρ Dry bulk density $[kg/m^3]$

ξ_u Moisture Capacity $[kg/m^3]$

ξ_w Specific Moisture Capacity $[kg/kg]$

A Adsorption coefficient $[kg/m^2 \cdot h^{0.5}]$

ACH Air Change per Hour $[1/h]$

ACH_{50} Air Change per Hour at 50 Pa $[1/h]$

Ap Surface of the pipe $[m^2]$

b_{mexp} Experimental moisture effusivity $[kg/m_2 \cdot Pa \cdot s^{0.5}]$

b_{mthr} Theoretical moisture effusivity $[kg/m_2 \cdot Pa \cdot s^{0.5}]$

b_m Moisture effusivity $[kg/m_2 \cdot Pa \cdot s^{0.5}]$

C Condensed water [g]

c Moisture concentration $[m^3/m^3]$

c_h Volumetric Heat Capacity $[MJ/m^3K]$

C_r Imperfect mixing reduction coefficient $[-]$

c_{vol} Volumetric Heat Capacity $[MJ/m^3K]$

D_m Diffusion coefficient [-]

D_W Vapour Diffusivity $[m^2/s]$

D_ϕ Liquid conduction coefficient $[kg/msPa]$

$EDRH$ Effective damped RH $[kg/h]$

G Moisture production [g]

g_w liquid transport flux density $[kg/m^2s]$

g_{wv} Water vapour transport flux density $[kg/m^2s]$

HIR^* Production interval adapted hygroscopic inertia $[kg/m^3 \cdot \%RH]$

$I_{h,d}$ Hygroscopic inertia $[g/m^3 \cdot \%RH]$

K_l liquid conductivity coefficient $[s]$

m Multiplier factor for EC [-]

M_a Moisture change in the room [g]

M_{diff} Water vapour diffusion through walls [g]

M_{Losses} Moisture exchange in the room through infiltration and moisture accumulated into the walls [g]

M_{mat} Accumulated moisture in walls [g]

$M_{vent-inf}$ Water vapour removed by ventilation/infiltration [g]

MBE_a Moisture Adsorption Effects) $[kg/kg]$

MBE_d Moisture Desorption Effects) $[kg/kg]$

MBV^* Production interval Adapted MBV $[kg/m^2 \cdot \%RH]$

MBV_{8h} MBV with 1 hour high humidity $[kg/m^2 \cdot \%RH]$

MBV_{8h} MBV with 8 hours high humidity $[kg/m^2 \cdot \%RH]$

MBV_{basic} Moisture Buffering Value Basic $[kg/m^2 \cdot \%RH]$

$MBV_{practical}$ Practical Moisture Buffering Value $[kg/m^2 \cdot \%RH]$

$MBV_{theoretical}$ Theoretical Moisture Buffering Value $[kg/m^2 \cdot \%RH]$

N Air change rate $[h^{-1}]$

p_n Capillary pressure $[Pa]$

p_v Water Vapour pressure [Pa]

p_s Saturation pressure [Pa]

p_t Barometric pressure [Pa]

Q_{50} Air Flow Rate at 50 Pa $[m^3/h]$

Q_{inf} Infiltration air flow Rate$[m^3/h]$

Q_{Vent} Ventilation Air Flow Rate $[m^3/h]$

RH Relative Humidity [%]

S Surface $[m^2]$

t Time $[s]$

t_p Time interval [s]

TG Vapour production period [h]

$UMBV$ Ultimate MBV $[kg/m^2 \cdot \%RH]$

V Volume $[m^3]$

v Air speed $[m/s]$

w Moisture content $[kg/m^3]$

w' humidity ratio with hygroscopic materials $[kg/kg]$

w_ind indoor absolute moisture content [g]

w_inlet absolute moisture content in the inlet duct of the ventilation system [g]

w_m Moisture content in [kg/kg]

w_n water content $[kg/m^2]$

w_out outdoor absolute moisture content [g]

w_outlet absolute moisture content in the outlet duct of the ventilation system [g]

w_0 humidity ratio with no hygroscopic materials $[kg/kg]$

w_h Humidity ratio injected by the air conditioning system $[g/kg]$

w_l Humidity ratio in the room $[g/kg]$

x_{Eff} Effective penetration depth [mm]

x_{Th} True penetration depth [mm]

Z_p Moisture surface resistance $[m^2 \cdot \%RH/kg]$

List of Acronyms

AAC aerated autoclaved concrete. xiv, 12, 13, 224

AC air conditioning. 3

ACH air change per hour. 118, 123, 124

AHU air handling unit. 28

ANN artificial neural networks. 19

BRP Building Research Park. 4, 6, 41, 110, 113, 115, 182, 186, 228

CFD computational fluid dynamics. 17

CoV coefficient of variation. 42

CS Campbell Scientific. 111, 112

DVS Dynamic Vapour Sorption. 47

EC effective capacitance. 16

EDRH effective damped relative humidity. 28

EMPD effective moisture penetration depth. 16, 17, 34

GHG Green House Gas. 1

HAMT heat, air and moisture transfer. 15, 17–19

HVAC heating, ventilation, and air conditioning. 31, 34, 35

MBV Moisture Buffering Value. iii, 12, 14, 17, 19, 21–23, 25, 49, 55, 59, 60, 63

MIP Mercury Intrusion Porosimetry. 42

MRI Magnetic Resonance Imaging. 33

NHL natural hydraulic lime. 41

NZEB net zero energy Building. 1

RAM Random-Access Memory. 15

RH relative humidity. iii, 2, 3, 9, 12, 13, 17, 18, 20–24, 27, 28, 31, 32, 34, 39, 41, 43, 45–47, 49, 65, 72, 84, 104, 105, 111, 115–117, 119, 129, 131, 132, 134, 154

SBS sick building syndrome. 2

TMPD true moisture penetration depth. 13

WUFI Wärme Und Feuchte Instationär. xv, 6, 17, 18, 114, 183, 184

1. *Introduction*

The building sector is responsible for 19% of Green House Gas (GHG) emissions, 32% of the world's total energy consumption and 51% of global electricity consumption (on Climate Change, 2015). Overall, carbon emission of buildings rose to over 35%, of which on average 20% is produced during construction works and 80% due to the use of buildings (included heating and air conditioning usage) (Eurostat and européenne. Commission européenne, 2016).

By putting legal targets to reduce the impact of human activity on climate change, policy makers have taken the first steps. Through the Kyoto Protocol and the "Climate and Energy Package" (Morlot et al., 1999), the United Nations and in particular the European Union are pushing individual nations towards a limited consumption of non-renewable resources and energies, and towards the development of environmentally sustainable technologies. In this regard, the European Parliament Directive 2010/31/EU (amended in 2018/844/EU) on the energy performance of buildings (2010) has been launched, with the main target for new buildings to guarantee energy self-sufficiency through the decarbonisation of electricity supply after 31 December 2020, while existing ones will be converted into net zero energy Building (NZEB).

It is clear that the main focus for the construction industry is to reduce energy demand in the use of buildings, which implies high standards in the design of technological systems and passive solutions, such as photovoltaic systems and passive ventilation strategies. This approach to low impact buildings takes into account the design of wall assemblies and, in particular, the capacity of the enclosure to reduce heat losses. The improvement in air tightness of building envelopes, by heavily insulating walls and by applying air tight barriers and sealants, leads to an increase of energy efficiency of buildings. However, as Mahdavi and Kumar (1996), and Crump, Dengel and Swainson (2009) state, the consequences of this approach has led to the reduction of the indoor air quality, occupant's hygrothermal comfort and wall durability.

The definition of comfort includes multiple aspects of people's well being in enclosed spaces. It embraces both physical and psychological conditions, which all aim to create a comfortable environment. Spending prolonged time in enclosed spaces may cause an

increase of occupant stress level, but it can also be the cause of several health problems, such as asthma, allergies and sick building syndrome (SBS) (Veitch, 2008), due to people's high exposure to indoor pollutants and mould. For these reasons, designers and researchers have been trying to optimise different aspects of the indoor environment quality. In particular, the hygrothermal comfort aims to achieve the highest possible percentage of people, occupying that particular space, to reach thermal neutrality. The thermal neutrality is reached when a person would not prefer either a warmer or cooler surrounding. Together with the thermal comfort, another important objective is also to minimise pollutants and contaminants indoors, in order not to effect occupants health.

The most important variables that influence hygrothermal comfort can be classified in environmental and human factors (Table 1.1). As Fanger et al. (1970) demonstrate, among the ambient variables, air temperature and radiant temperature play a more important role, and therefore, more accurate measurement of these two variables are necessary. On the other end, RH is not recognised as a key factor. Fanger et al. (1970) considers RH as spatially uniform. Consequently, only an approximate spot measurement of the humidity level is necessary for the thermal comfort assessment. ASHRAE-55 (2017) does not specify RH limits, but only prescribes to not reach a humidity ratio (mass of water vapour per unit mass of dry air) lower than 0.012, which corresponded to a dew-point of 16.8^oC indoor. ASHRAE-55 (2017) only mentions that a lower humidity limit might be considered, if low humidity levels produce discomfort. Other standards, such as the *BS EN ISO 13788* (2002), only require the RH to be low enough to avoid surface condensation.

Table 1.1. Main hygrothermal comfort variables (Fanger et al., 1970)

Environmental Factors	Human Factors
Air Temperature	Metabolic Rate
Radiant Temperature	Clothing Insulation
Air Velocity	
Humidity	

More accurate strategies to measure and control RH are, however, necessary. High levels of indoor humidity could lead to condensation formation, decay of materials, mould proliferation and an increase of indoor pollutants, released by solvents, building materials and furnishings (Arundel et al., 1986). Regulating RH levels in buildings can potentially reduce health issues and improve people's perception and satisfaction with the indoor environment (Arundel et al., 1986; Wyon et al., 2006; Tsutsumi et al., 2007). If RH is ideally maintained between 40% and 60%, the indoor air quality is optimised (Arundel et al., 1986). Outside this range, low RH levels increase concentration of noxious chemicals in the air, which exposes people to respiratory infections and skin diseases. High RH levels alter the temperature perception in the room, increase the emission of Volatile Organic Compounds from materials and provide conditions for the proliferation of viruses and mould spores (Fig. 1-1).

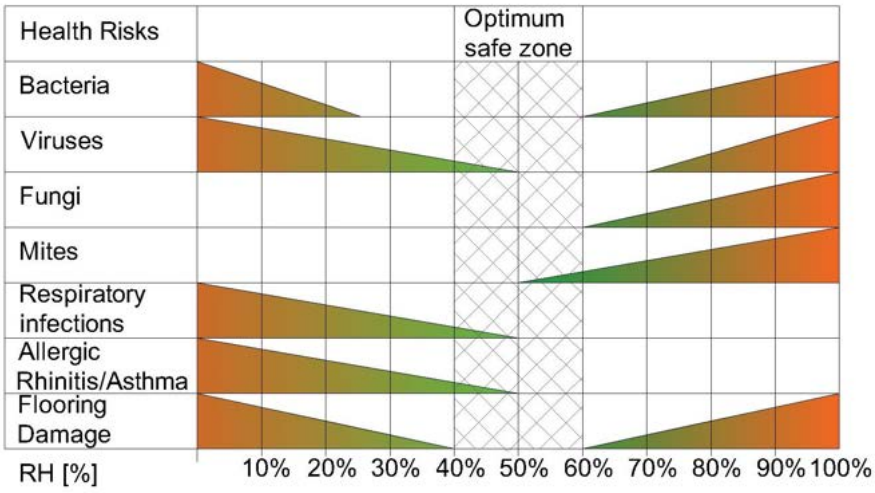

Fig. 1-1. The impact of humidity on human health (Arundel et al., 1986)

Energy consuming mechanical devices, such as air conditioning (AC) systems, are commonly used to cool an environment and maintain optimal RH levels (Di Giuseppe and D'Orazio, 2014; Besant and Simonson, 2000). However, these systems demand regular maintenance, which is not often systematically done, and a good understanding of their functioning and optimal use. There are also concerns about installation costs, other than the significant energy consumption during the usage (Isetti, Laurenti and Ponticiello, 1988; Osanyintola and Simonson, 2006; Crump, Dengel and Swainson, 2009).

Low energy design strategies aim to provide comfortable and healthy indoor climates, whilst minimising overall mechanical ventilation and AC energy consumption. One potential solution is the wider use of hygroscopic materials on building indoor surfaces, which have the ability to moderate indoor humidity fluctuations through exposure to the room air. This can be achieved by using specific building materials, which reduce the peaks of internal RH due to their ability to adsorb and desorb moisture, a process referred to as moisture buffering (Padfield, 1998). This property can reduce condensation risks and the decay of materials sensitive to moisture, but it may also reduce AC operational energy use, due to the air conditioning latent load reduction by porous materials during the exchange of moisture with the indoor air (Isetti, Laurenti and Ponticiello, 1988).

Experimental tests (Rode et al., 2005; Padfield, 1998; Yang et al., 2014) and theoretical models (Woods, Winkler and Christensen, 2013; Abadie and Mendonça, 2009; Zhang et al., 2017) were developed to characterise the moisture buffering properties of materials. It is not clear how these methods can represent the real moisture buffering behaviour of finishing materials. Laboratory tests are run in controlled environments and different tests lead to different results, whilst theoretical models are based on simplifications and on laboratory tested material properties.

Therefore, there is not an agreed interpretation of moisture buffering, due to the complexity of moisture exchange between materials and the environment.

1.1 Aims and Objectives

The overall aim of this thesis is to develop a method that can assess the ability of hygroscopic materials to regulate the indoor RH in a real environment. To pursue this, moisture buffering mechanisms at the material level and at the system level were investigated, by analysing the interconnected influence between materials and the indoor environment. The impact of environmental factors on the moisture buffering capacity of materials was observed in laboratory testing, whilst the influence of hygroscopic materials to moderate the indoor humidity together with ventilation strategies was investigated in the full-scale testing and hygrothermal simulations. Through the combination of these three levels, and, in particular, through the full-scale work, the foundation for developing a laboratory protocol that can predict the impact of the materials on the environment, can be laid. This will lead to develop a classification system, which will guide designer to select a material depending on the desired indoor environmental conditions.

The specific objectives of this PhD are to:

- Analyse the moisture buffering response of materials to variations of different parameters in laboratory testing, such as air velocity, temperature and humidity functions. By using as baseline existing protocols, each factor was individually varied to investigate its impact on the dynamic sorption capacity of materials. Temperature was considered for the first time as a variable factor in moisture buffering investigation, whilst sinusoidal RH signals were applied to materials, rather than the standard square wave signal in existing protocols.
- Devise and conduct experimental testing to define a method to quantify moisture buffering in real-scale buildings. An affordable and easily reproducible testing set-up was planned to monitor and investigate the moisture buffering capacity of hygroscopic walls in three testing facilities at the Building Research Park (BRP).
- Analyse the sensitivity of the moisture buffering capacity of walls to boundary conditions and environmental factors by using a hygrothermal simulation model.
- Analyse through simulations the behaviour of different coatings and the involvement of sub-layers in the walls to moderate the indoor humidity.
- Investigate and compare full-scale and existing laboratory scale testing.

1.2 Scope

The focus of this study is the moisture buffering capacity of materials to moderate the internal humidity fluctuations. The energy related aspect of the moisture buffering capacity of the materials was not investigated, as literature review presented contrasting results in terms of the impact of moisture buffering on the energy performance of the buildings (Chapter 2). The ability of hygroscopic materials to buffer moisture has been widely demonstrated, so therefore the aim of this work is to understand the environmental factors affecting the moisture buffering capacity of hygroscopic materials applied on indoor surfaces. Through the systematic measurement of the joint impact of hygroscopic materials and ventilation in the humidity moderation in full-scale rooms and the analysis of a variety of parameters that influence the dynamic sorption capacity of materials, this work provides the tools to accurately evaluate the moisture buffering capacity of materials. Coatings such as clay, gypsum, lime and plasterboard were used for the study as widely used on indoor surfaces and commercially available. There is a variety of other materials that have similar or better moisture buffering capacity (such as wood or novel plasters). However, the use of widely used materials allows a direct focus on the impact of environmental factors on materials rather than on their characterisation and composition. As Ramos, Delgado and de Freitas (2010) indicated, plasters are usually covered by paints and wall paper, which reduce the moisture buffering capacity of materials. In this study, materials were not coated, to better evaluate the moisture exchange mechanisms between hygroscopic materials and indoor environment. It is not in the scope of this thesis to analysis the impact of coatings on the moisture buffering performances of the walls.

The main experimental work for this study involved acquiring reliable moisture buffering data either in the laboratory and full-scale testing. For the laboratory scale testing the NORDTEST (Rode et al., 2005) protocol was used as baseline instead of other methods (*ISO-24353*, 2008; *JIS A 1470-1*, 2002), as it is widely used and it could be carried out during working hours. The use of other protocols would have given a wider analysis into the impact of different time interval and different RH ranges. Therefore, this study did not focus on this specific aspect, but on the shape of the RH signal, temperature and air velocity, as time intervals and RH levels have been widely investigated elsewhere. The NORDTEST protocol was also applied in test rooms, to directly compare the laboratory testing with the full-scale tests. In full-scale testing three test-rooms located in Wroughton, UK were used.

As this study was limited to few cases and carried out in a West of England specific climate zone, further studies on different constructions and climate are necessary in future for validation. Weekly tests were run on the test rooms to reproduce the six cycles of the laboratory moisture buffering test. One year test were not feasible due to time restriction and technical limitation of the equipment, as explained in Chapter 4.

In the full scale testing plasterboard was tested, as it had been applied in previous tests in the test-cells (Latif et al., 2016) and tests were performed, when outdoor temperature were low (winter-spring), as the rooms did not have a cooling system that would have permitted testing during warmer periods. Tests were not carried out in inhabited buildings, as it required building users to apply hygroscopic materials to the interior surfaces. Moreover, it is necessary to monitor participants' behaviour to accurately estimate people's impact on the moisture regulation of the building.

The use of alternative coatings were analysed through hygrothermal simulations. WUFI® Plus software was preferred as it is a commercially available, and it is widely used both in academia and in practice. The software has got some limitations as explained in Chapter 5. However, past studies (Barclay, Holcroft and Shea, 2014) and a comparison between simulation and full scale in this thesis gave confidence to the reliability of the software. Moreover, the use of simulation software also provided the opportunity to discuss about the suitability of hygrothermal models to predict moisture buffering.

1.3 Structure of the thesis

The PhD was divided in three interlinked phases:

- Laboratory-scale experimentation;
- Full-scale testing at the University of Bath's BRP, at the the Science Museum, Wroughton, UK;
- Hygrothermal simulation analysis.

The outcome of the three phases were then combined into the final phase of the research project, where full-scale data were combined with the laboratory test to investigate possible improvements on the evaluation of moisture buffering.

Following the same scheme, this thesis is comprised of six chapters. Each chapter, excluding the literature review, developed individually each phase of the research work then combined in the last two chapters (Chapter 4 and Chapter 5). For this reason each chapter is provided with a methodology, results, discussion and conclusion.

Chapter 2 reviews the moisture buffering background by explaining its theoretical fundamental and the development of experimental testing. A detailed review of studies on this subject was reported, where different approaches to moisture buffering were summarised and classified to criticise and identity aspects of moisture buffering that needs to be further investigated or introduced. The definition of moisture buffering is also presented, followed by the impact of this property on the indoor

humidity moderation and the consequent improvement of the health and comfort of people indoors.

Chapter 3 collates all the work focused on the materials characterisation and laboratory testing. Samples of plasters were analysed and their hygrothermal properties were experimentally determined and discussed with reference to the literature. This allows for a better understanding of their moisture buffering performances. Moisture buffering performances of the samples were then investigated, first following the existing protocols and successively by modifying some factors to reproduce similar behaviour as in real buildings.

Chapter 4 focuses on the full-scale experimental analysis, where the impact of hygroscopic materials on the indoor moisture moderation is analysed in existing testing facilities. The testing rooms were set up to control and monitor the indoor RH, which allowed analysis on the wall's response to the increase and reduction of humidity indoors. Ventilation and infiltration were also controlled and monitored to understand the influence of these factors on the moisture balance and moisture buffering capacity of the walls.

Chapter 5 continues the full scale analysis but with the support of simulations. This allows investigations into the impact of all the wall components on moisture buffering. Moreover, it was possible to vary elements of the testing, such as variation of the ventilation rate, moisture load and plasters applied on the indoor surfaces, so it was possible to look at moisture buffering from different points of view than the one analysed in Chapter 4. Chapter 5 also merges elements of Chapter 3 and 4. The experimental and simulated full-scale data were compared and divergences and similarity were observed and analysed.

Finally, Chapter 6 concludes the thesis and outline recommendation for future works.

1.4 Dissemination

Journal and Coference Papers

Cascione, V., Maskell, D., Shea, A. and Walker, P., 2019. A review of moisture buffering capacity: From laboratory testing to full-scale measurement. Construction and Building Materials, 200, pp.333–343.

Cascione, V., Maskell, D., Shea, A. and Walker, P., Mani, M., 2020. Comparison of moisture buffering properties of plasters in full scale simulations and laboratory testing. Construction and Building Materials, 252 119033.

Cascione, V., Maskell, D., Shea, A. and Walker, P. 2020. The moisture buffering

performance of plasters when exposed to simultaneous sinusoidal temperature and RH variations. Journal of Building Engineering. 101890.

Cascione, V., Hagentoft, C.E., Maskell, D., Shea, A. and Walker, P. 2020. Moisture buffering in surface materials due to simultaneous varying relative humidity and temperatures. Experimental validation of new analytical formulas. Applied Science. 10(22), 7665.

Conference Papers

Cascione, V., Maskell, D., Shea, A. and Walker, P., 2019c. Full-scale simulation of indoor humidity and moisture buffering properties of clay. Earthen dwellings and structures. Springer, pp.395–406.

Cascione, V., Cavone, E., Maskell, D., Shea, A. and Walker, P., 2019a. The effect of air velocity on moisture buffering. Matec web of conferences. EDP Sciences, vol. 282, p.02007.

Cascione, V., Lim, D., Maskell, D., Shea, A. and Walker, P., 2019b. The response of clay plaster to temperature and RH sinusoidal variations. Matec web of conferences. EDP Sciences, vol. 282, p.02005.

2. *Literature Review*

2.1 Introduction

Vapour responsive materials, defined as hygroscopic, have generally good moisture buffering capacity (Padfield, 1998). Indoor air quality and hygrothermal comfort significantly improve, when timber (Hameury, 2005), clay (McGregor et al., 2016) and other novel materials, such as zeolite (Sagae et al., 1994) and mineral based plasters (Stahl, Vonbank and Holzer, 2013), are applied indoors. Simonson, Salonvaara and Ojanen (2004) demonstrated that when the internal surfaces of a building were hygroscopic, the maximum RH in the room was lower compared to case with "non-breathable" surfaces, and overall, RH dropped by 20%. Salonvaara et al. (2004) showed that materials such as wood maintain the mean RH at around 40% in the 24h tests, which is within the optimal RH range for the health and comfort of building occupants (Rode et al., 2005).

As Osanyintola and Simonson (2006) indicated that moisture buffering may also directly and indirectly effects the energy use in buildings. As direct effect, in winter it may reduce heating energy consumption, due to the latent heat generated by hygroscopic materials, when moisture is adsorbed from the air (Kraniotis et al., 2016). In the cooling season hygroscopic materials reduce the use of energy to cool the room, as they keep humidity lower and decrease the room entalphy (Osanyintola and Simonson, 2006). Indirect energy saving are also possible, thanks to the indoor air quality and hygrothermal comfort improvement. With lower ventilation rate or lower and higher indoor temperature in winter and summer, respectively, it is still possible to guarantee a good air quality and comfort. This allows to reduce heating/cooling energy waste, by turning down total energy consumption in buildings (Zhang et al., 2017; Nore et al., 2017). However, there are uncertainty on the impact of moisture buffering on the energy usage. Osanyintola and Simonson (2006); Nore et al. (2017); Woloszyn et al. (2009) highlighted that good temperature and ventilation control strategies are mainly responsible to improve the energy performance of buildings, while moisture buffering has a marginal impact.

Even though the energy aspect of moisture buffering is of interest, the primary role of

hygroscopic materials is the moderation of the indoor humidity level. Other than a positive impact of people's thermal comfort and health moisture buffering also improves the durability of building components and reduces the decay of construction materials (Wu et al., 2015; Padfield and Jensen, 2010). The reduction of the highs and lows of humidity can significantly reduce condensation risk and can avoid "drying cracks" on mortar materials (Lombardi, 2005). Moisture accumulation can produce ornamental damages, such as formation of stains on surfaces, but also structural problems through the corrosion of steel and weakening of bricks (Lombardi, 2005). Moreover, the thermal conductivity of materials is increased with higher moisture content, reducing the insulation value of the building envelope (Budaiwi and Abdou, 2013). Moisture buffering can help to prevent high accumulation of moisture in the inner layers that can prevent damage and reduce the risk of the losses of the enclosures thermal performances.

Even though an increased interest in the moisture buffering capacity of hygroscopic materials has been showed, as yet there is not an agreed interpretation of this property, due to the complexity of moisture exchange between materials and the environment, and because of its definition itself. Moisture buffering is a physical quantity that refers simultaneously to a material property and building space characteristic at the same time. Moisture transport through walls has been always related to the temperature, vapour pressure and RH differential between the indoor and outdoor (Ojanen, Kohonen and Kumaran, 1994). However, in 1960 Künzel (1960) started considering the exclusive time-dependant moisture sorption process between finishing materials and indoor RH regulation. This property involves only indoor surfaces and it is not directly linked to outdoor/indoor humidity and temperature correlation. Künzel (1960) defined this property as moisture adsorption, which refers exclusively to a material property. Forty years later Padfield (1998) used the word moisture buffering, to describe the consequent effect of porosity and adsorption on the indoor moisture balance. The dynamic adsorption capacity has been consequentially gained interest and it has been studied in terms of theory, experiments and numerical simulation (Zhang et al., 2017; Woods, Winkler and Christensen, 2013; Allinson and Hall, 2010), looking for a connection between moisture transport mechanism in hygroscopic materials and the effects on the indoor hygrothermal comfort.

The term hygrothermal is used in building physics as the reference to heat and moisture transmission of materials. Even though heat and moisture transmission are interlinked, they are usually approached independently. The heat is transferred through conduction, convention and irradiation. Conduction is a characteristic of solid bodies. The heat propagates from a body to an adjacent one, due to a temperature differential. Convention happens between a solid and fluid, when the fluid is subjected to a temperature variation that moves the fluid away from the solid surface at a different temperature. This movement produces the transport of energy

in the form of enthalpy. The irradiation exchanges heat as electromagnetic heat radiation between surfaces. These three heat exchange mechanisms, when applied to buildings, are then combined in the heat flux equation:

$$\phi = -U(T_i - T_e)[\frac{W}{m^2}] \tag{2.1.1}$$

Where ϕ is the heat flux (W/mK), T_i and T_e are respectively the internal and external temperature (K), U is the thermal transmittance (W/m^2K) that is defined as:

$$U = (\frac{1}{h_i} + \frac{s}{\lambda} + \frac{1}{h_e})^{-1} \tag{2.1.2}$$

Where h_i and h_e represent the heat exchange for convention and irradiation (W/m^2K), while λ and s represent the thermal conductivity (W/m^2K) and thickens (m) of the body.

The moisture is exchanged between a solid and a gas, while it diffuses through a solid, when a moisture differential between the indoor and outdoor is present. The moisture exchange between solid and gas can be described as:

$$g_v = -\beta_p(p_i - p_e)[m^2/s] \tag{2.1.3}$$

Where g_v is the moisture flux, p_i and p_e are respectively the internal and external vapour pressure (Pa), β is the moisture exchange between a solid body and a fluid (s/m). The moisture transport through a solid can be distinguished between the water vapour diffusion and liquid transport. In the water vapour diffusion, moisture transport mainly happened in dry pores at low humidity level. In the vapour diffusion, water molecules transfer is represented, similarly to the heat transfer, as proportional to a vapour pressure differential and the water vapour permeability of the material (δ_p).

The liquid transport can be further distinguished between surface diffusion and capillary transport. The surface diffusion and capillary transport happen in smaller pores and capillaries at higher humidity levels. In the surface transport the water molecules stack on the pores surface and start to layer up forming hydrogen bonds until the pore saturates. The capillary transport is generated by the surface tension between the capillary surface and water molecules that contributes to the moisture distribution into the material. These two phenomena are more complex to determine than the vapour diffusion, and, consequently, different mathematical representations were developed, as described in Section 2.3.2.

Heat and moisture transfer happens simultaneously, influencing each other. By increasing the moisture content in the material, the thermal conductivity proportionally increases (Künzel, 1995). On the contrary, it is more complex to

determine the influence of the temperature on the moisture transfer (Feng and Janssen, 2016).

2.2 Theoretical Models

According to the definition given by the NORDTEST (Rode et al., 2005), moisture buffering can be evaluated by the MBV, which can be estimated by direct experimental measures or by an approximate model, based on Fick's principle on the diffusion of water vapour in a porous material (Alvarez, 1998). The theoretical Moisture Buffering Value ($MBV_{\text{theoretical}}$) is defined as the amount of water adsorbed and desorbed from materials through 1 m^2 surface exposed to certain RH variations, over a defined period of time:

$$MBV_{\text{theoretical}} \approx 0.00568 p_{\text{s}} b_{\text{m}} \sqrt{t_{\text{p}}} \tag{2.2.1}$$

$MBV_{\text{theoretical}}$ is a function of the saturation vapour pressure p_{s} [Pa], time period t_{p}[s] and moisture effusivity, $b_{\text{m thr}}$ $[kg/(m^2 \cdot Pa \cdot s^{1/2})]$:

$$b_{mthr} = \sqrt{\frac{\delta_{\text{p}} \xi_w}{p_{\text{s}}}} \tag{2.2.2}$$

Where δ_{p} is the water vapour permeability and ξ_w is the moisture capacity $[kg/m^3]$.

$MBV_{\text{theoretical}}$ does not represent the real capacity of materials, because it mixes steady-state properties, defined under steady state and equilibrium conditions with the dynamic buffering behaviour. Water vapour permeability and sorption isotherm are an example of steady-state properties. These properties are measured at a specific temperature and RH and are mostly considered invariable in different environmental conditions, which is not always realistic as Reuge et al. (2020) demonstrated. Peuhkuri and Rode (2005) demonstrated the dissimilarity of MBV, when b_{m} is calculated through Eq. 2.2.2 and when it is experimentally determined from adsorption and desoprtion cycles, based on 8/16 h square wave humidity steps between 33% and 75% RH (Fig. 2-1). The measured effusivity ($b_{\text{m exp}}$) is determined from the measured MBV and derived from Eq. 2.2.1. As shown in Table 2.1, $b_{\text{m exp}}$ for Autoclaved Cellular Concrete (AAC) is lower than the theoretical ($b_{\text{m thr}}$), as $b_{\text{m thr}}$ does not consider the dynamic rate and amount of moisture exchanged between materials and the environment. It is clear that $b_{\text{m thr}}$ indicates only the specific moisture capacity for equilibrium conditions. However, also experimental results may be not representative of the real dynamic behaviour of materials, because they are only related to a specific humidity variation function.

Table 2.1. Determination of Moisture Effussivity for AAC (Peuhkuri and Rode, 2005)

Method	b_{m} $[kg/(m^2 \cdot Pa \cdot s^{0.5}]$
Theoretical	$2.66 \cdot 10^{-7}$
Experimental	$1.96 \cdot 10^{-7}$

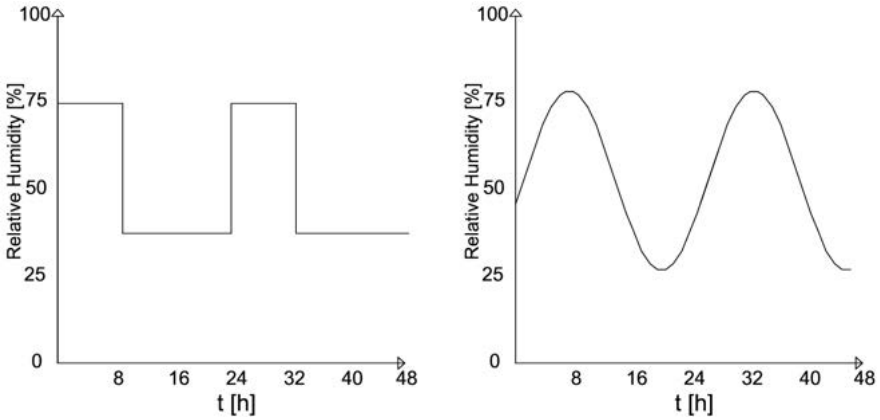

Fig. 2-1. Square wave humidity cycle and sinusoidal humidity variation

Similarly, the theoretical definition of penetration depth is also based on steady-state properties. The penetration depth is an essential property to determine the thickness of hygroscopic materials to make the most of moisture buffering potential (Rode et al., 2005). It defines how deep moisture infiltrates from the indoor air into the material for a given time period. Maskell et al. (2018) underlined the theoretical models overestimate the moisture penetration depth, as these methods are also based on numerical approximations.

In the calculation of the true moisture penetration depth (TMPD) (Equation 2.2.3), the moisture diffusivity is considered constant (Arfvidsson, 1999).

$$x_{Th} \approx 4.61\sqrt{\frac{D_W \cdot t_p}{\pi}} \tag{2.2.3}$$

Where x_{Th} is the true penetration depth [mm], D_w is the vapour diffusivity $[m^2/s]$, t_p is the time period [s]. Even though Abadie and Mendonça (2009) stated D_W can be assumed constant, as material's hygric properties within the RH interval 30%-70% are almost unvaried, Kreiger and Srubar III (2019) highlighted the importance to consider the diffusivity as variable value, as it depends on the moisture concentration and on the chemical and physical structure of materials.

Interestingly, Equation 2.2.3 was developed considering a semi-infinite body in contact with an environmental subjected to sinusoidal variation. The penetration depth of materials exposed to non-symmetrical square wave variation may be different. For all these reasons, Maskell et al. (2018) pointed out the necessity to quantify the penetration

depth through direct measurement.

Maskell et al. (2018) results on clay plasters showed the moisture buffering capacity is limited only to the first few millimetres of the material in tests with short cycles. It means that thickness of materials above their penetration depth do not improve the moisture buffering capacity, as the MBV stays constant. However, tests were performed only with earthen materials. The use of other materials, like hemp lime and rape straw lime, showed a continuous increase of the MBV with the thickness (Rahim et al., 2016), which indicates the difficulty to measure experimentally the penetration depth, when materials have a significant dynamic sorption capacity. At the same time, the quantification of the penetration depth becomes more complex, when multi-layer wall assemblies are taken into consideration. As Kaczorek (2019) demonstrated, the moisture moves into the wall depending on the single materials properties and their location in the stratification.

To reduce the gap between the theoretical models and experimental tests, Zhang et al. (2017) developed a new mathematical expression for MBV. The basic Moisture Buffering Value (MBV $_{\text{basic}}$) is applicable either with harmonic or square waves function of humidity (Fig. 2-1). The MBV $_{\text{basic}}$ function is dependant not only of the time period, but also of time variation of the indoor condition, when high humidity is kept for αt_{p} hours and low humidity is maintained to $(1-\alpha)t_{\text{p}}$ hours, as shown in the Eq. 2.2.4:

$$MBV_{\text{basic}} = 1.27[\alpha(1-\alpha)]^{0.535}\sqrt{\delta_{\text{p}} \cdot \rho \cdot \xi_u}\sqrt{t_{\text{p}}} \tag{2.2.4}$$

Where: δ_{p} is water vapour permeability $[kg/m \cdot s \cdot Pa]$, ξ_u is moisture capacity $[kg/kg]$ and ρ is density $[kg/m^3]$. Eq. 2.2.4 is applicable only for square wave moisture variation. However, it can be indirectly used for harmonic function of humidity, if multiplied by a correction factor β, which is derived from quasi-harmonic humidity variation equations.

Roels and Janssen (2006) highlighted that there are other discrepancies between the theoretical model and experimental results, as the effect of the moisture surface resistance, Z_{p}, in the moisture exchange process with the air is not considered. The $MBV_{\text{theoretical}}$ supposes the moisture exchange happens on the material surface, but in reality it takes place on a thin air layer above the surface, where either convective moisture flows in the air and the intrinsic materials resistance are present. As Rode et al. (2007) showed, $MBV_{\text{theoretical}}$ is comparable to the practical verification only if Z_{p} is zero, materials are homogeneous and their thickness is at least equal to their penetration depth.

2.3 Simulation models

Simulation models evolved quickly to systematise the global analysis of building hygrothermal performances, by taking into account heat and moisture transfer in buildings. Climate, location, building geometry and enclosure's structure are necessary input data to model the hygrothermal behaviour of an enclosure. In particular, to have accurate predictions of indoor temperature trends, the capacity of the enclosure to transport and store heat is assessed through wall's components properties, such as thermal conductivity, specific heat capacity, density, and their dependency on the moisture content in the enclosure. As an example, if the moisture content increases, the thermal conductivity increases too. Instead, to obtain a detailed evaluation of the indoor relative humidity in a variable regime (variable vapour production, ventilation and outdoor vapour pressure), the influence of porous materials needs to be included in the models. However, it is necessary to introduce various simplifications, to reduce computer Random-Access Memory (RAM) usage and calculation time. Each numerical model provided different simplifications, and for this reason they need to be first classified, in order to understand the reason of such simplifications.

As Kreiger and Srubar III (2019) explained, hygrothermal simulations can be initially divided into three groups:

- Empirical,
- Semi-Empirical,
- Physics Based.

This classification divided the models depending on the the use of experimental data in the development of the tools. The empirical models use experimental data as foundation of the tool, while physics based methods use physics fundamental equations to develop a model, which is later validated with experimental analysis. Semi-empirical models are in between the previous two cases, where physics based methods are improved by introducing inputs from experimental testings. In general, this classification can be further simplified, dividing the models to simplified simulations (empirical and semi-empirical) and heat, air and moisture transfer (HAMT) models (physics based).

2.3.1 Simplified Methods

Simplified mathematical models have been developed, usually by introducing correction factors from experimental data. The uncertainty of this method is the assumption that the correction coefficients can be applied to any building, when they are usually

obtained from experimental rooms or few full-scale testing (representative of a small climate zone) (Section 2.5).

For example, Tsuchiya (1980) model is based on factors measured experimentally, which makes his model only suitable for a specific tested room. However, Tsuchiya (1980) is one of the first to introduce moisture buffering in the mass balance equation as average moisture content of a thin indoor surface layer, which instantaneously reaches equilibrium. The storage capacity is limited to a few millimetres of the surface and calculated only as a function of the dry mass of the surface material.

The effective capacitance (EC) model (Stehno, 1982) links both the capacity of the finishing material and the room air to store moisture: moisture buffering is considered as an increment of the air capacitance of the room. The EC is a highly simplified model, which does not require many input data, because it assumes the air in the room is well-mixed and with uniform properties. Moreover, it does consider the wall moisture content always in equilibrium with the room air humidity, while the wall humidity increment is assumed as a qualitative multiplier factor (m), which is not well defined (Woods, Winkler and Christensen, 2013).

Later Woods et al. (2014) developed the effective moisture penetration depth (EMPD) model (Cunningham, 1992). This method considered the moisture capacitance of the wall as the combined work of a surface layer, which is responsible of the short term fluctuation and a deep layer for long term fluctuation. These two nodes represent the moisture buffering as a combination of the mass transfer resistance between the air and the surface, and the diffusion resistance into the material, respectively. The thickness of these layers is defined by the effective moisture penetration depth (Equation 2.3.1).

$$x_{Eff} = \sqrt{\frac{\delta_p \cdot p_s \cdot t_p}{\rho \cdot \xi_w \pi}} \tag{2.3.1}$$

Where δ_p is the water vapour permeability $[kg/m \cdot s \cdot Pa]$, p_s is the saturation pressure [Pa], t_p is the time interval, ρ is the dry density of the material $[kg/m^3]$ and ξ_w is the specific moisture capacity [kg/kg]. The EMPD is a semi empirical model, as it perfected the moisture capacitance model with inputs taken from experimental measurement in one single building. The experimental inputs (Surface area S, specific moisture capacity ξ_w, moisture permeability δ_p, effective penetration depth x_{Eff}) could be extracted through a moisture balance equation, by forcing humidity square wave fluctuation in the analysed building. Clearly, a specific equipment and set-up was necessary, such as that explained in §2.6. Successively, the model was improved and validated with more buildings (Woods and Winkler, 2016, 2018), showing a small sensitivity of the model to inputs variations. However, this model does not consider the moisture transport through walls and moisture buffering potential of furniture, as well as it needs further verification of the influence of location and square metering of buildings.

Other developments of this method were possible, by introducing computational fluid dynamics (CFD) in the EMPD model. As the EMPD model assumed the temperature and water vapour in the room are well-mixed and homogeneous, Steeman et al. (2009) highlighted that CFD allows to predict local distribution of temperature and humidity. In this way, it was possible to improve results obtained, but increasing significantly the simulation time. Consequently, it was so stated that the well-mixed air model give good prediction of the average RH in a room. Therefore, the CFD-EMPD should be applied only for the prediction of local hygrothermal behaviour or damage control.

The EMPD was also used by Abadie and Mendonça (2009), who looked for a method to apply the $MBV_{practical}$ in building simulations. Abadie and Mendonça (2009) found a way to convert experimental data, obtained in a certain experimental condition into the desired environmental condition to use in a lumped model, by looking into the correlation between $MBV_{theoretical}$, $MBV_{practical}$, RH and surface resistance (Z_p). Even though this model was based on several simplifications (constant moisture diffusivity, constant temperature, materials' thickness bigger than the penetration depth), it is a good starting point for looking into the correlation between theory, small scale testing methods and full-scale analysis.

2.3.2 HAMT Models

HAMT models are considered the most theoretically correct method for building simulations, as they analyse the simultaneous impact of temperature, humidity and barometric pressure on a simulated building. Consequently, HAMT give a better interpretation of the moisture storage capability of walls than the simplified methods. Due to the link between simultaneous heat, air and moisture transport through the building envelopes and the simulated hygrothermal condition in the room model, moisture buffering can be considered as part of the heat and moisture transfer between the surface and the indoors.

All the models are based on Fick's law for moisture. The main differences between each method are the level of complexity in the theoretical description of physical phenomenon, as well as the spatial and time discretization. The application of different strategies to describe physical mechanisms leads to divergent results. A clear example is the difference between Delphin® (Nicolai, 2017) and WUFI® (Antretter et al., 2015). Both software described the water vapour diffusion as follow:

$$g_{wv} = -\delta_p \cdot S \cdot \nabla p_v \tag{2.3.2}$$

Where g_{wv} is the water vapour transport flux density $[kg/m^2 s]$, δ_p is the liquid diffusivity coefficient $[kg/m \cdot s \cdot Pa]$, S is the surface area $[m^2]$ and p_v is the water vapour pressure $[Pa]$. However, there are significant differences in the materials'

liquid transport description. WUFI® assumes the liquid water moves in the pores, following the water concentration gradient. The liquid transport is consequently described as in equation Equation 2.3.3.

$$g_w = -D_W \nabla w_n \tag{2.3.3}$$

Where g_w is the liquid transport flux density $[kg/m^2 s]$, D_W is the liquid diffusivity coefficient $[m^2/s]$ and w_n is the water content $[kg/m^2]$.

On the other hand, Delphin® considers the capillary vapour pressure as driving force (Equation 2.3.4).

$$g_w = -K_l \nabla p_l \tag{2.3.4}$$

Where g_w is the liquid transport flux density $[kg/m^2 s]$, K_l is the liquid conductivity coefficient $[s]$ and p_n is the capillary pressure $[Pa]$. The main difference in the results can be seen in the moisture content of the layers. Generally, Wufi® presents higher moisture content values compared to Delphin®, as showed by Hagentoft (2002).

Considering the discretization, depending on the granularity of both air volume and enclosure of buildings, it is possible to focus simulations on the energy performances or on the enclosure properties. Enclosure focused simulation models (WUFI®, Delphin®) usually have intermediate to fine discretization for the walls, and a coarse indoor air granularity (Janssen and Roels, 2009). The coarseness leads to the assumption of perfectly mixed air and equal temperature and RH in all rooms, while intermediate-fine grained models generate 1-D models and 2D-models, respectively. Even though there is not an updated list of currently existing simulation models, more details on the main HAMT programs and their differences until 2010 can be seen in Straube and Burnett (2001); Woloszyn and Rode (2007); Delgado et al. (2010).

Although bands of acceptance for simulations were introduced (Hagentoft, 2002), to assure the reliability of simulation models, it was shown that numerical results still presented differences, due to different numerical techniques and levels of complexity (Hagentoft, 2002). Delgado et al. (2010) also highlighted, there is not yet a clear link between theory and the real dynamic sorption processes. Calculation methods may not represent moisture buffering in real buildings, because they are only based on a few case studies and very specific full-scale test set-up. Due to the complexity of the moisture transport mechanisms, a standard experimental validation technique does not exist and consequently it leads to different simulation results and evaluations.

In the last ten years existing software have been updated and improved, but new challenges have been undertaken. New models have been introduced, which stand out from the traditional HAMT (Van Belleghem et al., 2014; Dubois et al., 2014; Tijskens,

Roels and Janssen, 2019). Dubois et al. (2014) introduced an inverse modelling approach, which applied the HAMT and the experimental MBV, to estimate the hygric parameters of building materials. Contrary to the previous studies, this method aimed to use the MBV as a data source, allowing the prediction of materials properties, which are usually measured through time-consuming, steady state tests.

Another important challenge is the introduction of probabilistic evaluation in hygrothermal simulation. As deterministic simulation models become more computationally demanding and more targeted to highly specialised users, the application of this new approach aims to reduce the uncertainty, due to unknown materials and environmental properties, and at the same time reduce calculation time. Tijskens, Roels and Janssen (2019) applied an artificial neural networks (ANN) model to building physics. The ANN is an information-processing system, composed of small processing nodes and weighted interlinked connection between units. This system took inspiration from biological brain, which needs to be "trained" using an existing data set. In this way, the model learns how to predict the correct output. This method shows good agreement with experimental data, but it is at the beginning of its development for building physics applications, and needs more experimental data for its development.

2.4 Laboratory Scale Experimentation

This section presents some laboratory methods used to characterise the dynamic water sorption properties of building materials. There have been various laboratory protocols to determine moisture buffering (Künzel, 1965; Padfield, 1998; Rode et al., 2005), and these can be generally divided into two groups: tests performed through the step-response method and the ones performed in a flux chamber. The main difference between the two is the humidity variation function (square waves and harmonic). However, this simple distinction may prove to be restrictive, as some experimentation are a combination of the two.

2.4.1 Step-Response Method

The simplest laboratory-based experimental method for the moisture buffering capacity is the step-response method, developed by Künzel (1965). It measures the weight variation of samples, when they are subjected to an adsorption phase for a set time, followed by a desorption step (Fig. 2-2).

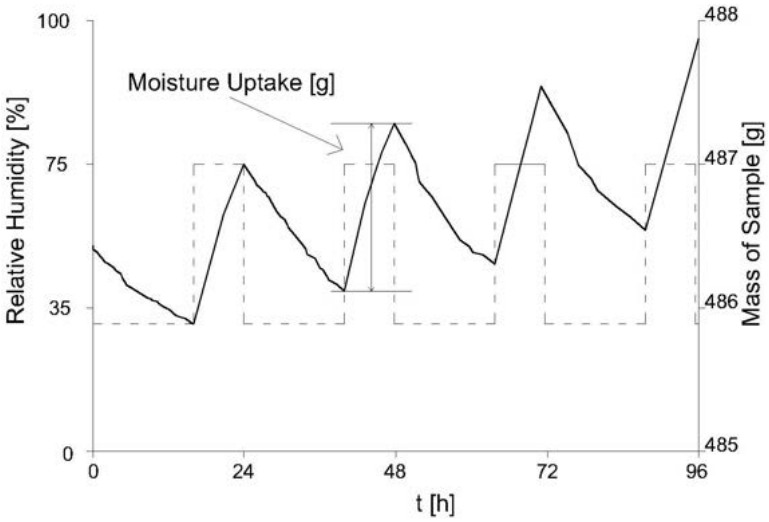

Fig. 2-2. Cyclical moisture uptake and release of hygroscopic materials as function of RH in isothermal conditions (Rode et al., 2005)

Moisture buffering was defined by Künzel (1965) as function of time through an adsorption coefficient A $[kg/m^2\sqrt{h}]$, which links the moisture uptake (kg/m^2) and the square root of time $(\sqrt{h})$. However, as Svennberg et al. (2007) discussed, in this first configuration of the step-response, air movement, sample size and experiment set-up were not standardised and the humidity generation interval to define RH-steps were always variable. RH interval length is strictly dependent on the vapour diffusion resistance of materials, size of the chamber and the way to determine the moisture equilibrium. In particular, equilibrium was considered to have been reached, either after a predetermined time frame or if the weight variation was small (Svennberg et al., 2007). Both methods might deviate from the true equilibrium and led to errors (Wadsö, 1994). Furthermore, the method supposed that the material reached again the hygric equilibrium in the chamber before another cycle started, which never happens in reality. As a consequence, the test results were not comparable to each other and did not represent a realistic situation in a whole building.

The NORDTEST project (Rode et al., 2005) improved and standardised step-response test introducing the Practical Moisture Buffering Value ($\mathrm{MBV_{practical}}$), described as $[kg/m^2 \cdot \%RH]$. It is based on the Künzel's method as it varies cyclically the RH from 33% to 75%. This method tries to supposedly replicate periodically the daily humidity exposure in a building of Nordic countries, assuming 8 h of high humidity and 16 h of low RH in an ambient with air velocity around 0.1 m/s and constant temperature. This is generally not representative of indoor daily humidity fluctuations, as it is unrealistic to have for a prolonged time extremely high humidity levels and than drop it to really low RH levels (Saito, n.d.). Rode et al. (2005) stated that 75%RH was chosen as threshold, above which the risk of condensation and corrosion is high. It is, however, not specified the reason of the 33%RH. The difference with the previous methods is also in the definition of moisture buffering, which is not a function of the square root

of time but a function of RH variation, and it requires a controlled environment for precise test performances.

Together with NORDTEST (Rode et al., 2005), other standards were introduced, such as the *JIS A 1470-1* (2002), *DIN 18947* (2013) and *ISO-24353* (2008), which present similar experimental procedure but use different time-steps and propose three RH levels. McGregor et al. (2014a) and Roels and Janssen (2006) highlighted how those differences influence the adsorption curves, as shown in Fig. 2-3. Janssen and Roels (2007) recognised that the NORTEST does not fully characterised moisture buffering in real buildings, due to the single time-steps interval. So Janssen and Roels proposed the Production-Adapted MBV (MBV*), which introduces another time-interval other than the one presented by the NORDTEST (Janssen and Roels, 2007):

$$MBV^* = \alpha MBV_{8\text{h}} + (1-\alpha)MBV_{1\text{h}} \tag{2.4.1}$$

where α is a weighting factor and 1h and 8h are the moisture generation time.

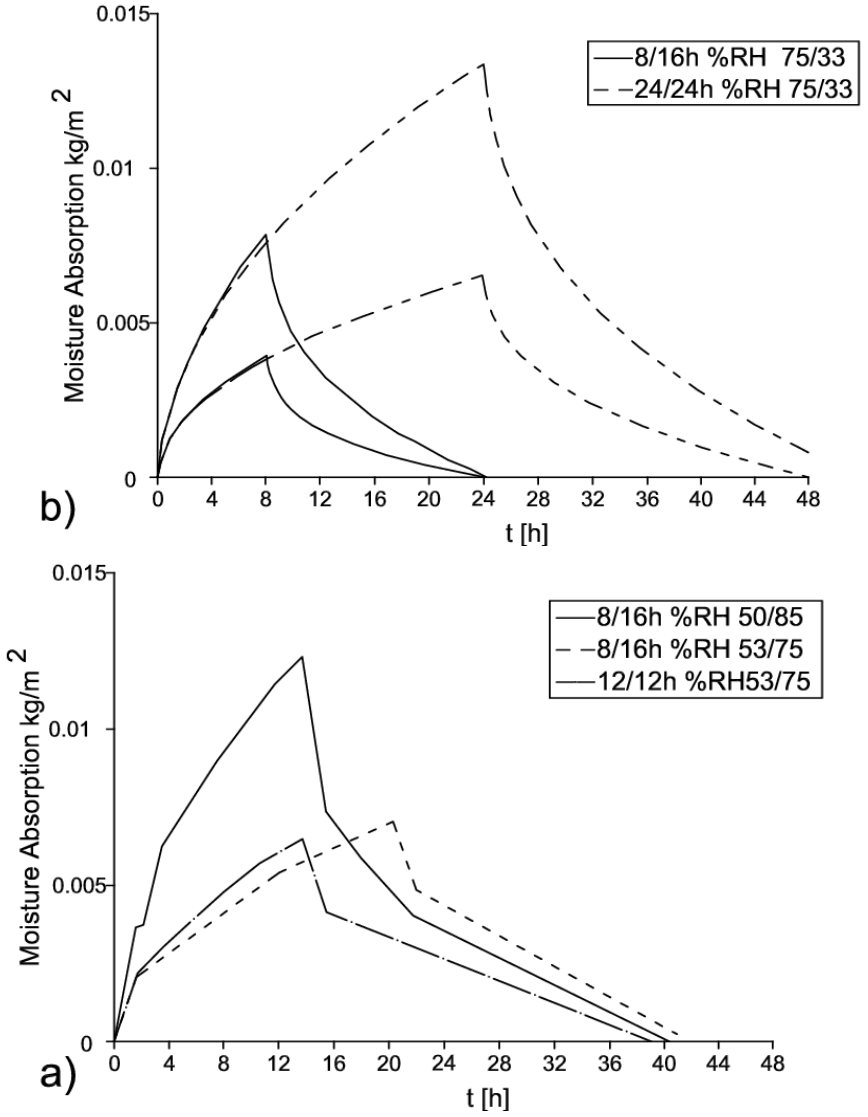

Fig. 2-3. Comparisons between different moisture buffering tests:a) ISO and NORDTEST (McGregor et al., 2014a); b) JPN and NORDTEST (Roels and Janssen, 2006)

Further development were introduced by Wu et al. (2015), who transformed the MBV in the Ultimate Moisture Buffering Value (UMBV). It is defined as:

$$UMBV = \sum_{k=I}^{III} \alpha_{\mathrm{i}} MBV_{\mathrm{i}} \tag{2.4.2}$$

Where α_{i} is the time coefficient defined as $t_{\mathrm{i}}/24$ and I, II and III are the time intervals of the test. Each phase simulates respectively sample pre-conditioning (23°C, 50% RH) summer (40°C, 98% RH) and extreme winter (18°, 3% RH) conditions. This method measures the behaviour of a material not on daily basis, but yearly because it considers only seasonal outdoor weather variations.

All these methods are quasi steady state, which means materials need to achieve a quasi equilibrium state. The methods prescribed preconditioning before testing and that the change in mass between adsorption and desorption is within a predefined threshold (the NORDTEST prescribes the weight amplitude between three consecutive cycles should not deviate to more than 5%). In addition, in real buildings RH varies together with the temperature, which is still not clear how it might influence moisture buffering. Rode et al. (2005) explained that temperature affects the water vapour transport, due to its influence on vapour pressure and other unknown transitory effects during temperature variation. Therefore, it is important to better understand the role of temperature in the dynamic vapour sorption, as temperature in indoor environments is always variable.

Even though a lot of improvement has been given to the test-response method, air movement, air speed, temperature and the surface resistance coefficient inside the climatic chamber are assumed constant. For this reason, Gómez et al. (2011) built another test facility that reproduced the effect of air movement for natural and forced convection on a surface. A test specimen was placed in an air tunnel (Fig. 2-4), which had an adjustable speed fan. The air flow passed first through a stagnation chamber and a flow guide, before reaching specimens, in order to obtain a laminar flow. The instrumentation was placed in a sealed box, where humidity was controlled by salt solutions. Following the NORDTEST protocol, Gómez et al. (2011) checked the influence of the coefficient of surface resistance on the sorption process through Lewis's correlation (Rode et al., 2005) and air speed, revealing a strong correlation between convective moisture flows and MBV. Allinson and Hall (2012) also highlighted that MBV increases, when air speed increases and vice-versa. The developed testing facility brought an effective improvement of the step-response method, as it demonstrated the importance of accurately measure the air velocity. Gómez et al. (2011) found an effective solution to this problem, but the instrument is a very precise apparatus, which might not be easy to replicate and it does not consider the effects on results of different time period and humidity levels, together with the air velocity. Furthermore, Gómez et al. (2011) apparatus controlled the air speed in a laminar environment, while common environmental chambers cannot control the air velocity and the air distribution. Consequently, different results may be obtained within the same chamber depending on the location of the sample inside the unit (Holcroft, 2016b).

Recently Zu et al. (2020) investigated an innovative method to consider accurately the surface resistance, which consisted in curve fitting the moisture buffering experimental data. The measured soprtion curve was compared with a theoretical curve. By varying the vapour permeability, the theoretical curve was varied until it matched with the measured one. The variable parameter, referred as to lumped vapour permeability, contains intrinsically the surface resistance factor at the test environmental conditions.

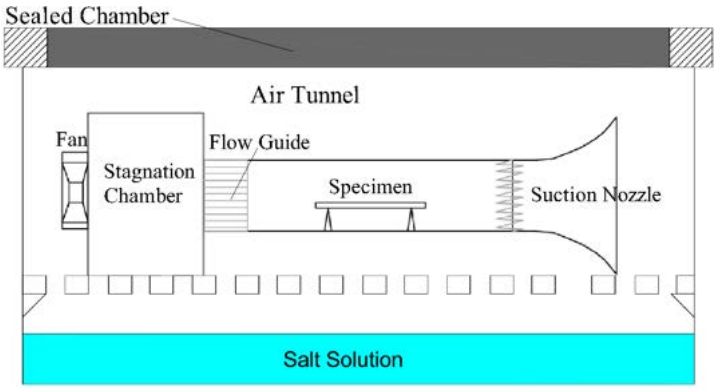

Fig. 2-4. Test configuration of Gómez et al. (2011) and 126 x 58 x 4 mm sample

2.4.2 Flux Chamber

Step-response tests are carried out by varying humidity from high level to low, following a square-wave function. However, in real buildings RH changes are more complex (Simonson, Salaonvaara and Ojanen, 2004). Padfield (1998) developed a different experimental facility, which recreated human moisture production through a 'harmonically changing RH'. The so-called 'flux chamber' did not measure directly the moisture adsorption capacity of materials but it measured the RH variation in the cell and calculates the difference between a known amount of water introduced in the cell through humidification and the moisture recollected in a water tank during the de-humidification. This method is more suited to the comparison of the influence of materials on the indoor environment, but it does not allow analysis of the impact of moisture on the material sorption process. For a complete understanding of moisture buffering, either the moisture storage capacity and their impact in the environment should be considered

Ramos and de Freitas (2004) developed a similar equipment in which the room ventilation is replicable. Their facility is placed in a climatic chamber, where it is possible to control the temperature and RH of the air injected in the flux chamber and the humidity generation is strictly controlled. Ramos and de Freitas (2004) test was based on the step-response method but they also looked for correlation between the daily RH variation and the hygroscopicity level of the room. Those two factors are represented respectively by relative daily average amplitude of a RH variation and Hygroscopic Inertia $I_{\mathrm{h,d}}$, defined as:

$$I_{\mathrm{h,d}} = \frac{\sum_{k=i}^{n} C_{\mathrm{r,i}} \cdot MBV_{\mathrm{i}} \cdot S_{\mathrm{i}} + \sum_{k=j}^{m} C_{\mathrm{r,j}} \cdot MBV_{\mathrm{obj,j}}}{N \cdot V \cdot TG} \tag{2.4.3}$$

Where: $\mathrm{MBV_i}$ is the moisture buffer value of element i ($g/m^2 \cdot \%RH$), $\mathrm{S_i}$ is the surface of element i (m^2), $\mathrm{MBV_{obj,j}}$ is the moisture buffer value of complex element j ($g/\%RH$),

C_r is imperfect mixing reduction coefficient (-). N, V and TG are respectively the air exchange rate (h^{-1}), the room volume (m^3) and the vapour production period (h). MBV is measured through the NORDTEST protocol ((Rode et al., 2005)) and it is applied also to complex interior finishes or objects ($MBV_{obj,j}$).

Overall, the flux chamber reproduces a small scale room condition (0.40 m^3), but needs more verification with full-scale testing, because there are other factors of influence in a room which are not considered or are assumed constant, such as the moisture transport through the wall, the outdoor weather condition and air speed. In Table 2.2 laboratory scale methods have been summarised.

Table 2.2. Comparison of laboratory methods

Author	Definition	Unit	Facility	Temperature
Künzel (1965)	adsorption coefficient	$[kg/m^3\sqrt{h}]$	Climatic chamber and jar	20°C
Rode et al. (2005)	MBV	$[kg/m^2 \cdot \%RH]$	Climatic chamber	23°C
Janssen and Roels (2007)	Production-Adapted MBV	$[kg/m^2 \cdot \%RH]$	Climatic chamber	23°C
Wu et al. (2015)	Ultimate MBV	$[g/m^2\%RH@12/8/4h)]$	Climatic chamber	variable
Padfield (1998)	Water vapour in the air	$[g/m^3]$	Flux chamber	20°C
Ramos and de Freitas (2004)	Hygroscopic Inertia	$[g/m^3 \cdot \%RH]$	Flux Chamber	23°C

2.5 Full-Scale Testing

Full-scale investigations are necessary for experimental validation of hygrothermal simulations and laboratory scale tests. There are no standard methods for moisture buffering verification testing, but several test configuration and test facilities for the moisture buffering validation process have been developed. Mitamura et al. (2004); Yang et al. (2009); Meissner et al. (2010) replicated a full-size room in a climatic chamber, which ensures a better control of the boundary environmental conditions. Rode, Sørensen and Mitamura (2001); Künzel, Zirkelbach and Sedlbauer (2003); Simonson, Salaonvaara and Ojanen (2004) built experimental spaces in direct contact with the outdoor environment or tested existing dwellings, to gain a more complete picture of all phenomena that may influence the moisture buffering. These approaches are reviewed below.

2.5.1 Room in a Climatic Chamber

Mitamura et al. (2004) placed a 4.62 m^3 scale model room in an environmental chamber, in which temperature and RH were kept constant. The purpose of the test was to measure the RH variation, by changing the ventilation rate through a forced ventilation system and changing the location of the tested hygroscopic materials on the surrounding walls. At the same time a small sample of the surface material was weighed on a scale inside the room, to compare the mass change of the material and RH fluctuation in the room. Although it is not clear if infiltration and moisture gain/losses through the ventilation system were considered, Mitamura et al. (2004) were among the first to design this kind of facility.

Yang et al. (2009) built a two storey structure placed in a climatic chamber, which simulated typical Canadian outdoor conditions. They calculated the accumulated moisture value into the surface (M_{mat}) through the moisture balance equation (Eq. 2.5.1), where not only moisture diffusion through the envelope, but also the moisture removal through ventilation were evaluated.

$$M_{mat}(t) = (-M_a(t) - M_{diff}(t) - M_{vent-inf}(t) + G(t)) \tag{2.5.1}$$

Where M_a is the moisture change in the room, M_{diff} is the vapour diffusion through the walls, $M_{vent-inf}$ is the water mass removed by ventilation and infiltration and G is the moisture source.

The accumulated moisture removal ($M_{\text{vent-inf}}$) is defined through the Condensed Water Method:

$$M_{\text{vent-inf}}(t) = C(t) + ACH\dot{(}w_{\text{h}} - w_{\text{l}})t \tag{2.5.2}$$

Where C is the condensed water, ACH is the infiltration rate calculated through T and RH sensors and w_h and w_l are respectively humidity ratio injected by the air handling unit (AHU) and the one in the environmental chamber. This method is dependent on the design of AHU (Fig. 2-5), which weighs the condensed water and controls all psychrometric parameters.

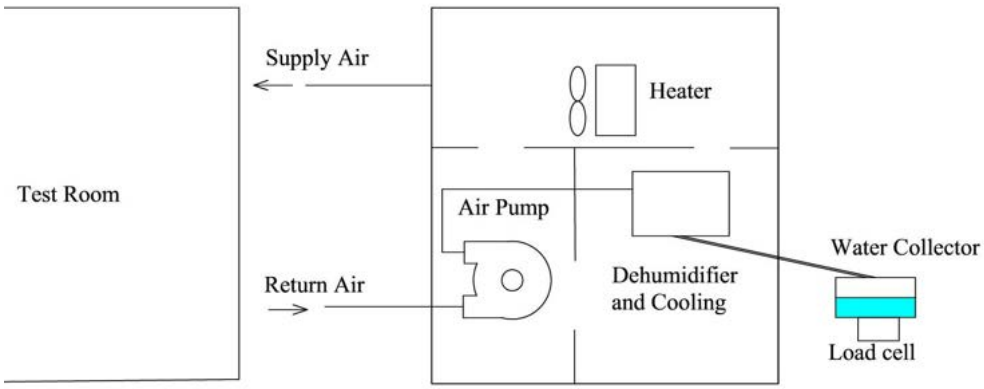

Fig. 2-5. Test configuration of Yang et al. (2007)

Later on, Li, Fazio and Rao (2012) refined the test procedure in the same facility measuring directly the moisture dissipation through moisture decay in the air after humidity generation stops and the room is not ventilated. They also developed another moisture buffering index, the effective damped relative humidity (EDRH):

$$EDRH = \frac{P_t \Delta w_{max}}{P_s(0.622 + \Delta w_{max})} \tag{2.5.3}$$

Where P_t is the barometric pressure, P_s is the saturation pressure at 21°C, Δw_{max} is the difference of average humidity ratio increases, comparing the RH level during the test with the one measured with the same experimental condition but in a non hygroscopic room. Eq. 2.5.3 also introduced a numerical factors to the moisture losses through building leakages, which includes measurement uncertainty.

Meissner et al. (2010) developed another set-up to apply the same principles of NORDTEST to a full scale facility. This is comprised of a timber structure mounted on four load cells, which measured the weight variation of the specimen, supported by a wood frame. The 8 m^3 'built-in test-cell' was supplied with an air tunnel (Fig. 2-6), which provided specific hygrothermal conditions inside the structure. However, problems related to the step-response test are not solved and infiltration rates and mass transfer through the structure are not measured. Table 2.3 compared the room in a climatic chamber methods.

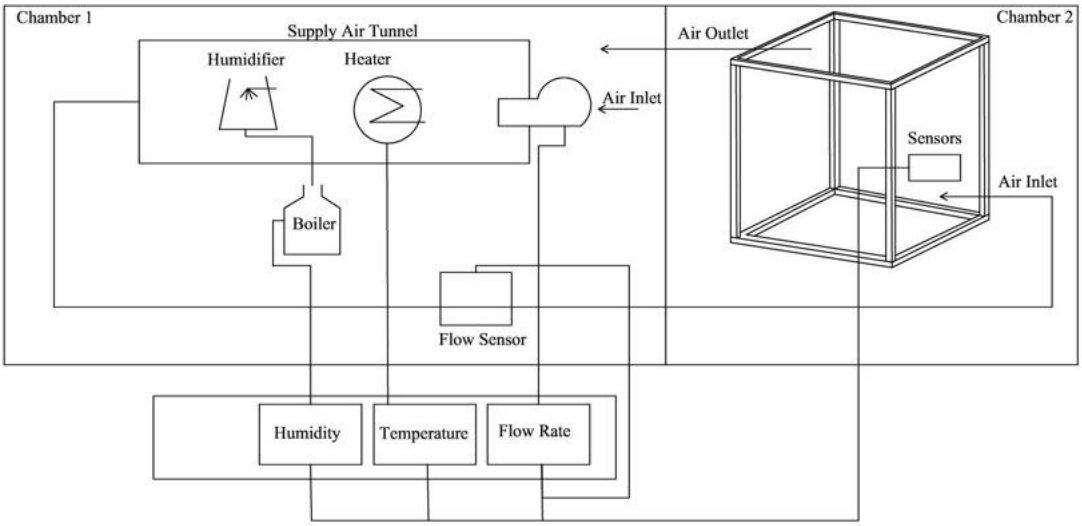

Fig. 2-6. Test configuration of Meissner et al. (2007)

Table 2.3. Comparison of methods for test facilities in climatic chambers

Author	Method	Moisture exchange		Chamber T and RH	Room T
		Infiltration	Ventilation		
Mitamura et al. (2004)	RH variation	Not measured	Not measured	20°C,50 % RH	20°C
Yang et al. (2009)	Moisture balance	Not specified	Condensed water	-10 °C, 45 %RH	20-21°C
Li, Fazio and Rao (2012)	Moisture balance	Moisture decay	Condensed water	-5 °C, 68 %RH	20°C
Meissner et al. (2010)	NORDTEST	Not measured	Not measured	outdoor condition	23°C

2.5.2 Experimental Rooms in the Outdoors

Another typology of test facility is the one in direct contact with the outdoor environment. An example is Rode, Sørensen and Mitamura (2001), who used an insulated steel box equipped with a condensation/evaporation supply, inspired by Padfield (1998) (Fig. 2-7), which simulated the effect of ventilation in the mass balance. They measured the RH variation inside the room, comparing the mass change of specimen boards placed on a scale and RH variation. This method does not consider the influence of the mass transfer through the wall and the effects of infiltration and ventilation on the mass balance and transfer surface resistance, due to the absence of a ventilation system.

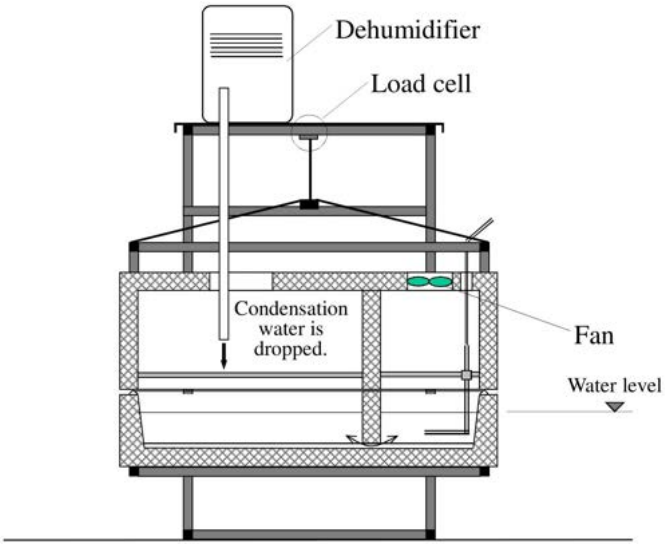

Fig. 2-7. Test humidifier/dehumidifier developed by Rode, Sørensen and Mitamura (2001)

Künzel et al. (2004) set up a test room, where samples were directly applied on the wall but separated by an aluminium foil from the enclosure, to exclude any mass transfer from or to the outdoor. Infiltration are measured through Blower Door test (Keefe, 2010) and a ventilation system is designed to control the air flow. Inside the test room the temperature is kept constant and the RH is free to vary, depending on the moisture buffering effects and the influence of moisture injected from the humidifier and the ventilation system. Künzel et al. (2004) consider the dynamic weather conditions an important factor for moisture buffering determination, due to the influence of outdoor temperature and RH through ventilation in the indoor mass balance.

Recently Nghana and Tariku (2018) conducted a similar study, where two 17.8 m^2 test cells were used. Two different materials were tested in each room, which was provided of heating, ventilation, and air conditioning (HVAC) system and humidifier that simulated human moisture production. Differently from Künzel et al. (2004), their facilities were provided of an HVAC system, which allows a better control of the

ventilation rate and RH. However, Nghana and Tariku (2018) focused on the correlation between RH variation in the indoor, moisture production and ventilation rate without considering the moisture exchange through ventilation, building infiltration and walls moisture diffusion.

2.5.3 Existing Building Testing

The evaluation of moisture buffering potential on existing building gives a better comparison for empirical models and more information about the real behaviour of hygroscopic materials, but it is more complex to isolate moisture buffering effects from all phenomena in inhabited buildings, and to evaluate results with higher levels of uncertainty. Due to the complexity of the moisture exchange in buildings, Kalamees et al. (2009a) pointed out that moisture buffering effects in inhabited houses is negligible because it depends on occupant behaviour, ventilation rate and the hygroscopicity of the enclosures.

In contrast, Simonson, Salaonvaara and Ojanen (2004) demonstrated that a well-designed hygroscopic wall improves air quality and thermal comfort. Simonson, Salaonvaara and Ojanen (2004) focused not only on the moisture buffering properties of the enclosure but also on the water vapour transfer through walls. They compared building reaction to moisture, testing a house, first covering walls with plastic, and then removing it. It was demonstrated that the permeability of the envelope reduced the humidity peaks. However, there are uncertainties and discrepancy in the study due to measurement errors when outdoor RH became higher than the indoors, and due to solar radiation, mass transfer unknown effects on moisture buffering and air distribution.

Zhang et al. (2017) also highlighted the role of hygroscopic material in a real building. They compared moisture buffering in a test room inside a climatic chamber and in an existing building. They also compared the humidity ratio between a non-hygroscopic reference room and an hygroscopic one. From this comparison Zhang et al. (2017) proposed the Moisture Buffering Effect, a new evaluation method expressed as Moisture Adsorption/Desorption Effect ($\mathrm{MBE_a}/\mathrm{MBE_d}$), where:

$$MBE_{\mathrm{a}} = \frac{\sum_{k=0}^{t} (w'(t) - w_0(t))dt}{\sum_{k=0}^{t} (w'(t) - w_0(0))} \tag{2.5.4}$$

$$MBE_{\mathrm{d}} = \frac{\sum_{k=0}^{t} (w_0(t) - w'(t))dt}{\sum_{k=0}^{t} (w_0(0) - w'(t))} \tag{2.5.5}$$

where w' and w are respectively the indoor humidity ratio when there is moisture buffering and when there are no hygroscopic materials in the room. The moisture concentration is obtained by a simplified moisture balance equation, where the contribution of ventilation and moisture diffusion through walls are not included. Zhang et al. (2017) demonstrated that by increasing the hygroscopic surface ratio in houses and decreasing the ventilation rate, moisture buffering has an important impact in the humidity moderation of buildings, but it is, however, hard to quantify the effects of such materials.

Altogether, full-scale testing does not have a standard procedure, which ensures comparable results and the isolation of moisture buffering from other moisture exchange processes. Testing in a climatic chamber simplifies moisture buffering evaluation, but it does not consider secondary effects, such moisture transfer through walls and variable climatic conditions, on the dynamic adsorption process of finishing materials. On the contrary, testing in real buildings have too many variables to consider and there still not a complete understanding of all factors, which may influence moisture balance and transport.

2.6 Scaling from Laboratory to In-Situ Experiments

It is clear that moisture buffering still needs to be explored and explained at all scales. It is important to understand the correlation between material characteristics and the indoor environment. Sagae et al. (1994); Hameury (2005); Vereecken, Roels and Janssen (2010); Woods et al. (2014) have stated the importance to combine and compare laboratory scale and full-scale tests results in order to better understand the physical principles that regulate the connection between material properties and their influence in a building.

Sagae et al. (1994) analysed zeolite panels at three test scales: in a climatic chamber; in a steel box placed in the outdoors and in a storage room of a museum. Their research considered each test scale independent of each other, in order to evaluate different properties, such as the maximum water amount adsorbed in 24 hours, the damping effects and the humidity control ability of the material. These parameters correlated but were not complementary in the definition of the moisture buffering effects at different scales, as not performed by following a common testing procedures.

Hameury and Sterley (2006) linked directly moisture distribution in materials, observed through the Magnetic Resonance Imaging (MRI), to step-response humidity cycles, developing an alternative method to NORDEST. The cyclically adsorbed and desorbed moisture was estimated, but it is limited to few millimetres of the surface and it is applicable only to small specimens. Hameury and Sterley (2006) also tried to quantify the moisture buffering capacity of walls in a real building, recording the moisture

content with ±0.5% accuracy pin-type moisture meters, applied in the first 3 mm of the surface. Difficulty to apply sensors at the same width and the impossibility to insert them deeper make it impossible to measure the direct quantification of the moisture buffering process. Recently, a new technique was developed to measure the moisture content in wood (Bylund Melin et al., 2016), in which RH and temperature were measured inside the material at different depths, and then the data were converted in moisture content, by taking into account the material's hysteresis and dependency of the sorption isotherm to the temperature, as described by Bylund Melin et al. (2016). Even though this method gave a good fit with the Fickian moisture transport equation Equation 2.6.1, it requires an elevated number of properties for the conversion of RH into moisture content, and it is probably not applicable to plasters, as those materials are too fragile to drill.

$$\frac{\partial w_m}{\partial t} = D_m \cdot \frac{\partial^2 w_m}{\partial x^2} \tag{2.6.1}$$

where w_m is the moisture content [kg/kg] and D_m is the diffusion coefficient [-].

Vereecken, Roels and Janssen (2010) verified the applicability of a new definition of moisture buffering (HIR*), which combine the MBV* (Eq. 2.4.1) to the Hygroscopic Inertia (Eq. 2.4.3) , to full-scale simulation. The HIR* value is measured in a laboratory and then implemented in the EMPD.

$$HIR^* = \frac{\sum_{k=i}^{n} (S_{\mathrm{i}} \cdot MBV^*{}_{\mathrm{i}}) + \sum_{k=j}^{m} MBV^*{}_{\mathrm{obj,j}}}{V} \tag{2.6.2}$$

The methodology validation is carried out either in a test room or in a real building, where NORDTEST protocol is followed. There is a good agreement with the empirical model, but the validation is limited only to a single case where ventilation and infiltration moisture moisture exchange is not measured and infiltration rate and indoor humidity are assumed constant.

Similarly to Vereecken et al., Woods et al. (2014) and later Woods and Winkler (2018) verified the applicability of the existing EMPD simulation model, to predict the moisture buffering capacity of hygroscopic materials in a house. They also developed a new experimental set-up, which is applicable both in the laboratory and in real buildings. The main component is the HVAC system, which controls the moisture removal and addition to a water tank placed on a mass balance and keeps the temperature constant in the house (Fig. 2-8).

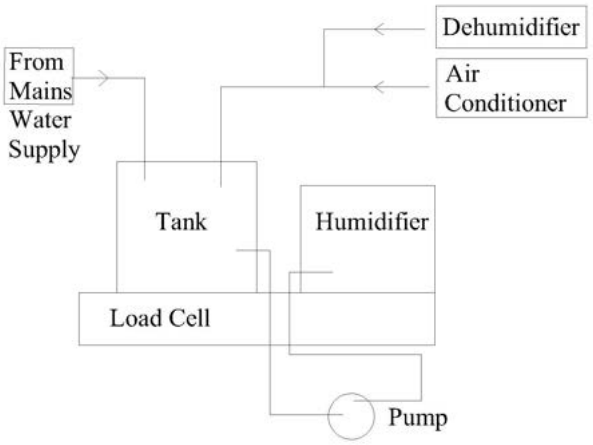

Fig. 2-8. HVAC system developed by Woods et al. (2014)

Moisture buffering is calculated from the mass balance equation, which includes measured moisture gains and losses through infiltration and the HVAC system, and compare results with the classical step-response method. The good agreement between the two methods in a climatic chamber led Woods and Winkler (2018) to conduct their new method in an existing building. From the results obtained by their experimental set-up they derived inputs for building simulations from house testing, and improve the correlation between properties materials and the indoor humidity variation in the dwelling. In Table 2.4 all previous methods are summarised.

Overall, in full-scale testing there are still some aspects to improve and consider as the moisture diffusion through the walls, the effects on the model of less accurate HVAC and ventilation systems, the influence of temperature fluctuation, the effect of different weather conditions and different enclosures.

Table 2.4. Comparison of outdoor test facilities

Author	Method	Moisture exchange		Wall assembly	Room T	Location
		Infiltration	Ventilation			
Rode, Sørensen and Mitamura (2001)	RH/Weight variation	Gas decay	No ventilation	Insulated steel	20°C	Denmark
Künzel et al. (2004)	RH variation	Not specified	Not specified	Bricks	$20°C$	Germany
Nghana and Tariku (2018)	RH variation	Not measured	Not measured	Steel frame	$21°C$	Canada
Kalamees et al. (2009a)	RH variation	Not measured	Not measured	170 assembly	variable	Netherlands
Simonson, Salonvaara and Ojanen (2004)	RH variation	Gas decay	Condensed water	Timber frame	Variable	Finland
Zhang et al. (2017)	RH variation	Not measured	Not measured	Timber frame	20°C	Not specified
Sagae et al. (1994)	RH variation	Not measured	Not measured	Not specified	Not specified	Japan
(Hameury, 2005)	Water content	Not measured	Not measured	Massive Wood	Variable	Sweden
Vereecken, Roels and Janssen (2010)	RH variation	Not specified	No ventilation	AAC	Not specified	Belgium
Woods et al. (2014)	Moisture Balance	Gas decay	Condensed water	Tmber frame	21-25°C	USA

2.7 Summary

From the review of the existing research the lack of a globally agreed method to measure transient moisture transport and accumulation properties of hygroscopic materials is evident. Laboratory scale investigations are performed with different test conditions and test arrangements, making direct comparisons between different experimentation not possible. Consequently, moisture buffering measurements vary depending on the test set-up and the different interpretations of moisture exchange phenomenon. Those tests were also mainly developed as a relative indicator of the performances of the materials, rater then to be applied in building simulations. For this reason, simulation tools were developed from steady-state material properties, such as vapour permeability and sorption isotherm, which do not sufficiently represent dynamic material behaviour.

There are also uncertainties on the full-scale experimentation, which are essential to validate material scale testing and simulation. Moisture buffering in real building is influenced by other moisture transport mechanisms, which make it more difficult to isolate the dynamic water sorption process and quantify its impact on the environment. For this reason, it is necessary to have more full scale testing and develop a standard procedure to evaluate moisture buffering performance of a building, to allow systematic and replicable verification methods.

Overall, there is a need to better understand the impact of hygroscopic materials on the indoor climate control and how they may play an important role in ventilation and conditioning design. It is important to help designers estimate and quantify the influence of exposed surfaces in the indoor on the RH, by using full-scale testing. The development of a method for testing the impact of materials on the environment will improve simulation and laboratory experimental testing. This will stimulate development and improvement of new moisture control materials and promote their use to improve indoor hygrothermal comfort and reduce air conditioning energy consumption.

3. *Laboratory Testing*

As already highlighted in Section 2.4, existing moisture buffering tests in laboratory are usually performed at constant temperature, specific air velocity and following RH square wave functions. The outcome of these laboratory tests may not be representative of the materials behaviour in a real building, as environmental conditions are more complex and not under steady boundary conditions. Moreover, the use of steady-state hygric properties, such as water vapour and sortpion capacity, in moisture buffering theoretical definition may not be representative of the dynamic response of materials to variable environmental conditions.

In this chapter, materials were first tested by applying the NORDTEST protocol and a correlation between steady-state measured hygrothermal properties and the dynamic sorption capacity was investigated. Successively, temperature, air velocity and RH signal were investigated, in order to analyse the response of coatings to different boundary conditions. The aim of this chapter is to reproduce similar environmental conditions of a real building to analyse the response of materials. In this way, the moisture exchange mechanisms between the environment and the materials could be explored. This will lead to a modification or introduction of new testing protocols that can quantify the impact of materials to regulate the indoor RH. All testing in this chapter were repeated three times, using three specimens of each sample. Table 3.1, a summary of the test performed in this chapter is provided.

Table 3.1. Summary of all tests performed in this chapter

Tests	Aim	Expectation
Materials properties	Evaluate the influencing properties on moisture buffering Identification of more influencing material characteristics	Find strong pattern between moisture buffering and material properties Better comprehension of moisture transfer in materials
Air Velocity	Evaluate the impact of air velocity on moisture buffering to predict materials behaviour in buildings	Find an increase of moisture buffering with increase of air velocity
Climatic Chamber monitoring	Investigate the reliability of the climatic chamber to maintain programmed conditions	Find a good agreement between programmed and measured environmental conditions If a disagreement is found, calibrate or consider impact on experiments
Moisture buffering at different temperatures	Verify the impact of temperature on moisture buffering	Significant variations of moisture buffering performances with temperature
Temperature fluctuations at constant RH	Verify the impact of temperature variations on the materials moisture storage capacity at different humidity levels	Observe variations in the moisture storage capacity of materials due to temperature fluctuations. Isolate the influence of temperature on materials
Simultaneous temperature and RH variations	Verify the impact of simultaneous temperature and RH variations on moisture exchange to investigate response of material in a dynamic environment	Demonstrate the significant impact of dynamic environmental conditions on materials moisture buffering capacity that needs to be considered in real buildings, in which temperature does vary
Sinusoidal temperature and RH variations	Investigate the impact of sinusoidal environmental conditions on materials	Find differences with square wave signal in the NORDTEST Better understand the correlation between environment and material moisture transfer
Modelling of the response of materials to variable temperature and RH variations	Investigate the weight of temperature and RH variation on moisture storage capacity	Mathematically quantify the impact of environmental conditions on the moisture buffering

3.1 Materials

Coatings were used for this study, due to their good moisture buffering capacity and their wide use to finish indoor surfaces. Samples of commercially available clay, gypsum and natural hydraulic lime (NHL) were cast and tested (Fig. 3-1). Plasterboard was also tested (Fig. 3-1d), as it is a conventional surface layer and used within the full scale wall constructions a the BRP (Chapter 4).

The clay plaster (manufactured by Claytec) was composed of 69% sand, 25% silt and 5% clay (Maskell et al., 2018), while gypsum (manufactured by British Gypsum) was a calcium sulphate hemihydrate. Lime (manufactured by Blue Circle) was a natural moderately hydraulic lime (NHL 3.5). Plasterboard was composed of a core of aerated calcium sulphate di-hydrate and 0.67 mm of paper, bonded with starch with an overall thickness 12.5 mm. The clay, gypsum and lime plasters, in a dry powdered form, were prepared by mechanical mixing in the laboratory. The mixing water amount was set according to the workability of the plasters. To the air dry clay plaster a further 20% mass of water was added. The lime plaster was mixed with fine aggregate sand (sieved to remove particles bigger than 1 mm and mixed in a ratio of 1.2:5 mass of lime:sand) and 30% mass of water. Gypsum was mix with 60% mass of water. Specimens were cast in 150x150x20 mm moulds made with phenolic-faced plywood. Thereafter, the specimens were stored for 28 days before testing in an environmental chamber at $20°C$ and 60% RH. Plasterboard specimens were cut from a 1.2 x 2.4 m panel, but the original thickness was preserved (12.5 mm).

All the specimens were tested to analyse their hygrothrmal properties in Section 3.2 and their response to the NORDTEST protocol (Section 3.3). Successively, clay and gypsum were selected to be further tested when the NORDTEST environmental conditions were varied in Section 3.4, Section 3.5 and Section 3.6. The choice not to focus on lime was due to the break of most of the lime specimens after the material characterisation. Plasterboard was not investigated due to later discussed considerations on the limited thickness and consequent limited moisture buffering potential of the material (Section 3.3).

In this chapter further materials were introduced to complete the investigation on the impact of air velocity and temperature on coatings. Hemp-lime was tested together with clay to have a wider understanding of the effect of air velocity on the moisture buffering of materials that have significantly different moisture buffering capacities (Section 3.4). In Section 3.5 high density specimens of clay and gypsum were cast by reducing the mixing water in order to double the density of the coatings. Variations on the material properties allowed to better understand the effect of temperature on the dynamic sorption capacity of materials. Description of the hemp-lime and the high density clay and gypsum can be found in Section 3.4 and Section 3.5, respectively

(a) Clay

(b) Lime

(c) Gypsum

(d) Gypsum plasterboard

Fig. 3-1. Moisture buffering specimens

3.2 Materials Characterisation

Dry density, porosity, sorption isotherm, water vapour permeability and thermal conductivity were measured as primary material properties necessary to better understand the moisture buffering behaviour of the materials (Section 3.3), as well as necessary for simulations (Chapter 5).

3.2.1 Density and Porosity

Materials density and porosity were measured, as important properties in the theoretical calculation of moisture buffering and because these factors are likely to influence moisture transport into materials. The bulk density was measured after drying the materials in the oven at $105°C$, until the weight stabilised. Results are shown in Table 3.2 with the coefficient of variation (CoV). The CoV represents the variation from the mean of the results obtained from the repetition of a test.

Porosity was determined by the Mercury Intrusion Porosimetry (MIP), using Pascal 140/440. The MIP set up data are shown in Table 3.3. The specimens were obtained by breaking into small peaces the original 15x15 mm samples. Porosity of clay, gypsum and lime was respectively 43.37%, 61.91% and 34.05%, while the porosity of plasterboard without paper was 75.55%. The MIP also provided skeleton density,

pore diameter, pore volume, surface area (Table 3.4) and pore size distribution, which is shown in Fig. 3-2 and Fig. 3-3. The skeleton density differs from the bulk density, as it is determined by dividing the dry mass by the solid volume of the materials, which excludes the pores, whilst bulk density was measured by measuring the dry mass of the specimen by the measured volume. It means that the volume includes the pores and solid components of the materials. However, the MIP cannot accurately obtain data on the skeletal density, when pores are smaller than the minimum pore size into which mercury can intrude. The reported data on the skeletal density are, consequently, not accurate.

Clay and lime presented mainly macro-pores, which have an average diameter of around 125 nm. Gypsum also had macro-pores of a significant bigger size (365 nm average), but it also presented micro-pores, as shown in Fig. 3-2b. Gypsum plasterboard had a more accentuate micro-pores presence and a significantly higher average pore diameter (631 nm) than standard gypsum. Overall, the gypsum and plasterboard showed a significant higher pore volume than clay and lime. Due to the more complex pore structure of gypsum and plasterboard, both vapour and liquid transport take place into the materials, when exposed to a RH and vapour pressure gradient, while in clay and lime only vapour transport occurs. Water vapour transport can take place in the macro-pores and its driving potential is the water vapour pressure, whilst liquid transport takes place in the micro pores, where the driving force can either be the relative humidity and the capillary pressure.

Table 3.2. Measured hygrothermal properties of four plasters

Material	$\rho_{dry}(kg/m^3)$	CoV (%)	$\mu(-)$	CoV (%)
Clay	1258	2.32	12.86	6.11
Lime	1576	1.69	9.65	2.60
Gypsum	856	0.95	8.84	9.66
Plasterboard	520	1.23	8.83	8.21

Table 3.3. MIP Information

Properties	Unit	Value
Mercury Surface Tension	N/m	0.48
Mercury Contact Angle	$\circ$	140

Table 3.4. MIP data

Properties	Unit	Clay	Gypsum	Lime	Plasterboard
Skeleton Density	kg/m^3	1360	950	1720	590
Inaccessible porosity	%	-12.03	-8.61	-19.95	-5.45
Total Pore Volume	mm^3/g	320.16	650.11	197.30	1263.61
Total Pore Surface Area	m^2/g	9.16	7.86	4.44	4.98
Average Pore Diameter	nm	141.21	338.59	212.89	1015.19

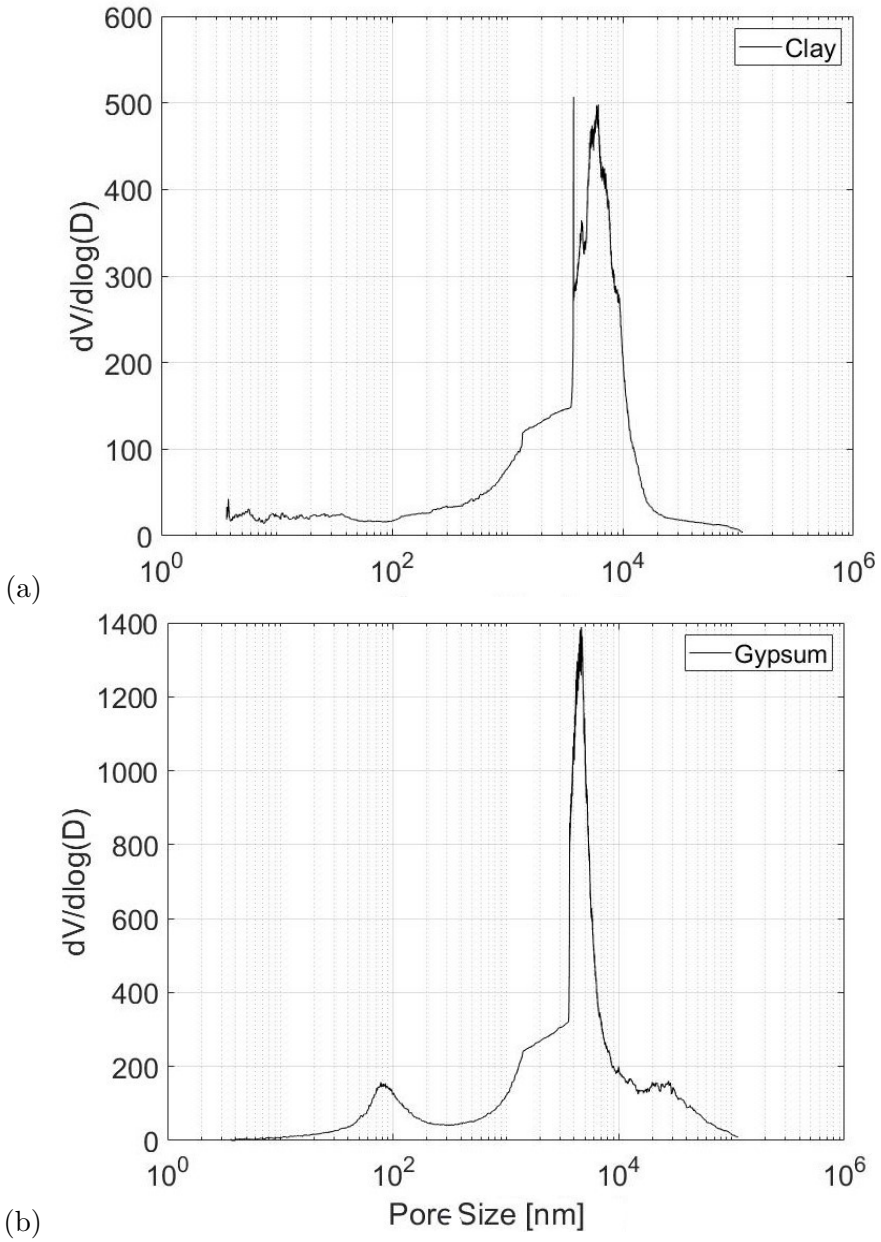

Fig. 3-2. Pore size distribution for (a) clay and gypsum (b)

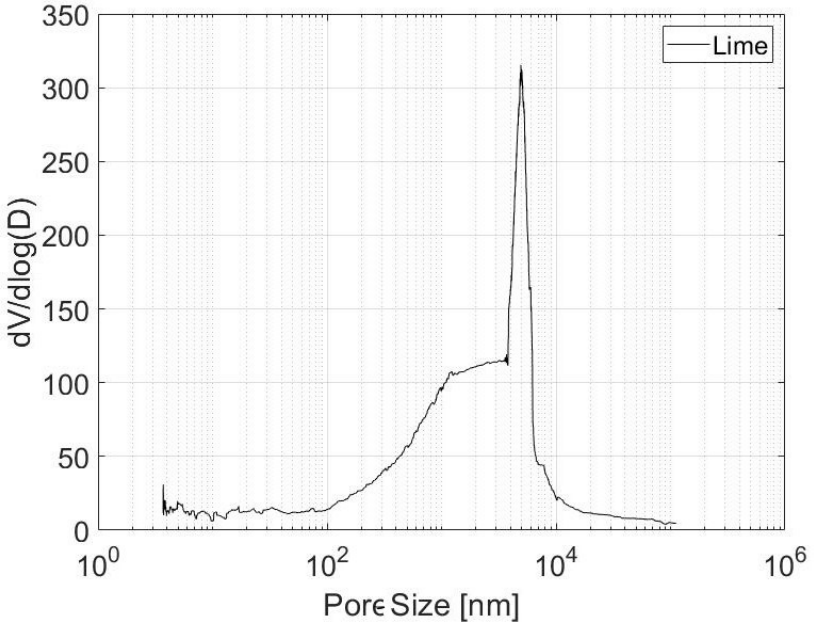

(a)

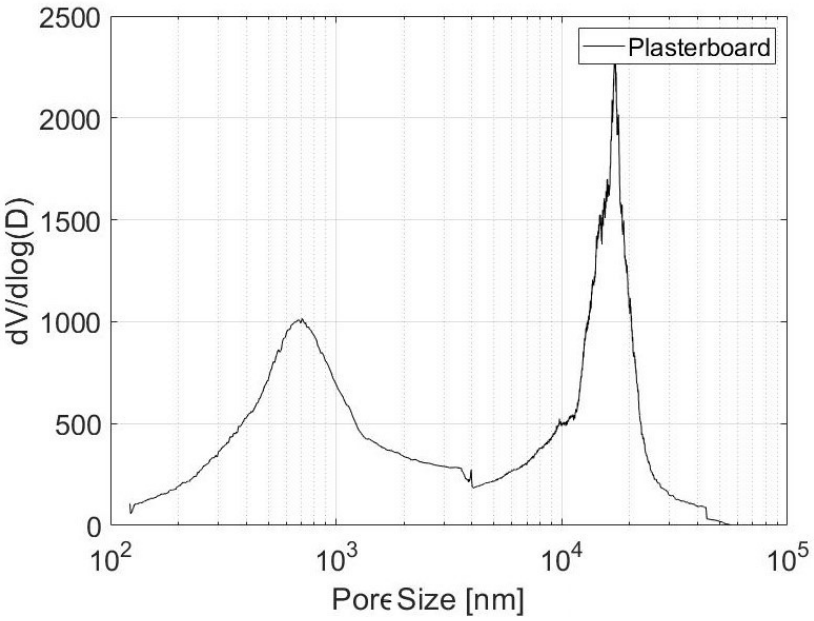

(b)

Fig. 3-3. Pore size distribution for lime (a) and gypsum plasterboard (b)

3.2.2 Water Vapour Permeability

The "dry" cup method (*ISO 12572*, 2016) was used to determine the vapour diffusion resistance factor of the specimens, as required by simulations. After the specimens were pre-conditioned in climatic chamber at $23°C$ and 50% RH for 24 hours, they were sealed with aluminium tape on the top of a plastic container, to ensure a vapour tight-seal. For the "dry" cup test Calcium Chloride ($CaCl_2$) was used to obtain 0% humidity inside the plastic container. As the *ISO 12572* (2016) requires, an air layer of 1.5 cm thickness was kept between the salt and the internal sample surface. The assembly was then placed in a climatic chamber (ACS DY110) at $23°C$ and 50% RH and weighed by

balance (Ohasus Pioneer±0.01 g readability) every 24 h until constant rate of change of mass was achieved. The test was repeated three times for each sample. From this test the water vapour resistance factor ($\mu[-]$) was calculated, following *ISO 12572* (2016). Results are shown in Table 3.2.

3.2.3 Thermal Conductivity

Thermal conductivity was measured on 75x75 mm specimens at ambient temperature ($19°C$ 63% RH), after 72 hours in an air conditioned room, where the test was performed. Tests were performed using a KD2 Pro at the Indian Institute of Science (IISc), Bangalore. The KD2 Pro (precision ±10%) is a transient method instrument, which is equipped with a dual needle inserted inside the specimen. The heat is applied to one of the two needles for a set time and the other one measures the temperature variations. For this study the holes for the needles were drilled before conditioning. During the test no filling liquid was applied between the needles and the specimen, as the adhesion was acceptable. The ambient thermal conductivity was measured 7 times with an interval of 15 minutes between a measurement and the other, in order to dissipate the thermal gradients.

It was not possible to apply the same method for the plasterboard, as its thickness was too small to fix the sensor into it. For this reason, the thermal conductivity of plasterboard and all other materials was measured again at the University of Bath using the Hot Disk (TPS 3500). Two specimens for each material were preconditioned and tested in the VWR climatic chamber at $23°C$. The functioning of the Hot Disk is similar to the KD2 Pro, with the only difference in the positioning and shape of the sensor. In this study a Kapton sensor was applied in between the surfaces of the two specimen, and preconditioning temperature was four degrees higher than previous test. Results can be seen in Table 3.5.

Table 3.5. Thermal conductivity (λ) and volumetric heat capacity (c_{vol}) measured at the IISc and University of Bath

Materials	IISc		University of Bath			
	$\lambda(W/mK)$	CoV (%)	$\lambda(W/mK)$	CoV (%)	$c_{vol}(MJ/m^3K)$	CoV (%)
Clay	0.44	1.23	0.55	0.24	621.75	0.88
Lime	0.38	0.63	0.64	0.67	599.27	1.04
Gypsum	0.18	0.89	0.20	0.45	755.81	0.60
Plasterboard	-	-	0.10	0.09	863.08	0.13

The discrepancies in the two tests can be due to the different testing temperatures, which influence the moisture content and, consequently, the thermal conductivity of the materials. The IISc data were initially used in simulations, but a sensitivity analysis on the impact of thermal conductivity on moisture buffering was performed with the

thermal conductivity data measured in Bath (Chapter 5). The comparison of the simulations results showed thermal conductivity variations did not impact the moisture buffering performances (less than 1.7% variations).

3.2.4 Water Vapour Sorption Curve

The sorption isotherm was measured by Dynamic Vapour Sorption (DVS) apparatus (Intrinsic Water Sorption Analyser) at the constant temperature of $23°C$. The humidity range was from 0% to 90% with the change in mass continuously measured. The temperature and RH precision of equipment are respectively $\pm 0.2°C$ and $\pm 1\%$ with an accuracy of mass change of 0.1 mg. Three specimens with a mass of approximately 0.3 g were placed on the DVS scale and the surrounding humidity was increased gradually in steps, until mass variations were less than 0.02 mg.

The sorption isotherm for clay, lime and gypsum is shown in Fig. 3-4. Two cycles were performed to ensure the stability of the sorption curves, with only the second cycle used for analysis. The test was repeated three times, by using different specimens. The sorption isotherm shown in Fig. 3-4 is the averaged curve of the three tests. The increase in water content from 0% RH to 90% RH for clay and lime can be approximated as linear, while gypsum shows a different sorption curve and greater gap between adsorption and desorption. The different behaviour of gypsum results in a Type IV curve (Kruk and Jaroniec, 2001; Sing, 1985), due to the bigger pore diameter and possible higher capillary condensation. Lime presented an anomaly, as there is a mass increase of 0.08% at the end of the full cycle of adsorption and desorption, indicating the lime binder may not have completed its hydration at the start of the test. Overall, gypsum reached higher values of moisture content, approximately 3.1% mass at 90% RH, compared to the clay (1.5%) and lime (0.7%)(Fig. 3-4). Plasterboard also showed similarity with gypsum, when no paper is applied on the material surface. The application of paper increases the plasterboard sorption capacity of 0.5% (Fig. 3-5). From the sorption curve, the moisture capacity (ξ_w) was calculated for the estimation of the penetration depth in Section 3.3. ξ_w was defined as the slope of the adsorption curve between 33% and 75% RH. The 33-75% RH interval was chosen, as it is the most significant interval for moisture buffering test in Section 3.3.

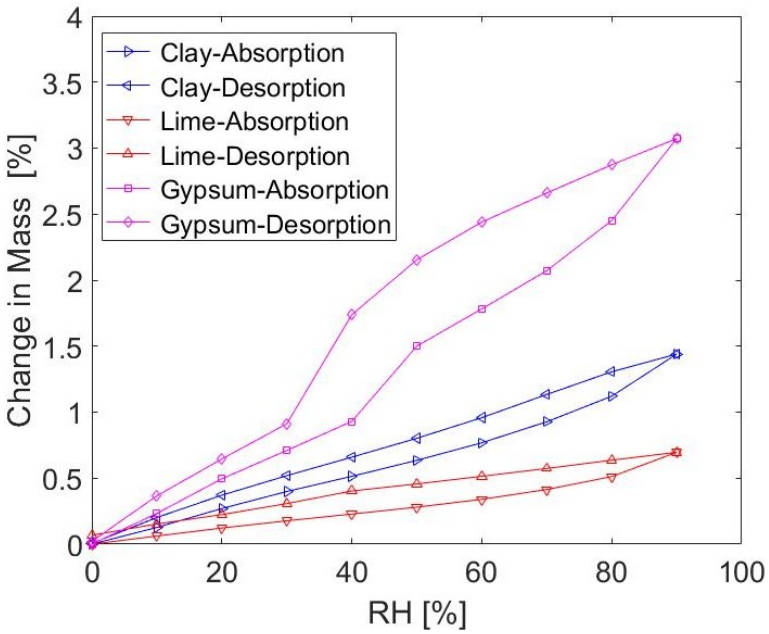

Fig. 3-4. Sorption isotherm curve profile of clay, lime and gypsum

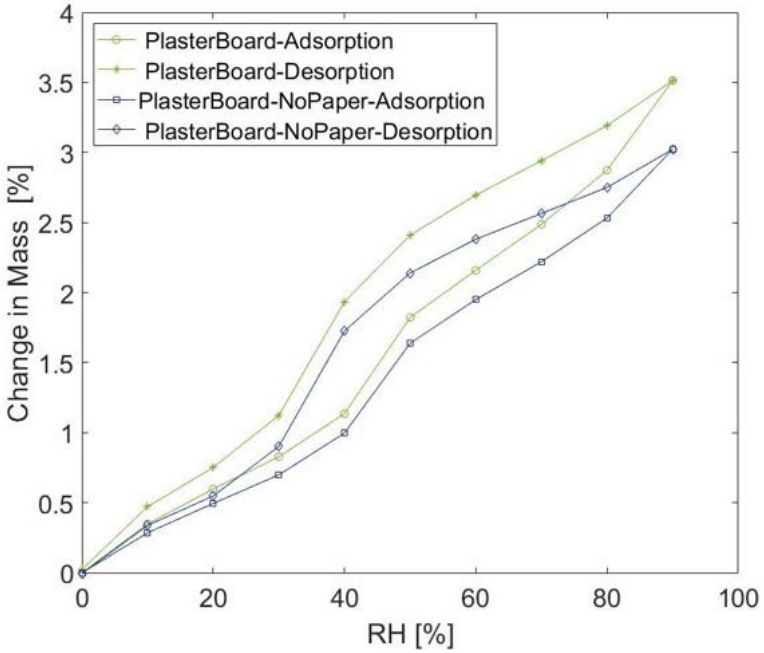

Fig. 3-5. Sorption isotherm curve profile of plasterboard

3.3 NORDTEST Protocol

In this section the NORDTEST protocol was applied to test the moisture buffering capacity of plasters and a correlation between material steady-state properties and dynamic sorption capacity was investigated.

3.3.1 Method

Three specimens for each coating were tested, following the NORDTEST protocol (Rode et al., 2005). The change in mass of the specimens was monitored every minute. The climatic chamber (ACS Compact Test Chambers DY110) was programmed to pre-condition the samples at 54% and 23°C for 24h, and to perform 6 cycles of 24h each at 75% RH for 8h and 33% for 16h. Specimens were surrounded by a net to reduce the air speed to less than to 0.1 m/s (Fig. 3-6). The air speed was measured with a hot wire anemometer (Extech 407119). Spot measurements were taken above the specimens. The MBV is expressed in $g/(m^2.\%RH)$. To ensure accurate measurement of the change in mass of the specimen, the sensitivity of the scales to humidity variation was initially tested, when no hygroscopic material is placed on it. The scale presented negligible and irregular fluctuation ($\pm 2.5 g/m^2$), which are 11% smaller than the smallest moisture buffering capacity recorded in this thesis and it is significantly lower than any materials tested by the NORDTEST (Rode et al., 2005). Consequently, the mass variations are negligible and linked to the chamber vibrations.

Fig. 3-6. Moisture buffering set up in the climatic chamber

3.3.2 Results and Analysis

Moisture buffering test results highlighted that lime did not reach a balance after 6 cycles. Tests were repeated and an increase of around 3% weight every cycle was again observed in Fig. 3-7, due to the hydration process (Sect. 3.2.4). The moisture buffering performance of the materials can be seen in Fig. 3-8. After 8 hours of humidification they reached respectively a moisture buffering capacity of 60.90 and 81.190 g/m^2, whereas lime reaches only 43.26 g/m^2. Plasterboard shows a good moisture buffering capacity (65.52 g/m^2), but the shape of the curve is significantly

different compared to the other cases. Plasterboard started presenting a plateau, which indicates that the thickness of the specimen was too small to use all the moisture buffering potential of the material. This would explain the lower moisture buffering capacity of plasterboard than gypsum, despite of its low density and permeability, and high porosity and moisture capacity (Table 3.7), which usually indicate a high moisture buffering potential.

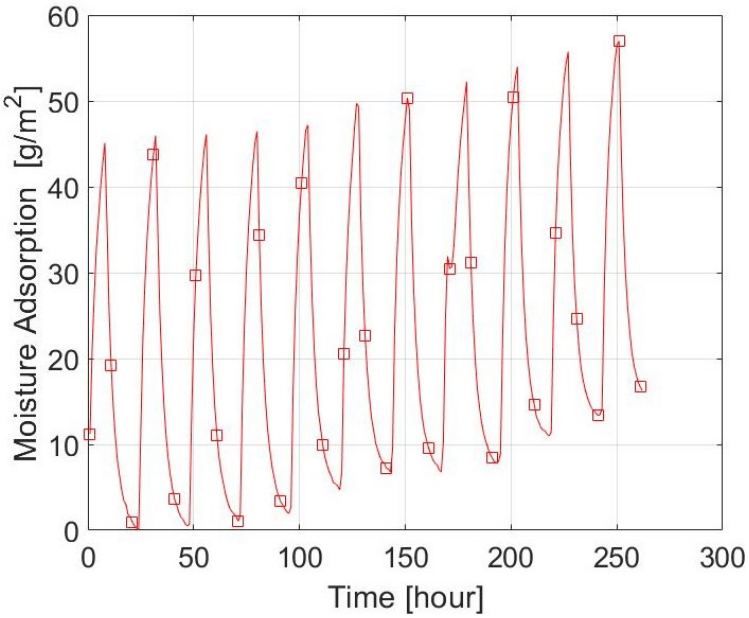

Fig. 3-7. Moisture buffering profile of lime

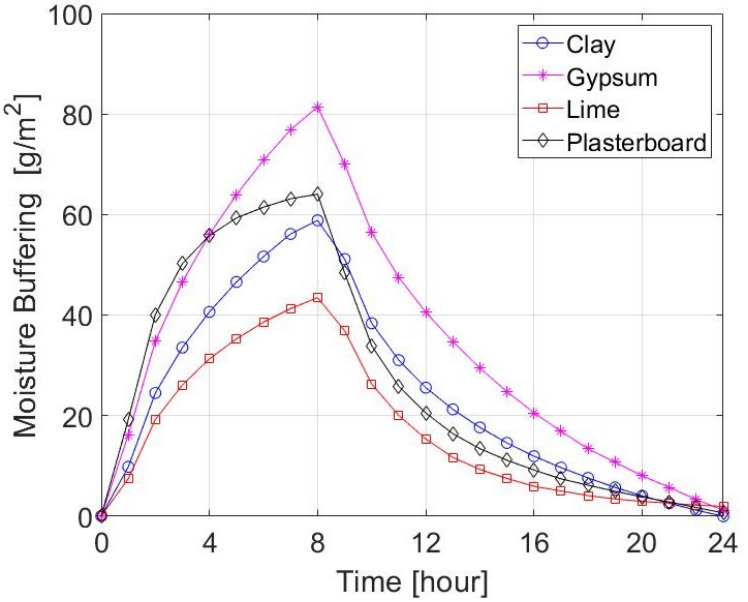

Fig. 3-8. Moisture Buffering profile of clay, lime, gypsum and plasterboard

As Maskell et al. (2018); Latif et al. (2015) demonstrated, when the moisture buffering curve starts to flatten, the water vapour penetration in the material is higher than

the sample thickness. For this reason, the true and effective penetration depth (x_{Th} and x_{Eff}) were calculated (Table 3.6), using Equation 2.2.3 and the Equation 2.3.1. The true penetration depth suggests all samples were thinner than their penetration depth. Nevertheless, all sorption curves did not present the plateau associated with the maximum capacity that confirms the specimens were thicker than their effective penetration depth. Table 3.6 shows the plasterboard effective penetration depth is smaller than the sample thickness, as the experimental data suggests. However, x_{Th} in this case may not predict accurately the penetration depth of plasterboard, likely due to the material multi-layers. Similarly, x_{Eff} also appears to overestimate the lime penetration depth, but the observation of the curve shows a beginning of the flattening of the curve (Fig. 3-8), which may suggest the material reached its maximum capacity. On the contrary, x_{Eff} did not indicate the plasterboard's plateau. In both cases a strong correlation between experimental data and calculate penetration depth was not found.

Table 3.6. Theoretical and Effective penetration depth

Material	x_{Th} (mm)	x_{Eff} (mm)
Lime	103.15	22.33
Clay	49.57	10.73
Gypsum	31.49	6.82
Plasterboard	21.95	4.57

As already explained in Section 2.2, steady-state properties can give a general indication of materials' moisture buffering potential, even though cannot give accurate prediction of moisture buffering. By analysing the correlation between moisture buffering and material properties, it was investigated that the materials in this study follow the general trend found by McGregor et al. (2014a) and Kreiger and Srubar III (2019).

Table 3.7 compares the moisture buffering capacity to the steady state material properties. As Fig. 3-9 shows, moisture buffering is inversely proportional to density (Fig. 3-9a), while it is directly proportional to porosity (Fig. 3-9b). This is in line with McGregor et al. (2014b) finding, which highlighted an inverse correlation between density and porosity in porous materials and a consequent linear relationship with moisture buffering. However, McGregor et al. (2014b) stated density did not show any direct correlation with moisture buffering, especially when considering clayey materials with similar density but different porous size distribution and mineralogy. The porous structure and porosity influenced significantly more the materials' moisture buffering potential.

Fig. 3-10a illustrates the direct correlation with the moisture capacity (ξ_u). Not many studies looked at the relationship between moisture buffering and sorption capacity. McGregor et al. (2014b) found a linear dependency, which demonstrated higher is

the moisture capacity (ξ_u), higher is the moisture buffering potential. However, the correlation should be further analysed, as it depends on the pore size and distribution.

In this study a relationship with the water vapour permeability was not found (Fig. 3-10b), because, regardless of the different properties of the materials, lime and gypsum presented similar μ value. McGregor et al. (2014b) study on unfired clay bricks presented an inverse correlation between the two properties, when the water vapour permeability is measured by wet cup method at $23°C$ and air velocity on the sample of 0.65 m/s. However, Kreiger and Srubar III (2019) demonstrated the lack of a link between moisture buffering and water vapour permeability when multiple studies are compared, due to the different boundary condition and test method applied for measuring μ.

Table 3.7. Moisture buffering and penetration depth of the plasters

Material	$MB(g/m^2)$	CoV (%)	$\rho_{dry}(kg/m^3)$	$\Phi(\%)$	$\mu(-)$	$\xi_w(kg/kg)$
Lime	43.26	8.28	1576	34.05	9.65	0.005
Clay	60.90	2.35	1258	43.37	12.86	0.013
Gypsum	81.90	0.84	856	61.91	8.84	0.032
Plasterboard	65.52	3.39	520	75.55	8.83	0.040

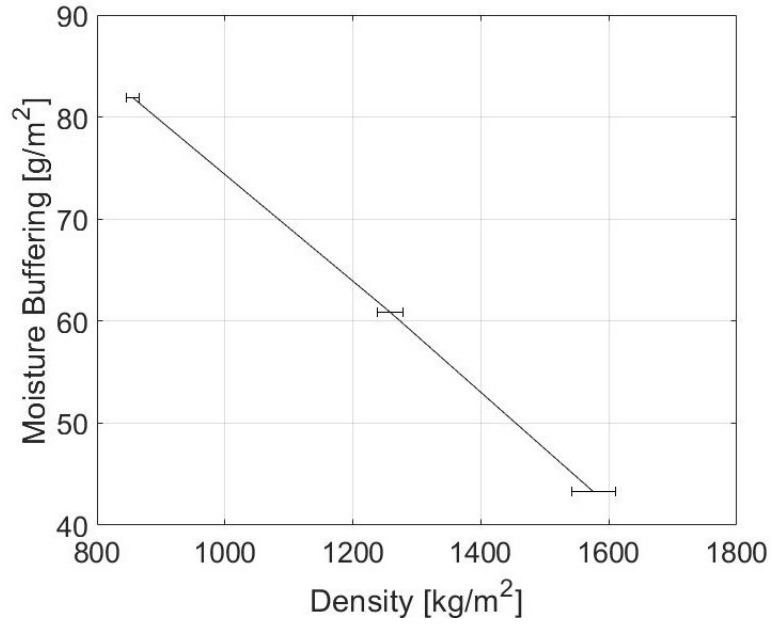

(a)

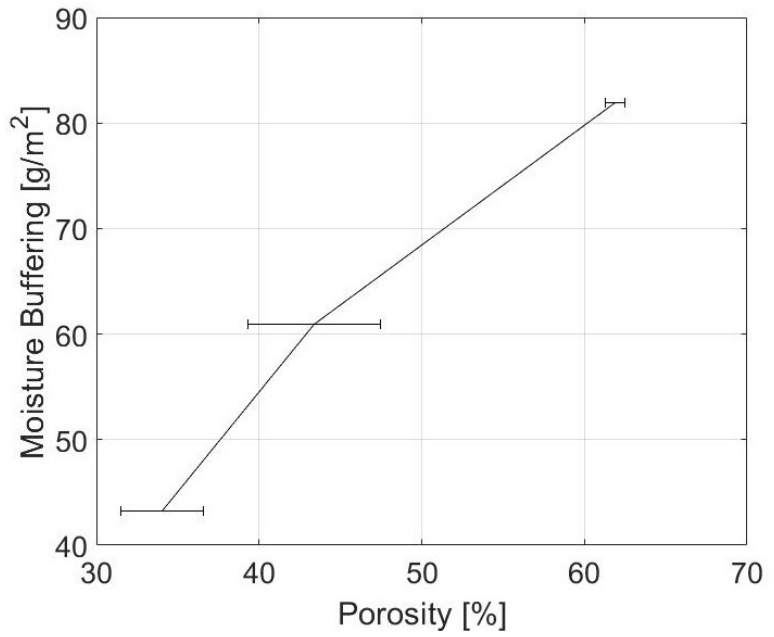

(b)

Fig. 3-9. Correlation between moisture buffering, density (**a**) and porosity (**b**) with their confidence interval

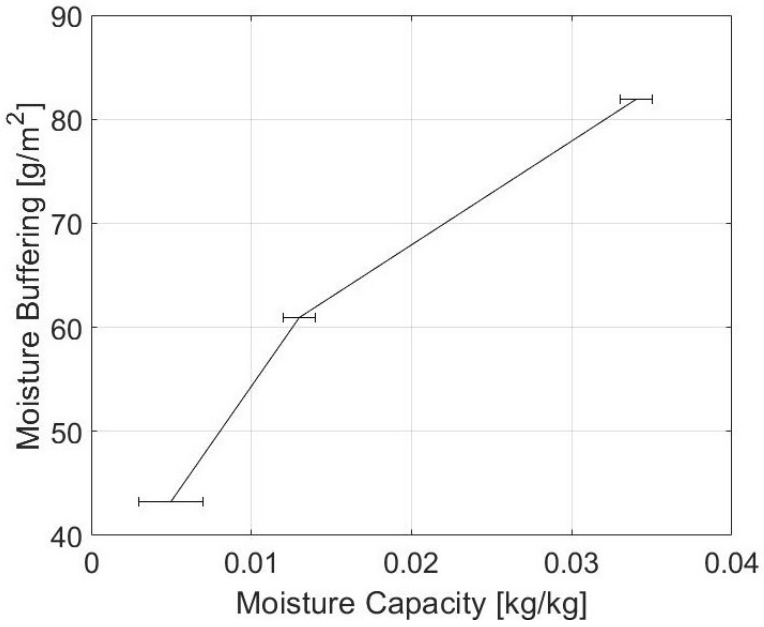

(a)

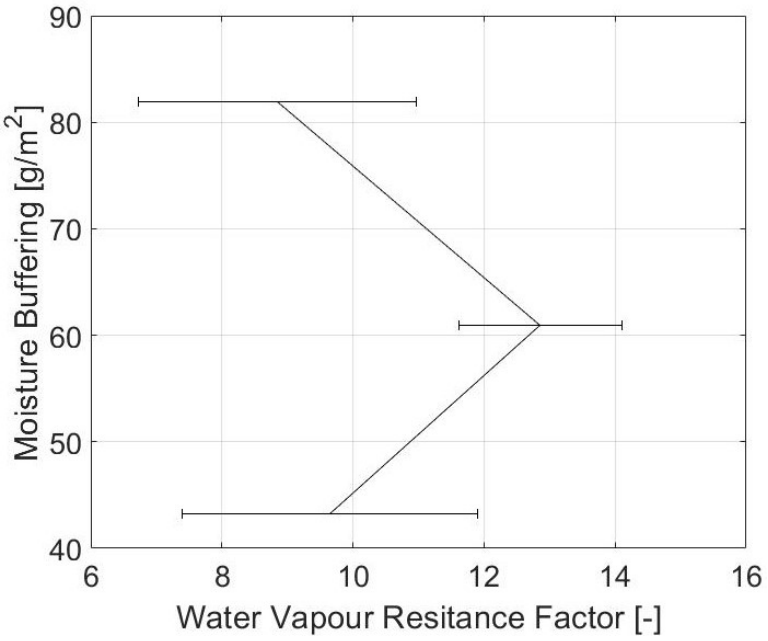

(b)

Fig. 3-10. Correlation between moisture buffering, moisture capacity (**a**) and water vapour permeability (**b**) with their confidence interval

3.4 Air Distribution in the Climatic Chamber

Moisture buffering protocols requires the air speed to be constant, as it is known it influences the dynamic water adsorption property (Gómez et al., 2011). Consequently, the NORDTEST protocol (Rode et al., 2005) prescribes the air speed on the specimen's surface to be 0.1 m/s during tests, which should equate to a surface film resistance of

$5.0 \times 10^7 m^2 s \cdot Pa/kg$. The *ISO-24353* (2008) recommends 13.3 $m^2 h \cdot Pa/\mu g$, which equate to $4.8 \times 10^{13} m^2 s \cdot Pa/kg$, while the *JIS A 1470-1* (2002) proposes a value between $2.4 and 9.4 \times 10^7 m^2 s \cdot Pa/kg$. The Japanese standard and the NORDTEST presented similar values. However, the value introduced in the *ISO-24353* (2008) shows a 10^6 higher values from the value proposed by the other two standards, which leads to different moisture buffering performances between the three protocols (McGregor et al., 2014a).

As tests are performed in climatic chambers (or in jars or boxes), which may not allow the manual control of the air speed, it is not easy to assure the prescribed surface resistance factor and air velocity. This may lead to different and non comparable MBV results. Roels and Janssen (2006) demonstrated that small decrease of the surface film resistance generated significant improvement in the moisture buffering capacity of wood fibreboard. As shown in Fig. 3-11, the MBV varied between 0.55 to 2.31 $g/m^2 \%RH$, due to the material's high sorption capacity. Roels and Janssen (2006) simulated also other materials with lower moisture buffering capacity, which showed smaller variations than wood. However, the authors highlighted that the differences in the sorption capacity were still not negligible.

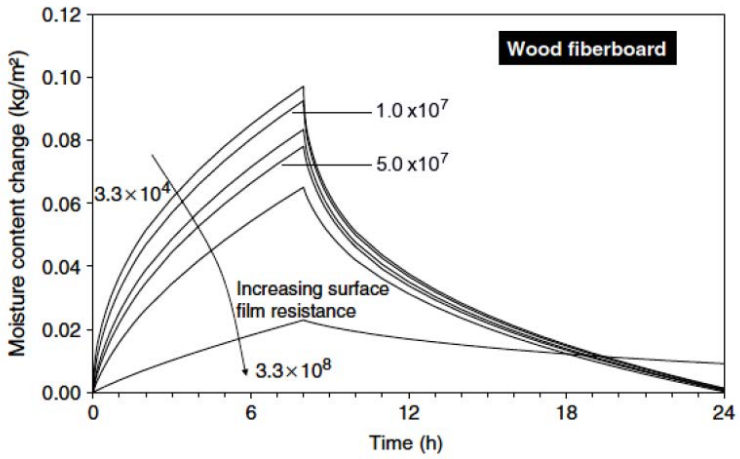

Fig. 3-11. Moisture Buffering profile of wood fibreboard (Roels and Janssen, 2006)

Holcroft (2016a) demonstrated the effect of non-homogeneous air velocity on the MBV of hemp-lime in climatic chambers. Similarly to Roels and Janssen (2006), the sensitivity of highly hygroscopic materials to air velocity changes across the same environmental chamber was demonstrated. Holcroft (2016a) found out that depending on the location of the specimen in the chamber, different MBV were obtained (Fig. 3-12). The difference in the sorption capacity highlighted the sensitivity of hemp-lime to small air velocity variations, which even changed the material's NORDTEST classification (Fig. 3-36).

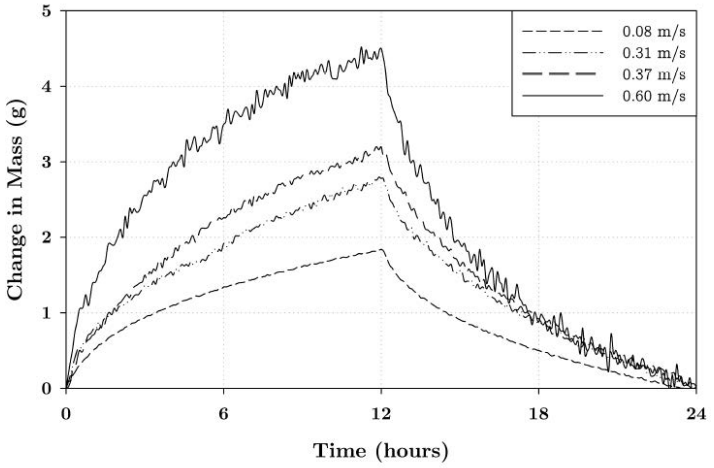

Fig. 3-12. Moisture Buffering profile of hemp-lime (Holcroft, 2016a)

3.4.1 Methods

The effect of air speed on the moisture buffering performance of clay plaster and hemp-lime was investigated. The NORDTEST protocol was repeated in different locations within the same climatic chamber. This study aimed to check that air speed, coming out from the inlet fan, is not higher than 0.1 m/s and the air distribution is uniform across the chamber, not leading to different air velocity and consequently, to different moisture buffering results. The significance of this section is also to check the sensitivity of moisture buffering to small air speed variations. The methodology can be dived into two sections: the measurements of the air velocity in the climatic chamber and the moisture buffering performances of materials, as the tests were performed separately. The comparison between materials with significant different hygric properties (clay and hemp-lime respectively) can also give a clearer idea of the impact of the air velocity, depending on the hygroscopic characteristic of the material.

3.4.1.1 Air Velocity Measurements

The air speed was measured in climatic chamber with a omni-directional, general purpose, air velocity transducer (TSI 8455) with ±2% accuracy. The climatic chamber was kept at constant temperature and RH (23°C and 50%). The air speed was measured in 27 different spots (at three different heights and 9 locations in the horizontal plane), as represented in Fig. 3-13. The air velocity was measured in an empty climatic chamber and the sensor was kept vertical. Records were taken every minute for 15 minutes, which is the time for the air speed to stabilise in the chamber.

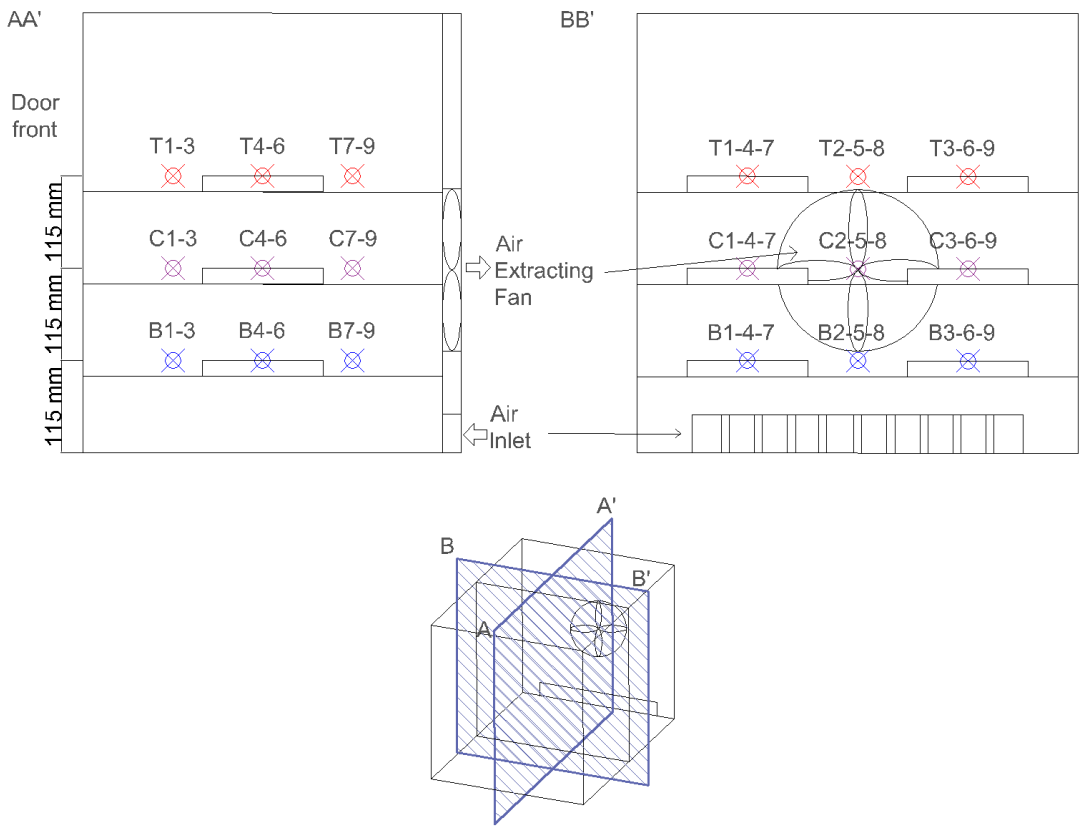

Fig. 3-13. Moisture Buffering profile of clay, lime and gypsum (T is top, C is centre and B is bottom)

3.4.1.2 Moisture Buffering Performances of Materials

Three specimens were preconditioned for 24h at 54% RH and 23°C, until the mass varied by less than 5%. The scales were placed at a measured height, in order to have the surface of the specimens at the same high of the spots, where the air velocity was previously investigated. The moisture buffering test was performed in 6 locations around the climatic chamber, as shown in Fig. 3-13. The moisture buffering capacity was initially performed only on clay, but, due to its low dynamic sorption capacity potential (Table 3.7), hemp-lime was also tested for its significantly higher dynamic sorption capacity and its sensitivity to the air velocity, as Holcroft (2016a) and Latif et al. (2015) showed. Hemp-lime properties can be see in Table 3.8.

Table 3.8. Hemp-Lime properties

Material	ρ	μ	ξ_w
Hemp-Lime	545	8.93	0.06

3.4.2 Results

3.4.2.1 Air Velocity

The average of the 27 air velocity measurements is presented in Table 3.9. The calculation of the confidence interval for each measurements showed variations were in 10^{-3} order, which assure the stability of the air speed during the tests. Each spot presented different air speeds, which demonstrated the air flow inside the climatic chamber is not constant. The results did not show a strong pattern, except that the back of the chamber (7-9) recorded overall higher values than the other locations. This highlighted the effect of the inlet and outlet fan on the air movement. In general, the variability between each location was significant, which indicated, the air movement in the chamber is not uniform.

Table 3.9. Average air speed values (m/s) for each location

Sensor location	Bottom	Centre	Top
1	0.77	0.23	0.82
2	0.93	0.21	0.47
3	0.33	0.26	0.27
4	0.37	0.64	0.60
5	0.39	0.23	0.36
6	0.47	0.30	0.87
7	0.41	0.88	1.07
8	0.52	0.53	0.50
9	0.47	0.71	1.52

3.4.2.2 Moisture Buffering

The clay adsorption and desorption curves are presented in Fig. 3-14. Adsorption is the highest, when the specimen is placed on the centre shelf on the left side of the climatic chamber (61.17 g/m^2 peak to peak), and it is the lowest, when it is on the centre shelf on the right ($48.8g/m^2$). The overall trend indicates that in the middle shelf the specimens presented higher differences between the left and right side. This is likely due to the proximity to the outlet fan, which probably generated positive/negative pressure in that specific shelf. The top shelf presented 6% variation between the two sides, while there is a 12% difference in the bottom shelf. The bottom specimens were near the inlet fan, which might explain the higher gap between the left and right side, compared to the top shelf. In general, the left side shows always higher sorption values, which corresponded on an increase of a 25% on the centre shelf, until a minimum of 6% on the top shelf. A statistical analysis was performed on these data, in order

to investigate the differences presented in Fig. 3-14 are significant. The two tailed Friedman-test analysis highlighted that there was in general no significant difference between the shelves ($p>0.05$). Only results in the centre showed statistically differences with the other MBV values across the chamber ($p=0.02$), as shown in Table 3.10.

Table 3.10. Moisture buffering values of clay in the six locations across the chamber

Moist.Buff (g/m^2)	Top Right	Top Left	Centre Right	Centre Left	Bottom Right	Bottom Left
Mean	52.08	53.76	49.56	62.16	51.66	57.54
CoV	1.30%	3.96%	7.25%	4.85%	1.49%	3.99%

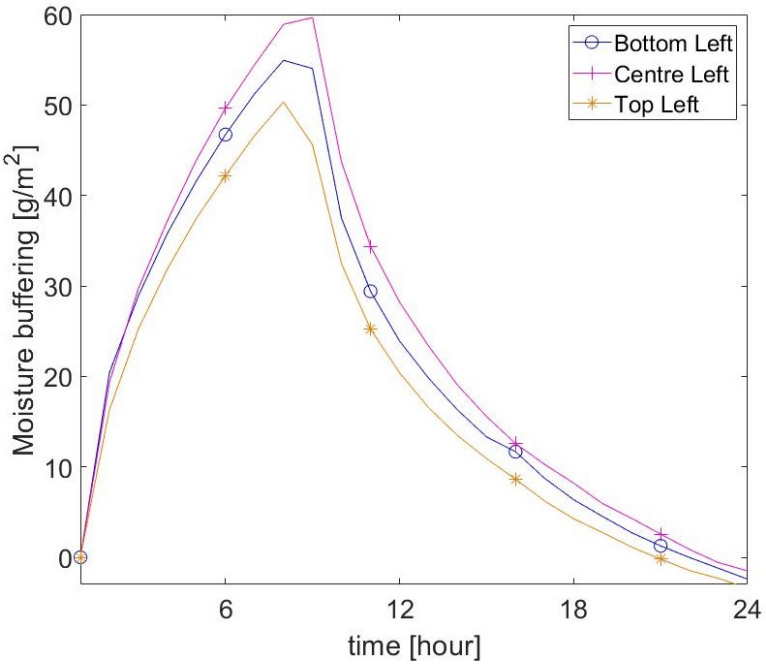

(a) Left

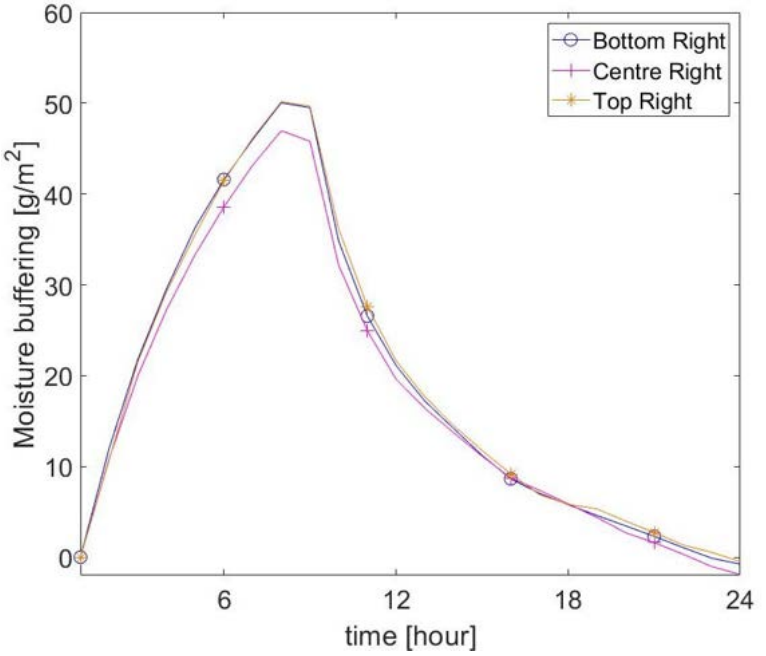

(b) Right

Fig. 3-14. Moisture Buffering profile of clay on the left and right side of the climatic chamber

The MBV values obtained for hemp-lime were significantly lower than the ones measured by Holcroft (2016a) and Latif et al. (2015) (Table 3.11). For this reason, the NORDTEST test was performed once on the original hemp-lime specimen (150x150x150 mm), which gave higher MBV values (over 2.2 $g/m^2\%RH$). Consequently, the 20 mm hemp-lime might not be effected in the same way as a thicker specimen by air velocity, as the limitation of the moisture buffering capacity

might also influence the sensitivity of hemp-lime to air velocity.

The results for hemp-lime are shown in Fig. 3-15. Compared to clay, hemp-lime presented smaller variations between the six locations. The Friedman test did not highlighted significant differences. The similar results obtained may be due to the machine calibration, which better regulated the moisture injection in the chamber than when clay was tested. Overall, the limitation of the hemp-lime's moisture buffering potential might also have influenced the results, which are significantly different from what Holcroft (2016a) found.

Table 3.11. Moisture buffering values of hemp-lime in the six locations across the chamber

MBV ($g/m^2\%RH$)	Top Right	Top Left	Centre Right	Centre Left	Bottom Right	Bottom Left
Mean	58.80	57.54	57.12	57.54	58.80	59.64
CoV	1.33%	1.75%	2.01%	0.62%	5.27%	2.76%

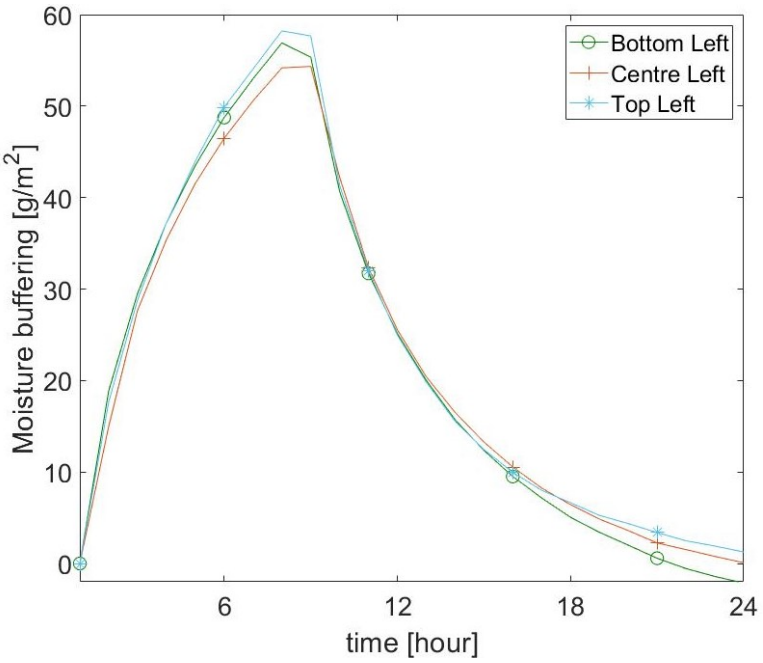

(a) Left

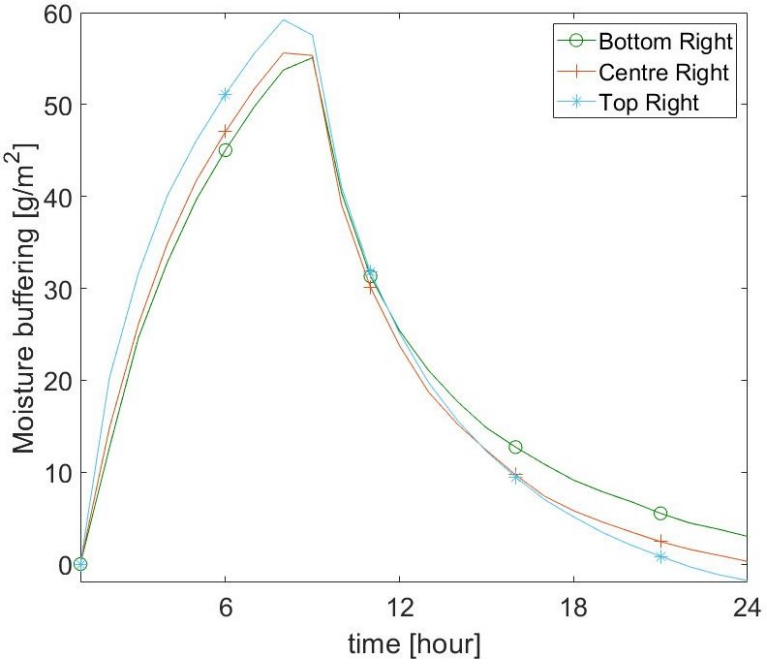

(b) Right

Fig. 3-15. Moisture Buffering profile of hemp-lime on the left and right side of the climatic chamber

3.4.3 Analysis and Discussion

The moisture buffering results were compared with the air velocity in Table 3.12. The final air speed was calculated based on the average air speed of spot 1, 4 and 7 for the left side and 3, 6, 9 for the right side (Fig. 3-16), as those spots covered the area, where

the specimens were placed.

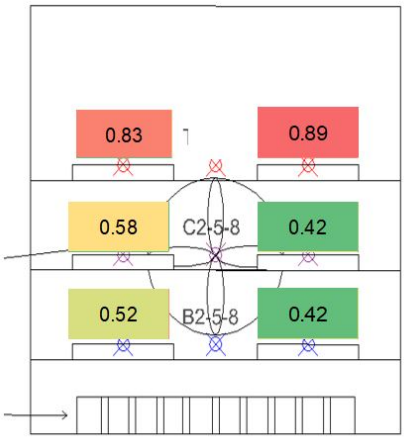

Fig. 3-16. Average air speed values (m/s)

Results in Table 3.12 showed different MBV values depending on the location of the sample. The top shelf had the highest air velocity, which produced slightly higher MBV values for hemp-lime compared to the other locations. The bottom left shelf also gave similar value of MBV, which can be due to the asymmetrical air velocity distribution in that spot. From Table 3.9, spot 1 presented 0.77 m/s and spot 4 and 7 have air speeds lower than 0.41 m/s. Probably, the higher air velocity on the front side of the chamber increased the overall moisture exchange mechanism in the bottom left shelf. Similar consideration can be done on the other spots, but it is necessary to measure the air velocity on top of the specimen, as the air velocity distribution might vary, when a volume (such as a scale) is placed into the chamber.

Table 3.12. Comparison air velocity and MBV for each location

Location	Air Velocity [m/s]	Hemp-Lime MBV $g/m^2\%RH$	Clay
Top Right	0.89	1.42	1.24
Top Left	0.83	1.40	1.29
Centre Right	0.42	1.35	1.18
Centre Left	0.58	1.33	1.48
Bottom Right	0.42	1.37	1.23
Bottom Left	0.52	1.41	1.37

A direct dependency between air velocity and moisture buffering performance cannot be found (Fig. 3-17). It is typically necessary to measure the air velocity directly on top of the specimen, when the moisture buffering test is performed. It could be noticed that the effect of such small air velocity variations on MBV did not lead to important changes in the MBV classification for both materials Rode et al. (2005). However, the

hemp-lime results might not be indicative, due to the material's thickness limitation. The only certainty is that the climatic chamber produced higher velocity than the ones prescribed in the protocols (Rode et al. (2005); *ISO-24353* (2008); *JIS A 1470-1* (2002)), and the different air velocities do not effect materials with moderate moisture buffering capacity.

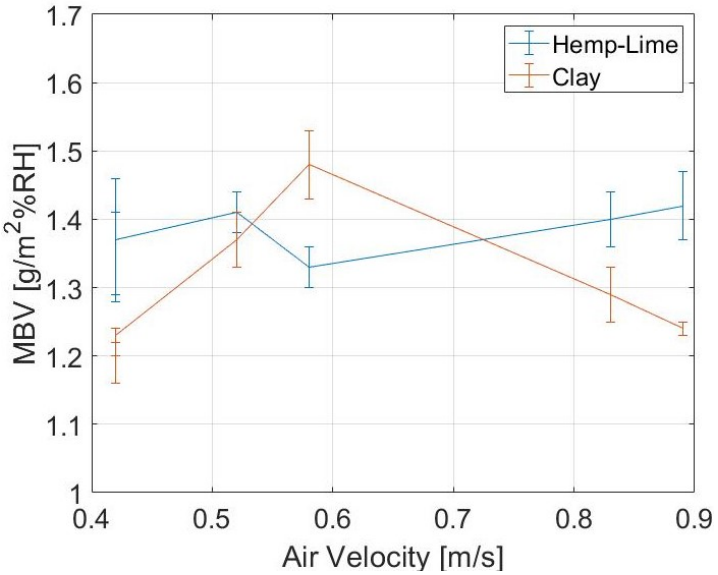

Fig. 3-17. Correlation average air speed values (m/s) and MBV

3.5 Effect of Temperature

As explained in Section 2.4, step-response tests do not consider the contribution of temperature on moisture buffering. However, indoor temperature in buildings is not constant, and its fluctuations may effect the real behaviour of hygroscopic materials indoors. In this section the NORDTEST was performed at different temperatures, in order to quantify the impact of temperature on the materials' sorption capacity. Tests were first performed by changing the prescribed temperature in the NORDTEST. Successively, the moisture buffering tests were repeated by dynamically varying the temperature. In this case the impact of temperature fluctuations was investigated when the materials were exposed either to constant RH and when temperature and RH vary simultaneously to isolate the effect of the temperature and RH on the moisture buffering capacity of the plasters.

3.5.1 Methods

The specimens were pre-conditioned for 24h in the climatic chamber at different temperatures and RH, depending on the environmental conditions that the specimens would be be subjected to during tests. In this way the materials would reach the

moisture balance with the environment at the specific temperature and RH of the test, as shown in Table 3.13. Two temperature and RH sensors (Tiny Tag TV 4505) were placed few centimetres above the two specimens inside the netted volume in order to monitor the environmental condition on the materials. Considering the internal size of the chamber is 550 x 443 x 551 mm, the specimen was placed toward the top of the chamber (at 432 mm from the bottom), to avoid the direct influence of the inlet and outlet fan at the back of the chamber. The accuracy of the temperature and RH sensors was $0.5°C$ and $\pm 3\%RH$.

Table 3.13. Preconditioning and test temperature and RH settings.

Tests	Pre Conditioning	T ($°C$)	RH (%)
RH Square 18	$18°C$ 54%RH	18	Square Fluctuation
RH Square 23	$23°C$ 54%RH	23	Square Fluctuation
RH Square 28	$28°C$ 54%RH	28	Square Fluctuation
T Square 33	$23°C$ 33%RH	Square Fluctuation	33
T Square 54	$23°C$ 54%RH	Square Fluctuation	54
T Square 75	$23°C$ 75%RH	Square Fluctuation	75
TRH Square	$23°C$ 54%RH	Square Fluctuation	Square Fluctuation

To investigate the sole impact of temperature on the dynamic sorption capacity, the modified tests followed the general guidelines of the NORDTEST protocol (Rode et al., 2005), but at different constant temperatures ($18°C$, $23°C$ and $28°C$). $18°C$ and $28°C$ are the acceptable maximum and minimum operating temperatures in buildings, in accordance to the ASHRAE-55 (2017), while $23°C$ is the temperature used in the NORDTEST protocol. The specimens were exposed to six cyclic humidities, where each cycle consisted of 8 hours of high humidity and 16 hours of low humidity (Fig. 3-18a).

Successively, temperature followed square wave fluctuation and RH was kept constant (Fig. 3-18b). Tests were repeated at different RH levels (33%, 54% and 75%) that are the minimum, mean and maximum RH in the NORDTEST. Finally, temperature was varied together with RH, by following an inverse function to RH fluctuation (8h of low temperature and 16h of high temperature), as daily temperature variations in real buildings are opposite to RH fluctuation (Chapter 4). The climatic chamber allows for simultaneous temperature and RH variations. When there is a change of temperature or RH, the chamber increases or decreases the amount of moist air. Due to its high level of accuracy, the chamber is able to auto-control the settings. The summary of all tests is shown in Table 3.13. The temperature fluctuated from $18°C$ to $28°C$. All tests were repeated three times to assure the repeatably and evaluate confidence intervals, CoV and other statistical analyses.

The choice to control the RH rather than the water vapour production was due to the

functioning of the climatic chamber. The machine injects an unquantified amount of moist air in the chamber, to keep the humidity level at the target RH. RH is the ratio of the actual amount of water vapour in the air and its saturation pressure, which are both values dependent on the temperature. To have a better understanding of the effect of temperature variation on moisture buffering, absolute humidity in the air should be measured instead. However, controlling the amount of water released in the chamber was not possible. This led the choice of RH as variable together with temperature, which is, commonly, used as indicator of the humidity level in buildings.

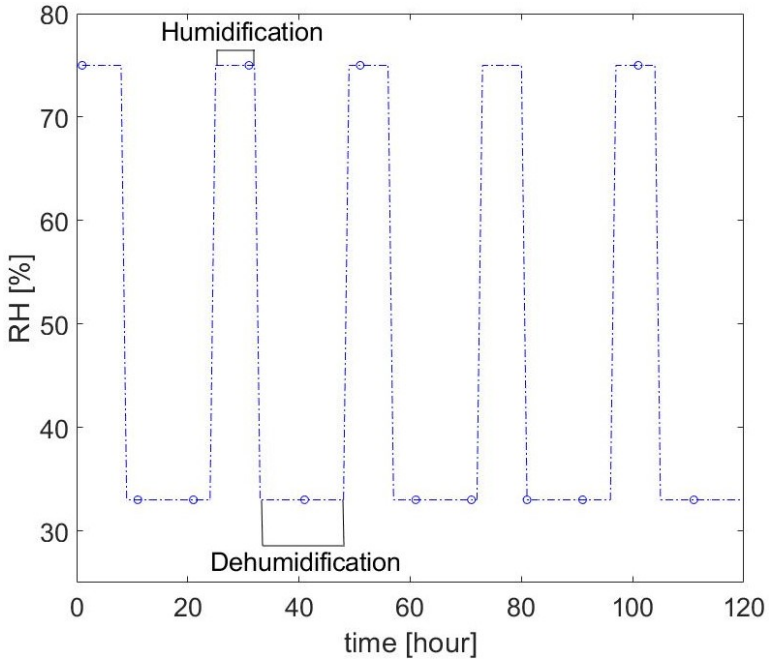

(a)

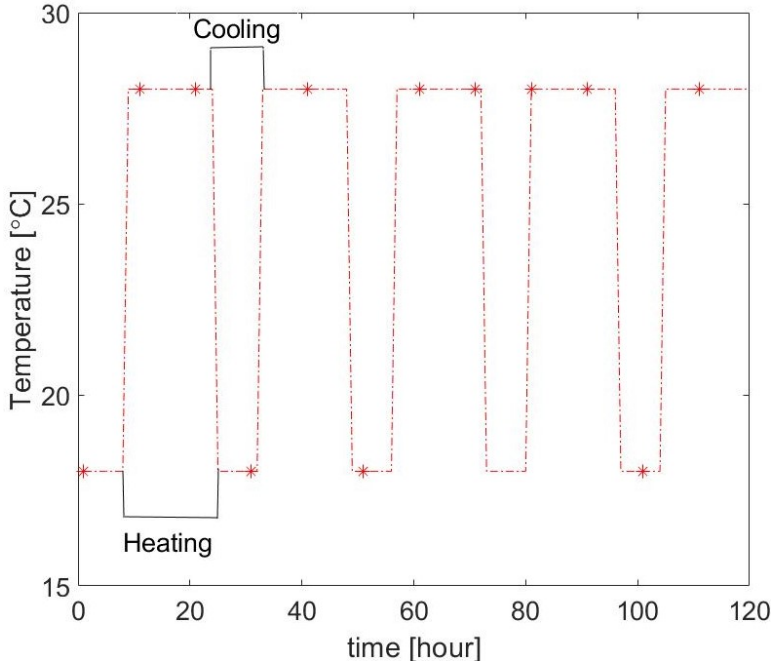

(b)

Fig. 3-18. Square fluctuations (**a**) and temperature square variations (**b**)

3.5.2 Results and Analysis

The results are divided into multiple sub-sections, in which different aspect of the testing were presented. The first sub-section (Section 3.5.2.1) investigates the reliability of the climatic chamber to follow the programmed environmental conditions. Section 3.5.2.2 shows the variability of the moisture buffering results,

when the NORDTEST is applied at different temperatures. This last section was further analysed in Section 3.5.2.3 by also looking at the influence of temperature on other specimens of clay and gypsum with different hygrothermal properties. In Section 3.5.2.4 the sorption capacity of materials was observed when the RH is kept constant and temperature varied, whilst Section 3.5.2.5 investigates the impact of the simultaneous variation of temperature and RH on the materials. Results shown in this section refer to the average data obtained by testing three specimens for each material.

3.5.2.1 Observations of the test chamber performance

The average data of the two RH and temperature sensors were shown to be in good agreement (less than 0.02^oC and 2% RH variations). The measured temperature and RH compared with the target curves are shown in Fig. 3-19 and Fig. 3-20. In Fig. 3-19a temperature followed the programmed curve, showing a square trend. It did not perfectly match the maximum and minimum target temperature, but there was less than $0.6°C$ shift, and the amplitude of the temperature fluctuations was preserved. Humidity presented small fluctuations, due to temperature variations. However, RH variations were less than $\pm 4.8\%$ in correspondence of the peaks, and the average RH was 1.12%RH higher that the programmed 50%RH (Fig. 3-19a). Fig. 3-19b shows a worse match between the target and measured RH, as there is a shift of more than 5%. The climatic chamber struggled to keep RH low, when the temperature dropped to $18°C$. Also the temperature curve does not match as good as in the previous case. The difference between the two curves is more than $1°C$ and also the fluctuation are $1°C$ more than the target one. In Fig. 3-20a a similar situation was found, as temperature is $1.52°C$ below the target temperature, and there is not a good agreement with the RH curve ($\pm 5.13\%RH$). Apparently the climatic chamber was not able to reach the lowest humidity, but the fluctuation amplitude was preserved. Fig. 3-20b presents similar issues for the RH curve ($\pm 5.02\%RH$), but there is a better match for the temperature curve ($0.70°C$). Fig. 3-21a presents a shift of ± 7.17%RH and $\pm 1.54°C$.

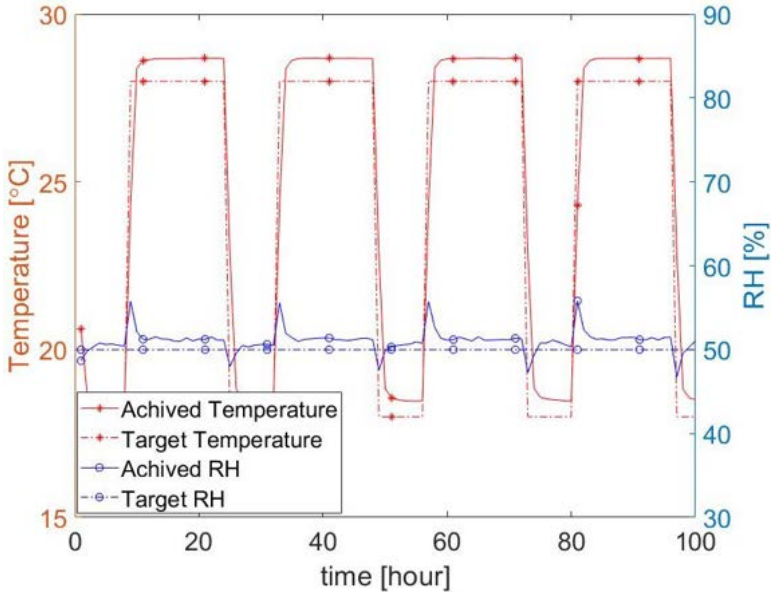

(a)

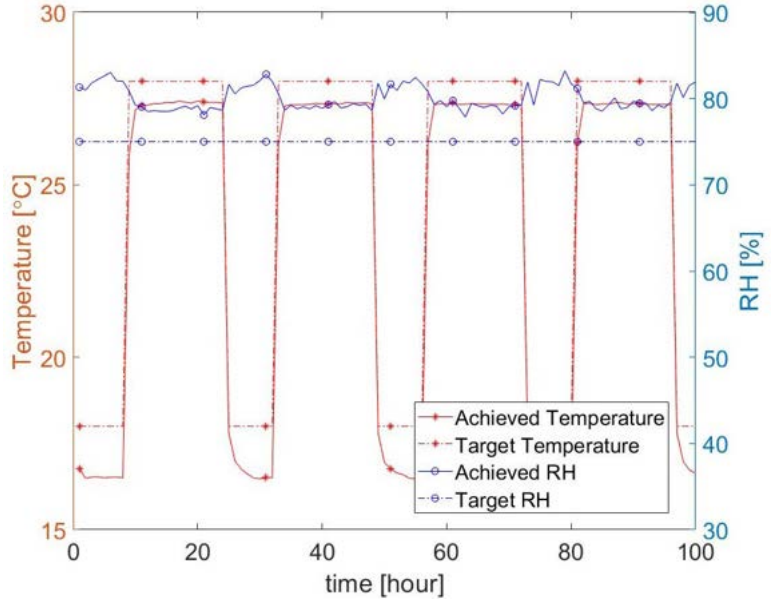

(b)

Fig. 3-19. Temperature square variation at 50% (**a**) and 75% (**b**)

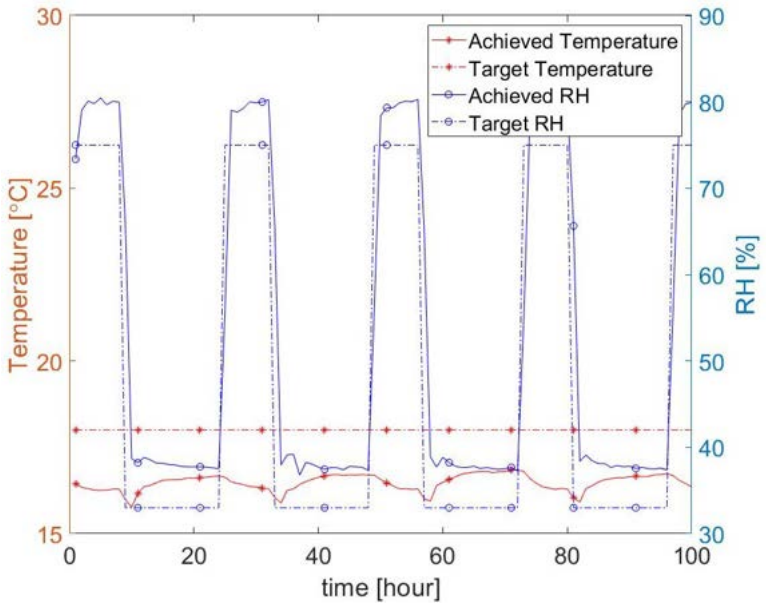

(a)

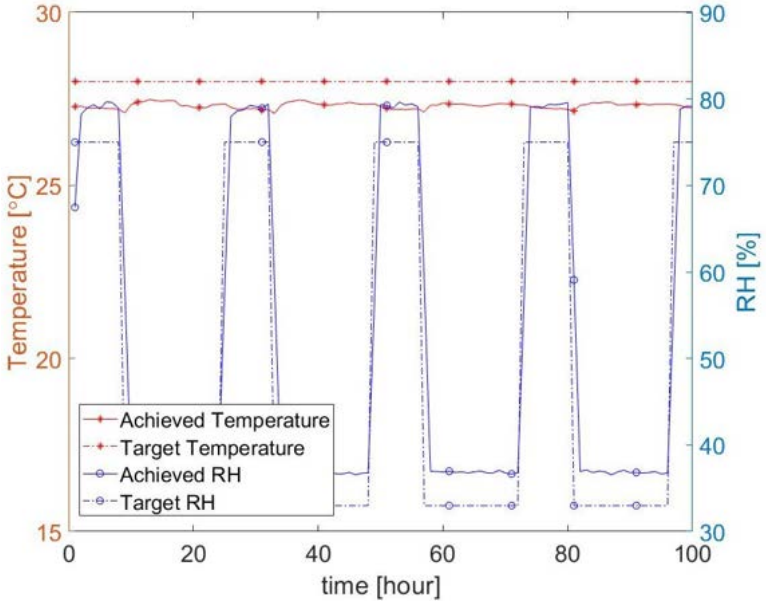

(b)

Fig. 3-20. RH square variation at $18°C$ (**a**) and $28°C$ (**b**)

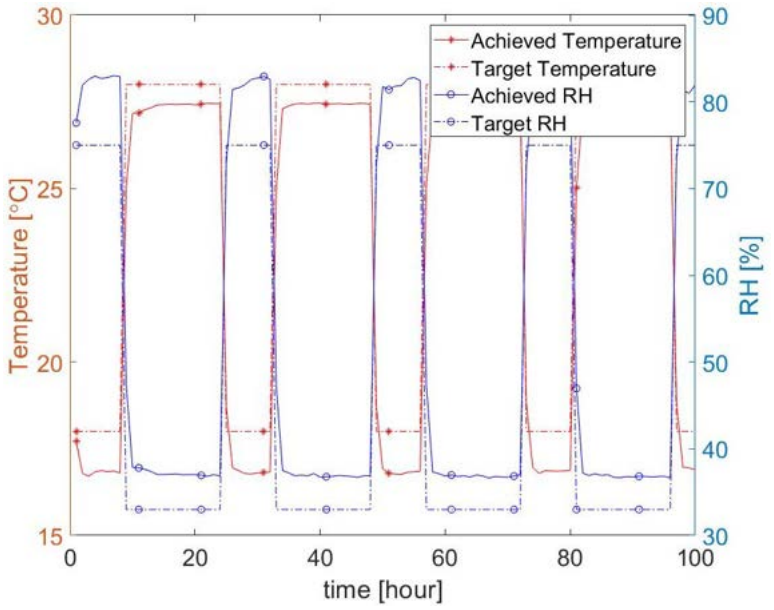

(a)

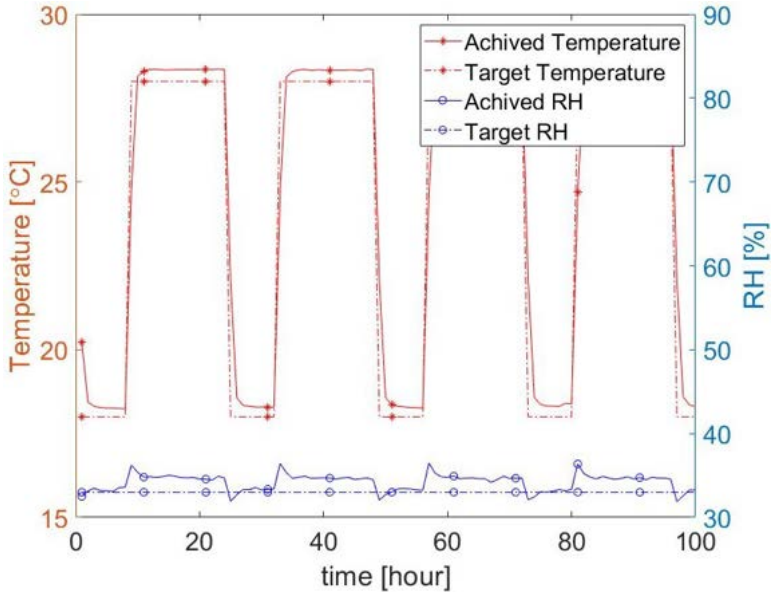

(b)

Fig. 3-21. Simultaneous RH and T variations(**a**) and T square variation at 33% (**b**)

The high variability of the results is due to calibration of the machine. Some tests were repeated shortly after the calibration of the machine, which showed a better agreement with the target function (Fig. 3-22). The curves in Fig. 3-21b had a better match than all previous curves, because the test was performed after the climatic chamber calibration (0.5%RH below the programmed 33%RH and $\pm 0.32°C$). The incapacity of the chamber to keep humidity and temperature continuously constant when the other parameter varies, can be due to the functioning of the machine. This issue can be mostly seen when high and low temperature are used. At $23°C$ and 50% there is usually a better match, because it is easier for the chamber to vary humidity and temperature

around the "average" value of the square function ($23°C$, 50%RH), rather than from the target maximum and minimum. In general, regardless of the temperature and RH set for the test, there is always an improved fitting with the programmed environmental conditions, when the climatic chamber is calibrated. As in this study the tests were started four months before the calibration, it is recommended precautionary to re-calibrate the chamber every 6 months, to always have reliable results for moisture buffering tests.

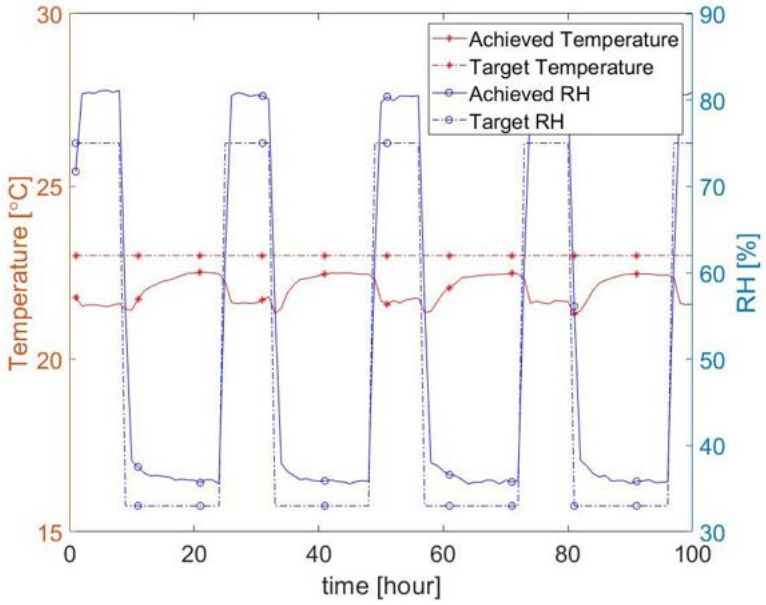

(a)

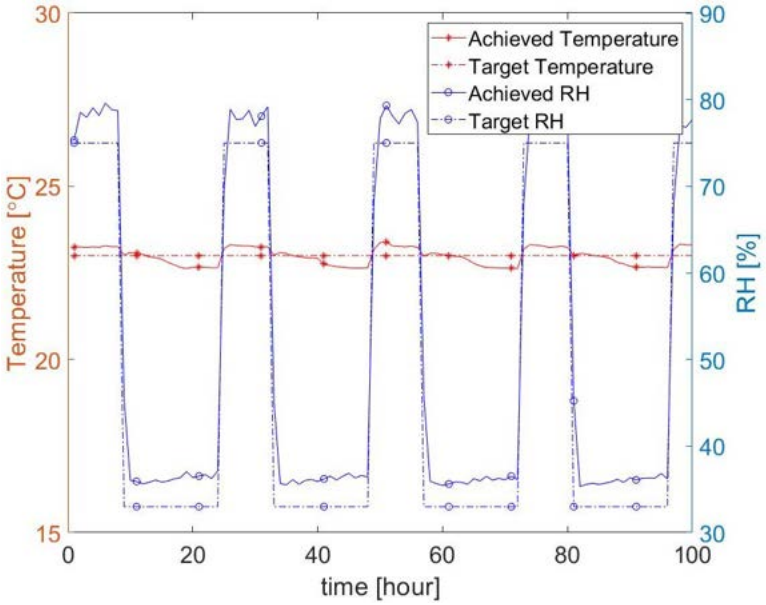

(b)

Fig. 3-22. RH square variation at $23°C$ before (**a**) and after calibration (**b**)

Overall, considering the accuracy of the climatic chamber was ±1% for RH and

$\pm 0.3°C$ for temperature, it wan noticed the climatic chamber did generally not maintain the programmed environmental conditions after more than 6 months from the annual calibration. Even though RH and temperature fluctuation amplitude was preserved, most of the tests were repeated, as after the calibration presented a better match with the target environmental conditions.

3.5.2.2 Moisture Buffering Capacity at different Temperatures

The response of clay and gypsum to the square RH variation at three different temperatures is illustrated in Fig. 3-23a and Fig. 3-23b. Temperature clearly influenced the sorption capacity of both materials. High temperatures yielded a greater amplitude of the curves, while lower temperatures generated a smaller moisture uptake and release.

At $28°C$ clay adsorbed 36% more than at $18°C$ and 14% more than at $23°C$ (peak to average). The desorption presented smaller differences (26.56 g/m^2 at $28°C$ and 21.20 g/m^2 at $18°C$), but there is still more than 10% difference in the moisture buffering capacity between the three curves). Overall, the Coefficient of Variation (CoV) at $18°C$, $23°C$ and $28°C$ was below 0.66%, 1.23% and 1.90% respectively. Gypsum presented a greater moisture buffering capacity than clay, but it was still influenced by the temperature in the same way. It stored and released respectively 56.22 and 42.84 g/m^2 at $28°C$, while its sorption capacity dropped around 56% at $18°C$ both in the adsorption and desorption phase, as shown in Fig. 3-23b. The CoV for gypsum at $18°C$, $23°C$ and $28°C$ was below 4.00%, 2.90% and 1.85% respectively. Table 3.14 summarises the adsorption and desorption capacity of clay and gypsum.

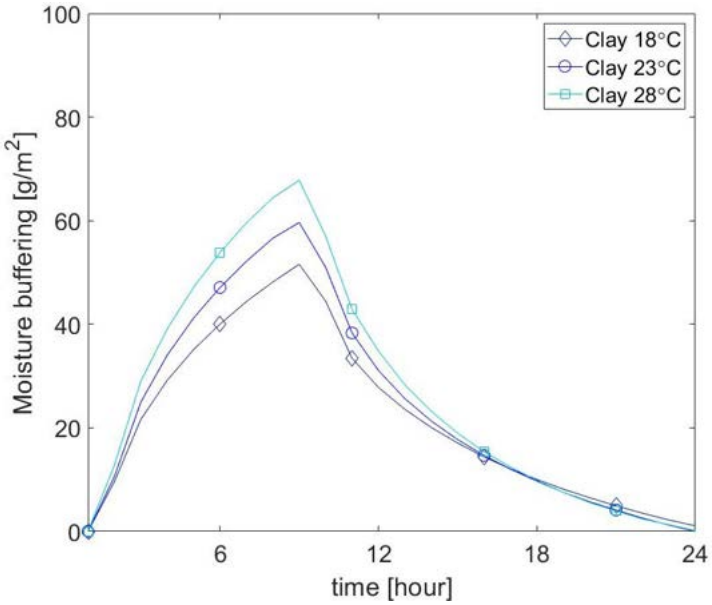

(a) Clay

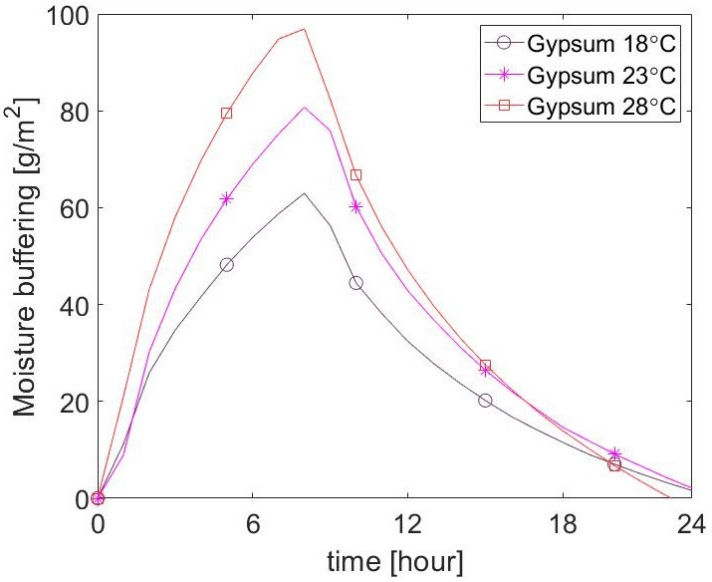

(b) Gypsum

Fig. 3-23. Sorption capacity of clay and gypsum at different temperatures

Table 3.14. Response and confidence interval of the specimens at variable RH and constant temperatures

Material	Curve	Adsorption (g/m^2)	Desorption (g/m^2)
Clay	RH Square 18	30.38 ±0.2	21.20±0.1
	RH Square 23	36.00±0.4	23.70 ±0.2
	RH Square 28	41.22±0.4	26.56±0.6
Gypsum	RH Square 18	36.00±1.0	27.04 ±0.7
	RH Square 23	45.90±1.1	34.82 ±0.9
	RH Square 28	56.22±0.9	42.84±0.9

In Fig. 3-24 the moisture buffering capacity was correlated with the temperature. A linear regression fit was modelled that resulted in a squared R of 0.99 and p-valued of 0.02 for both materials. It is evident there is a linear correlation between the dynamic sorption capacity and temperature for both clay and gypsum. Nevertheless, clay appears to be less sensitive than gypsum to temperature variation, as the slope of the two lines highlights. The clay moisture buffering capacity increased by 3.9%, while gypsum by 9.1%. The main reason can be due to the hygric properties of clay, together with the different pores distribution of the two materials.

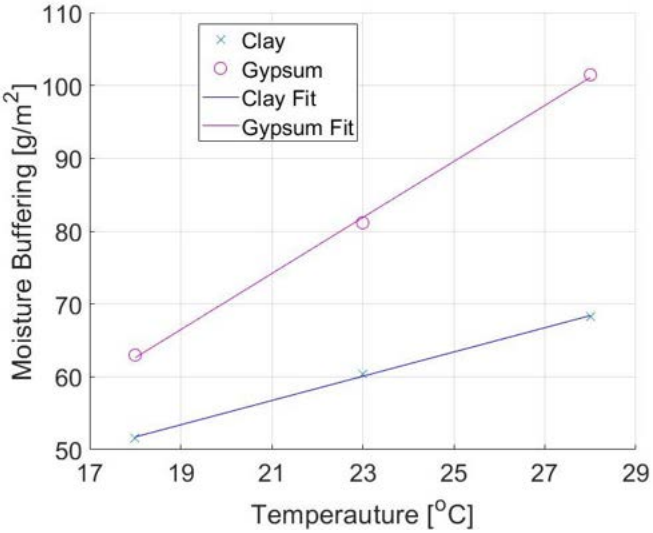

Fig. 3-24. Moisture buffering profile of clay and gypsum

3.5.2.3 Moisture Buffering Capacity at different Temperatures and variable Densities

To better understand the effect of temperature on clay and gypsum, the test was repeated on new specimens of clay and gypsum with different hygrothermal properties. Further gypsum specimens were cast, in which the water was halved (30% mass of water by air dry weight), to obtain a different density for the same material. The new clay specimens were cast for a previous study (Maskell et al., 2016). The new clay and gypsum presents higher density and lower hygric properties than the original materials. The properties for the new materials were measured, except for the porosity and pore distribution of clay, which were taken from Maskell et al. (2016). The high density (HD) materials' properties are showed and compared with the original clay and gypsum samples (LD) in Table 3.15. The high density specimens presented lower hygric properties and lower porosity, which indicates lower moisture buffering capacity. Gypsum HD presented a similar pore distribution of clay LD (Fig. 3-25 and Fig. 3-2a)

Table 3.15. Moisture Buffering Values at $23°C$, water vapour resistant factor (-), dry density (kg/m^3),specific moisture capacity (kg/kg) and porosity (%) of gypsum and clay.

Material	MBV	μ	ρ	ξ_w	Φ
Gypsum LD	1.95	8.37	856	0.034	61.91
Gypsum HD	0.97	10.75	1256	0.012	35.8
Clay LD	1.45	12.86	1258	0.013	43.37
Clay HD	0.95	19.21	1870	0.007	24.8

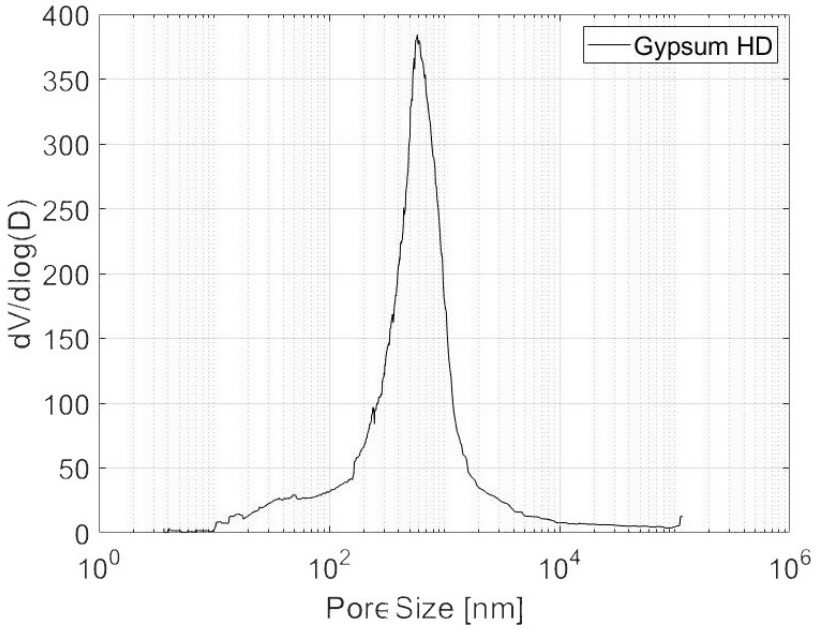

Fig. 3-25. Pore size distribution of gypsum HD

The sorption capacity of clay and gypsum HD was significantly reduced. The adsorption and desorption capacity of clay dropped 49% and 37% respectively, while for gypsum the moisture buffering potential decreased 90%. Fig. 3-26a illustrates the high density clay was still effected by temperature variation, but the difference between each curve was significantly smaller than in the LH specimens. At $18°C$ clay adsorbed 8% and 28% less at $23°C$ and $28°C$ respectively, and desorbed 11% and 26% less. The CoV for clay at $18°C$, $23°C$ and $28°C$ is 1.26%, 2.96% and 3.27% respectively. Gypsum showed more significant differences between the three curves than clay. At $18°C$ gypsum adsorbed and released 32% and 50% less than at $23°C$ respectively, and 67% and 65% at $28°C$. Gypsum presented a CoV of 4.09%, 2.93% and 1.85% at at $18°C$, $23°C$ and $28°C$ respectively. The significant reduction of the moisture buffering potential of gypsum is likely due to the change in pore structure. The lower mixing water content and probably small variations of the mixing procedure, resulted in different pore distribution. The high density gypsum did not exhibit the micro pore structure, that activates the liquid transport, consequently, reducing gypsum moisture buffering potential. Table 3.16

shows that the differences between higher density clay and gypsum were negligible.

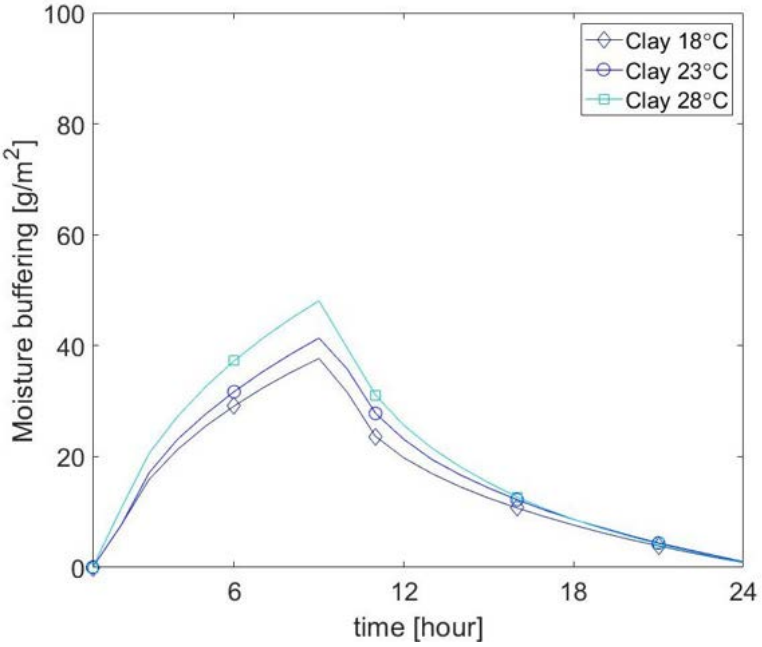

(a) Clay

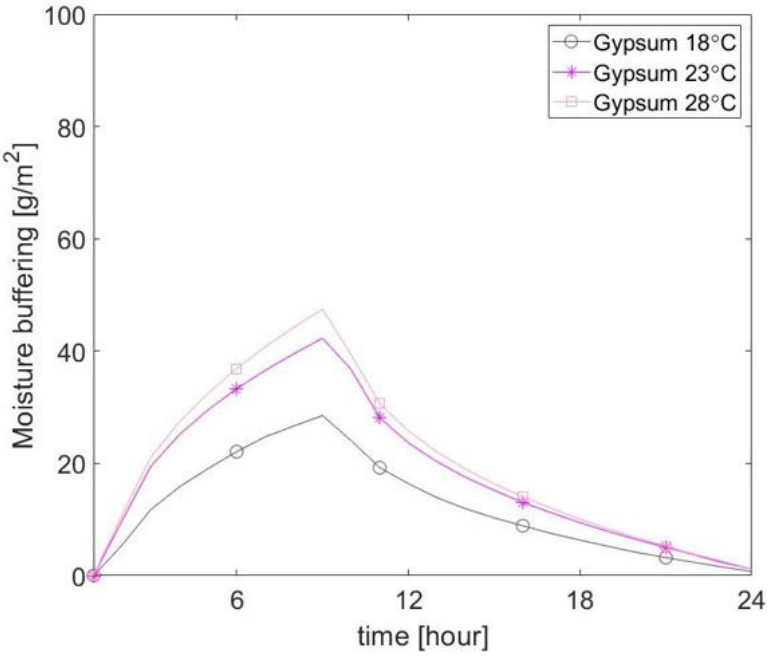

(b) Gypsum

Fig. 3-26. Sorption variation of high density clay and gypsum

Table 3.16. Response and confidence interval of the high density (HD) specimens at variable RH and constant temperatures

Material	Curve	Adsorption (g/m^2)	Desorption (g/m^2)
Clay HD	RH Square 18	22.20±0.2	15.48 ±0.2
	RH Square 23	24.11±0.5	17.26±0.4
	RH Square 28	28.57±0.7	19.51±0.6
Gypsum HD	RH Square 18	16.44±0.3	12.06 ±0.2
	RH Square 23	24.06±0.4	18.21±0.8
	RH Square 28	27.53±0.2	19.91±0.3

The correlation between temperature and the high and low density clay and gypsum is represented in Fig. 3-27. In this case the R squared in the linear regression was 0.94 and 0.87 for clay HD and gypsum HD, respectively, both with a p-value higher than 0.05. Even though the fit curve was not statistically significant, the slopes of the high density clay and gypsum is lower than the low density gypsum. However, clay high and low density and gypsum high density present similar slopes, probably due to similarity of the pores distribution curves. This resulted in the materials being effected in a similar way by temperature. The effect of temperature is higher on low density gypsum, due to the activation of liquid transport in micro-pores. It means that even though the materials present different density and porosity, the porous structure is the key parameter that determine the moisture buffering capacity of the materials.

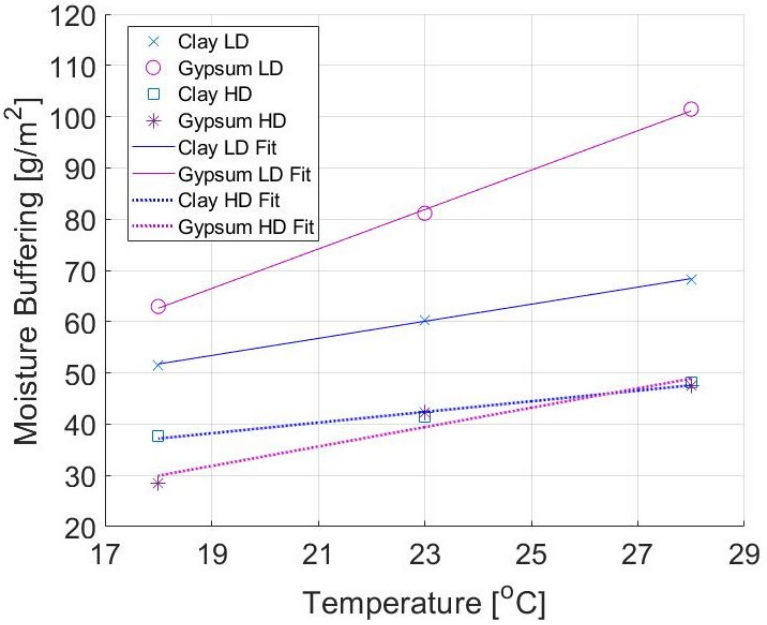

Fig. 3-27. Moisture buffering profile of clay and gypsum HD is high density and LD is low density

3.5.2.4 Temperature variation at constant RH

The sorption response of clay and gypsum to square temperature fluctuations is presented in Fig. 3-28 and Fig. 3-29. In Fig. 3-28a the sorption capacity of clay peaked, reaching (peak to maximum) 17.60, 5.24 and 31.46 g/m^2 at 33%, 50% and 75% with CoV below 10.46%, 11.86% and 1.50% between each cycle respectively. Desorption had similar values than adsorption at 33% and 50%, while at 75% presented higher values, as shown in Table 3.17. After approximately three hours the clay sorption curve flattened, until the temperature changed again (Fig. 3-28a). The peaks are due to the climatic chamber, as the sudden change of temperature brought to a jump in the moisture injected in the chamber, to keep the RH at the target value. The consequence of the increase/decrease of the air moisture content are the peaks in the moisture adsorbed in the materials in correspondence of such environmental variations. After the environmental chamber stabilised the temperature, the excess of moisture was adsorbed or desorbed by the material and the mass of the specimens stabilised. Fig. 3-28b illustrates the clay response in a 24h full-cycle. Eliminating the peaks, the temperature did not to influence the sorption capacity of clay (Fig. 3-28b), as the moisture content fluctuation are small and the difference between each curve is minimal, as shown after hour 12 in Fig. 3-28b.

Table 3.17. Response of the high density specimens at variable temperature and constant RH, when the peaks are considered

Material	Curve	Adsorption (g/m^2)	Desorption (g/m^2)
Clay	T Square 33	17.60±1.8	17.50 ±1.2
	T Square 50	5.24±0.6	7.38±0.4
	T Square 75	31.46 ±0.6	17.16±0.2
Gypsum	T Square 33	6.45±0.5	6.20±0.7
	T Square 50	8.14±0.6	8.03±0.4
	T Square 75	18.38±0.6	13.29±0.6

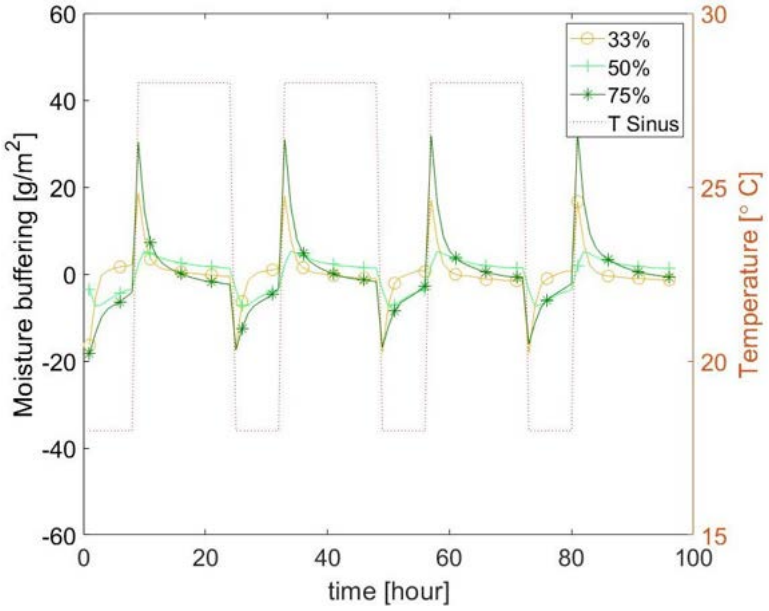

(a)

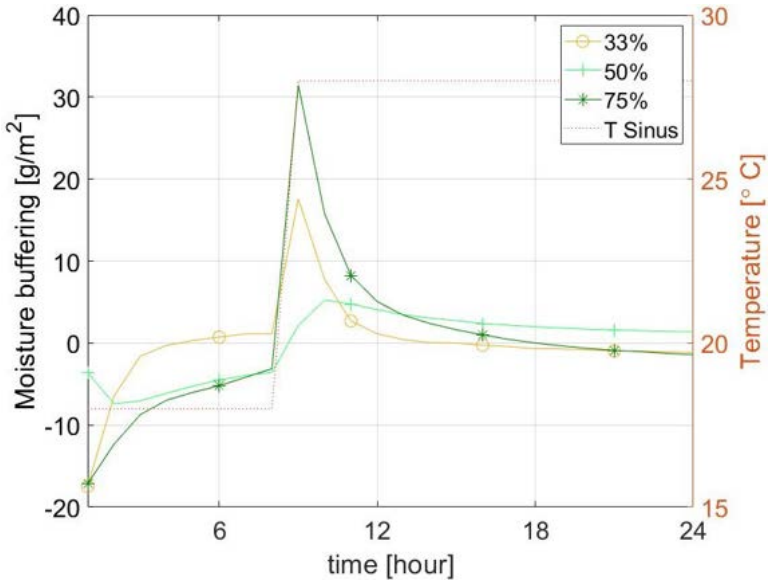

(b)

Fig. 3-28. Average sorption curve of clay: four cycles curves (**a**) and average 24h sorption curve (**b**) at constant RH and variable temperature

Gypsum had an average sorption capacity of 12.65, 16.17 and 31.67 g/m^2 at 33%, 50% and 75% with CoV below 7.27%. 7.27% and 2.90%. As Fig. 3-29a shows the peaks of the curves were smaller than for clay, which might be due to slight temperature and RH variations in the climatic chamber between each test. By increasing the RH, the sorption capacity of gypsum slightly increased, due to the larger amount of moisture content in the chamber necessary to reach higher RH. However, by eliminating the first three hours, the curves flattened similar to that observed for clay. Therefore, it can be stated that also in this case the temperature effect on moisture buffering is limited only in the first few hours of the temperature variation.

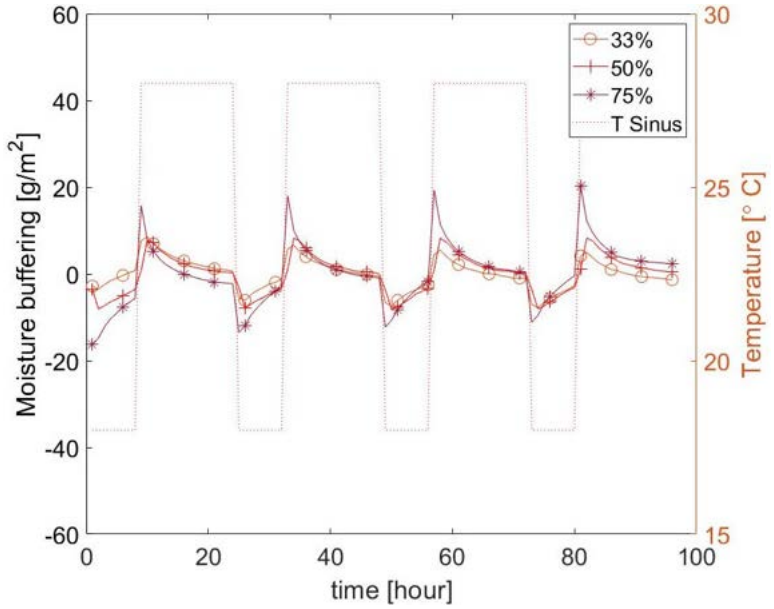

(a)

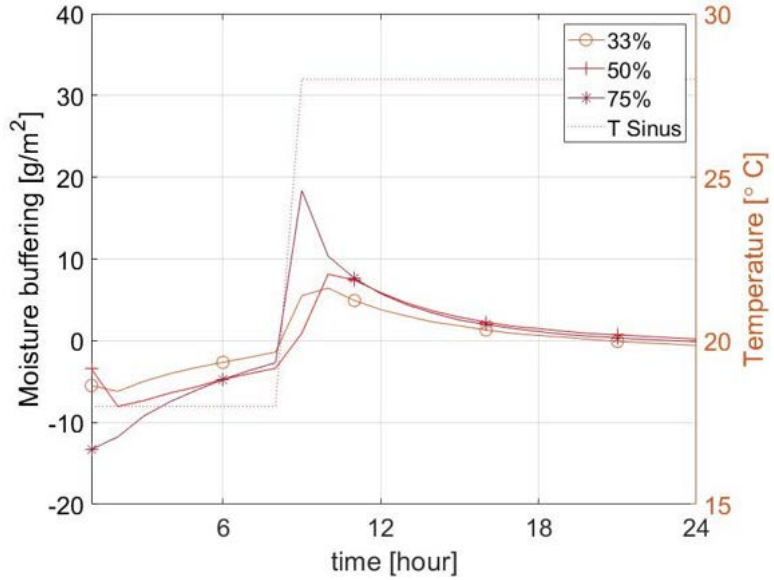

(b)

Fig. 3-29. Average sorption curve of gypsum: four cycles curves (**a**) and average 24h sorption curve **b** at constant RH and variable temperature

In Fig. 3-30 a correlation between the different RH applied to the test (33%, 54% and 75%) and moisture buffering was investigated. Both for clay and gypsum there was not any statistical significance with R squared of 0.22 and 0.88, respectively, and p-value higher than 0.05. Even though the p-value for gypsum was high, gypsum presented a better fit than clay, which might imply some error in the clay testing or some moisture transport/storage mechanisms that was not accounted for.

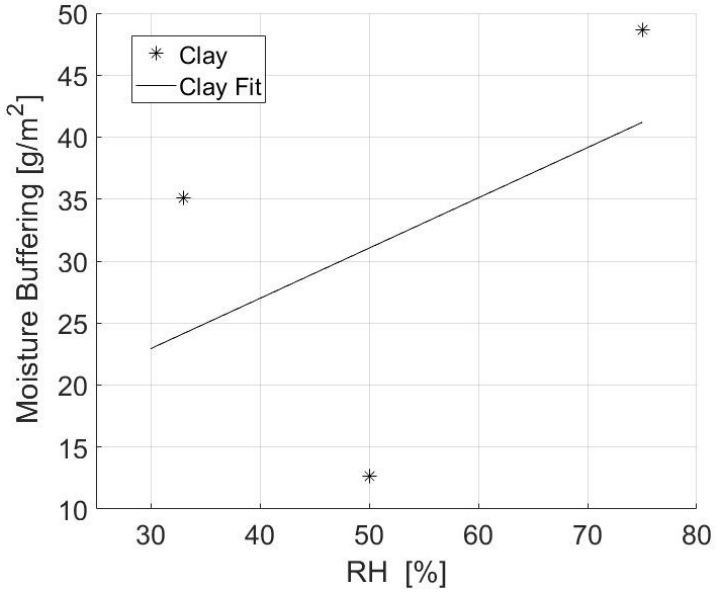

(a) Clay

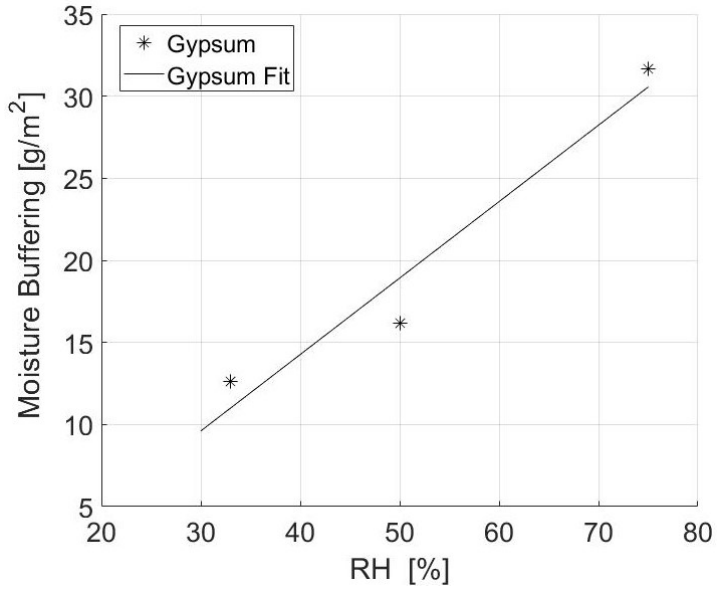

(b) Gypsum

Fig. 3-30. Correlation between RH and moisture buffering capacity for clay and gypsum

3.5.2.5 Moisture Buffering Capacity at Variable Temperature and RH

The behaviour of clay and gypsum, when subjected to simultaneous RH and temperature square variations is illustrated Fig. 3-31. Comparing the curves with the results obtained in Section 3.5.2.2, the sorption curves of the two materials had similar trend than the "RH Square 23" in terms of the overall behaviour. However, clay adsorbed and desorbed 7.16% and 8.31% less than "RH Square 23" (33.42 $g/m^2\%RH$ and $21.73g/m^2\%RH$), while gypsum adsorbed and desorbed 12% and 19% more ($51.42g/m^2\%RH$ and $41.44g/m^2\%RH$). The CoV for clay and gypsum is

1.80% and 1.72%. The different sorption capacity of materials in "RH Square 23" and "TRH Square" highlighted that the temperature influence the sorption capacity of materials. The decrease and increase for clay and gypsum in "TRH Square" respectively showed the different sensitivity of materials to temperature variations. In presence of micro-pores like for gypsum, the temperature increased the moisture transport potential, while for clay, which presented only macro-pores, the temperature variation decreased the sorption capacity, probably because pores dry quicker, after the moisture content in the chamber stabilised. Further observations on this phenomena were made in the following section (Section 3.6).

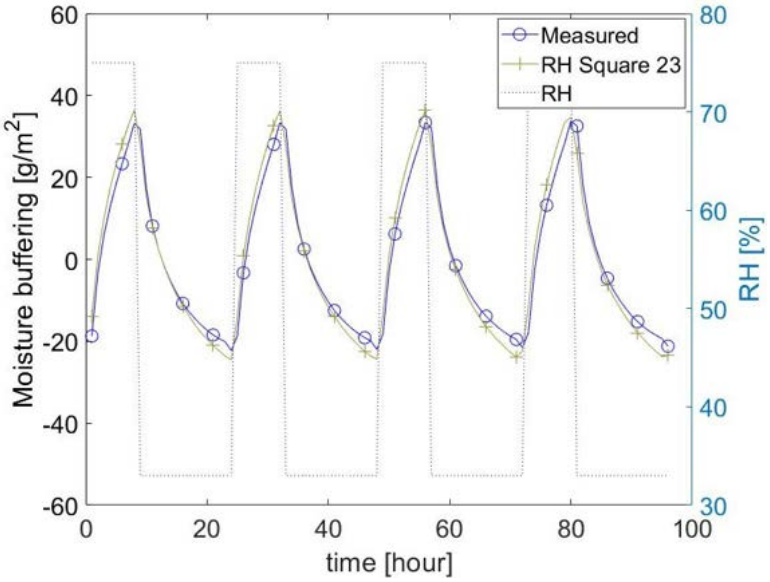

(a) Clay

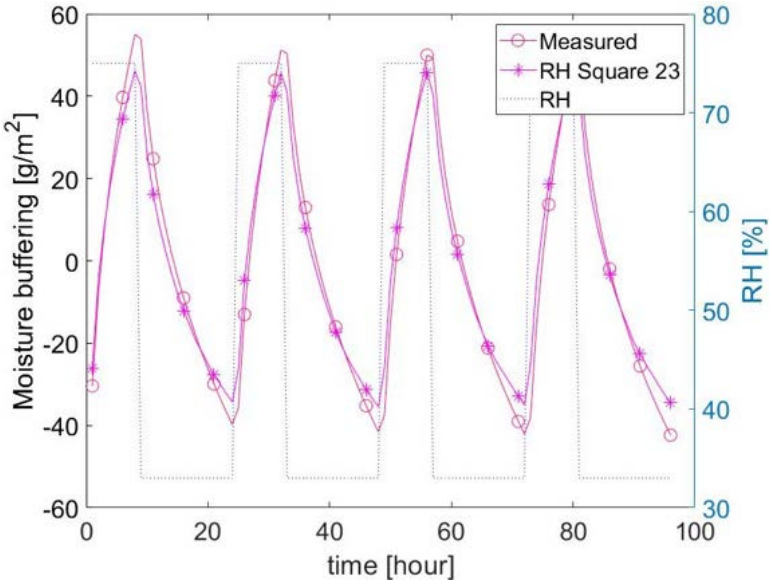

(b) Gypsum

Fig. 3-31. Sorption curve of clay and gypsum at variable RH and variable temperature

3.6 Investigation on Sinusoidal Humidity Variation

A new approach to measure moisture buffering in laboratory scale testing was developed in this section. The new protocol is based on the NORDTEST set-up, but the RH and temperature followed a sinusoidal variation function. This study aimed to show the complexity of the response of porous materials to sinusoidal and simultaneous humidity and temperature variations, which highlighted the importance to improve moisture buffering understating and testing practises. This section follows the same structure of Section 3.5, by first analysing the response of materials to sinusoidal humidity variations at constant temperature. Successively, materials were subjected to dynamic temperature variations at constant RH, and, in conclusion, temperature and RH are simultaneously varied.

3.6.1 Methods

Clay and gypsum specimens were exposed to six cyclic humidity and temperature sinusoidal changes. Each cycle consisted of 8 hours of high humidity (low temperature) and 16 hours of low humidity (high temperature). Temperature cycles were inversely proportional to the RH function. Materials were exposed initially only to temperature or RH sinusoidal cycles, while the other parameter was kept constant, in order to understand which of the two environmental factors influenced the dynamic sorption capacity most. Tests were repeated three times, respectively at different constant temperature ($18°C$, $23°C$ and $28°C$) and RH (33%, 54% and 75%), as shown in Table 3.18.

Table 3.18. Preconditioning and test temperature and RH settings.

Tests	**Pre Conditioning**	**T** ($°C$)	**RH** (%)
RH Sinu 18	$18°C$ 54%RH	18	Sinusoidal Fluctuation
RH Sinu 23	$23°C$ 54%RH	23	Sinusoidal Fluctuation
RH Sinu 28	$28°C$ 54%RH	28	Sinusoidal Fluctuation
T Sinu 33	$23°C$ 33%RH	Sinusoidal Fluctuation	33
T Sinu 54	$23°C$ 54%RH	Sinusoidal Fluctuation	54
T Sinu 75	$23°C$ 75%RH	Sinusoidal Fluctuation	75
TRH Sinu	$23°C$ 54%RH	Sinusoidal Fluctuation	Sinusoidal Fluctuation

The experimental RH and temperature sinusoidal variations are illustrated in Fig. 2-1. Differently from Section 3.5, the RH increase is represented by the section above the mean of the sinusoidal curve. The mean value and the starting RH humidification point was set to 54%, until it gradually reaches 75% and then back to 54%. The climatic chamber varies the RH circa every hour in the 8h. The humidity decrease phase starts at 54%, and the RH is decreased every two hours until it reaches the minimum 33%, and

then again up to 54% in 16 hours time frame. The climatic chamber cannot reproduce a perfect sinusoidal curve, for this reason, sinusoidal variations were approximated to a quasi sinusoidal curve, where the transition from high to low humidity (and vice versa) is distributed in eight smaller steps. The transition between one step to the other was automatically regulated by the chamber, by setting a "slope", which allowed a gradual increase/decrease of RH in between two steps. The slope is a setting of the climatic chamber that progressively increases/decreases the environmental conditions until the next temperature/RH is achieved. For the temperature, the curve was set to start at $23°C$, reaching within the 8 hours the minimum temperature of $18°C$, succeeded by a 16 hour ranging between $23°C$ to $28°C$. The temperature curve was programmed similarly to the RH.

In the sinusoidal test RH gradually reaches the maximum and minimum humidity level. As shown in Table 3.19, the chamber increased the humidity from 73.9% RH to 75%RH within one hour. After 30 minutes the RH was above 74%. The same procedure was applied when the RH jumps back from 75% to 73.4%RH. Overall, the RH between 74.5%RH and 75%RH was maintained for around one hour. The de-humidification process was similar but it took two hours reach the minimum RH. The water vapour variation of the simultaneous temperature and RH curve during the test can be seen in (Cascione et al., 2020a). The reliability of the climatic chamber, to maintain the sinusoidal variation, was checked with Tiny Tag sensors.

Table 3.19. Temperature and RH steps and time frame (hours) in detail

Steps	0	1	2	3	4	5	6	7	8	9	10	11	12	13	14	15	16
RH	54.00	62.04	68.8	73.4	75.0	73.4	68.8	62.0	54.0	45.9	39.1	34.6	33.0	34.6	39.1	45.9	54.0
Temp.	23.0	21.1	19.5	18.4	18.0	18.4	19.5	21.1	23.0	24.9	26.5	27.6	28.0	27.6	26.5	24.9	23.0
Hours	1	1	1	1	1	1	1	1	1	2	2	2	2	2	2	2	2

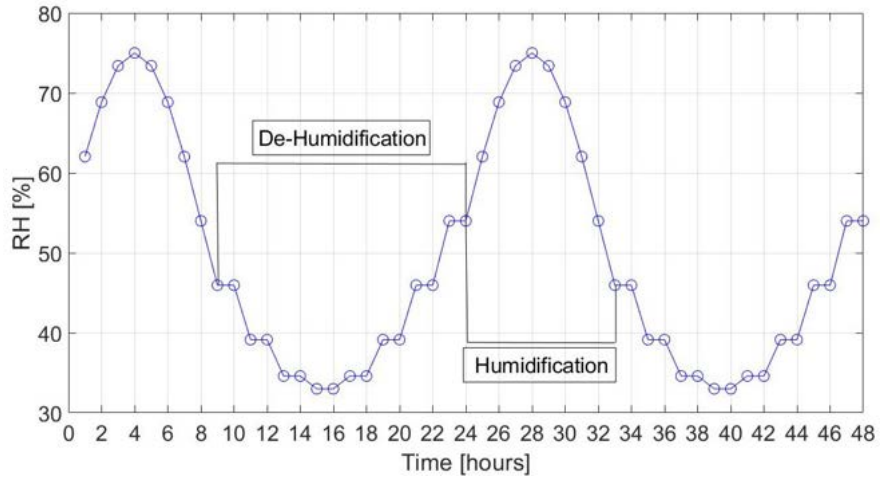

(a)

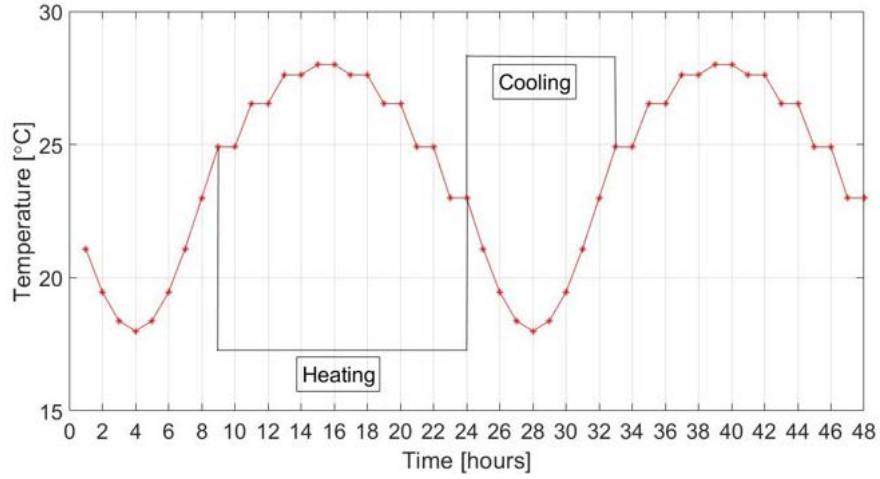

(b)

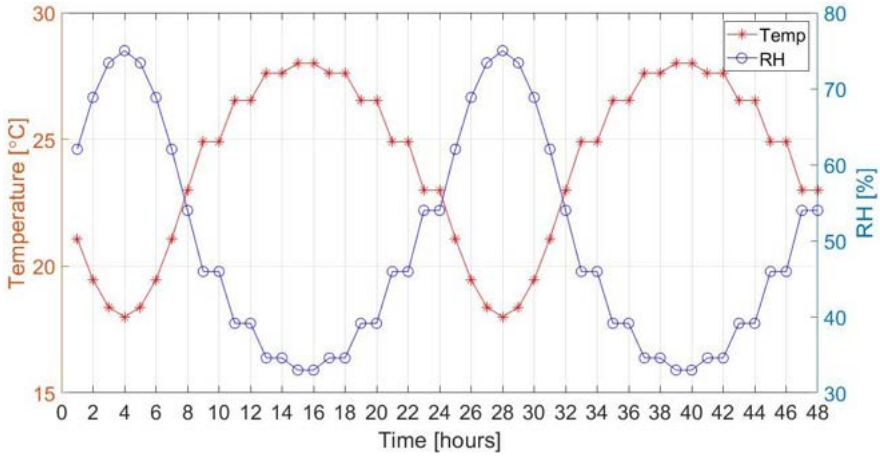

(c)

Fig. 3-32. Relative humidity sinusoidal fluctuation (**a**),temperature sinusoidal variation (**b**) and simultaneous variations (**c**).

3.6.2 Results and Analysis

The results are divided into multiple sub-sections, in which different aspect of the testing were presented. The first sub-section (Section 3.6.2.1) investigates the reliability of the climatic chamber to follow the programmed environmental conditions. In Section 3.6.2.2 the response of the plasters to square and sinusoidal environmental conditions were compared, whilst Section 3.6.2.3 analysed the impact of only temperature and RH on moisture buffering. Section 3.6.2.4 investigates the impact of the simultaneous variation of temperature and RH on the materials.

3.6.2.1 Observation of the Test Chamber Performance

The ability of the climatic chamber to maintain the sinusoidal variation, was compared to the measurements from the Tiny Tag sensors. The independent RH and temperature measurement confirmed that the chamber maintained the desired environmental conditions with only minor deviations. Fig. 3-33 and Fig. 3-34 show the actual average temperature and RH compared with the target curves. In Fig. 3-33a and Fig. 3-33b the temperature followed the programmed curve, showing a sinusoidal trend. It did not perfectly match the maximum and minimum target temperature, but there was less than $0.8°C$ shift, and the amplitude of the temperature fluctuations was preserved. Humidity presented small fluctuation, due to temperature variations. However, RH variations were less than $\pm 1.5\%$, and the average was 1.5% RH higher that the programmed 75%RH (Fig. 3-33a) and 0.5%RH below the programmed 33%RH (Fig. 3-33b). In "RH Sinu 23" (Fig. 3-34a) a better match was found, as temperature is only $\pm 0.4°C$ above the target temperature and there is a good agreement with the RH curve. When temperature and RH vary simultaneously (Fig. 3-34b) similar deviations for the RH curve were observed, but there was a good match for the temperature curve. The actual average temperature and RH compared with the target curves are shown in Fig. 3-33 and Fig. 3-34. Overall, the climatic chamber responded accurately and quickly to the temperature and RH variations.

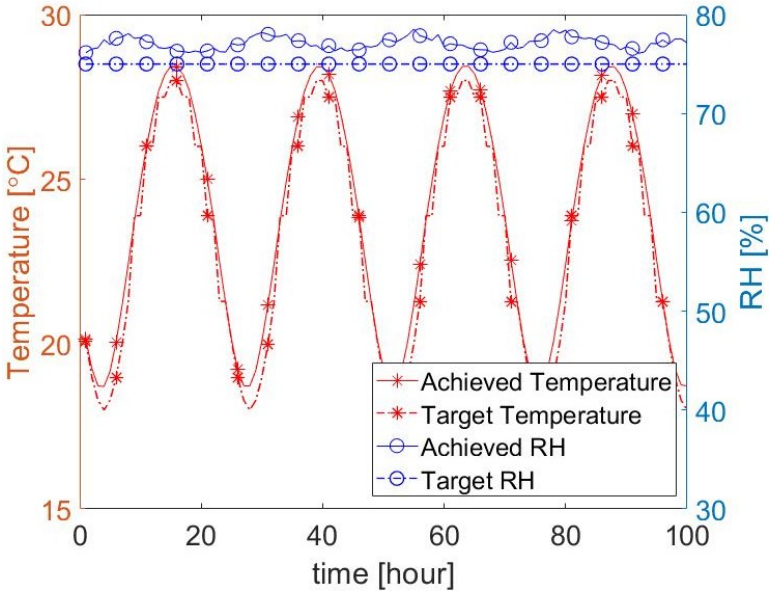

(a)

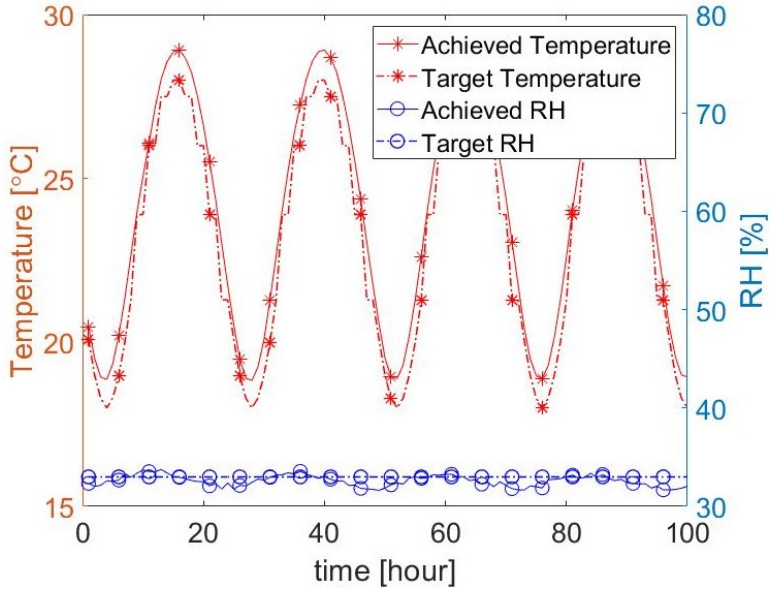

(b)

Fig. 3-33. Temperature sinusoidal variation at 75% (**a**) and 33% (**b**)

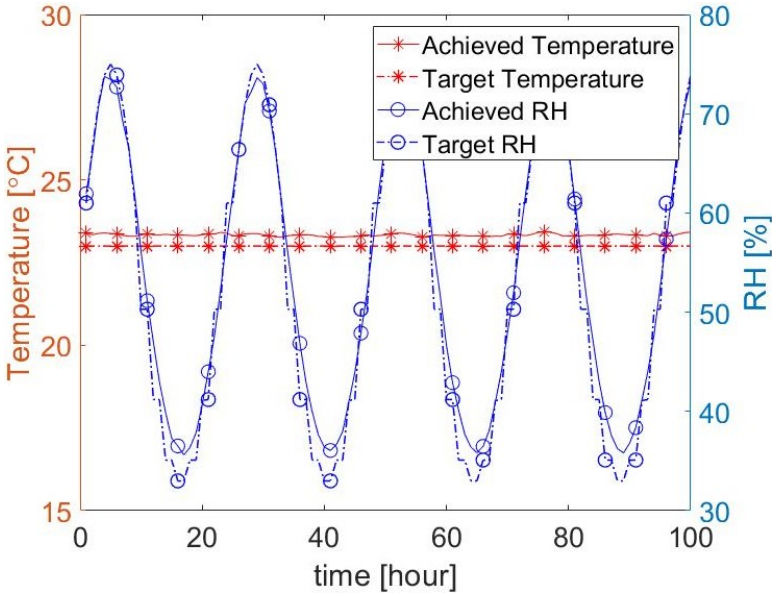

(a)

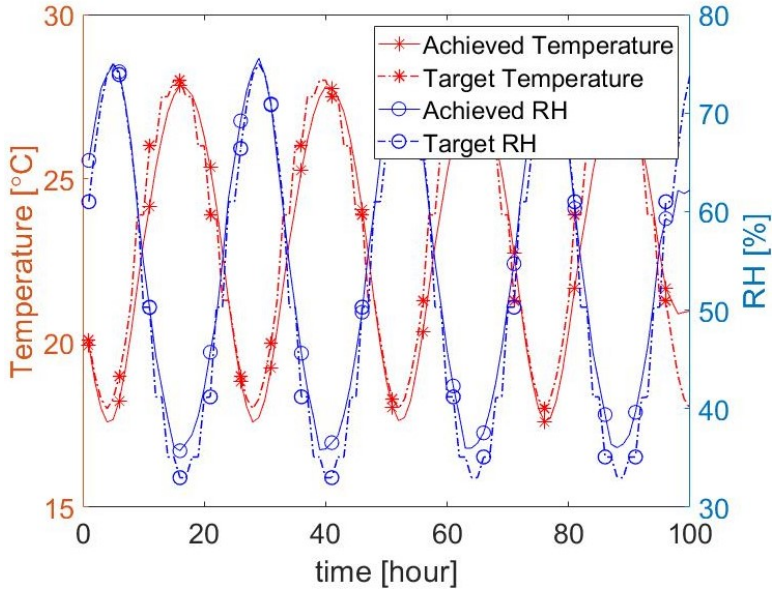

(b)

Fig. 3-34. RH sinusoidal variation at 23°C (**a**); Simultaneous temperature and RH sinusoidal fluctuation (**b**)

3.6.2.2 Comparison square wave and sinusoidal variations

The dynamic sorption curves, obtained by performing a standard square wave test and the sinusoidal tests, were compared in Fig. 3-35. In both cases temperature was kept constant at 23°C and the humidity varied between 75% and 33% RH in 24h. The main difference between the two methods is in the humidification process. In the square wave test humidity instantaneously jumps from high to low (and vice versa), and remains constant for 8 hours of humidification and 16 hours of de-humidification.

In the sinusoidal test the RH slowly moves from 75% to 33%RH. Table 3.20 shows the main differences. When sinusoidal RH variations were applied, the adsorption capacity dropped by 46% for clay and 60% for gypsum. The desorption is less effected by the change of the humidity function, as it was reduced by 14% for clay and 17% for gypsum. The reason of the small impact on the desorption is due to the longer de-humidification phase (16 hours). The transition between RH steps in the desorption can be considered as quasi-steady, as the specimens had a longer time to balance with the environment.

Overall, the moisture buffering capacity under sinusoidal variations was lower than under square wave, presenting lower values for both materials. An important difference is also in the response speed of the specimens to humidity variations. In the square wave tests the specimens quickly responded to humidity changes, presenting a synchronised response of the plasters with the humidity variations. The specimens started releasing moisture at the moment the RH in the chamber dropped to 33% and vice versa. In the sinusoidal test the materials reached the maximum moisture content 2 hours after the RH reached its peak. Accordingly, the materials do not respond as quick as in the square wave test, when humidity gradually changes.

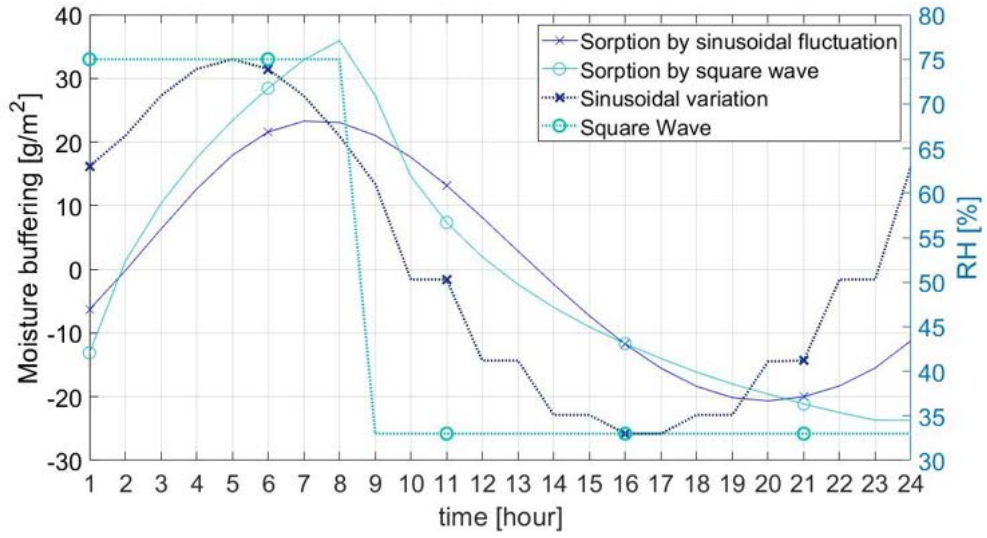

(a) Clay

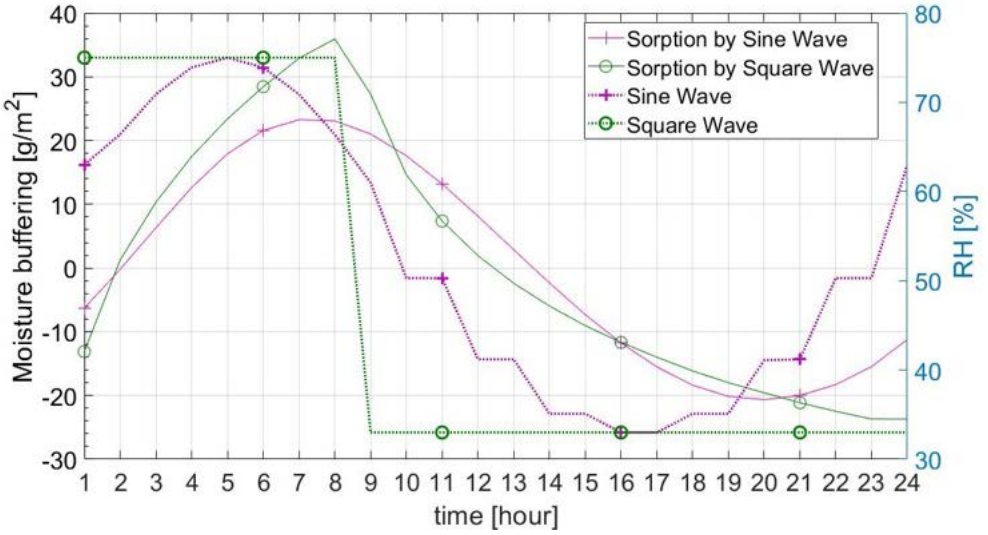

(b) Gypsum

Fig. 3-35. Comparison NORDTEST and sinusoidal RH variation for clay and gypsum

Table 3.20. Sorption capacity and MBV of clay and gypsum under square wave ans sinusoidal humidity variations

Properties	Clay		Gypsum	
	Square	Sine	Square	Sine
Adsorption $[g/m^2]$	33.93±0.4	23.27±0.2	49.48±0.4	30.82±0.9
Desorption $[g/m^2]$	23.70±0.4	20.65±0.2	34.82±0.8	29.07±0.9
MBV $[g/m^2\%RH]$	1.45	1.05	1.95	1.42

The lower sinusoidal MBV reduced the classification of both materials Fig. 3-36. Clay dropped to the lower limit of 'good', while gypsum moved away from the 'excellent' category to 'good'. However, the MBV is applicable only to the NORDTEST and should not be applied to the modified test, as the theoretical assumption of the MBV

are based on the square wave function. Both the *ISO-24353* (2008) and the *JIS A 1470-1* (2002) do not refer to this value and do not use the NORDTEST classification system.

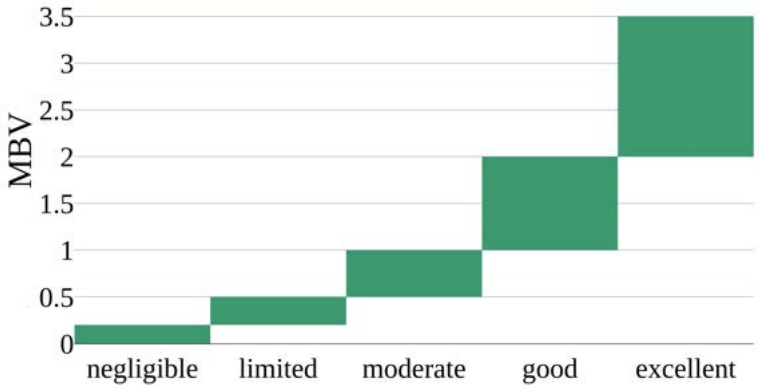

Fig. 3-36. NORDTEST Classification

3.6.2.3 Response of the samples to alternate temperature and RH variations

The gypsum and clay dynamic sorption curve under temperature and humidity variations are shown in Fig. 3-37 and Fig. 3-38. Fig. 3-37a and Fig. 3-37b illustrate the response of clay and gypsum to sinusoidal RH variations at three different temperatures. Temperature clearly influenced the sorption capacity of both materials. High temperatures yielded to a greater amplitude of the curves, while lower temperatures generated a smaller moisture uptake and release. At $28°C$ clay adsorbed 53% more than at $18°C$ and 31% more than at $23°C$ (peak to average). The desorption presented lower values (23.65 g/m^2 at $28°C$ and 15.45 g/m^2 at $18°C$), but there is still an important difference of the moisture buffering capacity between $18°C$ and $28°C$ (53% difference). Overall, the Coefficient of Variation (CoV) at $18°C$, $23°C$ and $28°C$ was below 2.12%, 0.16% and 0.32%, respectively. Gypsum presented a greater moisture buffering capacity than clay, but it was still influenced by the temperature in the same way. It stored and released respectively 23.08 and 20.55 g/m^2 at $28°C$, while its sorption capacity dropped approximately 50% at $18°C$ both in the adsorption and desorption phase, as shown in Fig. 3-37b. The CoV for gypsum at $18°C$, $23°C$ and $28°C$ was below 1.70%, 0.69% and 0.86%, respectively.

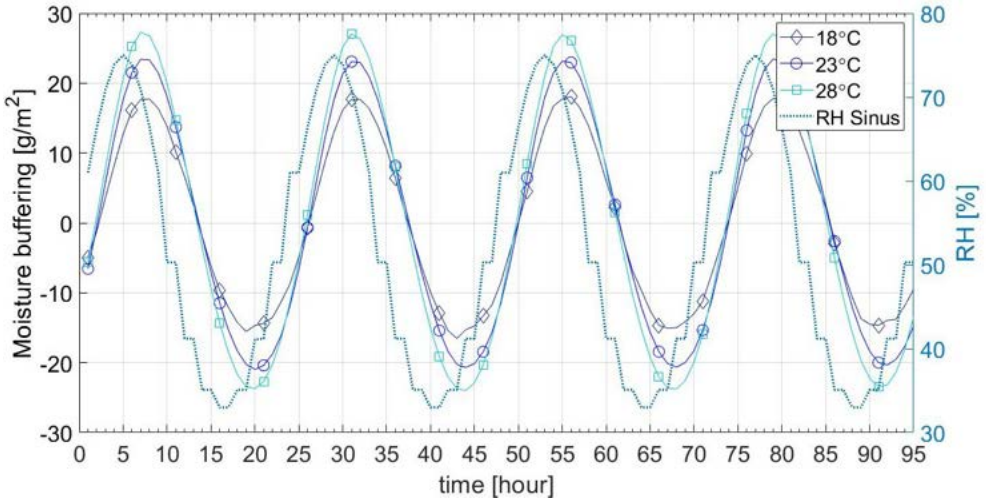

(a) Clay

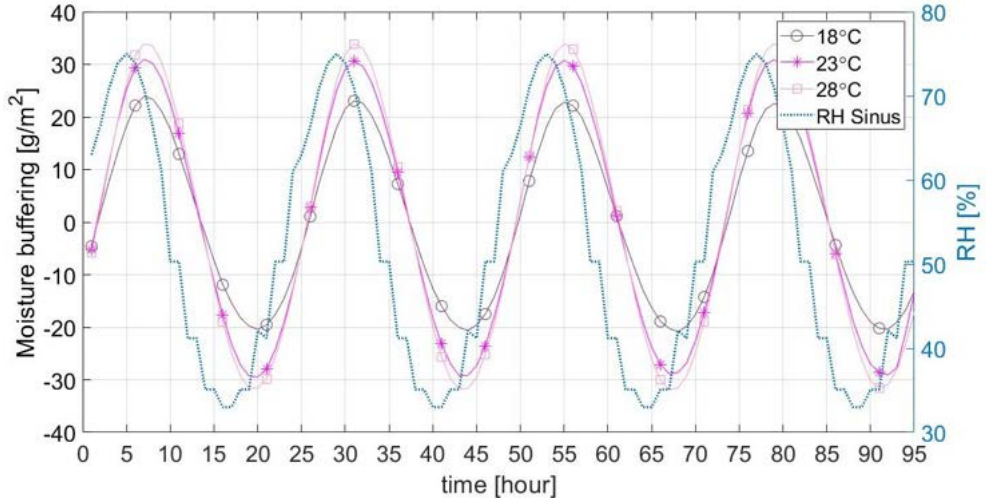

(b) Gypsum

Fig. 3-37. Relative humidity sinusoidal fluctuation for clay and gypsum

Independently to the temperature applied to gypsum, all curves exhibited a delay of around 2 hours in response to RH function peak points, while clay presented a higher lag at lower temperatures. In general, the reason of the lag is due to the short time in the adsorption phase for the specimens to balance their moisture content with the environment humidity. As the water vapour permeability decreases with the temperature (Galbraith et al., 2000), clay may have a lower water vapour permeability at $18°C$. Consequently, it takes longer for the moisture to move into the specimen to balance its moisture content with the environment, which explain the higher delay for clay. In general, this correlation is valid for both plasters, which explains the increase of the sorption capacity with the temperature. However, clay might be less responsive to the environmental conditions, due to its pore composition (Section 3.2.1).

The sorption response of clay and gypsum to sinusoidal temperature fluctuations is represented in Fig. 3-38a and Fig. 3-38b. The curves did not stabilise at 33% and

75% RH, which is likely due to the preconditioning period being too short. Due to the significant temperature difference between the control environment room, where samples were stored, and the testing environmental conditions, the specimens may not balance their moisture content in the 24h preconditioning before the start of the test. However, results were consistent and the sorption amplitude of clay was steady. The average sorption capacity of clay (peak to peak) was 5.45 and 6.82 g/m^2 at 33% and 75%, respectively, with CoV below 5.26% and 8.63%. Similarly, gypsum at 75% had an average sorption capacity of 7.01 and 11.35 g/m^2 at 33%RH and 75%RH with CoV below 3.04% and 3.97%.

Observing the mass variation, when subjected to temperature sinusoidal variations, the sorption capacity in Fig. 3-38a and Fig. 3-38b is significantly lower than under RH fluctuation (83.04% and 82.60% reduction respectively for clay and gypsum). The difference between the curve at 33% and the ones at 54% and 75% was respectively 15% and 78% lower for clay, and 43% and 53% lower for gypsum. The time lag response of the materials to temperature variations was in both cases one hour, as shown in Table 3.21 and Table 3.22. This indicates the sorption curves reach the peak one hour after the temperature peak regardless of the sorption in both coatings. Table 3.21 and Table 3.22 summarises all the results obtained for clay and gypsum specimens. It is clear that other than the influence of the temperature on the sorption capacity, RH has still an important role. By increasing the environmental RH, the moisture transport mechanism of the materials varies. As Holcroft (2016a) demonstrated, materials are sensitive to humidity. As an example, the water vapour permeability of materials increases, when the RH increases, which may indicate a raise of the sorption capacity with RH, due to the possible correlation between vapour sorption isotherm and permeability (Dongdong and Kefei, 2016).

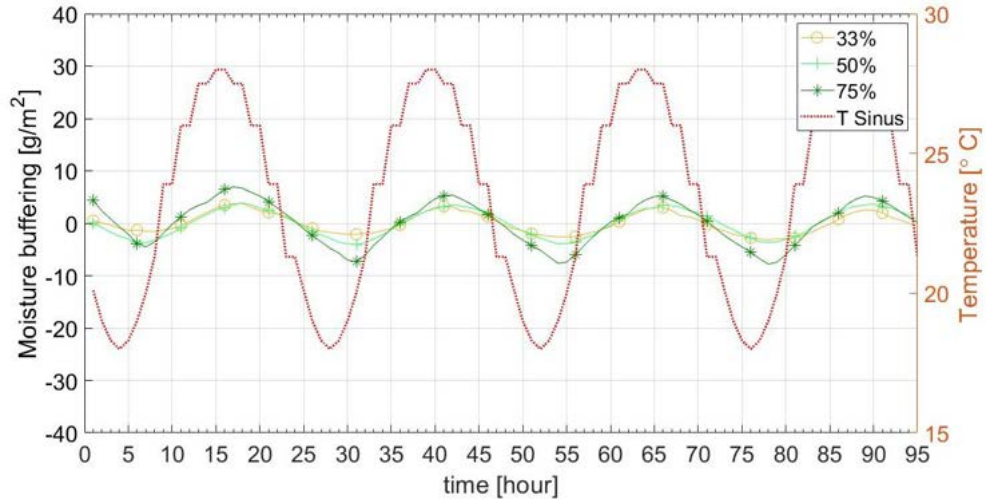

(a) Clay

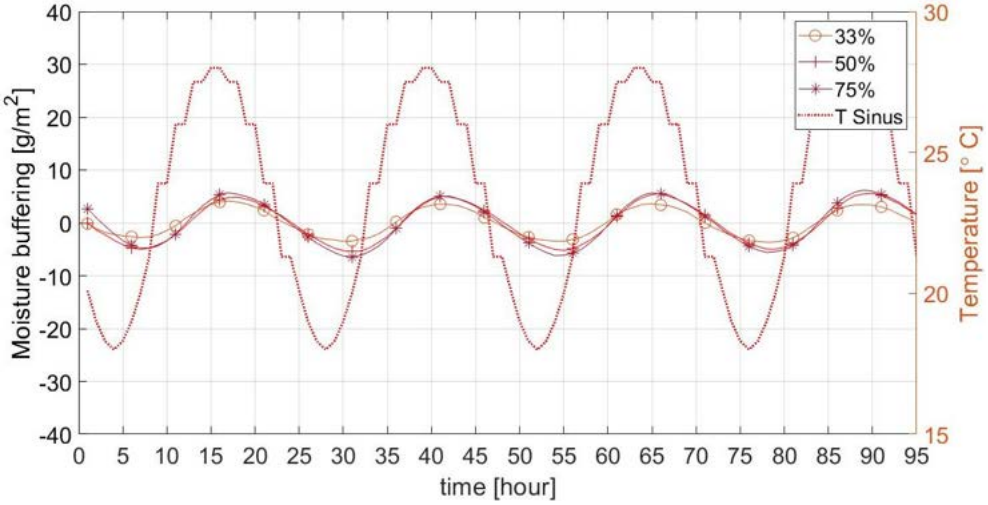

(b) Clay

Fig. 3-38. Temperature sinusoidal variation for clay and gypsum

Friedman's two way analysis of variance was performed, to determine if there is a statistical significance between the three sorption curves at constant temperature or between the three curves at constant RH. A confidence interval of 95% and a significance level of 5% were considered. The null hypothesis was that the distribution of the three sorption curves was the same. The significance value (Adjusted Sigma) was adjusted by the Bonferroni correction for multiple tests. Results showed that in most cases there are statistical differences between the three curves under sinusoidal temperature variations (Fig. 3-38a and Fig. 3-38b) and the ones performed under RH sinusoidal wave (adjusted sigma value below 0.043). Only the distribution of the sorption curves of both clay and gypsum between 33%RH and 54%RH, and the ones for gypsum between 18°C and 23°C were not statistically different. This indicates that differences between 18°C and 28°C and between 33%RH and 75%RH were always significant, whilst differences between 18°C and 23°C and between 33%RH and 54%RH are not always statistically

significant. Therefore, further investigations are necessary for environmental variations below 23°C and 54%RH.

Table 3.21. Results of the moisture buffering analysis of clay alternatively at constant temperature and RH.

Curves	**Adsorption** (g/m^2)	**Desorption** (g/m^2)	**Hygric Lag (h)**
RH Sinu 18	17.75±0.9	15.45±0.8	3
RH Sinu 23	23.27±0.2	20.65±0.3	2
RH Sinu 28	27.08±0.4	23.67±0.4	2
T Sinu 33	3.16±0.5	2.30±0.3	1
T Sinu 54	3.64±0.3	3.80±0.5	1
T Sinu 75	5.63±0.5	6.67±1.5	1

Table 3.22. Results of the moisture buffering analysis of gypsum alternatively at constant temperature and RH.

Curves	**Adsorption** (g/m^2)	**Desorption** (g/m^2)	**Hygric Lag (h)**
RH Sinu 18	23.08±0.7	20.55±0.8	2
RH Sinu 23	30.82±0.9	29.07±0.9	2
RH Sinu 28	33.93±0.7	31.73±0.7	2
T Sinu 33	3.68±0.4	3.24±0.8	1
T Sinu 54	5.28±0.5	5.14±0.5	1
T Sinu 75	5.66±0.6	5.70±0.6	1

3.6.2.4 Response of the samples to simultaneous temperature and RH variations

The response of clay and gypsum to simultaneous temperature and RH variations is shown in Fig. 3-39. It is evident that by storing 33.43 and releasing 34.20 g/m^2 gypsum performed better than clay (11.78 and 14.82 g/m^2 more than clay).

The time lag of the two curves both present 4 hours delays with respect to the RH sinusoidal curve. This is more than the delay of the sorption curve under RH sinusoidal fluctuation (2h) and the delay of change in mass of specimens under temperature sinusoidal variation (1h).

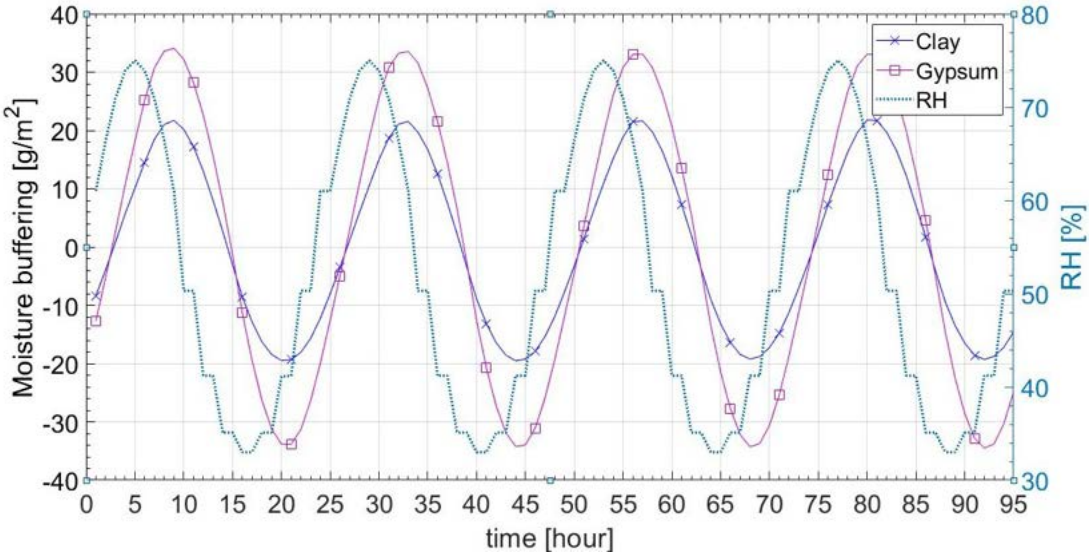

Fig. 3-39. Mass change of clay and gypsum, when subjected to simultaneous temperature and RH variation.

The "TRH Sinu" curves were compared with the "RH Sinu 23" and "T Sinu 50", to try to identify the impact of temperature and RH on the sorption capacity. The "TRH Sinu" curves had similar behaviour of the "RH Sinu 23" curves for both materials, whilst "TRH Sinu" showed an opposite trend of "T Sinu 50" (Fig. 3-40). However, "RH Sinu 23" did not perfectly match "TRH Sinu" in both cases. Clay "RH Sinu 23" adsorbed and releases 7.50% and 6.55% more moisture than "TRH Sinu", while for gypsum 8.50% and 17.61% less. The hygric lag is also different, presenting in both cases 2 hours delays between the "TRH Sinu" and "RH Sinu 23". It is evident temperature did not interfere significantly with the sorption capacity of the materials, but it delayed the response speed of the plasters to humidity variations.

The two plasters presented a different behaviour in the sorption process. The effect of the temperature variations on "TRH Sinu" reduced the sorption capacity of clay, while gypsum improved its moisture buffering capacity, when temperature varies sinusoidally. The discrepancy in the materials' behaviour, can be due to the plasters' porous structures and size. As Bennai et al. (2016) explained, moisture transport, which includes either vapour and liquid transport mechanisms, depends on to the pore geometry. Water vapour transport takes place in the macro-pores and its driving potential is the water vapour pressure, whilst liquid transport takes place in the micro pores, where the driving force can either be the relative humidity and the capillary pressure (Künzel, 1995; Scheffler and Plagge, 2010). The clay is mainly composed of macro-porous, which are mainly responsible of the water vapour transport. Gypsum is more sensitive to moisture and temperature (Murat and Attari, 1991), because it has both micro and macro-pores, which activated both the vapour and liquid transport simultaneously.

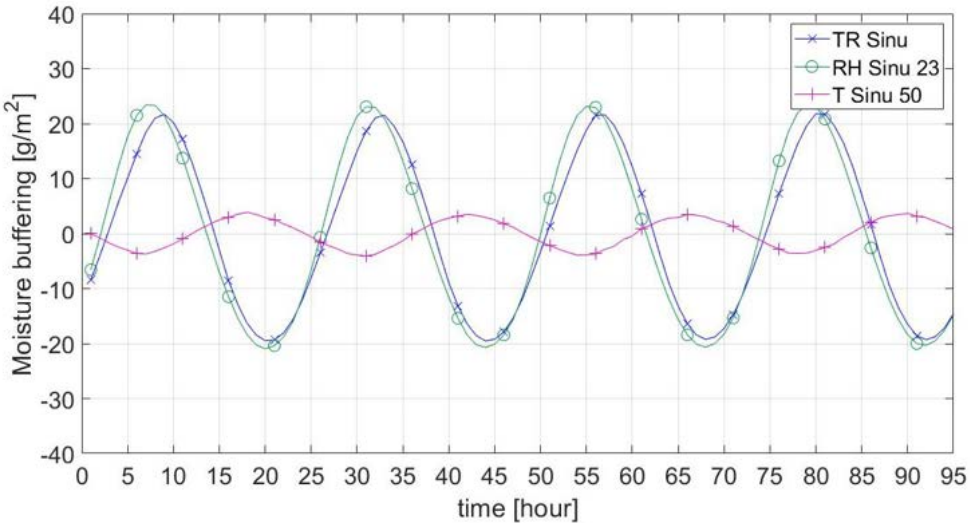

(a) Clay

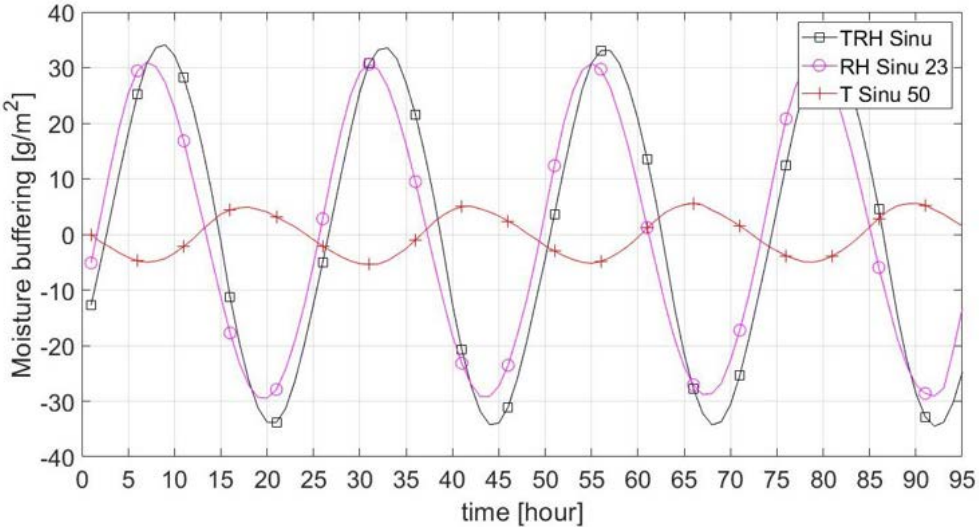

(b) Gypsum

Fig. 3-40. Measured mass change of clay and gypsum at simultaneous temperature and RH compared with mass change at 23°C and 54% RH

3.6.3 Discussions

To predict the behaviour of the coatings to simultaneous temperature and RH sinusoidal variation, the mass change curves, exposed respectively to variable temperature and constant RH, and variable RH and constant temperature, were arithmetically averaged. The predicted curves were then compared to the experimental results. The "TRH Sinu" test were performed by simultaneously varying the temperature and RH.

3.6.3.1 Modelled Sorption Curve

It is clear that the most important environmental factor in moisture buffering is the humidity level (specimens adsorbed more than 80% more moisture, when humidity varies), as shown in Fig. 3-40. Temperature still influences the response in the plaster, as its fluctuation impacts the moisture sorption and it delays the materials' response. The effect of the temperature and RH simultaneous varying may result in a combined effect on the moisture sorption capacity, as shown by "TRH Sinu" in Fig. 3-39. To investigate the individual effects of these two factors on samples subjected to dynamic temperature and RH fluctuation, the sorption curves at constant temperature were arithmetically combined with the sorption curves at constant RH, as shown in Fig. 3-41. Five curves were generated, by averaging the curves obtained at three different temperatures (Fig. 3-38a and Fig. 3-38b) and the curves at three different RH (Fig. 3-37a and Fig. 3-37b).

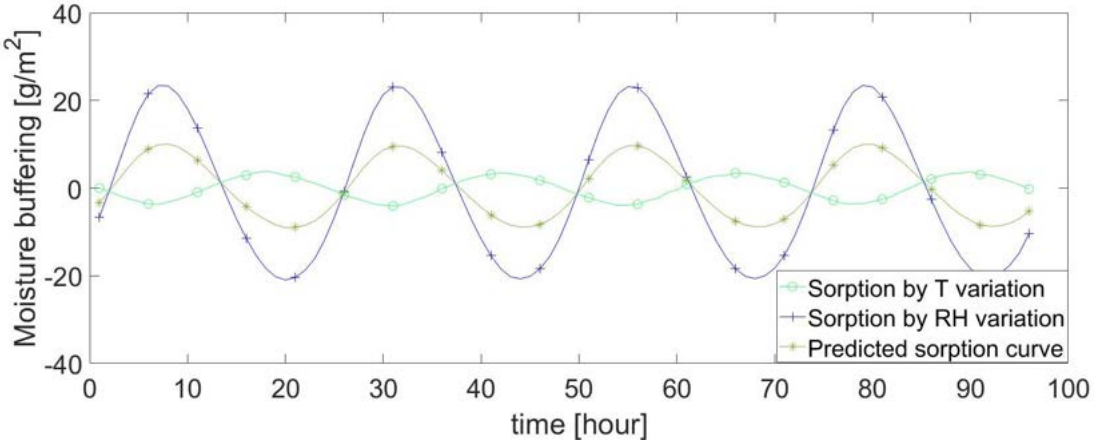

Fig. 3-41. Example of predicted curve with combined RH and temperature variation of gypsum

The results of some of the predicted curves are shown in Fig. 3-42. The results were obtained from the averaging of the experimental sorption curves for clay (Fig. 3-42a) and gypsum (Fig. 3-42b), while Table 3.23 and Table 3.24 represent the data for all the predicted curves. Dry and Humid correspond respectively to 33% and 75% RH respectively, and Cold and Hot to 18°C and 28°C. With this method it was possible to directly compare the measured sorption curve in Fig. 3-39 with the predicted ones, indicating how materials perform in different climates.

The combination of RH and temperature variation reduced the sorption capacity in the predicted curves than in "TRH Sinu", and in most cases it did not shift the time response of gypsum, whilst for clay the delays increased when the temperature and humidity decreased, as shown in Table 3.21 and Table 3.22. When the temperature was lower, the sorption capacity decreased independently of the humidity level (Table 3.23 and Table 3.24). Moreover, clay and gypsum responded better to humid environmental

conditions rather than dry, due to their sensitivity to the moisture.

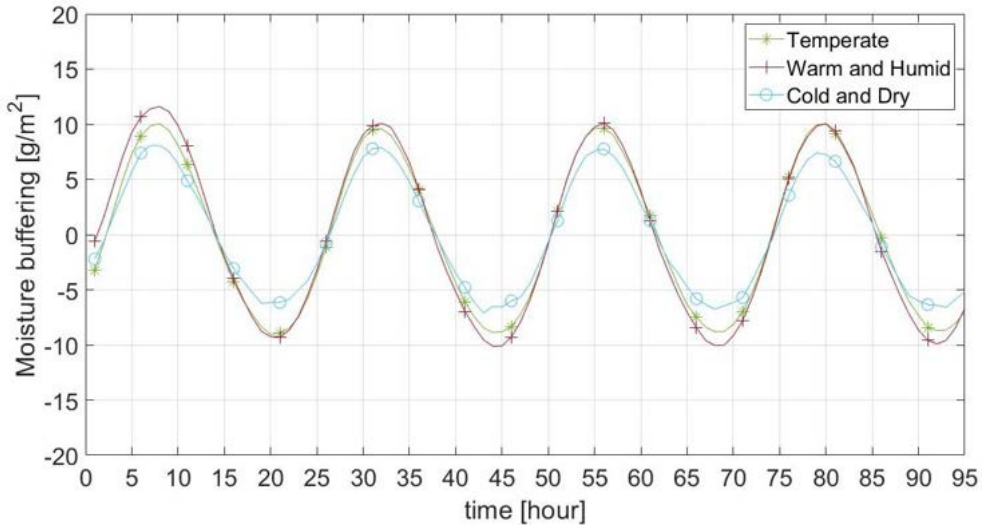

(a) Clay

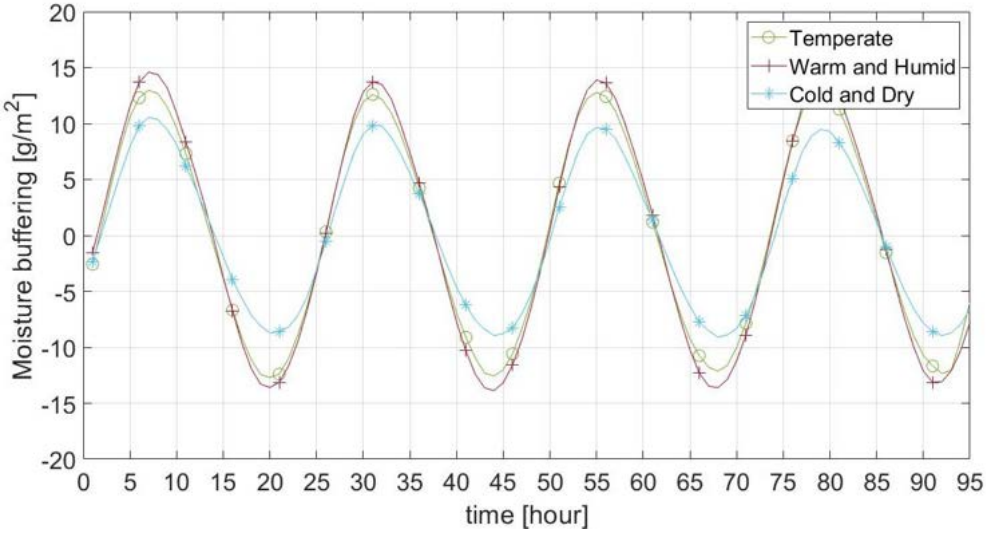

(b) Gypsum

Fig. 3-42. Predicted sorption curves for clay and gypsum

Table 3.23. Theoretical results of the moisture buffering analysis of clay.

Curves	**Adsorption** (g/m^2)	**Desorption** (g/m^2)	**Hygric Lag (h)**
Cold and Dry [$18^oC33\%$]	6.±0.2	5.68±0.3	4
Cold and Humid [$18^oC75\%$]	7.74±0.2	6.50±0.3	3
Mild [$23^oC50\%$]	9.82±0.2	8.85±0.3	3
Warm and Dry [$28^oC33\%$]	10.46±0.2	9.83±0.3	3
Warm and Humid [$28^oC75\%$]	12.39±0.2	10.93±0.3	2

Table 3.24. Theoretical results of the moisture buffering analysis of gypsum.

Curves	**Adsorption** (g/m^2)	**Desorption** (g/m^2)	**Hygric Lag (h)**
Cold and Humid [$18^oC33\%$]	8.69±0.3	8.10±0.4	2
Cold and Dry [$18^oC75\%$]	9.88 ±0.3	8.93±0.4	2
Mild [$23^oC50\%$]	12.84±0.3	12.44±0.4	2
Warm and Humid [$28^oC33\%$]	14.12±0.3	13.53±0.4	2
Warm and Dry [$28^oC75\%$]	15.30±0.3	14.36±0.4	2

3.6.3.2 Comparison between the Measured and Predicted Sorption Curve

The mild curve was taken as reference for the comparison with the measured sorption curve both for clay and gypsum, as it was hypothesised that the experimental curve had comparable average boundary condition than in the "mild" predicted curve (average temperature and RH were $23°C$ and 54%).

The differences between the predicted and measured sorption curves are illustrated in Fig. 3-43. It is evident that the mean curve, obtained by averaging the sorption curve at constant temperature and the one at constant RH, is not representative of the experimental curve, obtained when materials were subjected to simultaneous temperature and RH variations. The measured curve for clay adsorbed peak to peak 22.38 (g/m^2) more with respect to the calculated one (Fig. 3-43a). In gypsum this difference was more noticeable, as the predicted curve adsorbed 42.34 (g/m^2) less (Fig. 3-43b).

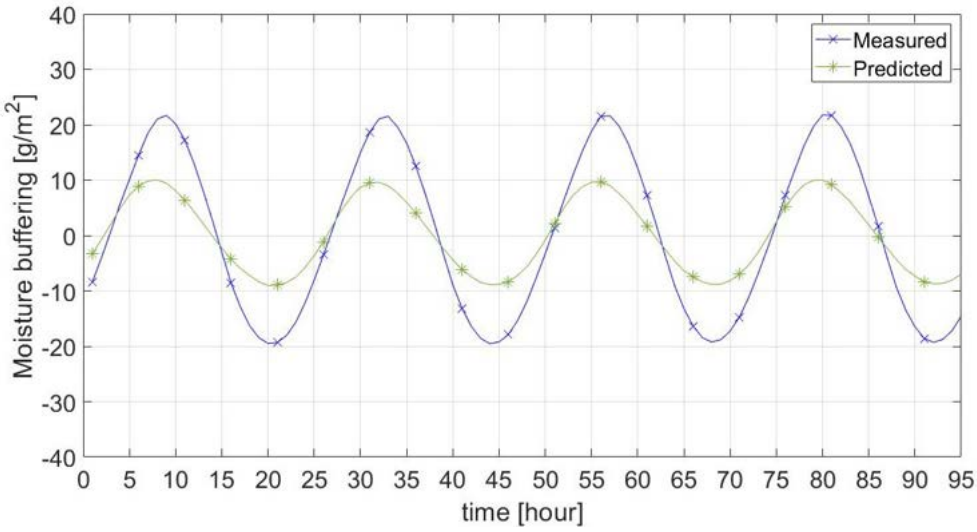

(a) Clay

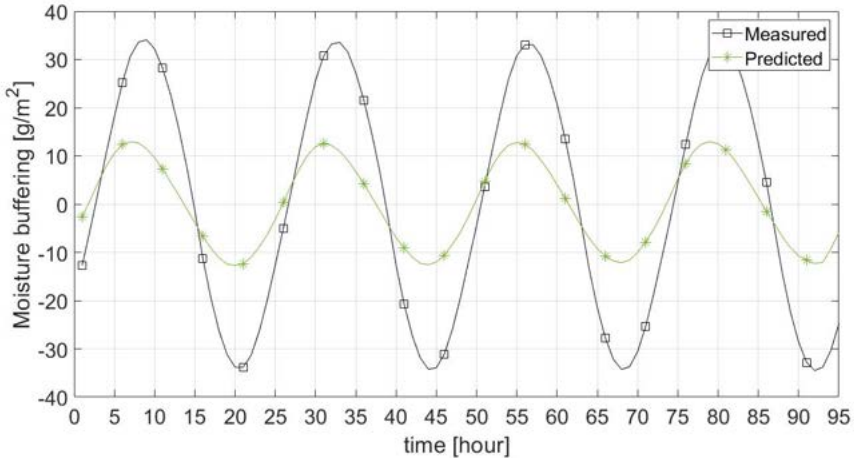

(b) Gypsum

Fig. 3-43. Measured mass change of clay and gypsum at simultaneous temperature and RH compared with the combined mass variation curves

The reason of this discrepancy is likely due to the pore structure and moisture transport mechanisms activated, due to the simultaneous temperature and RH fluctuation. The sorption capacity of gypsum with its higher percentage of micro-pores might be more influenced by the temperature variations As Peuhkuri, Rode and Hansen (2008); Yi et al. (2016) demonstrated, liquid transport is sensitive to temperature, as the water vapour permeability is effected by temperature at high RH levels. It was found that as temperature increases so does the permeability, showing bigger variation in materials with high porosity. This would explain the increase of the gypsum sorption capacity, when also temperature varied.

Feng and Janssen (2016) highlighted there might be temperature influences in the vapour sorption process (in particular during the desorption), but there it was not consistent with all materials, probably due to their pore structure. However, studies

for the verification of the temperature effect on moisture transport were carried in steady state environments, as the determination of the water vapour permeability by following the dry and wet cup test procedures for (Galbraith et al., 2000; Peuhkuri, Rode and Hansen, 2008) demonstrates. In a dynamic environment, it is necessary to consider the continuous variation of sorption isotherm, due to the continuous temperature variations. The moisture content balance changes each temperature step, as well as the water vapour permeability. The variable RH also influences the permeability, especially at higher RH levels (Holcroft, 2016a). Above 55% the permeability increases exponentially with the humidity. The simultaneous variation of both environmental parameters may activate other processes, and, as Yi et al. (2016) highlighted, temperature and pore geometry might produce independent effects on the hygric properties. Even though it is not possible to define the overriding influence of a specific pore size range (Lagouin et al., 2019), it is evident that a greater volume of pores in the micron-range increase the vapour permeability, sorption isotherm and moisture buffering capacity of hygric properties of the materials, independently from the temperature.

In conclusion, the predicted "mild" curve, average of "T Sinu 54" and "RH Sinu 23", might not be representative, as liquid transport were not considered. Giving the same weight to temperature and humidity variations in the empirical approach is not indicative of the real response of materials to simultaneous environmental variations.

Table 3.25 shows the adsorption, desorption and MBVs of the predicted and experimental curve. Both cases presented a MBV below the moderate class in the NORDTEST classification (Fig. 3-36), and gypsum and clay moisture buffering capacity was significantly lower than the equivalent values obtained in the standard NORDTEST and (Table 3.20), if square wave variations were applied on the same materials. The MBV classification and MBV values are not effective to dynamic temperature environments, as the theoretical formulation of the MBV is based on the assumption temperature is constant and materials' performances varies linearly with (Rode et al., 2005).

Table 3.25. Adsorption $[g/m^2]$, Desorption $[g/m^2]$ and MBV $[g/m^2\%RH]$ obtained from the predicted and experimental sorption curve

Curves	Clay			Gypsum		
	Adsorption	Desorption	MBV	Adsorption	Desorption	MBV
Mild	9.82±0.2	8.85±0.3	0.44	12.84±0.3	12.44±0.4	0.60
T Simu	21.65±0.2	19.38±0.2	0.98	33.43±1	34.20±0.9	1.61

3.7 Summary

Hygric properties and moisture buffering capacity of coatings (clay, lime, gypsum and plasterboard and hemp-lime) were determined experimentally. Density, porosity, water vapour permeability, sorption capacity and thermal conductivity were measured and compared with moisture buffering, calculated performing the NORDTEST procedure in a climatic chamber. The laboratory test showed gypsum stored and released more humidity than the other materials, due to the presence of micro-pores, and the consequent activation of liquid transport together with the water vapour transport in the macro-pores. A direct correlation between moisture buffering and hygric properties was found, which highlighted a significant correlation between porosity and the dynamic sorption capacity.

Clay and hemp-lime were tested, by applying the NORDTEST protocol and moving the samples in six locations in the climatic chamber, which presented different air velocities. The aim was to observe how materials' moisture buffering performance varied, by simply moving the sample around the climatic chamber, where different air velocities were recorded with an omni-directional anemometer. Moisture buffering test is sensitive to the air speed, as variation across the chamber may generate different moisture surface resistances on the materials and, consequently different moisture buffering results. The air velocity transducer measured higher air velocities on the top and back of the climatic chamber, but no significant correlation with moisture buffering was found. Even though the testing needed to be completed, the study highlighted the reliability of the climatic chamber to produce repeatable measurements, as it did not generate significant air velocities differentials, which might effect results. However, in all spots air velocity is always higher than the prescribed 0.1 m/s in the protocols.

The clay and gypsum were exposed to a modified NORDTEST protocol, where the specimens were subjected to different temperatures, other than the prescribed $23°C$. Results showed a direct correlation between moisture buffering and temperature, which is more significant in gypsum, due to the dependency of micro-pores liquid transport to temperature variations. As the impact of temperature variations on moisture buffering was not known, two other tests were performed. Specimens were exposed to variable temperature at constant RH and simultaneous temperature and RH square variation. When only temperature varied, the temperature was responsible of the initial increase of the plasters sorption capacity, as the quick change of the temperature during the test generated a disruption of the moisture balance between the specimens and the environment. When the moisture content in the environment stabilised together with the temperature, the materials did not present change in mass. Even though the impact of temperature may be considered negligible in this case, further study on the impact of plasters on the environment may highlight the importance of this finding. For example, when heat sources are turned on or off in buildings, creating a sudden increase

or decrease of temperature, plasters may help the room to regulate instantaneously the indoor RH.

When temperature and RH vary simultaneously, the response of the materials showed that moisture buffering performances were effected by temperature, but clay and gypsum responded differently to the variable environmental condition, due to their different pore structure. Gypsum with its complex pore structure, increased its moisture buffering, due to the higher impact of temperature on liquid transport. The RH and temperature gradient activated capillary transport and surface diffusion, when gypsum was subjected to simultaneous square wave variation. On the contrary, the moisture buffering capacity of clay was reduced probably due the combined effect of the saturation of macro-pores at high RH and impact of low temperature on the hygric properties.

The method of investigating a material moisture buffering capacity was further investigated by applying sinusoidal variation rather than square step functions. The modified test considered indoor RH as a quasi harmonic function, and introduces also the influence of sinusoidal temperature variation (opposite to RH) on moisture buffering. Similarly to the square wave tests, the tests were first performed at constant temperature and variable RH and at constant RH and variable temperatures, to understand the effect of temperature and RH sinusoidal variation on the specimens individually. Clay and gypsum showed similarity in their adsorption capacity, when subjected to sinusoidal variation at constant RH and constant temperature: when increasing temperature or RH, the materials' dynamic sorption capacity increased. Temperature did not impact the adsorption and desorption capacity of materials as much as humidity. On the contrary, temperature delayed materials' response to humidity changes. However, when temperature and RH changed simultaneously, differences between the response of clay and gypsum were observed, which can only be attributed to the activation to other processes related to the materials' porous structure and temperature influence. Overall, it can be stated:

- There are significant differences when RH variations do not follow a quasi steady function, as in the NORDTEST. Quick variation of the RH function leads to incapacity of specimens to reach the balance, causing hygric lags.
- Temperature effects both the sorption capacity and hygric lag, due to its influence on the sorption isotherm, water vapour permeability and moisture transport mechanisms. In general, increasing the temperature increases the equilibrium moisture content of materials at constant RH.
- RH has an effect on the moisture buffering capacity of the materials, effecting mainly liquid transport mechanisms. Increasing the RH increases the dynamic sorption capacity of materials.

- When temperature and RH varies simultaneously the pore structure and temperature impact the way materials adsorb moisture. It is necessary to further understand the impact of either pores and temperature on moisture buffering, as it was demonstrated their relevance in the moisture transport. However it is not clear whether these factors influence independently or jointly moisture buffering.
- As the NORDEST prescribes an isotherm environment, the MBV is not be applicable in a dynamic realistic scenario. For this reason, temperature variation should be integrated in the formulations of MBV, as different temperatures lead to different material's responses. It is also necessary to consider the hygric lag, as complementary parameter for the understating of the dynamic sorption capacity of materials. However, further analysis on the joint variation of the moisture transport mechanisms and equilibrium moisture content in variable environments should be performed.

4. *Full Scale Testing*

In laboratory testing, moisture buffering is considered as an independent variable, which is not influenced by other moisture transport and moisture exchange mechanisms (such as ventilation). On the contrary, in computational modelling moisture buffering is usually considered as part of the heat and moisture transport through the enclosure (Künzel et al., 2004), and not considered as an individual factor. Moisture buffering is clearly a property that relates to materials applied on the indoor surface (Rode et al., 2002; Maskell et al., 2018), but its impact on the whole building's moisture exchanges, and the interaction between moisture buffering and other moisture transport mechanism should be investigated. For this reason, it is important to identify the main factors that contribute to the indoor moisture balance and find their impact and relationship with moisture buffering.

There are multiple parameters to consider when looking into the moisture balance in buildings including infiltration, ventilation, and external weather conditions, as discussed in Section 2.5. Kraniotis et al. (2015) considered infiltration rate as an influencing phenomena on moisture buffering, as air leakages help finishing materials to dry faster. However, as the moisture exchange relies on the variable outdoor weather condition, it is possible that building infiltration transports humidity from the outdoor to the indoor, or vice verse, reducing or amplifying moisture buffering.

Yoshino, Mitamura and Hasegawa (2009) highlighted the direct impact of ventilation on moisture buffering. Higher the air speed and ventilation rate, lower is the sorption capacity of finishing materials, until a maximum ventilation rate is reached, which, as Kalamees et al. (2009b) stated, makes moisture buffering impact in houses negligible. Ventilation can also add or remove moisture in buildings, depending on the outdoor weather conditions and the environmental conditions differential between the indoor and outdoor. In wet or rainy locations, ventilation moves the moist air indoors, while in dry environments, the indoor moisture migrates outdoors. It is evident that the outdoor weather influences the indoor environment (specifically the humidity). Consequently, the geographical location of the buildings is always to be considered, when analysing moisture buffering, as demonstrated by Nguyen, Schwartz and Dockery (2014) through statistical linear correlation between indoor and outdoor environmental conditions from experimental data.

In this chapter, a study on the impact of building infiltration, ventilation and weather variations on moisture buffering were analysed. Three full scale single room buildings (test cells) were monitored, so that one room could be used as reference room (non-hygroscopic) and the comparison of the other two could give a better control of the consistency results. Each room presents a different wall design with same finishing material (gypsum plasterboard), which allowed a comparison of the behaviour of the three test rooms at different sources of humidity and to isolate the moisture buffering involvement to balance humidity from building infiltration and ventilation. Infiltration was analysed through a decay test, when rooms were sealed and no ventilation system was installed. Ventilation was analysed successively together with moisture buffering tests. The impact of the weather on the indoor environmental conditions was analysed through the whole testing campaign. In order to make results between full-scale and laboratory scale comparable, moisture decay and buffering tests were performed, following NORDEST time-steps (Rode et al., 2005), as discussed in Section 3.3. The tests results were successively used in Chapter 5, to build an indoor moisture balance equation, which quantified the moisture buffering contribution of gypsum plasterboard. The aim of this chapter is to quantify the moisture buffering capacity of hygroscopic materials in a realistic full-scale environment, to successively use the testing results in the laboratory testing to modify or introduce a protocol that quantifies the impact of the materials on the environment. Table 4.1 shows a summary of the tests performed in this chapter.

Table 4.1. Summary of the tests performed in this chapter

Tests	Aim	Expectation
Instantaneous Injection	Evaluate the suitability of the test cells for the moisture buffering testing	Find significant differences in the moisture moderation between the hygroscopic/non-hygroscopic cells
Moisture Decay	Quantify the impact of walls to moderate the indoor moisture content	Quantify the moisture buffered by the walls, by comparing the hygroscopic/non-hygroscopic cells
Moisture Decay: Statistical correlation humidification/weather	Investigate the impact of outdoor weather on the indoor moisture variations during the humidification	Find a significant correlation between the humidifier moisture load variations and outdoor environmental variations
Moisture Decay: Statistical correlation de-humidification/weather	Investigate the impact of outdoor weather on the indoor moisture variations during the de-humidification	Quantify the impact of the outdoor weather on the moisture decay and find a significant correlation between the de-humidification curve and weather variations
Moisture Decay: Statistical correlation between the test cells	Compare the three test cells during the de-humidification	Find significant differences between the three room to extrapolate the walls intervention in the moisture regulation
Moisture buffering at constant temperature	Reproduce the NORDTEST test set up in a realistic full-scale environment	Calculate through moisture balance equation the moisture buffering capacity of walls and find differences with the NORDTEST to then implement changes in the protocol
Moisture buffering at variable temperature	Investigate the impact of temperature variations on the moisture buffering capacity of walls	Find a significant reduction of the moisture buffering capacity of walls in an conditioned environment
Correlation laboratory/ full-scale testing	Compare moisture buffering of specimens of the same materials in laboratory and full-scale	Find significant discrepancy between NORDTEST protocol applied in full-scale and laboratory environment

4.1 Test Cell Case Studies

Three test rooms, located at the University of Bath's BRP, Wroughton, UK were selected (Fig. 4-1). Fig. 4-1a presents the three of the five cells tested in this study (Fig. 4-2), which were built in 2016 for the HEMPSEC project. HEMPSEC is an European Union project aimed at expanding the market for a pre-fabricated system of hemp-lime construction (HEMPSEC, 2014). The test cells external dimension are 4.34 m x 4.34 m x 2.94 m high, while the internal dimension is defined by the walls thicknesses, which differ for every room (Table 4.2), so that a consistent design U-value of $0.15\,W/m^2K$ could be assigned to each room. Floor and ceiling are timber sandwich panel structure of PIR insulation and particle board with a total thickness of 350 mm (Fig. 4-1b). Floor and ceiling have a calculated U-value of $0.10\,W/m^2K$, determined following the *BN EN ISO 6946* (2007). Fig. 4-3 shows the three typologies of cells enclosures. The floors, ceilings and doors were covered with an impermeable layer, to ensure that the room moisture balance was not affected by the particle board. The PIR insulated timber structure was entirely covered by an impermeable sheet ($s_d = 4000m$), in order to use it as reference room or as room, which does not have any moisture buffering property.

Table 4.2. Internal dimension of the test building

Rooms	Width [m]	Height [m]	Wall Surface [m^2]	Volume [m^3]
PIR	3.82	2.4	14.59	35.02
Concrete	3.54	2.4	12.53	30.08
Wood Fibre	3.63	2.4	13.16	31.60

(a) Outdoor (b) Indoor

Fig. 4-1. Test buildings

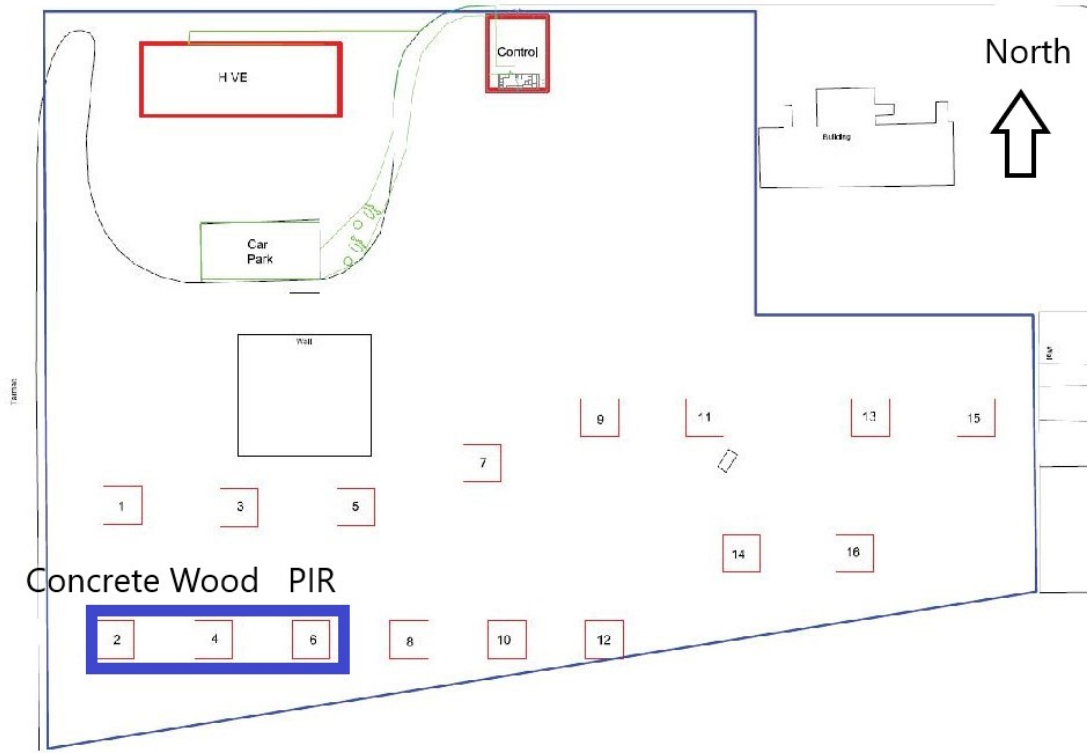

Fig. 4-2. Plan of the BRP and the location of the three testing rooms

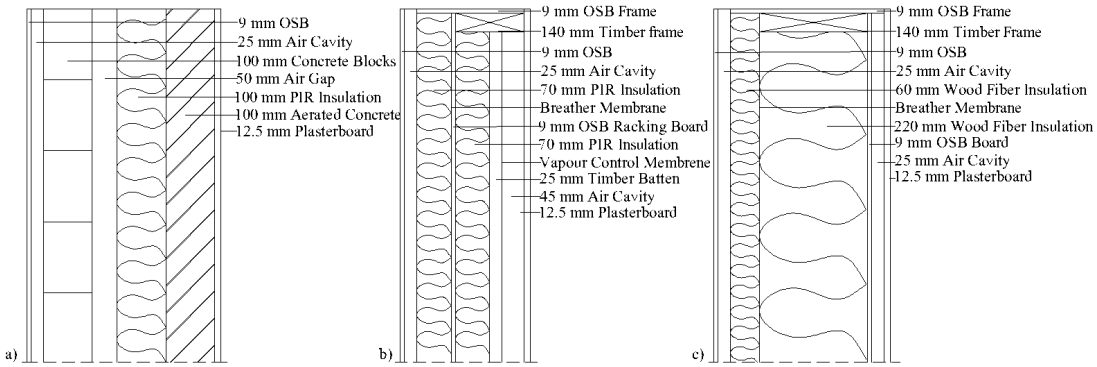

Fig. 4-3. Section of the test cell walls a) Concrete Blocks Cell, b) PIR insulated timber cell, c) Wood fibre insulated timber cell

4.2 Test Room Set Up

Rooms were equipped with 240 W heaters and thermostat (Inkbird ITC-308), to keep the temperature inside the room at 23°C (±0.4°C). Each room temperature and RH were monitored by four Campbell Scientific (CS) CS215 sensors ($\pm 0.4°, \pm 2\% RH$). One sensor was placed in the middle of the room, and the other three were placed at three different height (500 mm, 1200 mm and 1700 mm from the floor) in a corner (the North-West for moisture decay and South-West for moisture buffering) of each room at 500 mm from the walls. Before testing, temperature and RH were monitored across

the cells and it was assured by moving the sensors across the rooms, temperature and RH were uniformly distributed (Fig. 4-4). The temperature fluctuation are due to the heater turning on and off.

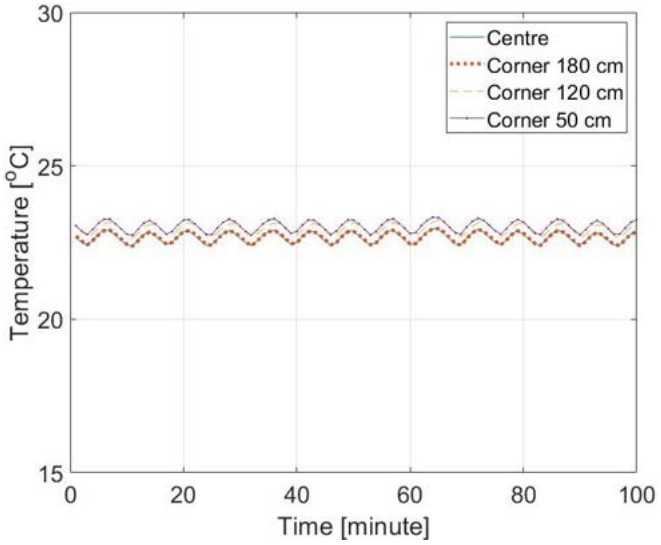

(a) Temperature

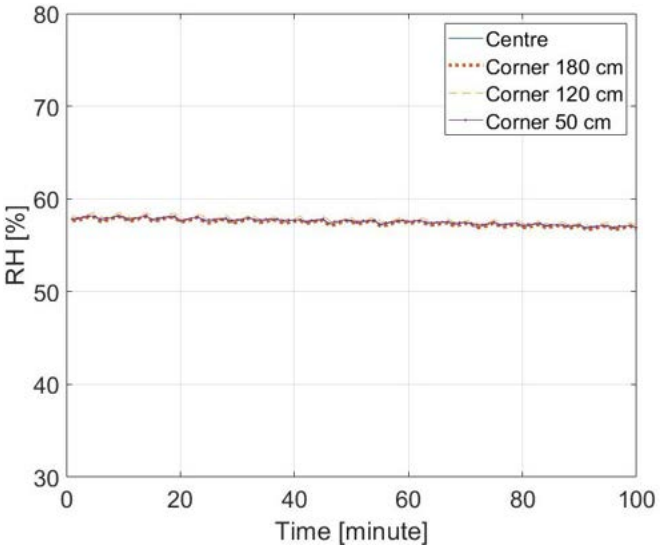

(b) RH

Fig. 4-4. Temperature (**a**) and RH (**a**) in the wood fibre room

A fan was used to mix the air and an energy meter was used, to monitor how often fan and heaters turned on and off. The U-value of the walls was measured on the North wall, to remove the influence of solar radiation on the measurement. Two heat flux plates (HukseﬂuxHFP01), two Type-T thermocouples and a thermistor (CS 107) were used to measure the heat flux and the indoor and outdoor surface temperature, respectively. Walls have a measured U-value of $0.31\,W/m^2K$ for the concrete room, $0.19\,W/m^2K$ for the PIR timber and $0.13\,W/m^2K$ for the wood timber. For the sensors data collection a CS data logger (CR1000) was used. Measurements were taken every

30 seconds and data were then averaged every 5 minutes.

A humidifier regulated the moisture content into the cells, as described in Section 4.2.1. The target was to maintain the humidity at 75%RH for 8 hours, followed by a de-humidification phase, in which the air moisture was slowly dissipated both by the building fabric and ventilation. The test was designed to reproduced similar conditions to the NORDTEST laboratory protocol, by providing 24 hour cycles, which comprise 8 hours of high humidity and 16 hours at low humidity. The main difference with the laboratory testing was in the de-humidification. No de-humidifier was used, and, consequently, the RH did not always reach the prescribed 33%RH, as the minimum RH conditions of the cells were dependant on the weather conditions. A moisture decay test (Section 4.3) and a moisture buffering (Section 4.4) test were performed in the rooms. Both tests comprised 8 hours humidification at 75%, whilst the de-humidification was 40 hours long in the decay test and 16 hours in the moisture buffering test. In the moisture buffering tests the cells were subjected to six 24 hour cycles, similarly to the laboratory test (Section 3.3). Tests are further described in Section 4.3 and Section 4.4.

The outdoor climatic data were taken from the BRP weather station (Gill Instruments MetPak II plus RM Young tipping bucket rain gauge, and Delta T devices SPN1 Sunshine Pyranometer), placed around 20 m from the test room (Fig. 4-5). Before the start of every test, the doors were sealed, and a PIR insulation panel was inserted in between the internal and external door, to avoid thermal bridges and to reduce air infiltration from the doors (Fig. 4-6).

Sensors, included the weather station, were not calibrated before testing. However, Temperature and RH sensors readings were monitored in the laboratory climatic chamber. The good agreement between the chamber environmental setting and the sensors gave confidence on the sensors reliability. The weather station data were compared also with temperature, RH and solar radiation sensors, barometric pressure placed outdoors, whilst wind speed and direction were compared with live data of nearby weather stations.

Fig. 4-5. Weather Station

(a) (b)

Fig. 4-6. Door sealing: indoor door (**a**) and PIR insulation panel between the indoor and outdoor doors (**b**)

4.2.1 Humidifier and Pre Experimental Simulations

To estimate an appropriate moisture load in the room, pre experimental simulations with WUFI ® Plus were performed. The maximum water content to inject in the room

was evaluated, to avoid condensation and to reach the target RH level. Simulations were set as in Chapter 5. As simulation were performed, before the field testing, the outdoor climatic data were taken from Lyneham, UK, a weather station at around 10 miles from the location of the test rooms (Fig. 4-7). The weather data for Lyneham is representative of the West of England environmental conditions, and it follows a similar trend to the data collected later at the BRP, as shown in Section 5.1.3.

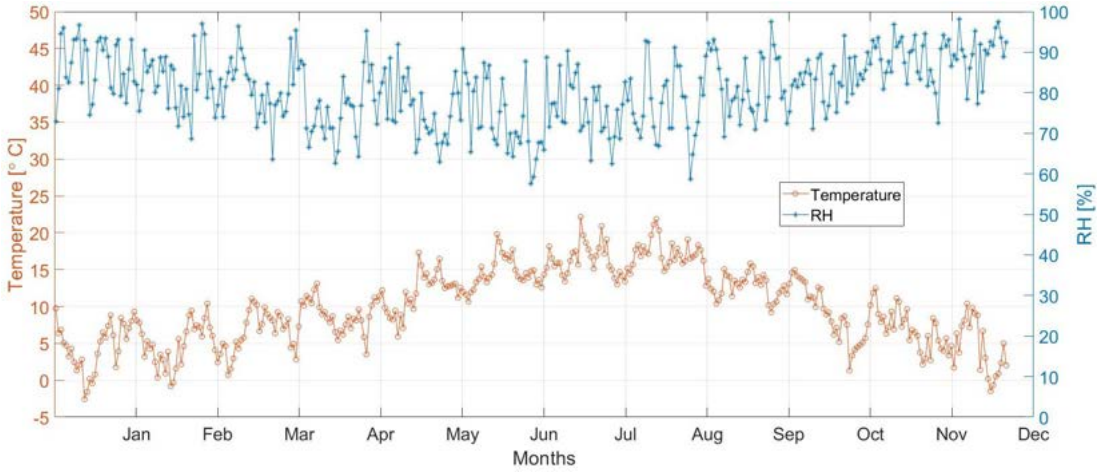

Fig. 4-7. Reference year for weather condition in Lyneham

For each room five simulations with different moisture loads were run, as shown in Table 4.3. The loads represented the "ideal" moisture flow that the humidifier had to inject, to reach 75% RH. Table 4.3 showed the optimal flow was 400 g/h either for the concrete and wood fibre room. The PIR room always reached condensation, regardless of the amount of water released. It indicated that the lack of ventilation and the impermeability of the wall did not allow moisture to be removed.

Table 4.3. Simulation of the indoor RH, when different moisture loads are present in the three rooms

Concrete		Wood Fibre		PIR	
Moisture Load [g/h]	RH [%]	Moisture Load [g/h]	RH [%]	Moisture Load [g/h]	RH [%]
700	86.10	600	86.4	600	100
600	84.9	500	85.3	500	100
500	83	400	84.1	400	100
400	70.4	300	73	300	100
300	57.6	200	59.7	200	100

The simulations results were used for the design of the humidification systems. A centrifugal humidifiers (HG-Hydroponics HR-15) were integrated with a pulse pause module and humidifier controller, to ensure a controlled steam flow in the room. The factory moisture flow for the humidifier (1.5 kg/h) was reduced to around 0.45 kg/h

by cutting down with a pulse module the time the humidifier was on. By turning the humidifier off every 20s for 40s, the moisture flow was limited to 450 g/h (Fig. 4-8). To avoid the risk of condensation in the PIR and to reach exactly the same RH in all rooms, the humidifier controller, connected to a RH sensor, turned off the humidifier, when RH reached 75%.

Simulations also estimated the water consumed for each humidification cycle was around 3L (always depending on the outdoor weather, as explained in Section 4.3.2.2). As the capacity of the humidifier' water tank was limited (1.5L), a water reservoir was connected to the humidifier, to increase the capacity of the humidifier water tank to 6L. For the moisture buffering testing, a third water tank (90L) was added, to allow multiple RH cycles for the week long tests. To monitor the amount of water released in the room, the water tank was placed on a scale (ATP FHB-6000, accuracy $\pm 0.02g$), which was logged to a Raspberry Pi B3 that recorded measurements every minute. A timer was used to control the humidification period, typically turning on the humidifier before and after the 8 hours de-humidification.

- Water tank
- Water tank
- Controller
- Data logger
- Scale
- Timer
- Humidifier

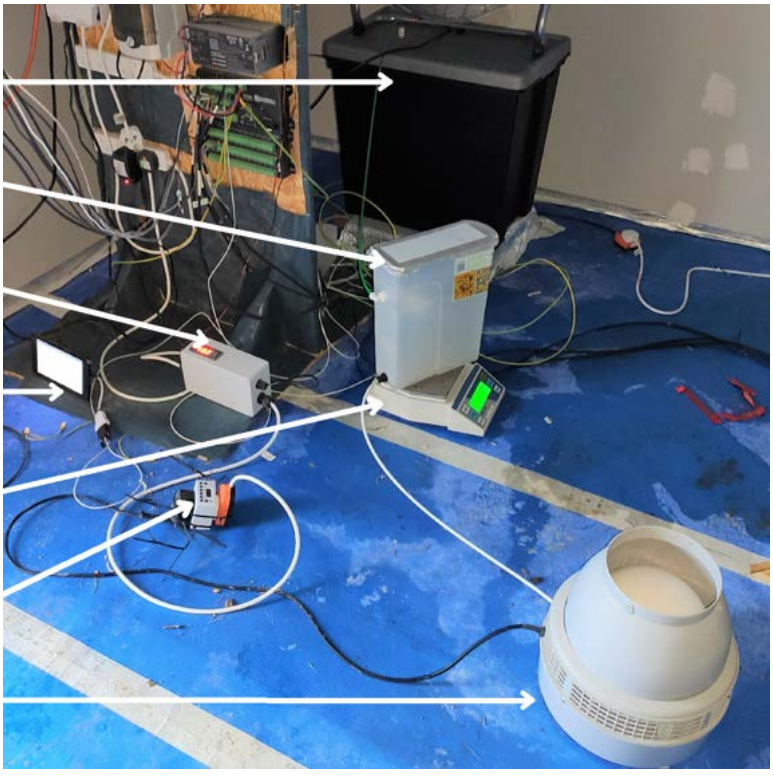

Fig. 4-8. Humidifier set up

4.3 Air Infiltration, Instantaneous Moisture Release and Moisture Decay

To test the response of the rooms to humidity loads, a moisture decay test and a instantaneous moisture release test were performed. Both tests were carried on, to quantify the effect of moisture adsorption, building infiltration and weather influence on the moisture balance of the rooms and on moisture buffering. Particular focus was also given to the determination of air leakages of the test-cells enclosures through the fan pressurisation method (*BS EN ISO 9972*, 2015) and gas decay test (*BS EN ISO 12569*, 2017).

The instantaneous moisture release test was performed to evaluate the suitability of the three rooms to the moisture buffering testing. The test consisted in injecting a known amount of water for a short time in the rooms without any control on the RH level. The objective of this test was to investigate and compare the response of the rooms to quick variations of moisture loads, when plasterboard is covered (non-hygroscopic) or not (hygroscopic) by an impermeable sheet.

The decay test combined elements of the co-heating test (Latif et al., 2016) and parts of the gas decay test (*BS EN ISO 12569*, 2017). The moisture decay test consisted in injecting moisture in the rooms for 8 hours and successively measure the decrease of humidity levels over the time. The injection phase followed the same guidelines of the co-heating test, in which the water consumed by the humidifier, to maintain the RH at 75%, was monitored. In the decay phase, the reduction of the RH is observed, until the indoor humidity reached the initial RH before the test. The results obtained were analysed together with the tracer gas and blower door test, to investigate the correlation between building infiltration. moisture transport and storage in the wall build up.

4.3.1 Method

4.3.1.1 Air Infiltration Tests

The gas decay test was performed once in each room. CO_2 two point decay tests were performed by following the *BS EN ISO 12569* (2017). CO_2 was realised for 15 minutes, reaching 3000 ppm ±50. The decay was observed for 40 hours. A TSI Q-Trak 7575 was used to monitor the CO_2 decay. Fig. 4-9 shows the test set-up. The decay is calculated as follow:

$$ACH = \frac{1}{t_2 - t_1} \cdot log_e \frac{c(t1)}{c(t2)} \tag{4.3.1}$$

Where air change per hour (ACH) is the air change [1/h], t_1 and t_2 are the time at the beginning and at the end of the test [s], c is the gas concentration $[m^3/m^3]$

- CO_2 sensor
- CO_2 inlet
- Fan
- CO_2 bottle

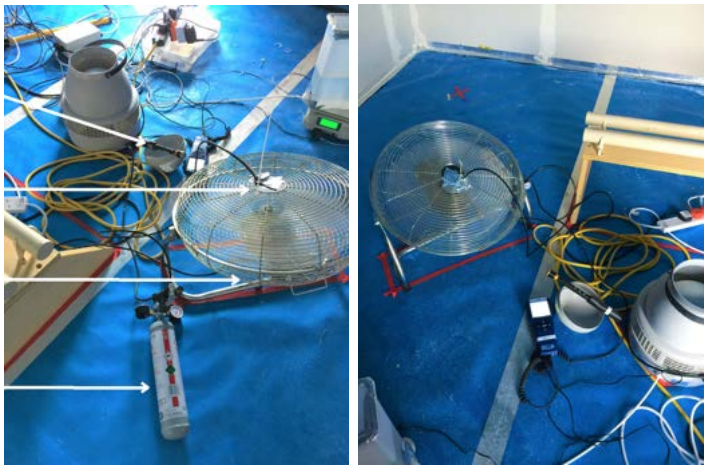

(a) (b)

Fig. 4-9. Gas decay test set-up: CO_2 bottle and CO_2 sensor place at the centre of the room

For the blower door test a Minneapolis blower door, equipped with a DG-700 differential pressure gauge and a C3 fan ring, was used (Fig. 4-10). Pressurisation tests were performed three times for each room, starting from low pressure differential (around 15 Pa) until 70 Pa. Indoor and outdoor temperature was also measured in both tests. The results were then analysed and corrected by following the *BS EN ISO 9972* (2015).

Fig. 4-10. Blower door test

4.3.1.2 Instantaneous Injection and Moisture Decay

In the instantaneous injection test, the humidifiers were filled with 1L of water. The humidity flow was not controlled by the humidifier controller and timer, using the humidifier at its maximum capacity (1.5L/h) until the water tank was empty. The test was performed in the three rooms simultaneously, ensuring that the rooms were exposed to the same weather conditions. The test was repeated twice with plasterboard exposed in the concrete and wood fibre rooms, and it was repeated successively applying the impermeable sheet in all rooms. Temperature was always kept at $23°C$. The moisture load was injected for 40 minutes, to reduce the risk of damaging the equipment with high humidity levels. At the end of each test, the room was ventilated, to remove any residual condensation.

Similarly to the instantaneous injection, the moisture decay test was performed when plasterboard was in direct contact with the room environment (hygroscopic test) in the concrete and wood fibre rooms. The comparison between the hygroscopic and non hygroscopic test (PIR cell) allowed to isolate the impact of building infiltration on the decay of moisture concentration in the rooms at the same weather conditions. The test was performed seven times, to assure the repeatably of the test.

The rooms were first humidified for 8 hours (between 9.00 a.m. to 5.00 p.m) and, successively, the RH decay was monitored for 40 hours after the humidification process.

As the humidifier responded with few seconds delay to humidity changes in the room, the humidifier controller sensor was set at 73% RH, to keep humidity in the room below 75% (± 2) and avoid condensation. The amount of water consumed by the humidifier was measured in each cycle. Temperature was monitored, showing a good capacity of the heaters to keep the temperature at 23°C (Fig. 4-11). The scale of Fig. 4-12 shows the rooms set-up.

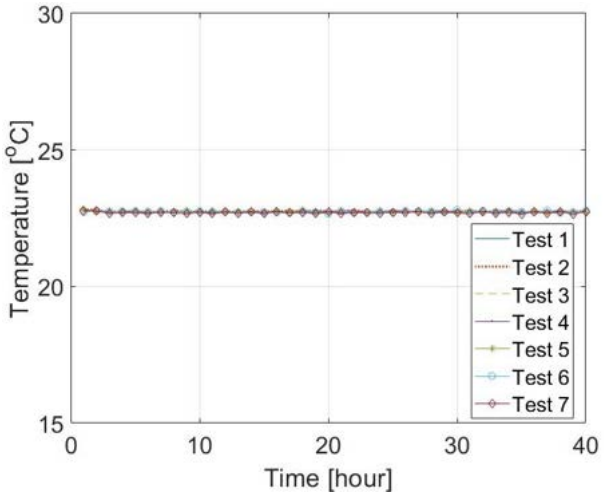

(a) Concrete

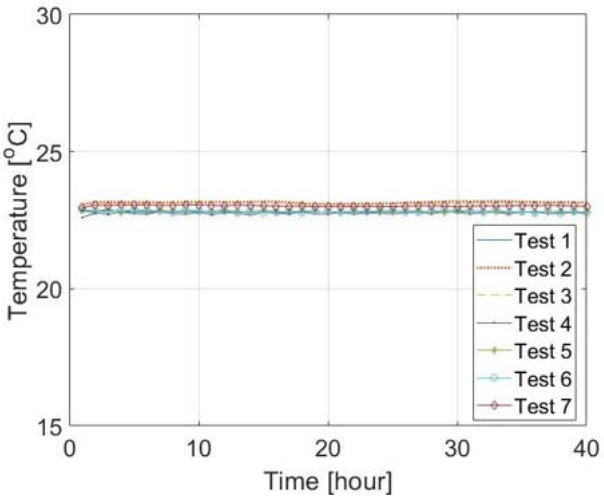

(b) Wood fibre

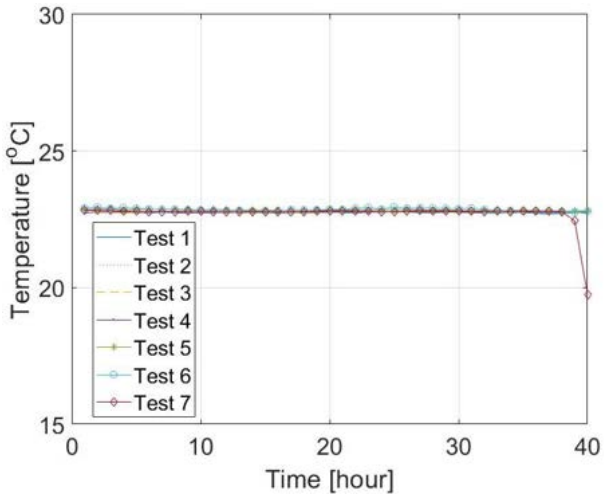

(c) PIR

Fig. 4-11. Temperature in the concrete, wood fibre and PIR room during the decay test

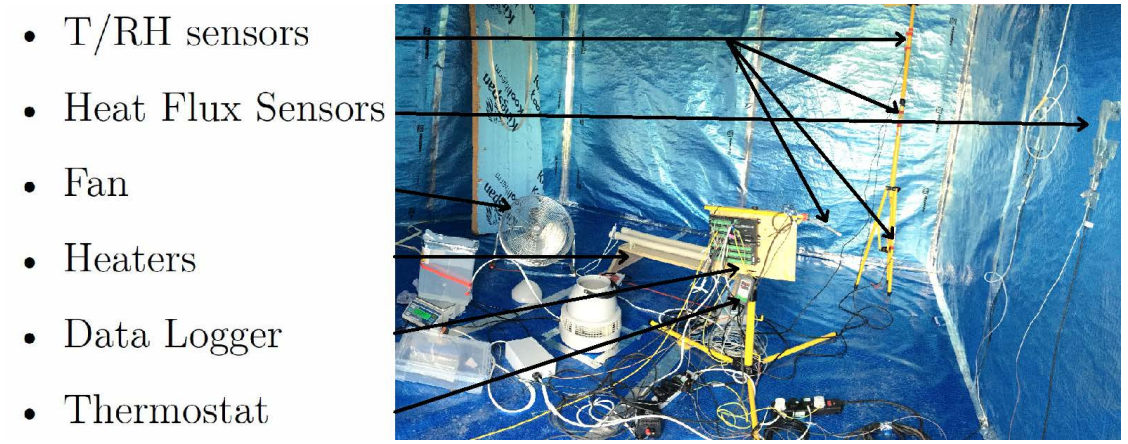

(a) PIR

(b) Concrete

Fig. 4-12. Moisture decay set-up: non-hygroscopic (**a**) and hygroscopic (**b**)

4.3.2 Results, Analysis and Discussions

In this section the analysis on the infiltration rate measurement, instantaneous injection test and on the moisture buffering test is presented. The humidification phase of the decay and the de-humidification phase were analysed separately. The humidification phase corresponds to the eight hours of moisture injection into the room, followed by 40 hours de-humidification, in which the moisture dissipation was observed after the humidification process ended (Fig. 4-13). These two phases of the decay test was due to the different behaviour of the rooms to high and low humidity levels, as it is discussed in the following sections.

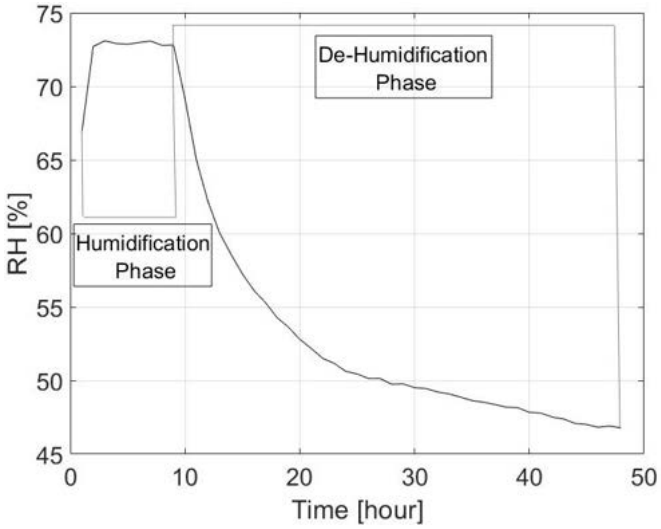

Fig. 4-13. Moisture decay phases

4.3.2.1 Gas Decay and Blower Door tests

The results of the gas tracer and blower door test are shown in Table 4.4. The variations between the two tests are likely due to the different testing methods. The blower door test applies elevated pressure in the the rooms, which are 50 times higher than the normal pressure at ambient conditions. The high pressure differential forces the indoor air out through the joints and cracks of the buildings, which do not usually affect the air tightness of the building at ambient conditions. The gas decay test injects a known amount of CO_2 at ambient pressure, which is slowly removed through the building. Patel et al. (2011) investigated the comparability and differences of the two tests, pointing out the advantages and disadvantages of the two methods. The gas tracer test is sensitive to equipment precision and weather variations, but determines directly the air leakages at normal operating pressure. The blower door test provides the ACH regardless of the outdoor environmental conditions. However, the ACH is calculated following the corrections and conversion formulas prescribed in *BS EN ISO 9972* (2015).

To compare the two tests at ambient condition, the ACH was experimentally measured at different pressure differentials (from 15 to 80 Pa) in the blower door test to perform a linear regression analysis for each room (Fig. 4-14). The statistical analysis showed a good fit with the experimental data for the three rooms, presenting a R squared of 0.99, 0.98 and 0.94 for concrete, wood fibre and PIR, respectively and a p-value lower than 0.05. Through the resulting equations, the ACH for the three rooms was calculated, when the pressure differential between the indoor and outdoor was equal to 2 Pa, which was the average pressure differential measured during the tracer gas test. Concrete and wood fibre calculated ACH was 0.25/h and 0.22/h respectively, while for PIR the ACH was 0.30/h. The obtained values were in general higher than in the tracer test. In the gas tracer test the three rooms presented the same air change, and, therefore, higher air tightness of the cells than in the blower door test. The blower door test showed the concrete cell had the lowest infiltration rate, due to its thicker walls and its different building assembly. As the two tests are based on different test principles and methods, it is not possible to state which one of the two test is more reliable. However, for this study, the use of the gas decay test for the analysis was considered more appropriate, as the moisture decay test was performed at standard pressure differential and it followed the same principle of the tracer gas decay test.

Table 4.4. Air change per hour (ACH) and air leakage rate (Q) at 50 Pascal for the blower door test and at ambient condition for the gas decay

Room	Blower Door				Gas Decay	
	$ACH_{50}[1/h]$	$Q_{50}[m^3/h]$	$ACH_2[1/h]$	$Q_2[m^3/h]$	$ACH_2[1/h]$	$Q_2[m^3/h]$
Concrete	1.60	48.12	0.25	7.52	0.06	1.80
Wood	1.88	59.40	0.22	6.95	0.06	1.89
Pir	1.89	66.18	0.30	10.50	0.06	2.10

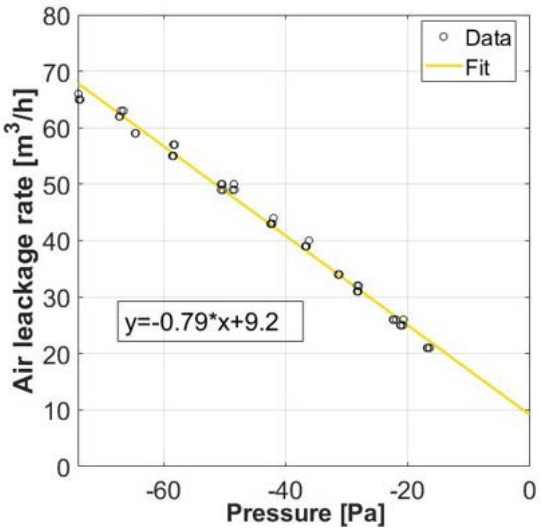

(a) Concrete

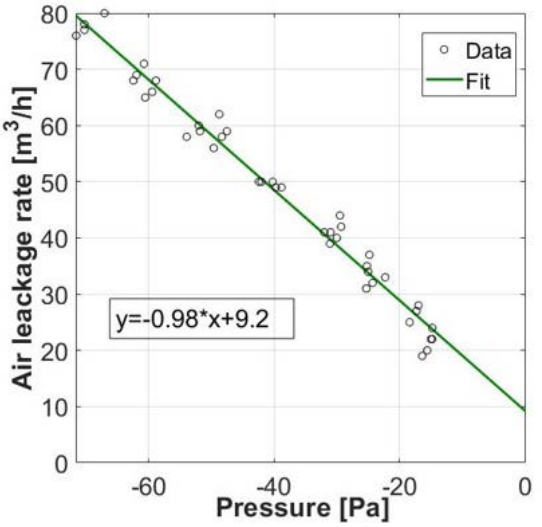

(b) Wood fibre

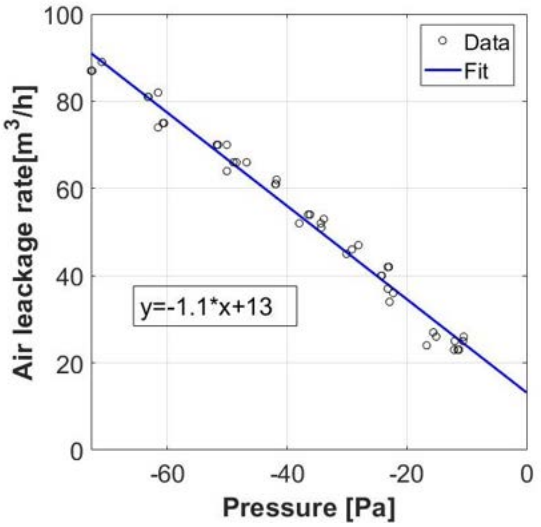

(c) PIR

Fig. 4-14. Linear regression of the air leakage rate for the concrete, wood fibre and PIR room

4.3.2.2 Instantaneous injection test

The instantaneous injection test results for the hygroscopic test are shown in Fig. 4-15. The hourly average data were calculated from the original minutely file. The concrete and the wood fibre rooms presented similar trends and reached similar peaks during humidification for Test 1 (80% and 77%, respectively) and Test 2 (77% and 75%, respectively). The moisture decay phase followed a logarithmic curve, showing variations of less than 3%RH between Test 1 and Test 2, probably due to the different weather conditions during the tests (Fig. 4-16). The variations between the two rooms were less than 5% difference. The wood fibre room kept the humidity level slightly lower than the concrete, probably due the possible higher penetration depth of moisture, or the higher moisture load in the room. The air gap may also play a role, and, for this reason, it was further investigated and discussed in Section 4.4.

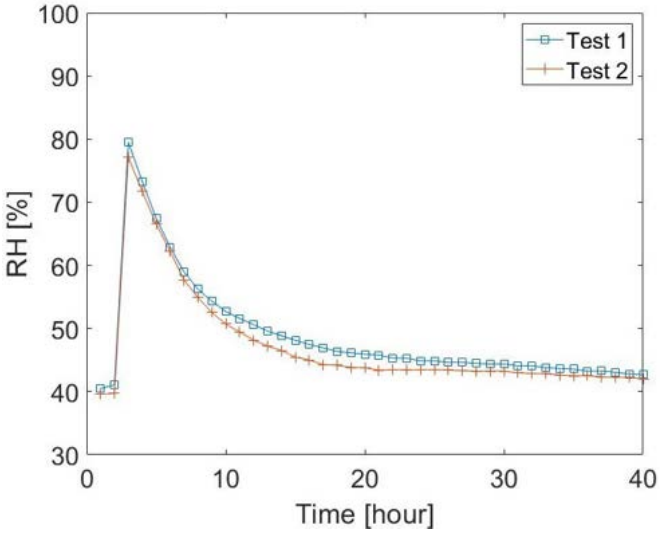

(a) Concrete

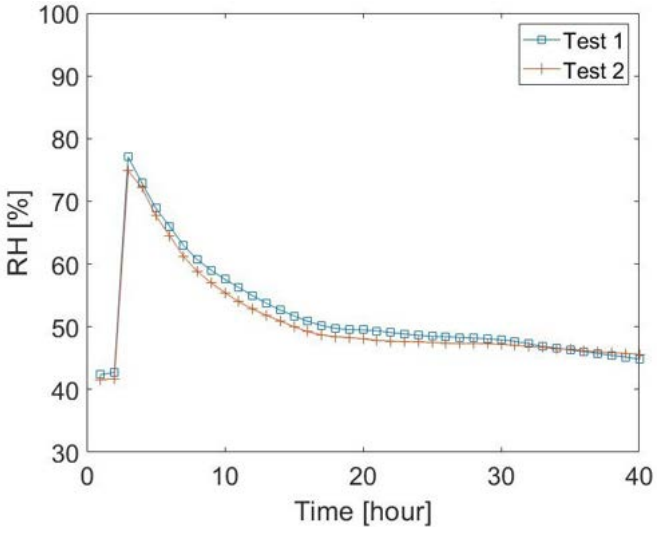

(b) Wood fibre

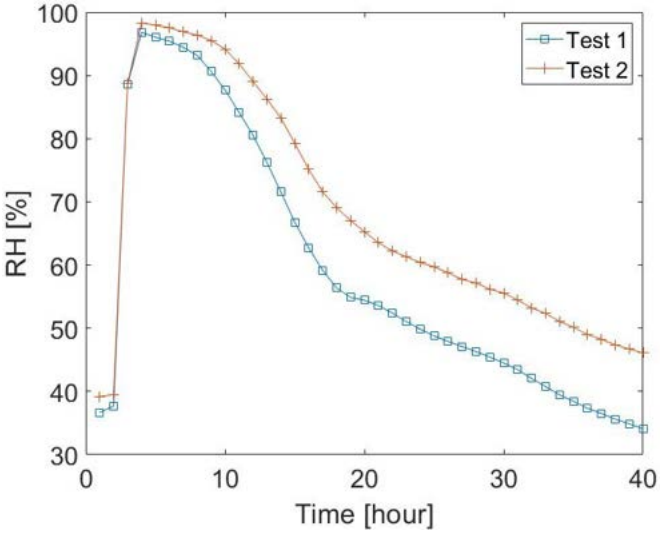

(c) PIR

Fig. 4-15. Instantaneous moisture injection in the three rooms

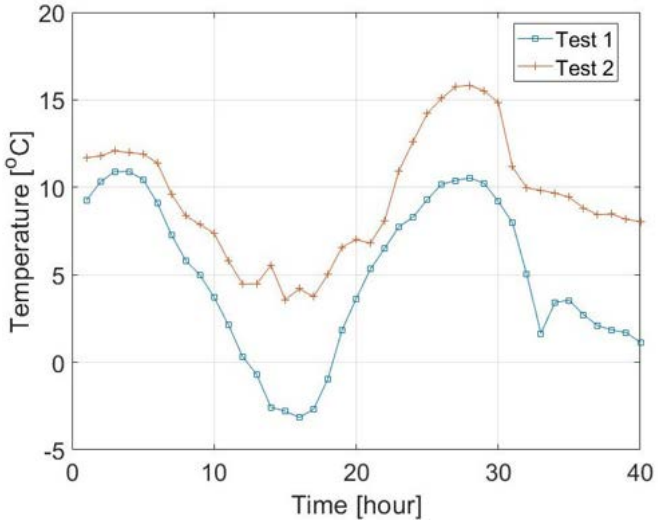

(a) Temperature

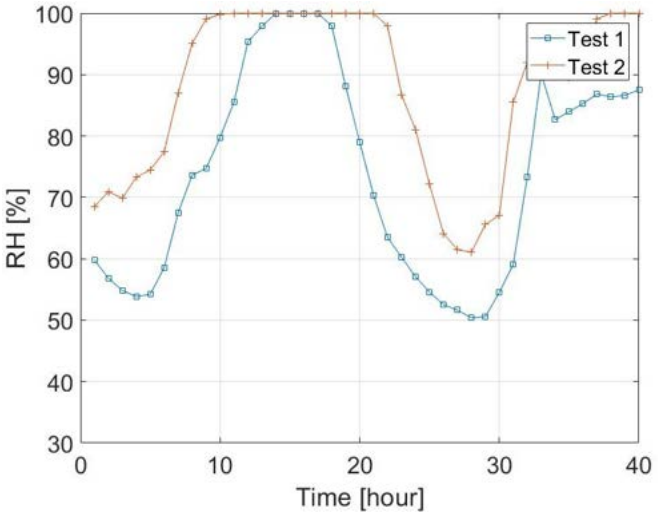

(b) RH

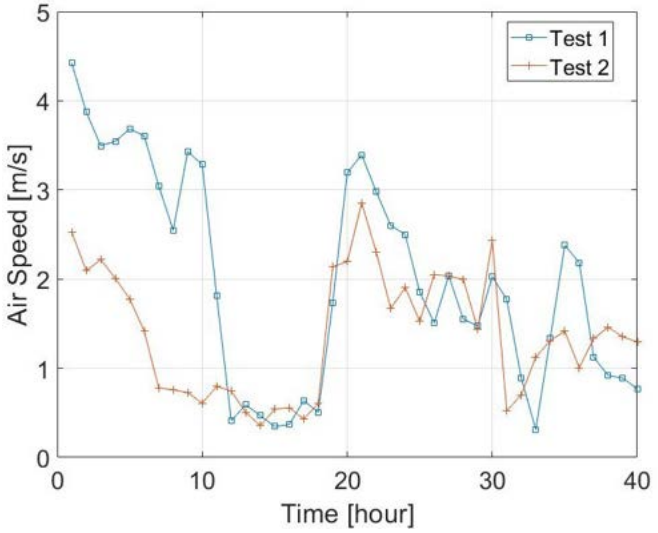

(c) Wind Speed

Fig. 4-16. Weather conditions in April during the instantaneous injection tests

The PIR room showed significantly different response to the instantaneous humidification. PIR reached 98% and 97% in Test 1 and Test 2 respectively, and it presented an anomalous decay and distinctly different from the other two. The moisture decay was slow in the first 7 hours after the humidification, as humidity could not be removed, and successively, it was expelled to a quicker rate than the other two rooms. This could be due to the higher partial pressure differential generated between the indoor and outdoor (Fig. 4-17), which also explains the remarkable difference between Test 1 and Test 2 in the PIR cell. In Test 1 the bigger partial pressure differential generated a steeper curve than in Test 2 (Fig. 4-17c), until the RH decay slowed down at Hour 19, once the partial pressure differential was reduced. In the other two rooms the partial pressure is significantly lower. Consequently, there may be a slower moisture exchange between the indoor and outdoor (Fig. 4-17a and Fig. 4-17b). The capacity of the concrete and wood fibre rooms to balance the indoor moisture content through the walls resulted in a reduction of the indoor/outdoor partial pressure differential, which explains the slow and steady RH decay, as also demonstrated in Section 4.3.2.4.

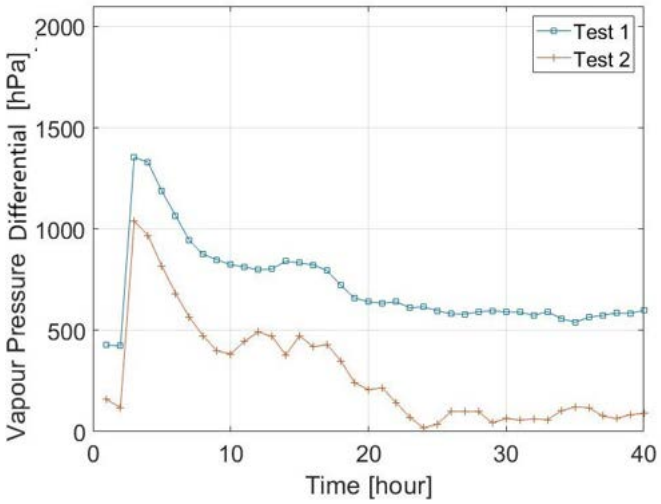

(a) Concrete

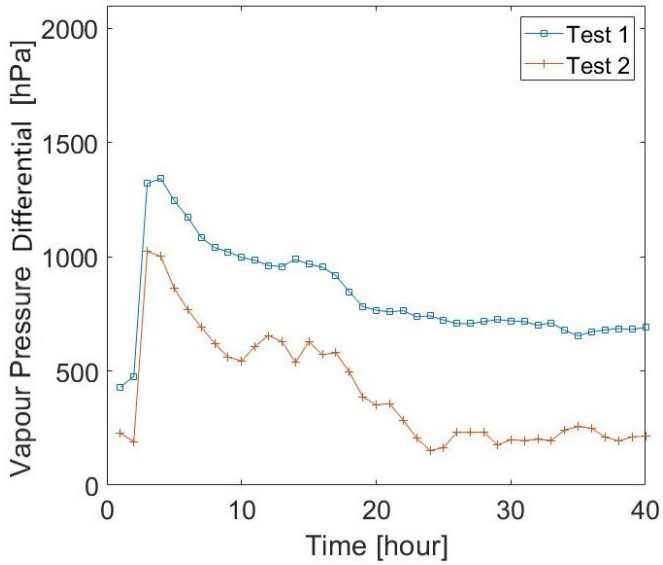

(b) Wood fibre

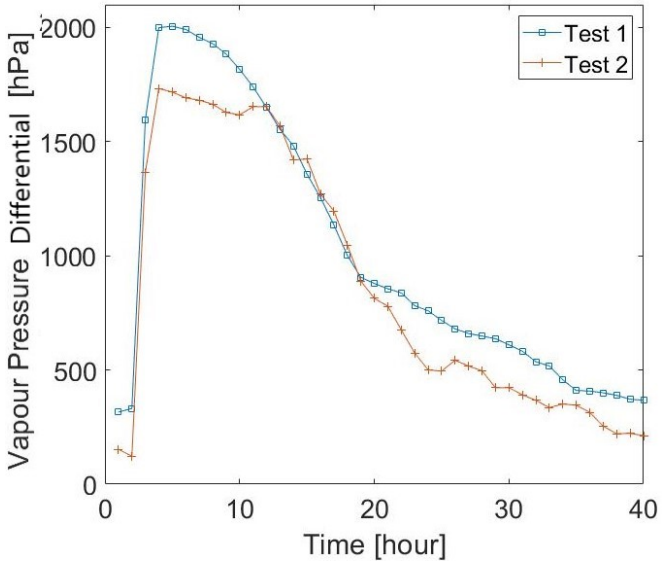

(c) PIR

Fig. 4-17. Vapour pressure differential between the indoor and outdoor in concrete, wood fibre and PIR room

Due to the different behaviour of the PIR room, the instantaneous injection test was then repeated with the concrete and wood cells also covered with the impermeable sheet, to confirm the response of non-hygroscopic walls to high humidity levels. This test was repeated after the ventilation system was installed for the moisture buffering tests in Section 4.4. To reduce the impact of a ventilation system on the tests, the ducts were sealed internally and externally, but it was still not possible to reproduce the same indoor environment as in the previous test. However, the wood fibre room still reached RH values as high as in the PIR room (more than 98%RH). All considering, the shape and the response of the wood fibre cell (Fig. 4-18) is not significantly different from the PIR cell (Fig. 4-15c), when walls are impermeable. The concrete cell presented significant differences probably due to higher air leakages from the ventilation system or from around the door opening. Nevertheless, the room reached 88%RH and the response showed an irregular shape, as expected for a non-hygroscopic test. Regardless of the differences in the rooms conditions, both concrete and wood rooms presented a significant difference between the hygroscopic and non-hygroscopic case. Consequently, the results obtained in the instantaneous injection investigation together with the simulation analysis in Chapter 5 pushed to pursuit the field testing, as demonstrated hygroscopic materials did impact the indoor RH.

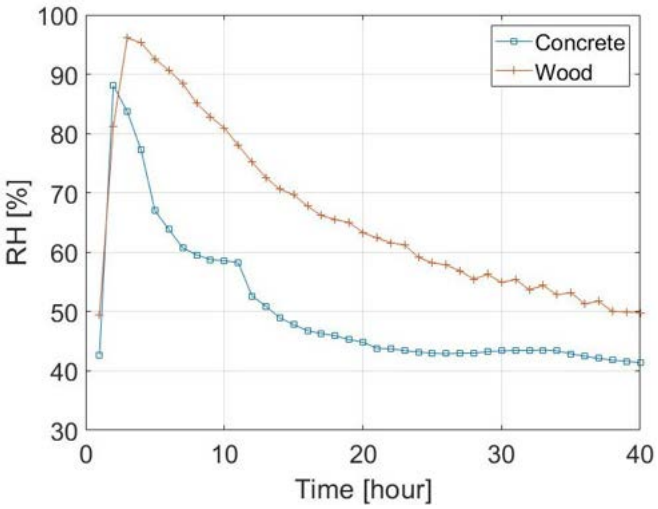

Fig. 4-18. Instantaneous moisture injection in the concrete and PIR rooms, when covered with the impermeable sheet

4.3.2.3 Humidification Phase of the Decay Test

In the concrete and wood fibre rooms the RH did not reach an average of 75%RH, because of the settings of the humidifier controller, described in Section 4.3.1 (Fig. 4-19a and Fig. 4-19b). The small fluctuations during the humidification phase represents the humidifier turning on and off. The slow response of the humidifier was more evident in the PIR room (Fig. 4-19c), due to the higher sensitive of the cell to humidity

variations. The humidifier's delay to switch itself off made the RH jump to more than 78%RH in the first few hours of the humidification in the PIR. After 5 hours the humidifier reached the target RH, as the controller kept the humidifier off for longer intervals and on for shorter time, allowing the RH to stabilise at 75%. The different functioning of the humidifier already showed an important difference between the three rooms. In the concrete and wood fibre rooms walls immediately moderate the indoor humidity content, making easier for the humidification system to reach the target RH. For PIR small injection of water made the RH increase quickly, as the non-hygroscopicity and highly air tightness of the cell did not allow moisture to be removed, reaching immediately the room saturation.

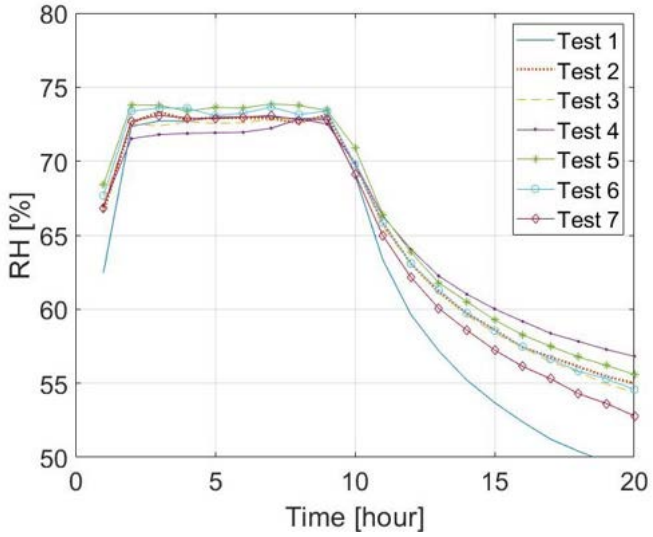

(a) Concrete

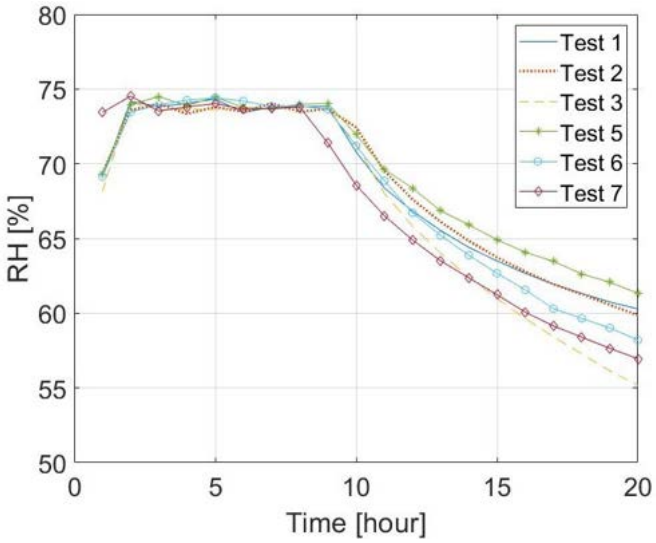

(b) Wood fibre

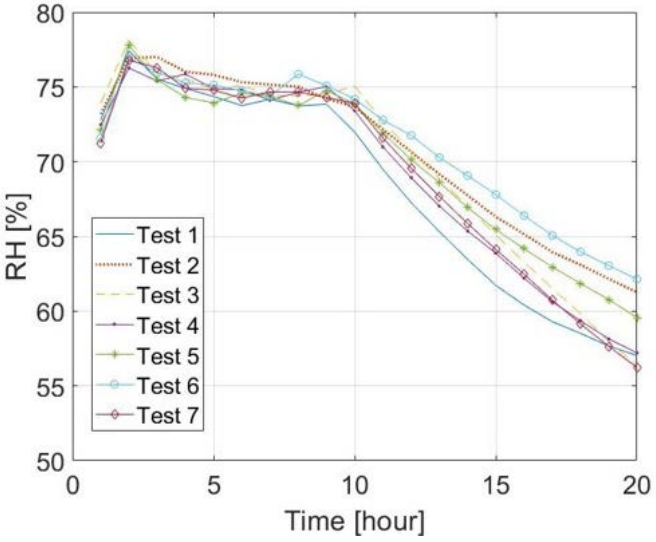

(c) PIR

Fig. 4-19. Results for the concrete, wood fibre and PIR room

The moisture decay test allowed for the investigation of a trend between the hygroscopic and non-hygroscopic rooms during the humidification phase. The amount of water injected in the rooms was measured, to investigate the water need for each room to maintain 75%RH, as shown in Table 4.5. There were not enough data for wood, but the differences between concrete and PIR cells showed the different behaviour between the non-hygroscopic and hygroscopic rooms. The PIR did not remove the indoor moisture as quick as the concrete room, for this reason the humidifier was kept off for longer time, consuming less water in the reservoir. Table 4.5 shows concrete and wood fibre rooms consumed double the amount of the water used in the non-hygroscopic cell. The wood fibre cell had similar behaviour of the concrete room, as it injected the same amount of water in Test 4, 6 and 7. The different response of the rooms to the moisture injection is due to the hygroscopicity of the walls. In the non-hygroscopic room walls were not adsorbing water from the air, whilst in the concrete and wood fibre rooms the use of water was higher because wall stored and transported water through the assembly, reducing the moisture content in the air.

Table 4.5. Water injected in each room

	PIR		Concrete		Wood	
	Total water [g]	Water per hour [g/h]	Total water [g]	Water per hour [g/h]	Total water [g]	Water per hour [g/h]
Test 1	-	-	-	-	2338.00	292.25
Test 2	1020.98	127.62	2100.89	262.61	-	-
Test 3	1113.00	139.12	2242.69	280.33	-	-
Test 4	1425.00	178.12	3096.37	387.04	2868.763	358.59
Test 5	920.30	115.03	1833.7	229.21	-	-
Test 6	958.7	119.83	1834.37	229.29	1892.57	236.57
Test 7	995.68	124.46	1957.42	244.67	1764.23	220.52

The water injected varied proportionally every week in all cells, probably due to the influence of the weather environmental variations. Outdoor temperature, RH, barometric pressure and wind velocity were monitored during the decay tests (Fig. 4-20 and Fig. 4-21), which was performed from February to April 2019. Considering only the first 8 hours in Fig. 4-20 and Fig. 4-21, the average, maximum and minimum values of the outdoor environmental factors during the humidification interval were calculated (Table 4.6). As RH depends on the temperature, the absolute humidity was calculated and investigated instead. There is no apparent correlation between the water injected and the outdoor environmental condition, except for the wind speed. It appears that higher the wind velocity, more water the room required to maintain 75%RH. Only in Test 4 rooms were not in line with this trend, but looking at the maximum and minimum wind velocity, the wind speed fluctuations in that week varied significantly. The wind speed was constantly above 7 m/s in the first 5 hours of the humidification, to suddenly drop to less than 5 m/s in the last 2 hours

of the test (Fig. 4-21b). Therefore, for the majority of the test the air speed was around the same speed as in Test 3, where similar conditions were observed.

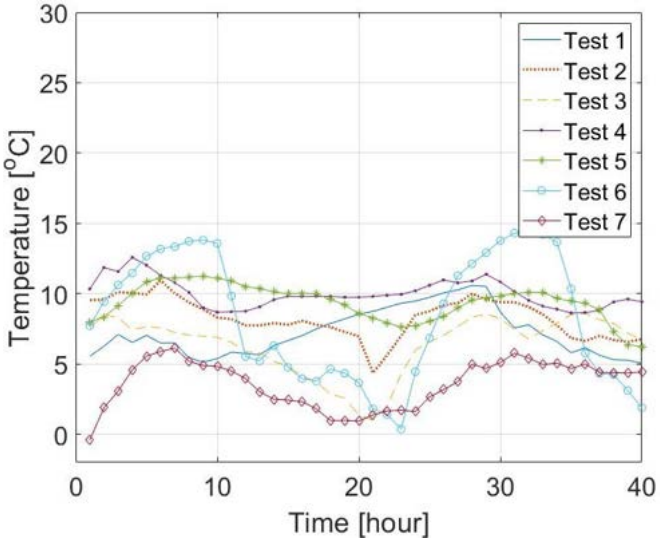

(a)

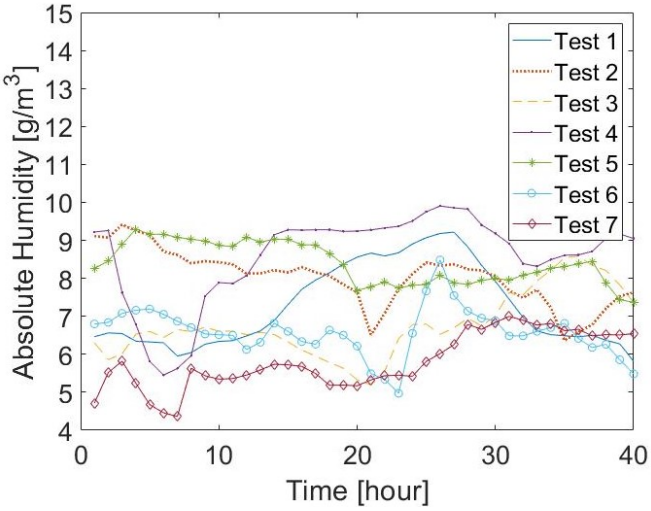

(b)

Fig. 4-20. Outdoor temperature (**a**) and outdoor absolute humidity (**b**)

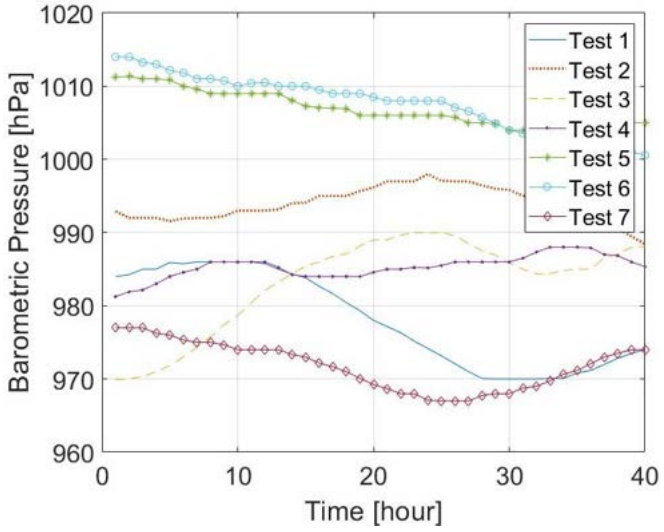

(a)

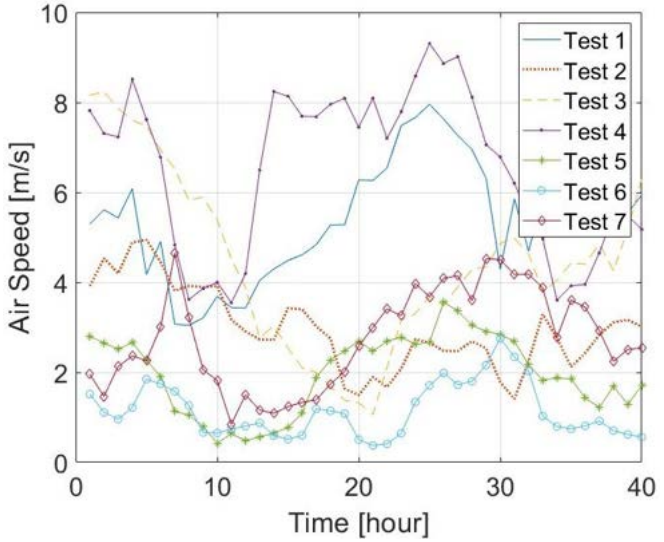

(b)

Fig. 4-21. Outdoor barometric pressure (**a**) and wind speed (**b**)

Table 4.6. Temperature,RH, barometric pressure and wind speed average, max and minimum

		Temperature [$°C$]	Abs.Hum. [g/m^3]	Bar. Press [hPa]	Wind Velocity [m/s]
Test 1	Mean	6.22	6.31	985.10	4.71
	Max	7.10	6.56	986.00	6.08
	Min	5.13	5.95	984.00	3.05
Test 2	Mean	9.83	8.96	992.16	4.30
	Max	10.94	9.41	993.00	4.94
	Min	8.89	8.39	991.58	3.81
Test 3	Mean	7.59	6.37	971.69	7.40
	Max	8.51	6.65	975.75	8.23
	Min	6.97	5.85	969.00	5.83
Test 4	Mean	11.06	6.97	983.21	6.92
	Max	12.58	9.25	986.00	8.59
	Min	8.99	5.45	981.00	3.62
Test 5	Mean	10.27	8.91	1010.27	1.94
	Max	11.25	9.29	1011.33	3.17
	Min	7.99	8.26	1009.00	0.42
Test 6	Mean	11.76	6.96	1012.27	1.32
	Max	13.81	7.19	1014.00	1.92
	Min	7.71	6.70	1010.00	0.65
Test 7	Mean	4.09	5.05	976.18	2.46
	Max	6.13	5.81	977.00	4.65
	Min	-0.41	4.36	975.00	1.09

A linear regression analysis for each room was also performed to statistically investigate the correlation between the water usage in the rooms and the average weather data. A regression test was performed for the PIR and concrete cells, which produced similar results in terms of test significance (Table 4.7 and Table 4.8). The level of significance of the linear regression was 0.05. Results showed that there was no correlation with temperature, absolute humidity and barometric pressure. By considering the small number of data, a power analysis was performed. The power calculation is generally carried out, when the null hypothesis is rejected ($p>0.05$), but a correlation between the two factors might still exist (type II error). As Field (2013) explained, the power analysis gives information about the statistical strength of the model, which is calculated through the R squared value. The power is a factor that varies between 0 and 1. In this study power values below 0.8 were observed, which indicated a type two error occurred. The general conclusion was that it was not possible to confirm if temperature, absolute humidity and barometric pressure

influenced the total moisture injection in the rooms. The only regression that presented a significant correlation was the analysis with the wind speed in the concrete room. Wind speed presented a p value smaller than 0.05. However, the R squared was quite low, which indicated the wind speed could predict only the 61% of the moisture load variations. The adjusted R squared also indicated some levels of error, as its values should not differ much from the R squared. It means that one or more data points (out-layers) did not follow the general trend of the correlations. Also in this case, more data points would reduce the effect of the out-layer and reinforce the prediction model.

Table 4.7. Linear regression correlation results for the concrete cell

Mean	R Square	R Squared Adj	p value	power
Temperature	0.02	-0.17	0.76	0.06
Abs. Humidity	0.02	-0.17	0.75	0.14
Bar.Pressure	0.23	0.07	0.28	0.21
Wind Speed	0.61	0.53	0.04	-

Table 4.8. Linear regression correlation results for the PIR cell

Mean	R Squared	R Squared Adj	p value	power
Temperature	0.04	-0.21	0.72	0.03
Abs. Humidity	0.04	-0.20	0.71	0.06
Bar.Pressure	0.24	0.05	0.32	0.18
Wind Speed	0.61	0.52	0.06	0.63

As in all tests (except for week 7), the wind speed was the highest in the first 5 hours of the humidification phase (Fig. 4-21b). Therefore, the correlation between the maximum wind velocity and the water usage was also investigated (Table 4.9). Results showed a better fit than in the previous case, presenting an R Squared of 0.69 and $p < 0.05$ both in the concrete and PIR room. Looking at the intercept and slope of the predicted fit curve (Table 4.10), it was observed that when the wind speed is 0, the wood fibre room needed twice the amount of water than in the PIR room, to maintain 75%RH. An interpretation of this is that the walls of the hygroscopic room were adsorbing half of the water to reduce the indoor level of humidity, while the other half was distributed in the air in the room or expelled through infiltration. The increase of wind speed generated two different slopes for the two rooms. The wind speed did effect more the concrete room, as the gradient of the curve was bigger. The highest gradient of the predicted concrete curve indicated that the wind speed might dry the walls due to the moisture transfer increase on the outdoor surface through convection, allowing for more moisture to be adsorbed by the walls. Another reason is the increase the partial pressure differential between the indoor and outdoor that might push moist air to be removed through the door. In the PIR cell the smaller variations suggested that in the non-hygroscopic room the walls were not participating to the moisture

balance, but infiltration through the door was still playing a role, by dissipating the indoor humidity accordingly with the wind speed. Overall, it was possible to observe significant differences between the hygroscopic and non-hygroscopic room. The wall did impact the indoor humidity content, by storing moisture in the materials and it could be quantified by comparing the two rooms, but to investigate the impact of the weather conditions on the room moisture balance, further data and analyses are necessary.

Table 4.9. Linear regression correlation with the maximum wind speed

Max	R Squared	R Squared Adj	p value
Wood Fibre	0.69	0.62	0.02
PIR	0.69	0.61	0.04

Table 4.10. Linear regression predicted intercept and slope with the maximum wind speed

Max	Intercept	Slope
Wood Fibre	1407.52 ±260.76	147.70 ±44.69
PIR	771.72 ±111.14	57.24 ±19.18

The test was supposed to be repeated with all three rooms covered with an impermeable layer, to verify that similar results to the PIR room were obtained. The repetition of the test was expected to show the water usage in the concrete and wood fibre rooms was halved compared to the equivalent hygroscopic test, and would have given more data points for the statistical analysis.

4.3.2.4 Moisture Decay

The second part of the moisture decay test consisted in the investigation of the moisture dissipation after the humidification phase. Seven tests were performed in the three rooms, presenting the results in Fig. 4-22. Inspecting all the RH decay curves, each test showed slight different steepness and curve shape. The majority of wood fibre and PIR room (Fig. 4-22b and Fig. 4-22c) tests resulted in a curve flattening from the 12^{th} hour of the decay, while the concrete room did not present this anomaly (Fig. 4-22a). The variations between each test were probably caused by the outdoor weather that influenced the indoor environment, but also likely depended on the wall design. The concrete room presented more steady and smooth decays, probably because of the combination of its probable higher air tightness and plasterboard participation to moderate the indoor environment, whilst PIR was the most influenced, due to the higher air leakages and non-hygroscopicity of the walls.

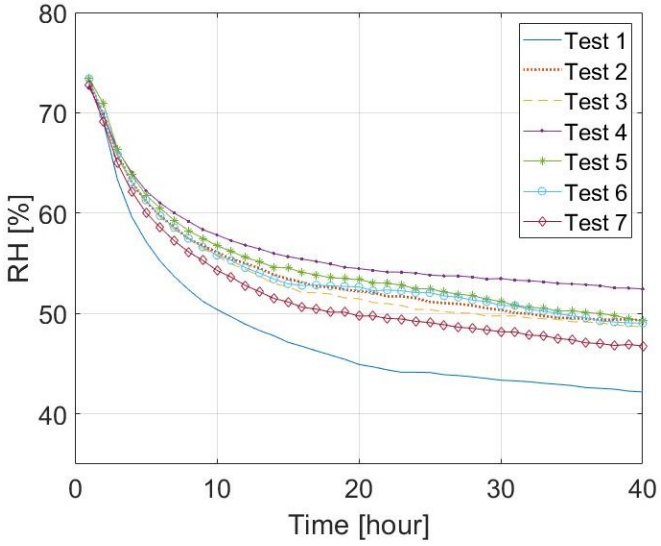

(a) Concrete

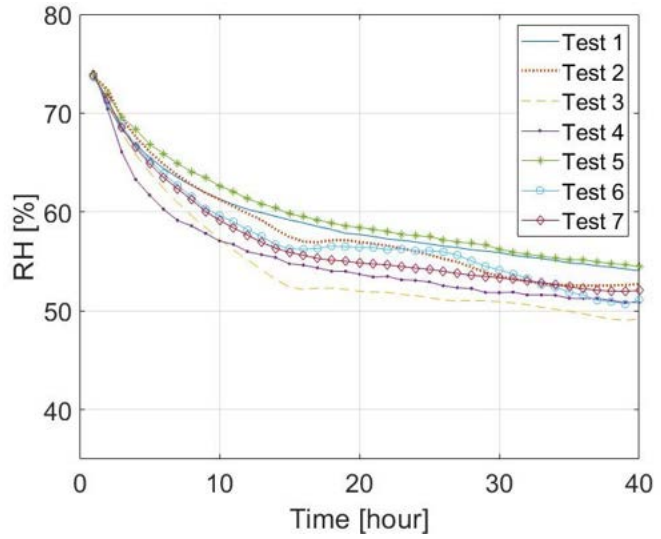

(b) Wood fibre

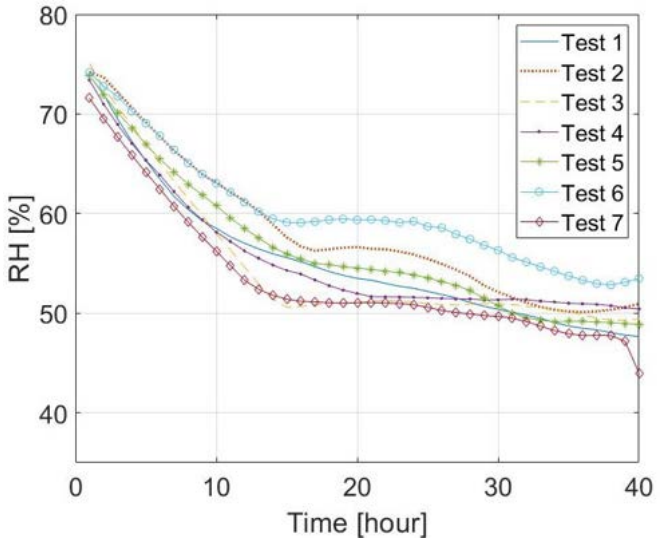

(c) PIR

Fig. 4-22. Decay phase for the concrete, wood fibre and PIR room

Observing the weather variations across the seven tests (Fig. 4-23 and Fig. 4-24), it was not immediately noticeable which outdoor environmental factor was actually differentiating the decays across the seven weeks testing. The indoor environment might be influenced by the simultaneous variations of all the weather factors or variations in the partial pressure differential between the indoor and outdoor, as already mentioned in Section 4.3.2.2 and Section 4.3.2.3.

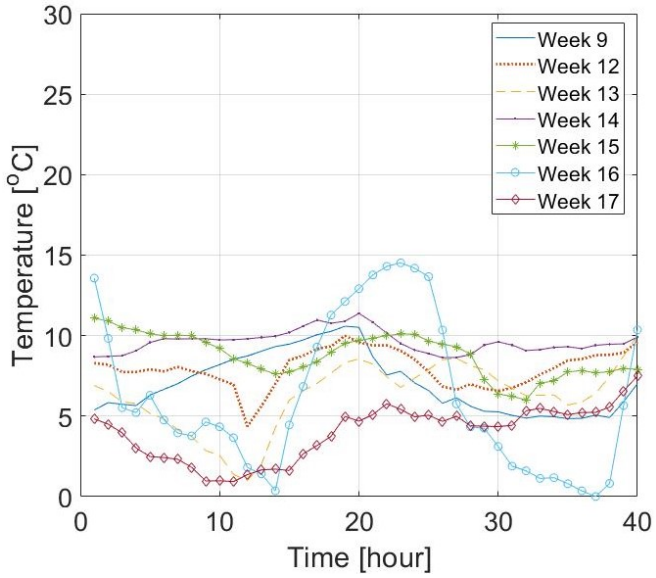

(a)

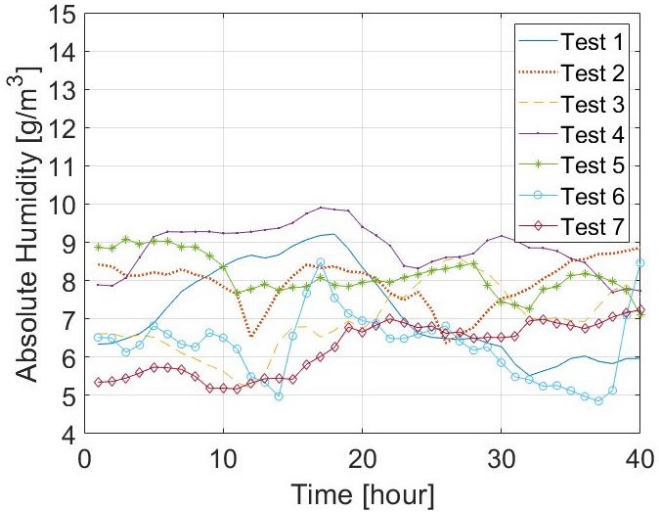

(b)

Fig. 4-23. Outdoor temperature and absolute humidity during the moisture decay

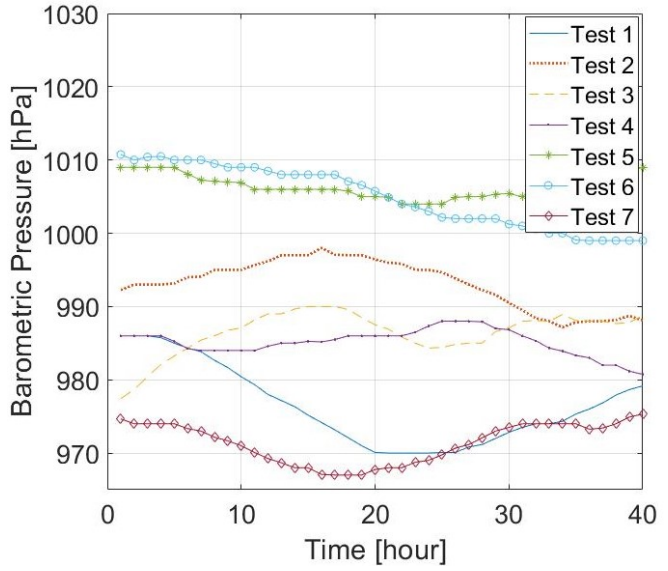

(a)

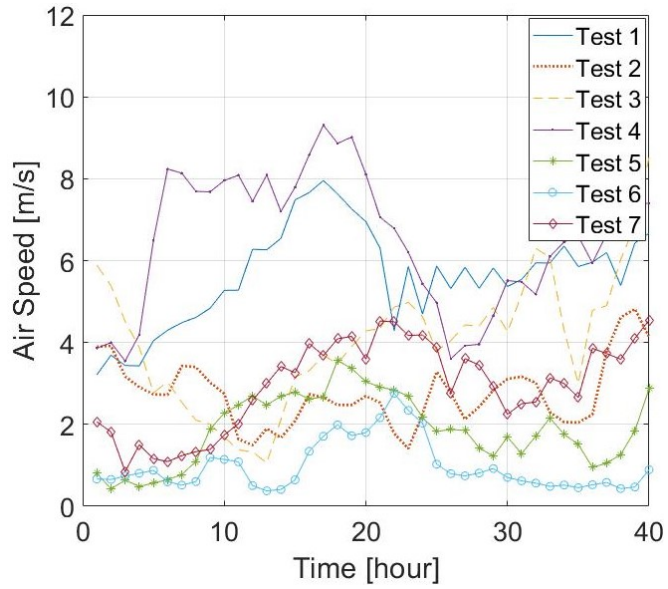

(b)

Fig. 4-24. Outdoor barometric pressure and wind speed during the moisture decay

By comparing the indoor and outdoor vapour pressures, it can be noticed that drops in the outdoor partial pressure generated the plateau in the PIR and wood fibre room, as shown in Fig. 4-25. Similarly, variations of the outdoor vapour pressure between each test generated different gradient of the curves (Fig. 4-26). However, it was not possible to observe a clear relationship in the decays of the rooms, because the three cells did not present persistent variations across each of test. Comparing Test 2 and Test 4 (Fig. 4-25), it can be noticed that in Fig. 4-25a concrete is the one with the highest gradient and quickest decay, while in Fig. 4-25b wood fibre and concrete presented a similar and slower decay. However, the final RH reached at the end of the 40 hours was similar in all the three rooms, regardless of the shape of the curve during the decay.

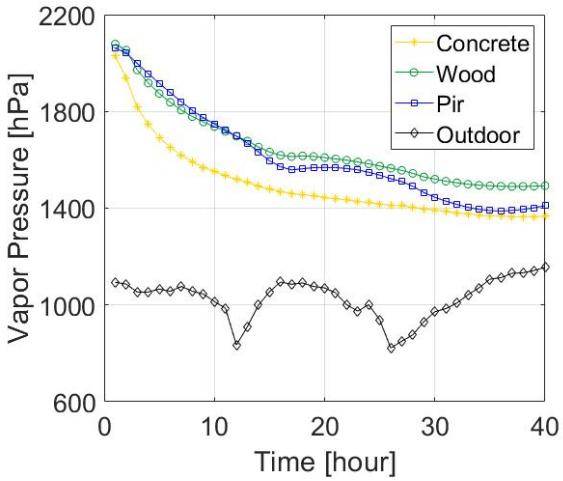

(a) Test 2

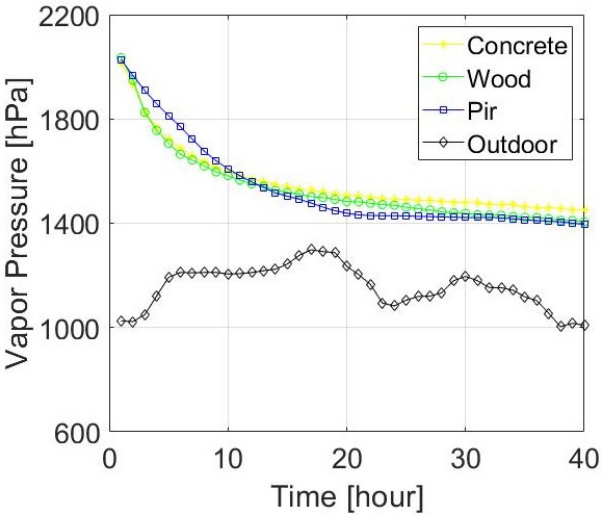

(b) Test 4

Fig. 4-25. Outdoor and indoor water vapour pressure in the three rooms in Test 2 and 4

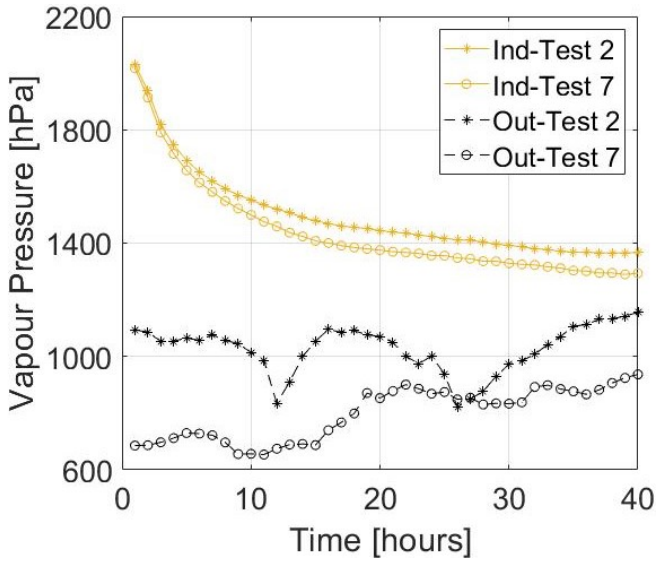

Fig. 4-26. Comparison of vapour pressure the indoor and outdoor vapour pressure in Test 2 and 7

Overall, it was not possible to observe a significant difference between the three rooms apart from the plateau region. Therefore, a statistical analysis was performed to quantify the impact of the outdoor weather on the indoor humidity and to, successively, standardise the curves, by counting for the effect of the weather. To apply the most suitable statistical model, an analysis of the data structure was necessary. The moisture decay measurements were performed multiple times on the same rooms, while subjected to multiple external factors, such as the outdoor weather. As the moisture decay changed over time, time had to be taken into account in the statistical model, as well as the dependency of each data point to the previous one. For example the humidity at time t depends on the humidity at time $t-1$. A repeated measurements mixed model was the most suitable, as it considered the dependency of the measurements and the multiple sources of variability. The outdoor weather was taken into account as fixed effect, as it was the same across the rooms. The structure chosen for the model was auto-regressive, due to the dependency of each data with the previous data. The absolute humidity both for the indoor and outdoor was considered instead of RH, in order to eliminate the dependency of RH on the temperature. The effect of the outdoor temperature, absolute humidity, wind speed and time (fixed effects) on the indoor absolute humidity was analysed, whilst comparing the three rooms performances. Barometric pressure was not considered, as it is correlated to the outdoor absolute humidity. Further details of this model can be seen in Field (2013).

The results of the statistical analysis (Table 4.11) showed that all the outdoor factors influenced the indoor absolute humidity, as they had a p-value lower than 0.05. The outdoor absolute humidity decreased the indoor humidity level, while wind speed and temperature increased it. Every hour the absolute humidity decreased of 0.13 g/m^3,

whilst variations of the temperature and wind speed raised the indoor moisture content of 0.063 g/m^3. Temperature and wind speed impact was significantly lower than humidity and time. The squared and cubic value of the time and the multiplied values (Weather by time) were introduced as they represent the curvature of the decay. The multiplied values did not impact the indoor moisture level, but did impact the steepness of the decay. The elimination of the squared values would have given a linear predicted curve instead, which would have not matched the experimental data. The introduction of time as a variable and as an influencing factor was a way to consider variables that could not be described by the measured weather data. Time can be considered as simultaneous impact of the rooms and the materials that over time changed their behaviour, like the walls absorbing less water, because walls are getting wetter, or water infiltrating through the impermeable layer or seals.

Table 4.11. Results of the mixed model analysis

Estimates of Fixed Effects			
Parameter	Estimate	Std. Error	p-value
Intercept	16.11	0.21	0.00
Hour	-0.50	0.015	0.00
$Hour^2$	0.017	0.00	0.00
$Hour^3$	-0.0002	0.00	0.00
Wind Speed	0.036	0.009	0.00
AbsHum Out	-0.13	0.018	0.00
T Out	0.027	0.004	0.00
Hour * Wind Speed	-0.0009	0.0004	0.02
Hour * AbsHum Out	0.004	0.0007	0.00

As shown in Table 4.12, the estimated values were calculated on the wood fibre room, and then an adjusting coefficient was introduced to adapt the equation to the other two rooms. The concrete and PIR predicted values were adjusted adding -0.11 and -0.13 to the general equation. However, the estimated values were not statistically significant, as the model considered all the rooms behaving in a similar way in terms of their capacity to reduce the moisture content over time.

The final equation to predict the decay for all rooms becomes:

$$\begin{aligned} AbsHum_{Ind} = 16.11 - 0.50(Hour) + 0.017(Hour)^2 - 0.0002(Hour)^3 \\ +0.1(T_{Out}) - 0.13(AbsHum_{Out}) + 0.027(WindSpeed) \\ +0.0037(Hour \times AbsHum_{Out}) - 0.0008(Hour \times WindSpeed) \end{aligned} \tag{4.3.2}$$

Table 4.12. Estimated contribution of the walls in the statistical analysis

Parameter	Estimate	Std. Error	p-value
Concrete	-0.11	0.24	0.648
PIR	-0.13	0.24	0.595
Wood	0.00	0.00	-

The comparison between the average decay curve of the seven tests and predicted curve with its confidence interval (95%) can be seen in Fig. 4-27. It can be stated the predicted decays are representative of the real behaviour of the rooms, as the statistical model matched the average decay curves.

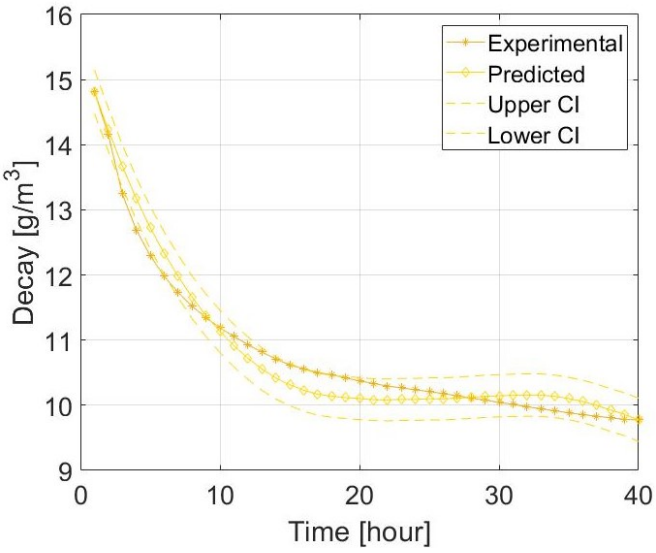

(a) Concrete

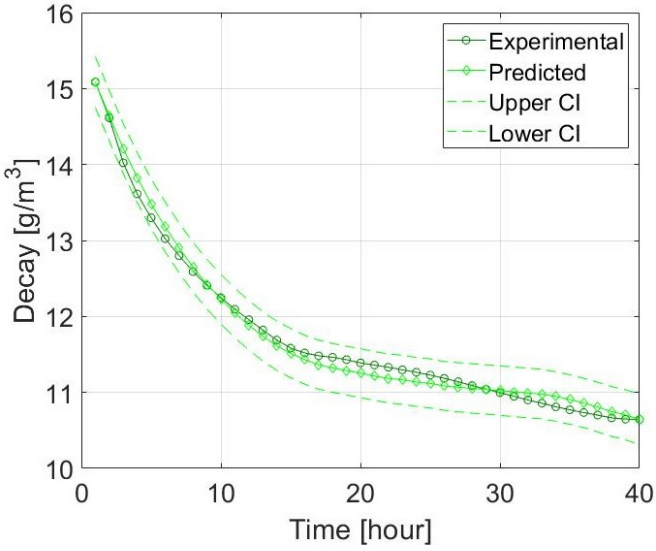

(b) Wood

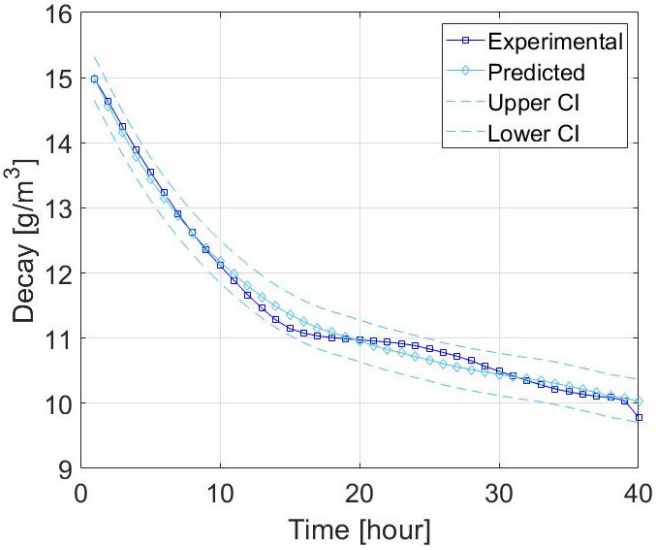

(c) PIR

Fig. 4-27. Comparison of the average decay curve and the predicted one with its 95% confidence interval

Once the effect of the weather was statistically quantified from the moisture decay, the resulting curves for each room were compared to analyse the differences between the three rooms (Fig. 4-28a). Even though there is not a significant difference in terms of humidity level, the curvature of the predicted curves differed (Table 4.13).

Table 4.13. Comparison of the curvature of the three rooms

Contrast	Curvature	Estimate	Std. Error	p-value
Concrete vs Wood	Hour	-0.16	0.02	0.00
	$Hour^2$	0.007	0.001	0.00
	$Hour^3$	0.00	0.00	0.00
Concrete vs Pir	Hour	-0.20	0.02	0.00
	$Hour^2$	0.01	0.001	0.00
	$Hour^3$	-0.0001	0.00	0.00
Wood vs Pir	Hour	0.03	0.02	0.95
	$Hour^2$	-0.003	0.001	0.008
	$Hour^3$	0.000	0.000	0.00

In summary, there were no significant differences between the rooms. As the rooms presented the same decay it implies that is not the wall which is eliminating the RH, but infiltration is playing an important role in the de-humidification. The door is likely not to be as air tight as the other components of the building and this led the moisture to migrate through it. However, the differences in the curvature of the moisture decay either in the predicted and measured case (Fig. 4-28) indicated the concrete and wood fibre walls reduced the humidity excess and smoothed the decay, by eliminating humidity fluctuation produced by the outdoor weather, while PIR was more sensitive to outdoor variations.

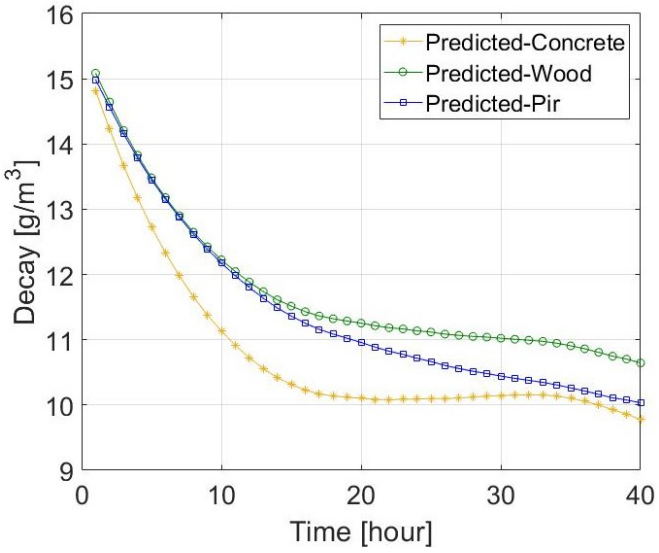

(a) Predicted

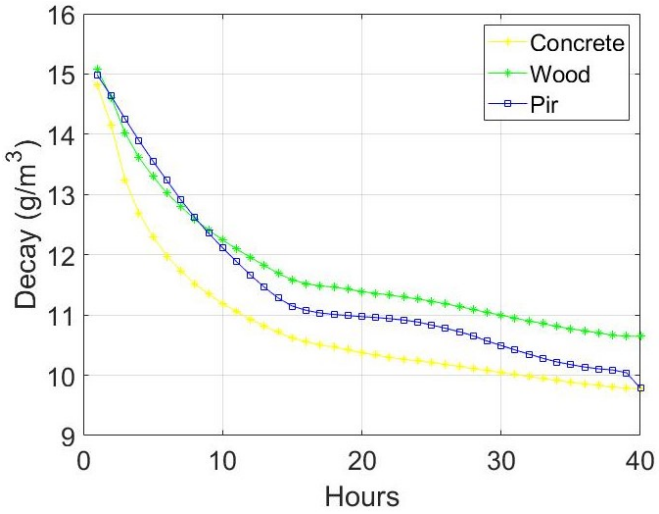

(b) Experimental

Fig. 4-28. Comparison of the predicted and averaged experimental curves

4.3.3 Partial Moisture Balance Equation

The moisture balance equation of the three rooms was calculated. by applying Yang et al. (2009)'s method:

$$w_{Ind}(t) \cdot V = G(t) - (M_{Inf}(t) + M_{Mat}(t)) \tag{4.3.3}$$

Where, w_{Ind} is the absolute humidity indoor and outdoor (g/m^3), G is the moisture load generated by the humidifier (g), V is the room volume (m^3), M_{Inf} are the ventilation and infiltration moisture gain/losses (g), M_{Mat} is the moisture uptake of the walls.

In the PIR cell the M_{Mat} was zero, as the room did non have hygrscopic surfaces.

Consequently the equation can be expanded to become:

$$(w_{Ind}(t) - w_{Ind}(0)) \times V = G(t) - Q_{Inf} \times (w_{Ind}(t) - w_{Out}(t)) \times t \tag{4.3.4}$$

Where, $w_{Ind}(0)$ and $w_{Ind}(t)$ are the absolute humidity in the rooms before and during the test (g/m^3), respectively, G is the moisture load generated by the humidifier (g), V is the room volume (m^3), Q_{Inf} is the infiltration rate (m^3/h) and $w_{Out}(0)$ is the outdoor humidity (g/m^3).

As the infiltration rate might vary depending on the vapour pressure differential, the moisture expelled by infiltration was indirectly calculated from the moisture balance equation in the PIR room. Results presented a variable ventilation rate (Table 4.14), which varied depending on the outdoor weather conditions. Values fluctuated between 0.59 and 0.89, which are eight times higher than the ventilation rate obtained with the gas decay test (Section 4.3.2.1), suggesting significant and variable partial pressure differential between the indoor and outdoor.

Table 4.14. Infiltration rate in the PIR room

	Test 2	Test 3	Test 4	Test 5	Test 6	Test 7
PIR	0.79	0.59	0.87	0.89	0.67	0.62

The same operation was repeated for the other two rooms. However, in the balance equation infiltration and moisture buffering were considered as a joint factor, as it was not possible to independently measure the impact of walls and infiltration. Eq. 4.3.4 becomes:

$$w_{Ind}V = G - (M_{Losses}) \tag{4.3.5}$$

Where, M_{Losses} is the sum of M_{Inf} and M_{Mat}.

Only Tests 4, 5 and 6 were analysed, as these were the only three tests where all three rooms had all the data necessary to calculate the moisture balance. Comparing the results (Figure 4-29), it is clear concrete and wood fibre had higher moisture losses than PIR. The reason of the discrepancy can be due to the either the infiltration or the the hygriscopicity of the rooms. The differences could be seen only in the humidification phase, whilst in the de-humidification negligible differences were observed, as also discussed in Section 4.3.2.4.

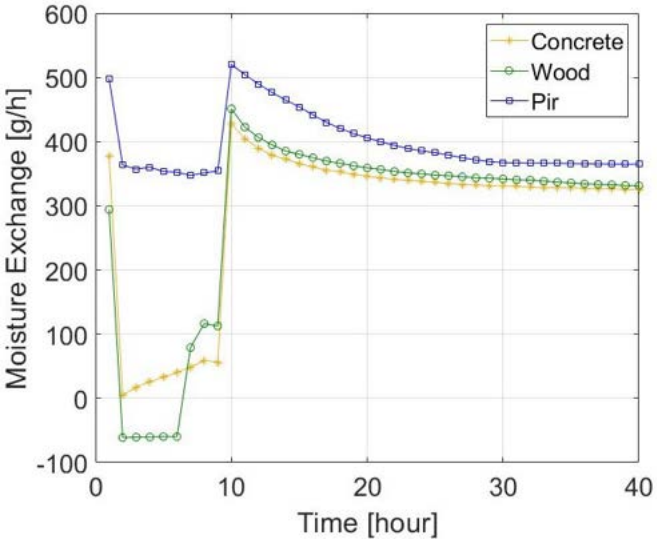

(a) Test 4

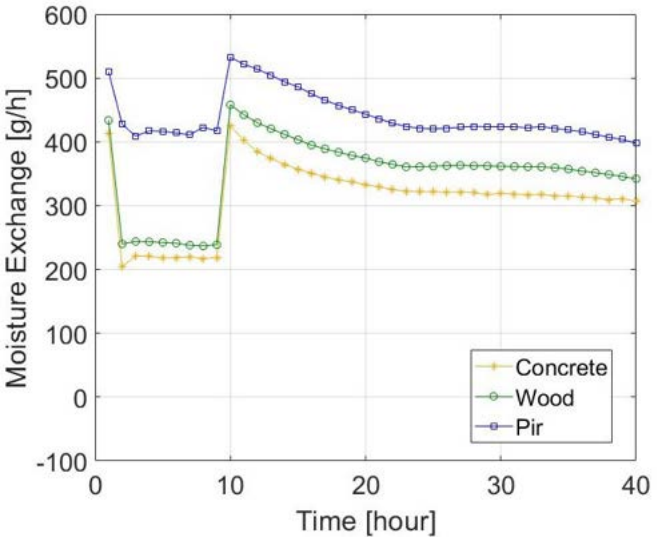

(b) Test 6

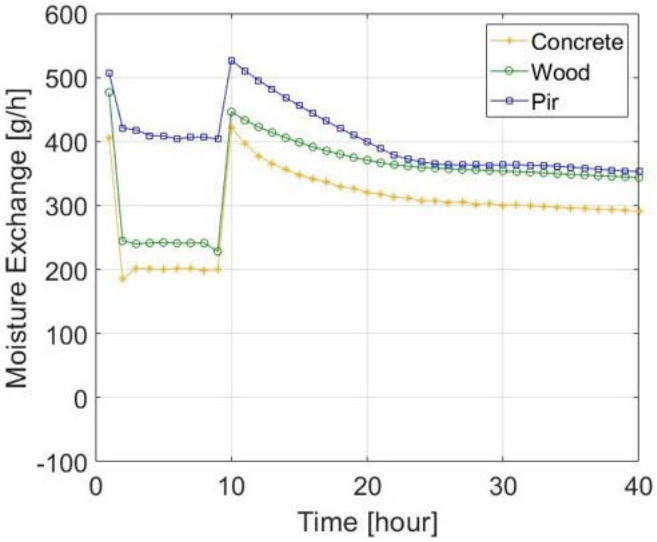

(c) Test 7

Fig. 4-29. M_{Losses} trough infiltration and walls

To determine the walls participation to the moisture balance of the rooms in the humidification phase, it was assumed that the three rooms had the same infiltration rate, which is justified by the analysis on the de-humidification of the decay test in Section 4.3.2.4 and by the gas decay test (Figure 4-29). Consequently, assuming that the infiltration rate was the same in all rooms, the infiltration rates calculated in the PIR (Table 4.14) were applied in the moisture balance equation of concrete and wood fibre. The results of this operation represent the moisture uptake of the walls of the hygroscopic rooms. By dividing the M_{Mat} by the surface area of the walls, an approximation of the moisture buffering capacity could be achieved (Table 4.15), which was in line with the results obtained on a similar study on plasterboard (Yang et al., 2007; Woods et al., 2014; Rode et al., 2002). Yang et al. (2007) applied a similar moisture balance equation to calculate the plasterboard moisture buffering capacity ($9.9\,g/m^2$), which was validated by moisture transmitters applied on the surface. Woods et al. (2014) and Rode et al. (2002) obtained around $8\,g/m^2$ for plasterboard placed on a mass balance in a non-hygroscopic room. However, data are not comparable, as the humidity level, fluctuation and signal differ in different ways from the RH conditions in this study.

Table 4.15. Moisture buffering capacity of the concrete and wood fibre room (g/m^2)

	Test 4	Test 6	Test 7
Concrete	7.40±1.8	5.46±0.2	5.97±0.4
Wood	8.11±2	5.80±0.05	7.16±0.1

4.4 Moisture Buffering

Moisture buffering was investigated in the three rooms, based on a comparable approach to that in Section 3.3. The humidity variations always followed the same principle of the NORDTEST (8 hours humidification at 75%RH and 16 hours de-humidification), but it was investigated under both constant and variable temperature. The two tests were carried on to observe the moisture exchange between the indoor and outdoor via a ventilation system and the effect of temperature on moisture buffering. From the moisture buffering testing a moisture balance equation was established to calculate the participation of walls to buffer moisture. A specimen of plasterboard was placed on a scale in one of the testing room, to monitor the change in water of the material during the full-scale testing. The experimental moisture buffering of the specimen was compared with the calculated moisture buffering value through the balance equation and with the laboratory testing (Section 3.3).

4.4.1 Method

The moisture buffering test at constant temperature was performed by keeping the temperature at 23°C. Four more heaters were added to the room for a total of six, to account for the additional ventilation heat losses through the ventilation system. In the variable temperature investigation, the heaters were switched off to leave the indoor temperature to vary according to the outdoor weather conditions.

In all three rooms a mechanical ventilation system was installed above the door, to reproduce realistically the indoor environment of buildings. The system was composed of an inlet and outlet duct. Similarly to Künzel et al. (2004), the inlet duct was composed of a volume flow controller (Trox VFC), which produced a constant and defined air flow, and a centrifugal fan (Xpelair XID100), which was wired to a fan controller (Fantronix 3Amp-ME1.3), to regulate the air speed, as shown in Fig. 4-30. The inlet overall length was around 1.8 m, whilst the outlet duct was 500 mm.

- Outdoor
- Fan
- Controller
- Indoor

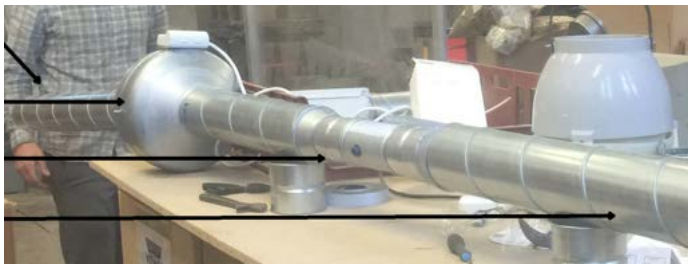

Fig. 4-30. Ventilation system before insulation

The ducts were than covered with a 4 mm aluminium insulation layer (λ=0.002 W/mK). To avoid condensation in winter, the minimum insulation thickness was calculated considering indoor temperature 23°C and outdoor -5°C, which was the lowest temperature recorder by the weather station in 2018. As the minimum calculated thickness was 7 mm, two layers of the insulation sheet were applied on the ducts. The system was mounted on top of the door, as shown in Fig. 4-31b. The different length on the inlet and outlet duct allowed for a good circulation of the air in the room (Fig. 4-31a), whilst on the outside 90° bend ducts were applied, to avoid interference between the inlet and outlet. The inlet pipe was designed to generate a laminar and controlled air flow at the end of the duct.

(a) Indoor

(b) Outdoor

Fig. 4-31. Ventilation system from the inside (**a**) and outside (**b**)

Temperature and RH in the ducts were measured by Tiny Tag sensors at 2 cm from the end of the internal side of the ducts both in the inlet and outlet. The ventilation flow was set to a constant $86\,m^3/h$ (2.8/h) that was calculated by considering the producer's specifications on the fan capacity and the fan controller set-up. The maximum fan capacity was $288\,m^3/h$, but it was reduced to still minimise the risk of condensation in the room, without reducing the moisture buffering potential of the walls. To investigate the water vapour transfer from the plaster to the other wall's components, temperature and RH in the air gap behind the plasterboard in the wood fibre room were also monitored by a Tiny Tag.

Four scales with sample of plasterboard, clay, gypsum and lime plaster were placed in the concrete room (Fig. 4-32). The weight of the specimens was monitored, to have an indication of the moisture adsorbed and released by plasterboard. The other three materials were used to compare laboratory moisture buffering results with the field-

testing data. The specimens were surrounded by a perspex structure that reduced the air speed to less than 0.1 m/s and placed at 1 m from the humidifier. The air speed was measured with a hot wire anemometer (Extech 407119). Spot measurements were taken above the specimens.

Fig. 4-32. Moisture buffering testing in the test cells at the BRP

4.4.2 Results, Analysis and Discussions

In this section the results of the moisture buffering testing are shown. The data available from the in-situ experimentation were analysed and successively used in simulations in Chapter 5 to calculate the moisture balance of the rooms. The full-scale room moisture buffering tests at constant temperature were analysed first and then used as reference for the testes at variable temperature. The ventilation moisture load and the materials moisture buffering capacity in the two tests were also investigated.

The lack of data due to the impossibility to complete all moisture decay and moisture buffering testing pushed to a wider use of simulations (Chapter 5). Originally, a final testing campaign was planned to have a perfected version of all the tests performed previously, which would have allowed a more accurate model construction. For these reasons, the in-situ moisture buffering test was criticised to show the improvement necessary to repeat the test.

4.4.2.1 Moisture buffering at constant temperature

The RH variations in the three rooms are shown in Fig. 4-33. Overall, the cells presented RH lower than 70%RH in most tests. The reason is likely due to low outdoor absolute humidity levels. Because of the low absolute humidity, the humidifiers were overloaded because could not generate more water vapour than they

were designed for. Consequently, humidifiers did not always manage to reach the target RH. In the PIR room the impact of the outdoor weather was more evident, as already discussed in Section 4.3.2.4. The pod reached only a maximum of 60%RH in most of the tests (Fig. 4-33c), as the ventilation system was continuously removing moisture from the room. The concrete and wood fibre cells managed to maintain higher RH levels, probably due to the walls contribution to compensate the moisture content eliminated by the ventilation system, as it will be demonstrated later in this chapter. By comparing the concrete and wood fibre rooms, the concrete room recorded a slightly worse behaviour to maintain the target RH, but it can be related to the calibration of the humidifier's RH sensor. After the testing session it was noticed the sensors was reading 7%RH less than the actual relative humidity.

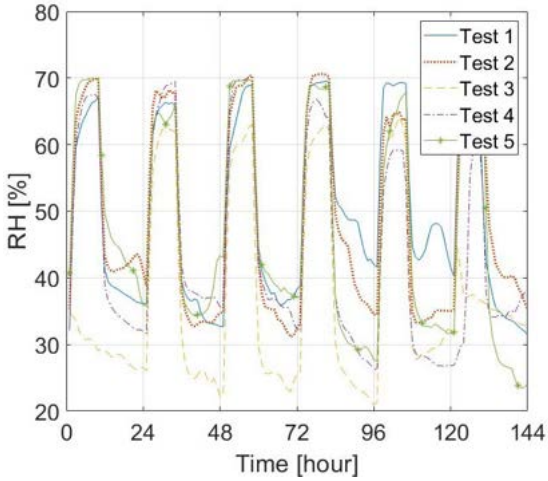

(a) Concrete

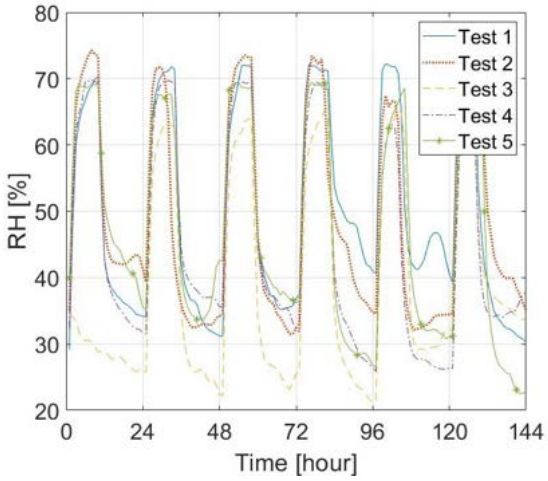

(b) Wood

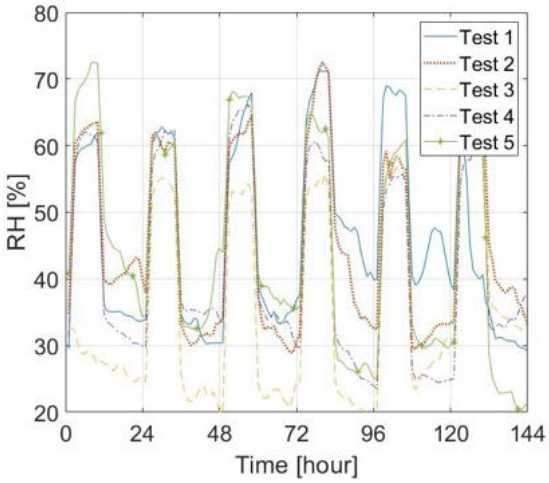

(c) PIR

Fig. 4-33. RH variations in the three rooms at constant temperature

The influence of the outdoor environment on the moisture content in the rooms is shown in Fig. 4-34. When the outdoor absolute humidity dropped, the indoor humidity also

decreased. Looking at the difference between the absolute humidity of the three rooms (Fig. 4-35), it is evident that the moisture content difference is small especially during the de-humidification phase, similarly to what was observed on the de-humidification phase in the moisture decay section (Section 4.3.2.4).

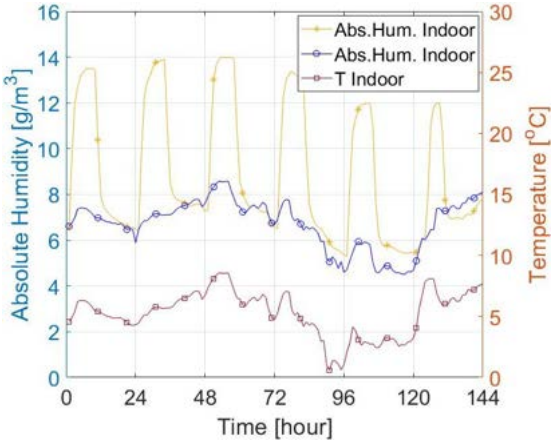

Fig. 4-34. Comparison of the concrete room absolute humidity with the outdoor humidity content

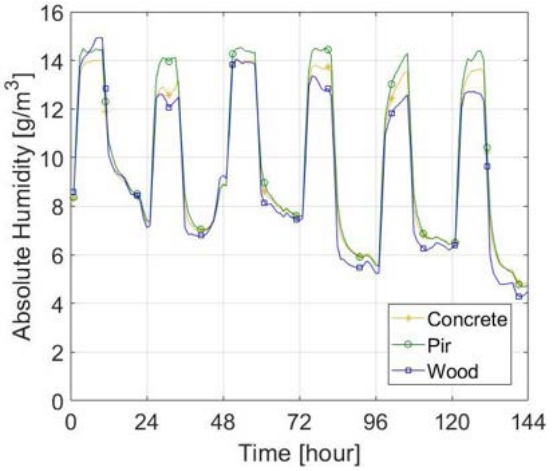

Fig. 4-35. Comparison of the absolute humidity in the three rooms

As observed in Fig. 4-36, even though the number of heaters was increased, the rooms still presented less than 0.5^oC decrease of the temperature in correspondence of the activation of the humidifiers. The sudden humidity increase in the rooms produced a decrease of temperature, as observed in the laboratory testing, due to inverse correlation between moisture content and temperature (Section 3.5.2.4). The small temperature fluctuations are, however, negligible, as they did not significantly influence the indoor moisture content

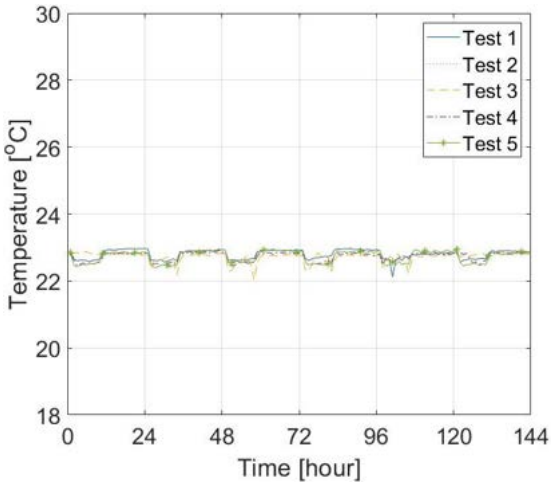

(a) Concrete

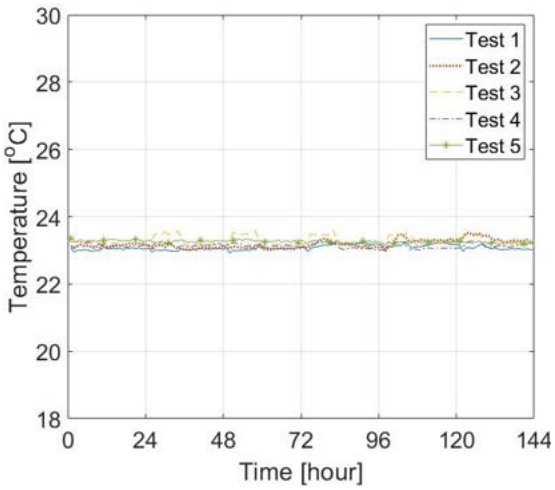

(b) Wood

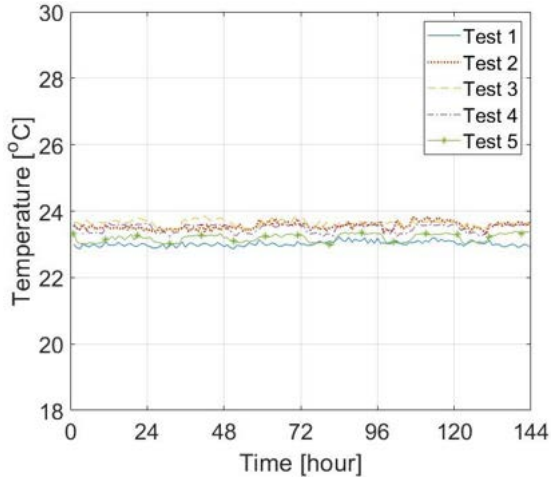

(c) PIR

Fig. 4-36. Temperature variations in the three rooms at constant temperature

The moisture load injected by the humidifier was monitored in the rooms. Due to the malfunctioning of the humidifiers/data-loggers, data on the humidifier water usage in

the concrete and PIR cells were not available. Only in few cycles in the wood fibre room the water used by the humidifier to increase the humidity at 75%RH was recorded. Therefore, the wood fibre room was used for the indoor moisture balance analysis.

The removed/added moisture through the ventilation system was calculated from the ventilation rate and the measurements of temperature and RH sensors that were placed in the air inlet and outlet ducts. The accuracy of this RH method is highly dependant on the accuracy of RH sensors (Yang et al., 2009). Therefore, the data obtained from the outlet and inlet Tiny Tag sensors were compared with the indoor temperature and RH probes placed around the rooms and with the weather station, respectively. The comparison showed a good agreement, confirming a good reliability of the Tiny Tags. Ventilation rate and the difference between the inlet and outlet moisture content were provided for the calculation of the moisture exchange, as specified by Yang et al. (2009). The ventilation rate was calculated by using the inline fan specification, whilst the absolute humidity was determined from the Tiny Tags temperature and RH measurements. The temperature and RH data necessary to calculate the moisture exchange through the ventilation system had several gaps, due to the Tiny Tag's limited memory and short battery life. The partial data were investigated instead and the analysis on the available results is shown in this section.

Fig. 4-37a shows the moisture removed by the ventilation system in the three rooms. The negative values indicate the moisture was removed, whilst positive values indicate the room gained moisture. The PIR cells always removed humidity during the humidification phase except for the few hours that corresponded to the beginning of the humidification process. In the other two rooms ventilation did not remove humidity during the de-humidification, but moisture losses increased significantly during the humidification (Fig. 4-37b). The higher humidity losses in the PIR cell through ventilation are linked to the non-hygrscopicity of the room, which needed to eliminate more moisture through ventilation to balance the indoor humidity.

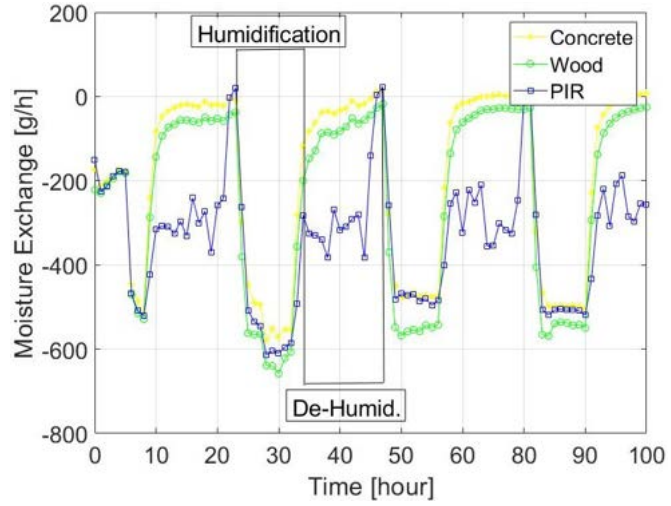

(a)

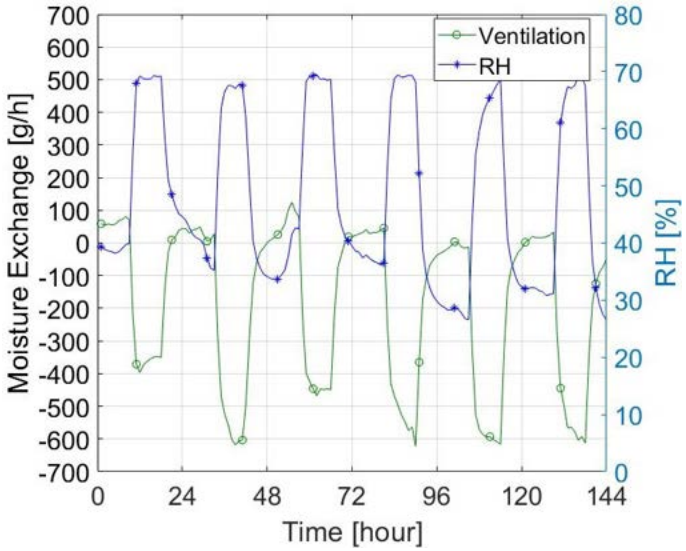

(b)

Fig. 4-37. Humidity gains and losses through the ventilation system

For the moisture buffering test it was not possible to directly calculate the moisture balance in all three rooms, as in each test one of the rooms had some information missingThe only room where it was possible to partially calculate the moisture balance was the wood fibre cell. Test 4 in the wood fibre cell provided all data necessary for the the moisture balance equation, as shown in Fig. 4-38. The moisture balance equation applied was the following:

$$w_{Ind}V = G + M_{Vent} - M_{Inf} - M_{Mat} \tag{4.4.1}$$

Where, w_{Ind} is the absolute humidity indoor and outdoor (g/m^3), G is the moisture load generated by the humidifier (g), V is the room volume (m^3), M_{Vent} is the ventilation moisture gain/losses (g), M_{Inf} is the infiltration moisture gain/losses (g), M_{Mat} is the moisture uptake of the walls (g).

Which expands out to:

$$(w_{Ind}(t) - w_{Ind}(0)) \times V = G(t) + Q_{Vent} \times (w_{Inlet}(t) - w_{Outlet}(t)) \times t \\ -Q_{Inf} \times (w_{Ind}(t) - w_{Out}(t)) \times t - M_{Mat}(t) \quad (4.4.2)$$

Where, w_{Ind} and w_{Out} are the absolute humidity indoor and outdoor (g/m^3), respectively, G is the moisture load generated by the humidifier (g), V is the room volume (m^3), Q_{Vent} and Q_{Inf} are the ventilation and infiltration rate (m^3/h), w_{Inlet} and w_{Outlet} are the humidity content of the inlet and outlet ventilation ducts (g/m^3).

The unknown variables in the balance equation were the infiltration rate and the moisture buffering capacity of walls. The infiltration rate from Table 4.14 was applicable in this section, due to the installation of a ventilation system that may increase the building air leakages. Therefore, the infiltration rate was calculated through the moisture balance equation of the three rooms in the instantaneous injection test, when covered by the impermeable membrane (Section 4.3.2.2). In the instantaneous injection test the ventilation system was turned off and sealed, and the total water load injected in the room was 1 kg. By applying Eq. 4.3.4 in Section 4.3.3, the infiltration rate of each room was estimated, as showed in Table 4.16.

Table 4.16. Air change rate in the three room after the installation of the ventilation system (1/h)

	Concrete	Wood	PIR
ACH	0.89	0.83	1.45

The moisture gain/losses through infiltration, ventilation and moisture buffering in the wood fibre room in the last two cycles of Test 4 are shown in Fig. 4-38. Ventilation, infiltration and walls were all participating to the moisture dissipation during the humidification. Ventilation had the highest contribution to remove moisture during the humidification phase, whilst during the de-humidification, the ventilation and infiltration impact was negligible after few hours from the end of the humidification. The walls one third less moisture than the ventilation during the humidification, but during the de-humidification, walls released moist air into the room, due to the low humidity level in the indoor (around 20%RH).

By standardising the moisture buffering capacity of the room for the plasterboard surface area, the calculated moisture buffering capacity of the walls was 13 g/m^2 and 18 g/m^2 in the first and second cycle, respectively. The higher sorption capacity of the walls than in the moisture decay test is explained by the higher amount of water used for the humidification, due to the lower humidity level and different weather conditions in the moisture buffering test.

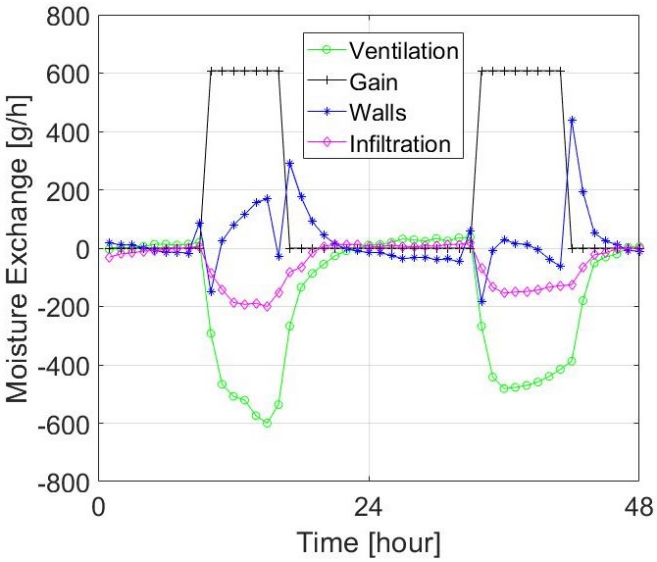

Fig. 4-38. Moisture balance in the wood fibre room in Test 4

4.4.2.2 Comparison of the Moisture Buffering Capacity of Plasterboard sample and Walls

To define the impact of the plasterboard on the indoor RH the mass variations of the plasterboard specimen were experimentally investigated, as described in Sect. 4.4.1. Moreover, the temperature and RH variations in the air gap behind the plasterboard were analysed. The moisture uptake varied in every test, depending on the moisture content in the room (Fig. 4-39a). Regardless of the RH levels, plasterboard followed the same trend of materials subjected to square wave variations in laboratory testing (Fig. 4-39b, as observed in Section 3.3. Comparing the calculated moisture buffering capacity of walls obtained in Section 4.4.2.1 with the specimen, plasterboard sample adsorbed 73% more than the calculated total moisture adsorbed by the walls. Plasterboard specimen adsorbed 57.65 g/m^2 and 67.22 g/m^2 for the two cycles analysed in Section 4.4.2.1, respectively. The discrepancy between the calculated and measured values may depend primarily on underestimation of the water usage in the room in the moisture balance equation. However it may also depend on the air velocity on the surface of the material. The plasterboard specimen was protected surrounded by a perspex structure to reduce the air speed to less of 0.1 m/s, while the walls were exposed to the air speed generated by the ventilation system and fan. Other reasons could be related to the horizontal position of the specimen, which may behave differently than when applied to walls. Also the presence of the under-layers and the effect of the outdoor environment on the walls moisture transport may reduce the moisture sorption capacity of plasterboard. Latif et al. (2015) showed, within a laboratory setting, that the application of only lime plaster kept the assembly's moisture buffering capacity higher than the other cases, where lime was applied on top of gypsum plasterboard or air barrier.

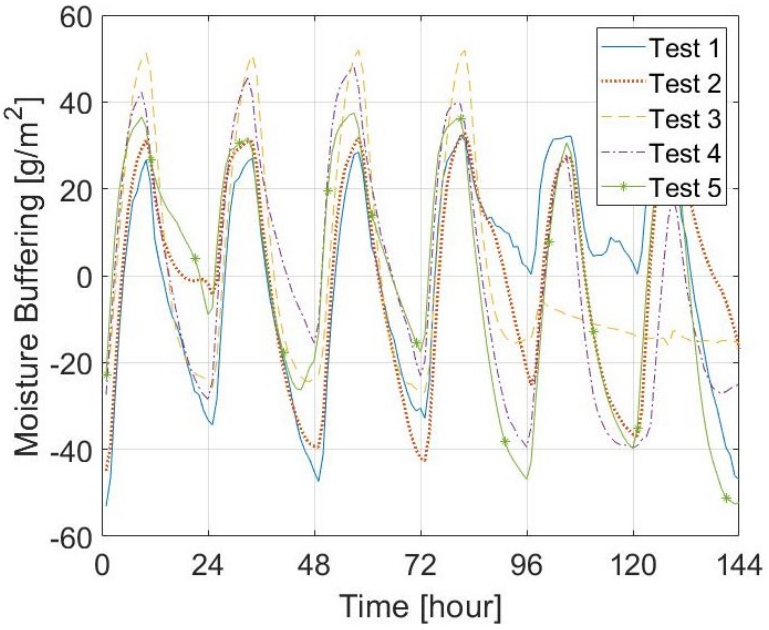

(a)

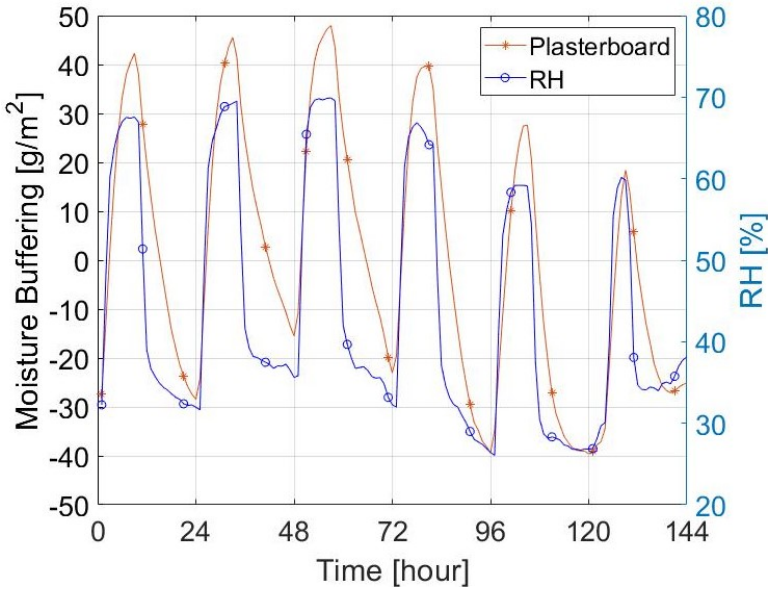

(b)

Fig. 4-39. Moisture buffering of plasterboard in the concrete room

The air gap followed the same RH fluctuation as the room (Fig. 4-40). It was expected to see a delay in the RH variations in the gap, as the moisture within the room would first have to be transferred through the plasterboard, which should have slowed down the vapour transport. The simultaneous variations of RH between the room and RH suggested the moisture moved into the air gap through any gaps between the plasterboard panels instead. The RH fluctuations in the air gap were, however, reduced by 18% compared to the room fluctuations, and the RH peaks followed the same curvature of the plasterboard sorption curve (Fig. 4-39b). These observations can be associated to the joint participation of plasterboard and the

under-layers (wood fibre insulation) that moderated the RH in the air gap, once the moist air moved into the cavity. Moreover, the air gap temperature presented slightly higher fluctuations than in the room, which suggested there may be convection air movement in the air gap. For all these reasons, it was not possible to quantify the amount of water that plasterboard transferred to the air cavity. The moisture transfer through the wall was further investigated in Chapter 5.

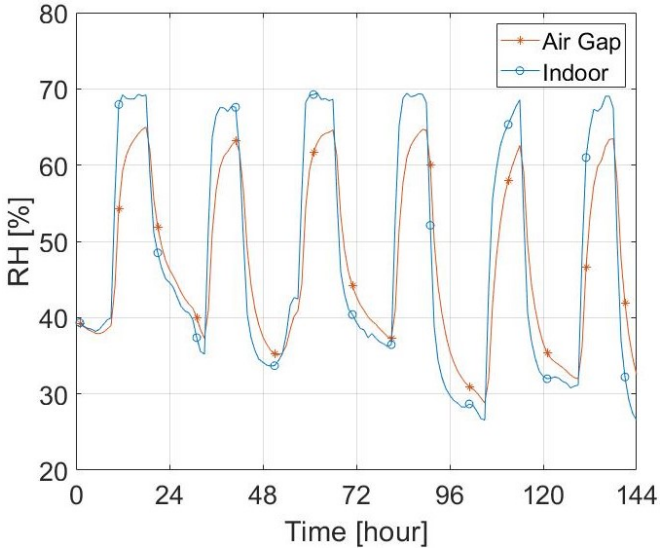

(a)

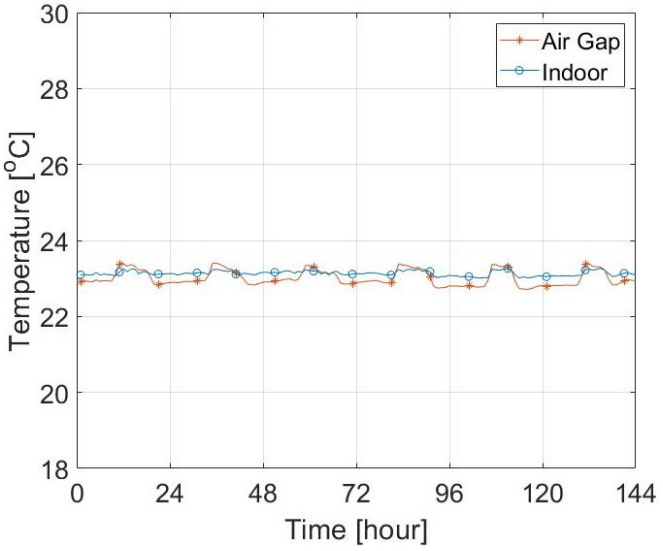

(b)

Fig. 4-40. Air gap in the wood fibre room at constant temperature

4.4.2.3 Moisture Buffering at Variable Temperatures

In this section the response of the rooms to variable temperature was investigated. The RH and temperature variations in the three rooms can be seen in Fig. 4-41 and Fig. 4-42. The RH fluctuation intervals were significantly smaller than at constant

temperature (less than 20%RH), especially when the outdoor humidity was higher than in the indoor. During these investigation the RH increased sharply above 75%, which did not allow for the activation of the humidifiers. As there was no active de-humidifier, it was not possible to reduce the humidity and continue the test in this situation. The RH variations in concrete and wood fibre were similar (Fig. 4-41a and Fig. 4-41b), while PIR presented significant lower variations, where the humidity never dropped below 70% (Fig. 4-41c). Temperature variation between the rooms were relatively small (Fig. 4-42), presenting a maximum temperature differences in some cycles of 2.30 ^oC. The highest differences were observed between the PIR and concrete room. The average daily temperature fluctuations for each room are summarised in Table 4.17. PIR showed slightly higher daily variations than the other rooms.

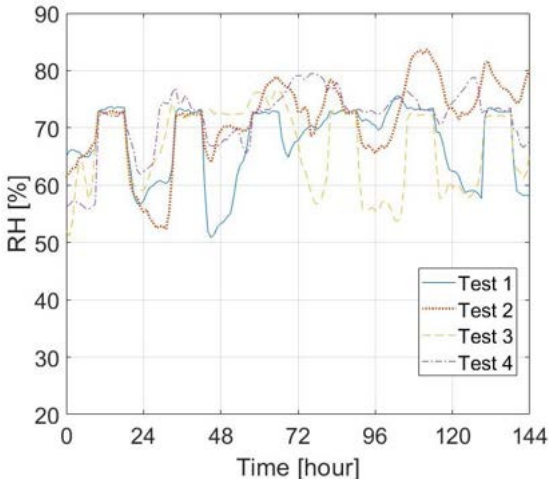

(a) Concrete

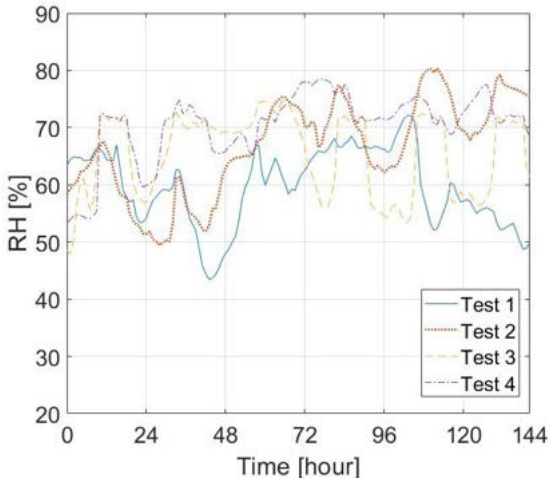

(b) Wood

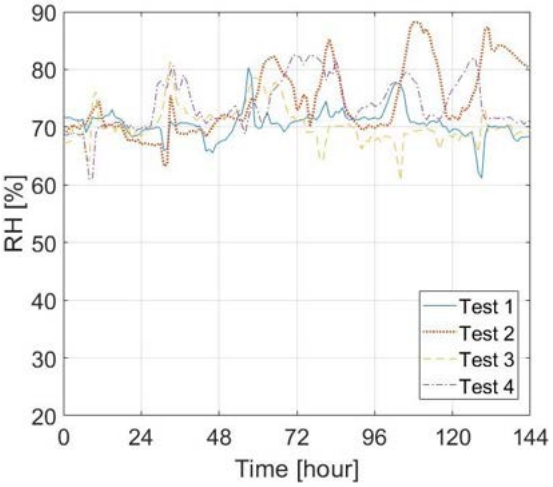

(c) PIR

Fig. 4-41. RH variations in the three rooms at variable temperature

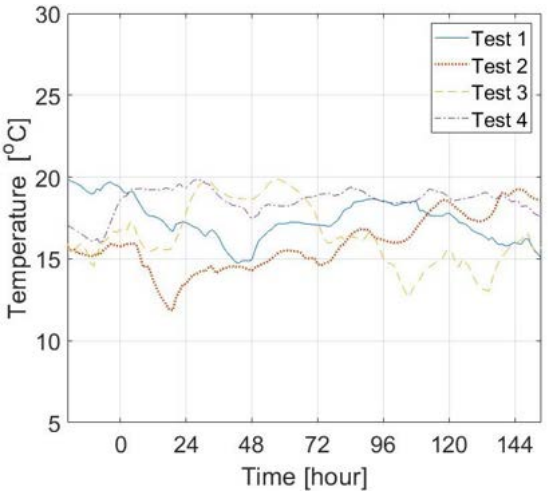

(a) Concrete

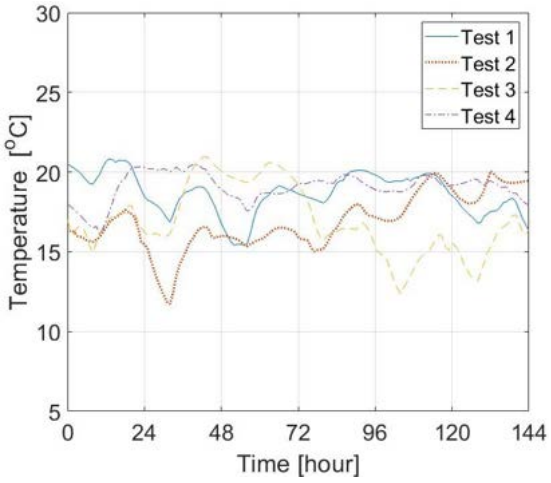

(b) Wood

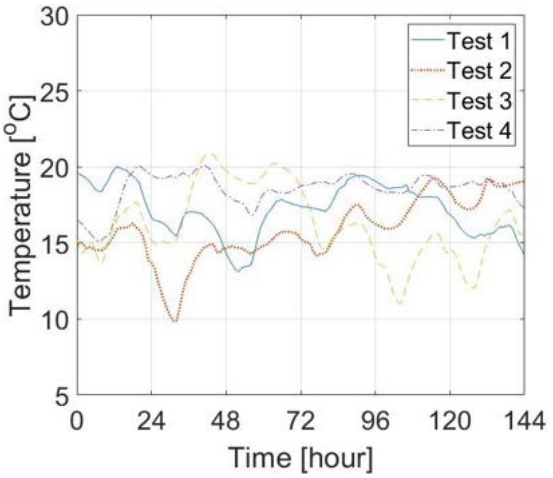

(c) PIR

Fig. 4-42. Temperature variations in the three rooms at variable temperature

Table 4.17. Daily temperature fluctuations (^oC)

	Concrete	Wood	Pir
Average	2.67	3.19	3.85
Max	4.16	5.90	6.42
Min	0.86	0.74	1.25

When the outdoor RH was lower than in the indoor, the humidifier activated. During the de-humidification, even though the outdoor humidity increased, the cells expelled the moisture produced by the humidifier (Fig. 4-43a), but to a lower rate than at constant temperature (Fig. 4-37). However, when the outdoor RH reached 100%RH for a prolonged time, as in Fig. 4-43b, the indoor RH increased significantly above 75%. In this case, the humidifiers did not turn on and the indoor RH followed the same RH variations of the outdoor, but presenting smaller fluctuations. The indoor temperature followed the outdoor, but the rooms reduced and shifted the indoor temperature variations, probably due to the thermal storage capacity of the walls and slight attenuation of the air temperature in the ventilation system (Fig. 4-43c). Indoors temperature and RH fluctuations presented an opposite trend, when the humidifier was not activated. When the temperature peaked, the RH reached its minimum and vice-versa.

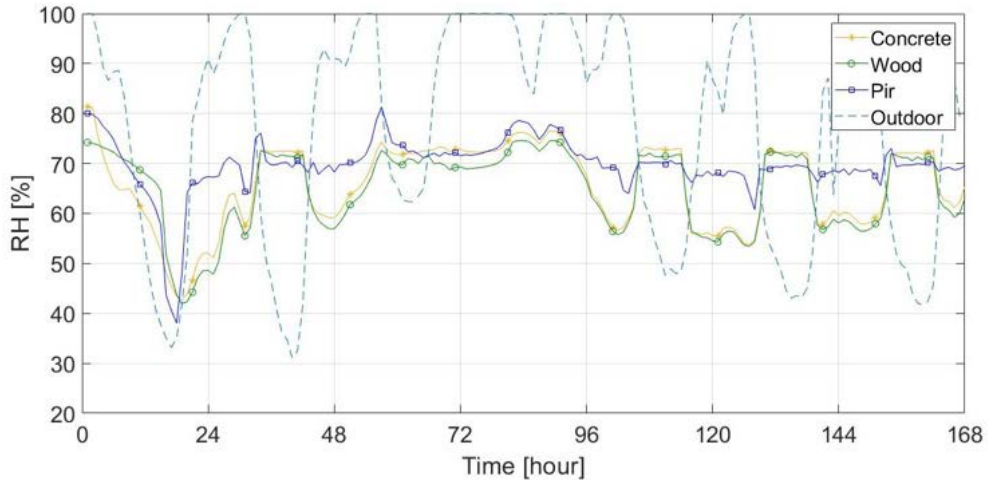

(a) Test 3

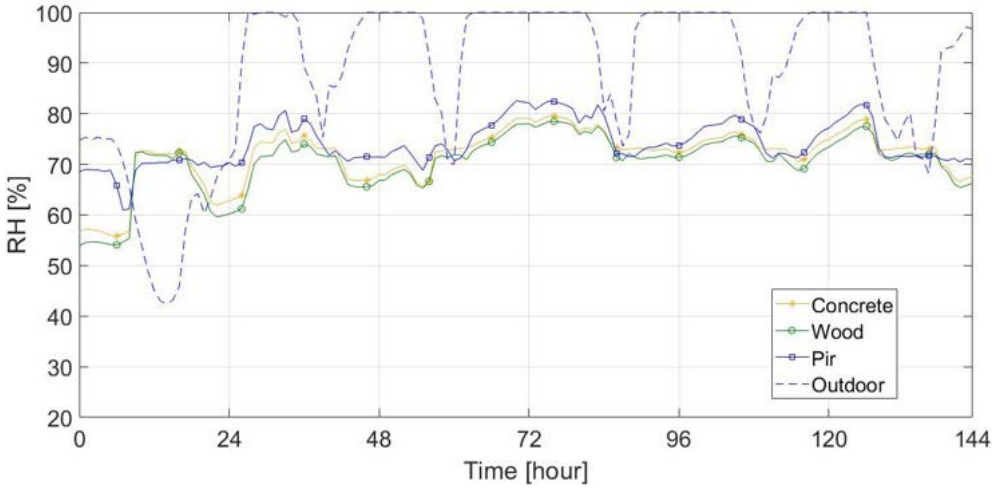

(b) Test 4

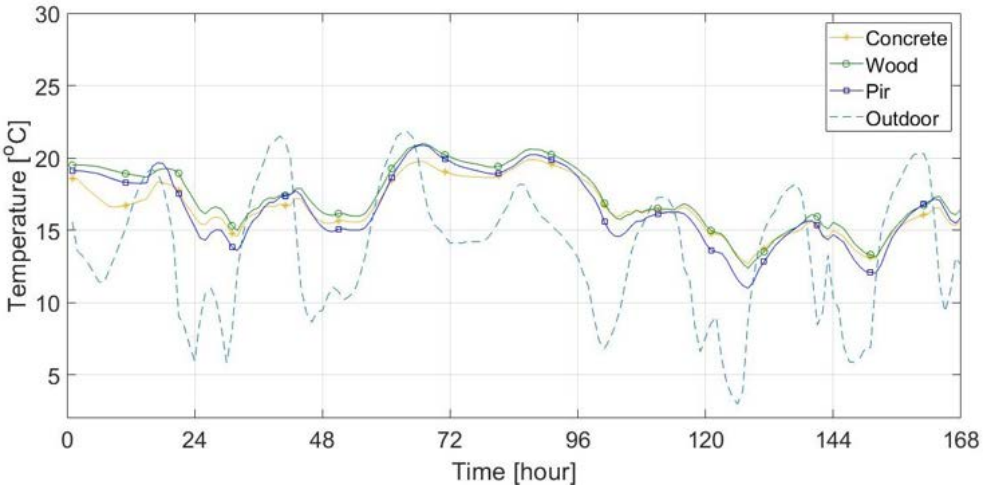

(c) Test 3

Fig. 4-43. Comparison of the temperature and RH variations in the three rooms and the outdoor at variable temperature and ventilation rate of 86 m^3/h

Even though there were differences between the RH in the three rooms, when

considering the absolute humidity there were no substantial differences (Fig. 4-44). This indicated that each room responded differently to achieve the same moisture balance, by regulating the temperature and the amount of water eliminated by ventilation and through the walls. Therefore, the humidifier moisture load, ventilation and walls adsorption were significant to observe the differences between the rooms.

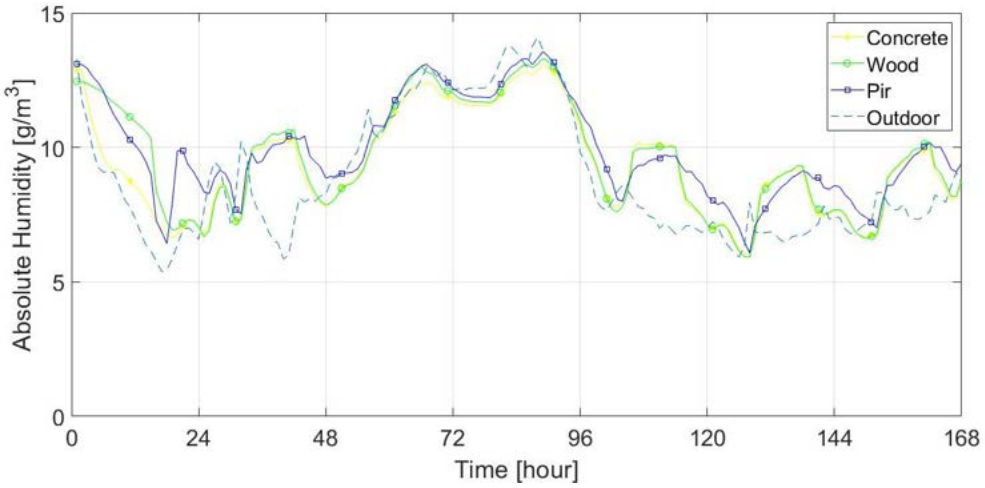

Fig. 4-44. Absolute humidity variations in the three rooms at variable temperature

Compared to the tests at constant temperature, the water usage of the rooms at variable temperature was significantly smaller (Fig. 4-45a). This is due to the overall higher indoor RH level, which reduced the time the humidifier was on during the humidification. As the water usage for this test was low, a smaller water tank without a water pump was used to supply the reservoir on the mass balance. Considering the water usage in the three rooms as seen in Fig. 4-45b, the water usage was less than 150 g per cycle, but it varied in each cycle and for each room. As there were some technical issue with the mass balance in the concrete room, the wood fibre and PIR cells were used to calculate the moisture balance equation.

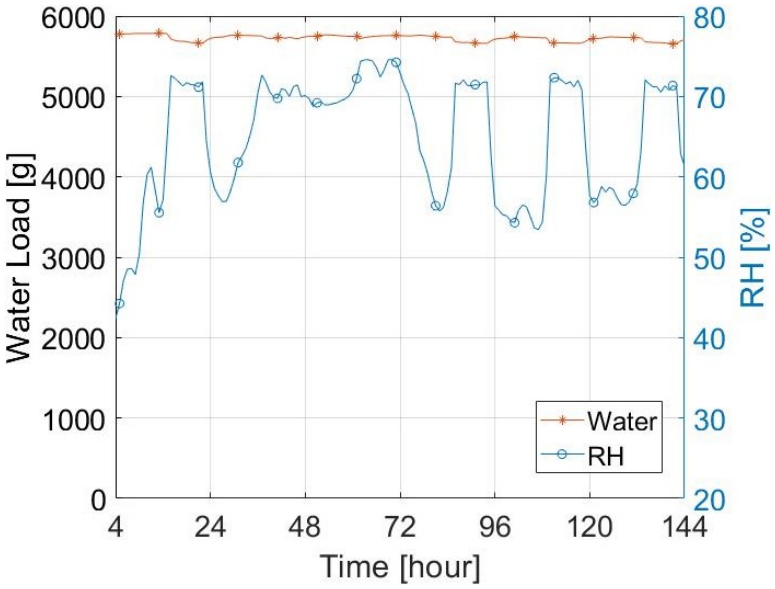

(a) Test 4

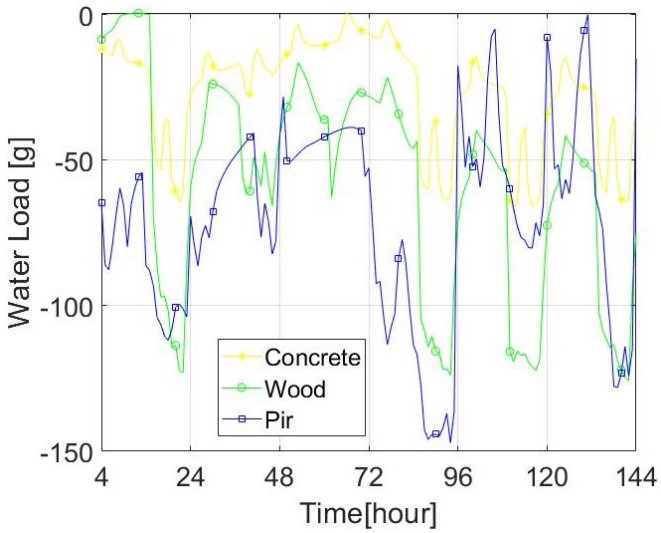

(b) Test 5

Fig. 4-45. Water load used by the humidifier at variable temperature

As already explained in the previous section, the moisture eliminated through ventilation increased during the humidification (Fig. 4-46a). However, less moisture was expelled than at constant temperature (circa 400 g/h less) and the ventilation system moved moist air into the room during the decay, due to the high outdoor absolute humidity level. This explained the significant indoor moisture content increase in some tests. When the temperature was not controlled the difference between the three rooms was small in terms of ventilation moisture removal. As shown in Fig. 4-46b, wood and concrete behaved similarly, while PIR removed slightly more water than the other two. The higher moisture removal of the PIR can be explained by the participation of the walls in the other two rooms.

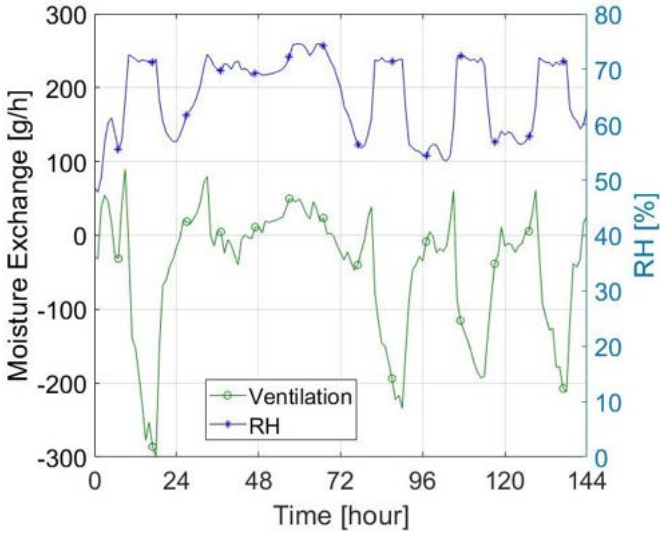

(a)

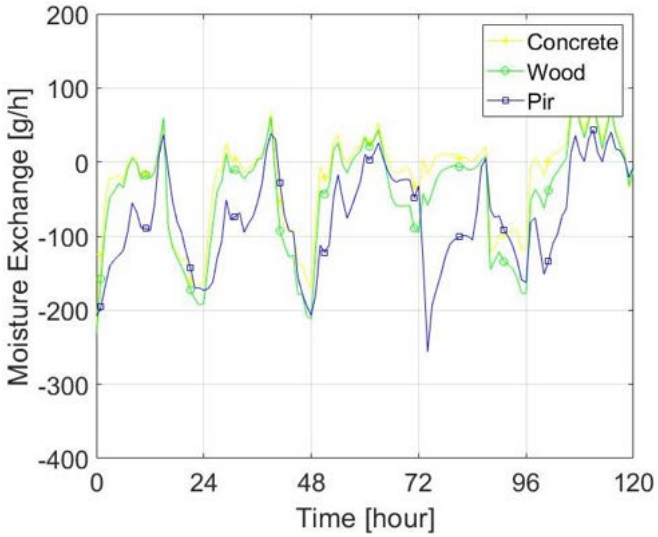

(b)

Fig. 4-46. Moisture gains and losses through the ventilation system compared with the RH variations

As in Section 4.4.2.1 and by applying the moisture balance equation (Eq. 4.4.1), the moisture gain/losses through infiltration/ventilation and walls were calculated for PIR and wood fibre (Fig. 4-47). The moisture balance suggested ventilation pushed moist air from the room to the outdoor, except when the humidifiers were not active. The ventilation participation to remove the moisture in the rooms was less significant than at constant temperature (Fig. 4-38). Infiltration had an opposite trend than ventilation due to the higher outdoor vapour pressure that moved moist air in the indoor, increasing the overall moisture content of the rooms. Walls did not have a great impact in the moisture elimination in the rooms during the humidification, as ventilation was already dissipating the moist air outdoor.

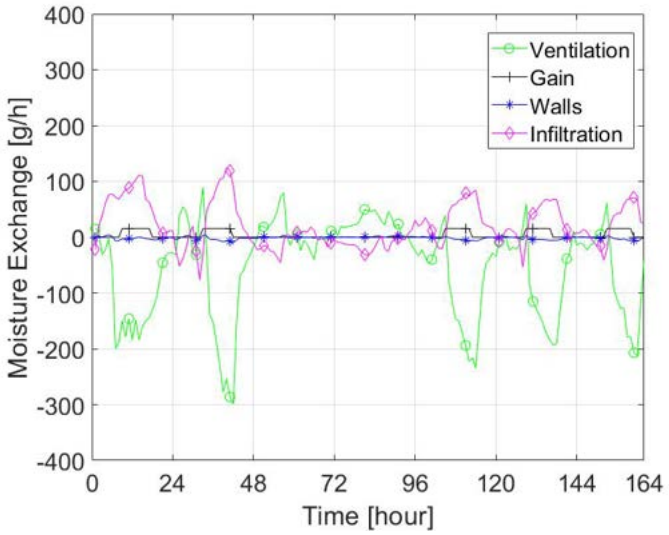

(a) Wood fibre

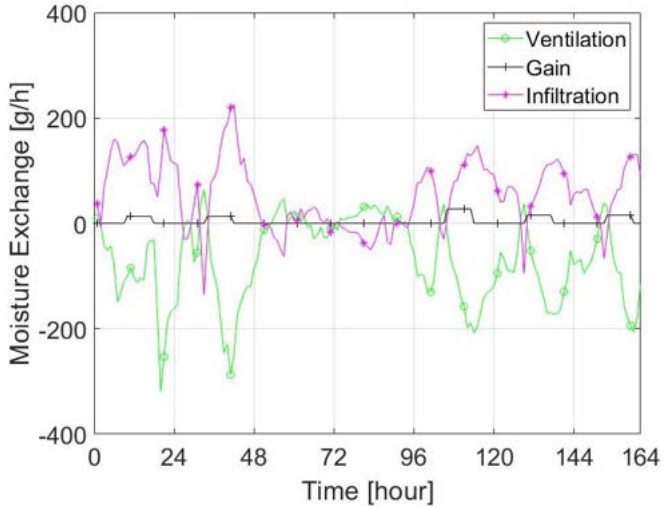

(b) PIR

Fig. 4-47. Moisture balance in the wood fibre and PIR room

The investigation of the mass variations of the plasterboard specimen (Fig. 4-48) confirmed the reduced capacity of plasterboard to store water, when temperature were low and variable. The measured moisture buffering capacity was around 13.70 g/m^2 (82% less than at constant temperature). Temperature appears to be a significant factor that regulate the moisture content indoors. The lower average temperature in the cells allowed for an higher RH that may have saturated and wet the plasterboard surface and paper coating.

Another reason of the reduced moisture buffering capacity could be linked to the smaller moisture load injected in the rooms, which was mainly removed through ventilation. This suggested that there was no necessity for the room to store water into the walls. However, the possibility that the water tank did not provide the real water usage needs to be taken into consideration. In this eventuality the moisture balance equation may

present different results.

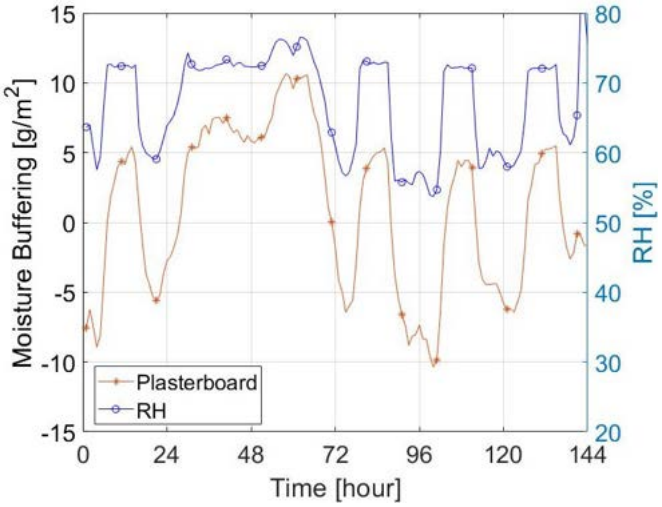

Fig. 4-48. Moisture buffering capacity of plasterboard at variable temperature

4.5 Moisture Buffering Performances of Plaster Samples in Laboratory and Full-scale testing

The comparison between experimental laboratory and full-scale testing is complex, as both tests were based on different set-ups and principles. Laboratory testing were performed in a climatic chamber, in which temperature and RH were easily and automatically controllable, although the amount of water used by the chamber to maintain the target environmental conditions was not monitored. On the contrary, in the full-scale room the amount of vapour injected in the room to keep the RH constant was monitored, but it was not possible to observe the change in weight of the walls. Therefore, for the in situ-testing the impact of the materials on the moderation of the indoor RH was investigated instead. The volume of the chamber and the rooms is another important difference in the test set-up. The released moisture in the two cases may differ, as the climatic chamber has a volume of 0.33 m^3 compared with the testing room of approximately 30 m^3, probably affecting moisture buffering. In this section the change in weight of four coatings in the test cells was investigated and compared with the laboratory moisture buffering protocol Section 3.3, to analyses discrepancies and similarity between the two scale testing.

4.5.1 Method

The moisture buffering capacity of the four coatings (clay, gypsum, lime and plaster board) tested in the laboratory and in one of the experimental room (concrete room) is compared. As already described in Section 4.4, in the in-situ rooms the NORDTEST

protocol was followed to allow the comparison with the laboratory testing. The in-situ NORDTEST test combined elements of the laboratory protocol, by placing a specimen of each material on a mass balance surrounded by a net to reduce the air velocity to 0.1 m/s, as described in Section 4.4.1. At the same time materials were subjected to a larger indoor environment that were influenced by the outdoor weather, ventilation and moisture load (Section 4.4), to reproduce realistic indoor environmental conditions, in which coatings are normally exposed. The change in wight of the coatings was monitored during the moisture buffering test presented in Section 4.4.

Due to the variable outdoor environmental conditions and only the use of an humidification system, the RH fluctuations did not always follow the 75%-33%RH square wave signal as in the laboratory testing. Therefore, each cycle in the full-scale testing was monitored and the cycles, where the RH fluctuations aligned with the ones in the NORDTEST (42 %RH amplitude and within the 75%-33%RH) were analysed. The change in weight of the four specimen in these cycles were compared with the laboratory testing (Section 3.3).

4.5.2 Results and Analysis

The moisture buffering capacity of the plasters within the 30 m^3 in-situ volume is shown in Fig. 4-49 and Table 4.18. In the full-scale testing, gypsum was the better performing material, as it presented higher moisture adsorption (88.63 g/m^2), whilst lime exhibited the lowest capacity (33.56 g/m^2). Plasterboard had lower values than gypsum (76.16 g/m^2) and similarly to the laboratory testing the material presented a plateau. Differences with the laboratory can be seen in Table 4.18. The variations between laboratory and in-situ testing were due to the variable fluctuation of the humidification system and errors in the measurements. Gypsum and plasterboard presented 7% and 15% higher sorption capacity than in the laboratory, whilst clay and lime showed 30% and 22% lower values, respectively. The reason of the higher moisture buffering values for plasterboard and gypsum are related either to the higher sensibility of the materials to moisture variations and to the possible uneven distribution of the moisture on top of the materials. Temperature and RH were not directly monitored above the specimens in the room, so environmental conditions may be slightly different than in the rest of the room and between materials.

Another difference may be also in the humidifier functioning. In the test cell the humidifier injected moisture from the bottom to the top of the room, which then fell back unevenly on the specimens, probably wetting more the surface of plasterboard and gypsum and increasing their overall weight. On the contrary, in the laboratory the climatic chamber releases moisture below the mass balances and a fan uniformly circulates the most air, so there is no direct injection of moisture on the materials. Moreover, in the chamber it was possible to achieve square wave RH fluctuations,

whilst the RH decay during the de-humidification in the test cells was slower than in laboratory and followed a logarithmic curve, changing the moisture buffering mechanisms of materials.

Table 4.18. Comparison of the moisture buffering capacity of plasters (g/m^2) and confidence interval

	Clay	Gypsum	Lime	Plasterboard
In-situ	46.79±3	88.63±8	35.37±3	76.00±7
Laboratory	60.90 ±1	81.90±1	43.26±4	65.52 ±2

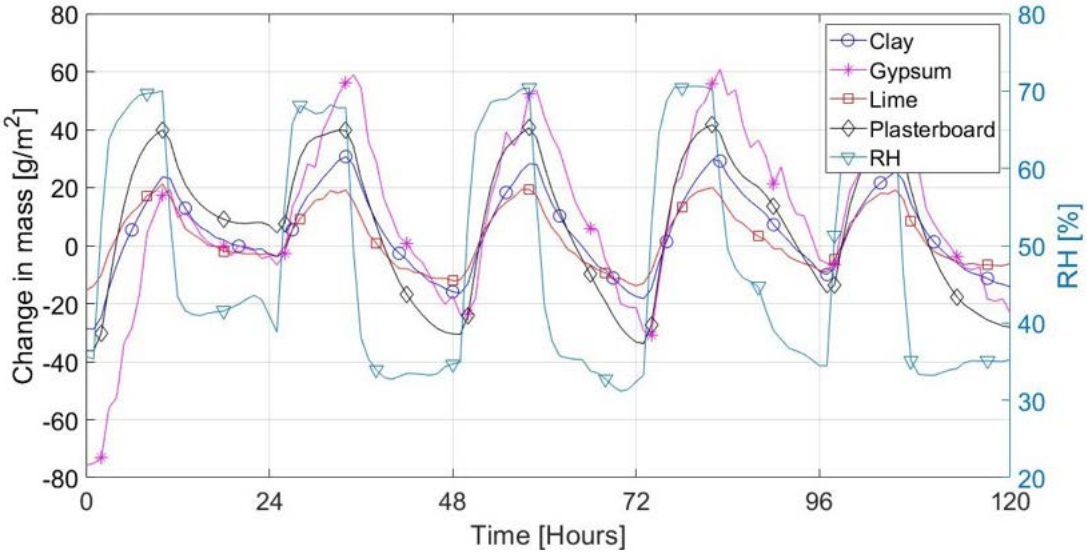

Fig. 4-49. Moisture buffering of the materials in the concrete cells at the BRP

4.5.3 Discussion

Even though the test cells had significantly higher volume than in the climatic chamber, the in-situ and the laboratory experimental testing showed some discrepancies that cannot be, however, considered significant. The discrepancies were generated by several uncertainties, such as the uneven moisture distribution and environmental conditions, and variations in the overall RH fluctuations in the room. This investigation indicated that moisture buffering is strongly dependent on the RH in the room. When the RH fluctuation and RH level are unvaried, either the volume of the enclosed space, moisture load and ventilation do not influence the coatings' dynamic sorption capacity, as it is also demonstrated in Section 5.2.4.

4.6 Summary

The effect of infiltration, ventilation, temperature and weather on the indoor moisture regulation capacity of hygroscopic walls was investigated in this chapter. Three rooms with different wall assemblies but the same plasterboard applied on the indoor surface were tested. One of the three rooms was covered with an impermeable layer, to be used as non-hygroscopic reference room, while the other two had the plasterboard exposed to the indoor climate. The two hygroscopic rooms presented two different wall structures. One room was a timber frame building insulated with wood fibre panels while the second cell was a concrete cavity wall filled with PIR insulation. The moisture exchange through infiltration and the influence of the weather on the indoor were first analysed through a moisture decay test.

A moisture decay test consisted of a humidification phase, where an humidifier injected a known amount of water into the rooms for 8 hours, to reach and maintain 75%RH. The humidification step was followed by a de-humidification phase, where the reduction of the RH level was observed until the rooms reached the initial RH observed before the tests. The humidification step showed that in the non-hygroscopic room the humidifier consumed half amount of water to maintain the moisture to 75%RH than the hygroscopic rooms. This demonstrated hygroscopic walls adsorbed water from the indoor to balance and reduce the moist air. Consequently, the concrete and wood fibre rooms needed more water to keep RH high. It was also observed that the water usage varied in each test, which suggested the outdoor weather influenced the indoor moisture content. A strong correlation between outdoor temperature and absolute humidity, and the indoor was not found. However, a correlation between wind speed and the humidifier water usage was found, which indicated there is a dependency of the moisture dissipation through infiltration on the wind speed. The wind impact on buildings needs to be integrated in the usual infiltration moisture removal calculation. Consequently, it might be possible to predict realistically the moisture removed through infiltration during the humidification, depending on the outdoor air velocity.

The de-humidification phase showed that the moisture reduction followed a logarithmic curve in all rooms. The moisture decay during the de-humidification did not present significant differences in the humidity level between the three rooms, as the three cells were similarly impacted by the outdoor temperature, RH and air speed. However, a statistical analysis demonstrated that the rate of change and speed of the de-humidification curve was significantly different in the three rooms. The concrete room was the one that smoothed the decay curve and reduced quickly the humidity level in the first twelve hours of the decay, while in the non-hygroscopic room the moisture decay curve was more influenced by the outdoor weather. The wood fibre room followed the same behaviour of the concrete room, but the decay was

slower and it was slightly influenced by the outdoor climate. It is not completely clear why the reference room was removing moisture quicker than the wood fibre room, but a reason could be due to the non-hygroscopicity of the room that generated an higher vapour pressure in the reference room, increased the infiltration rate through the door. Overall, the analysis of the decay phase highlighted moisture reduction was similar in all the rooms. The moist air was removed mainly through infiltration, while walls smoothed the decay and reduced the weather impact on the indoor.

A ventilation system was installed to investigate the impact of ventilation in the buildings. A moisture buffering test was carried on in the rooms. Six cycles of 24h, of which 8 of humidification at 75% and 16 of RH decay were performed. The test was performed at constant temperature and at variable temperature. In the first test the temperature was kept at 23^oC, whilst in the second the indoor temperature was not controlled. Results showed the moisture exchange through ventilation varied depending on the hygroscopicity of the room. In the concrete and wood fibre cells ventilation removed a similar amount of moist air, while in the reference room ventilation removed more moist air from the room, as the ventilation and infiltration were the only ways to regulate the moisture content in the non-hygroscopic room. In all rooms ventilation had a significant impact on the moisture exchange during the humidification phase, while in the de-humidification ventilation did not participate to the indoor moisture balance in the hygroscopic cells. The ventilation system in the reference room, however, kept actively removing moisture through ventilation also during the de-humidification.

The indoor environment in the test at variable temperature was strongly influenced by the outdoor. As tests were performed, when the outdoor moisture content was persistently high, the ventilation system kept pushing moist air indoors. In some cycles the indoor RH was above 75%RH and in most of the tests the indoor RH fluctuation in a daily cycle were less than 20%. Consequently, the water usage in the rooms was significantly smaller than at constant temperature, as well as the moisture load eliminated by ventilation was lower. Differences between the three rooms were minimal, showing the three rooms eliminated the same amount of moisture regardless of the room hygroscopicity and wall structure. This is due to the effect of the temperature fluctuations in the rooms, which auto-regulate the indoor moisture content.

A moisture balance equation was used to estimate the walls participation in buffering moisture in the three rooms. In the test at constant temperature significant differences between the reference room and other two cells were observed. In the hygroscopic rooms the balance equation showed that walls were participating to the moisture regulation, whilst in reference room the indoor moisture content was balanced solely by ventilation and infiltration. However, in the test at variable temperature walls were not strongly involved in the moisture balance during the humidification also in the hygroscopic cells, as small differences between the moisture balance in all rooms indicated. To better

understand the differences between the two tests, a plasterboard specimen, together with specimens of clay, gypsum and lime, were placed on a scale in the concrete room. The weight variations of the material in the test at variable temperature were on average 82% smaller than at constant temperature. That indicates that lower and variable temperatures, as well as smaller moisture fluctuations, reduced the capacity of the materials to adsorb water. The moisture buffering capacity of plasterboard at constant temperature was further compared with the moisture uptake value calculated through the moisture balance equation. The calculated moisture buffering capacity was significantly smaller than the weight variation of the specimen on the scale. This discrepancy needs to be further verified, but the reasons might be related to the air velocity on the wall surface and water transport through the walls.

The moisture buffering capacity of all plasters was also compared with the results obtained in the laboratory to understand the impact of a larger and more realistic environment on moisture buffering testing. The good agreement between the specimens placed in the room and in the laboratory confirmed that an higher volume of moisture in the room did not impact the dynamic sorption capacity of materials, when the RH fluctuations and interval are preserved.

5. *Hygrothermal Simulation of Buildings*

Full-scale experimentation on real buildings is not often possible or too complex (Section 4.4), leading toward the use of hygrothermal simulation that can give a realistic quantification of the dynamic sorption behaviour of the enclosure (Section 2.3). Hygrothermal models can be applied to any building and materials in any environmental condition. They can give a quick and detailed evaluation of the indoor relative humidity in a variable environment and perform global analysis on the simultaneous heat and moisture transfer through enclosures. In this chapter, simulations were used to continue and further analyse the experimental full-scale testing (Section 4.4), and to investigate the effect of ventilation and moisture transport into the walls. The influence of the wall components on the overall moisture capacity of the walls was analysed, looking into the moisture distribution and moisture transport into the concrete and wood fibre cells.

5.1 Method

In this chapter, simulations can be classified as 'pre-experimental simulations', 'experimentally based simulations' and 'investigatory simulations'. Pre-experimental simulations and investigatory simulations refer to simulations, in which specifications, such as boundary and initial conditions, were mostly user-defined. Pre-experimental simulations were run prior to the in-situ testing to initially plan the field work (Section 4.2.1), whilst the investigatory simulations were used after the experimental tests for complementary analysis to the full-scale testing. Experimentally based simulations are based on a hybrid mix of experimental data and user-defined properties applied to the model. The three simulation levels investigated different aspects of the moisture buffering capacity of walls, but the model set-up and some boundary conditions (such as building size, wall structure and thermal properties) were preserved for all simulations. Properties in common for all simulations are described in this section. The concrete, wood fibre and PIR rooms, previously experimentally tested in Section 4.4, were modelled in WUFI® (Wärme Und Feuchte Instationär). Details of the buildings are shown in Section 4.1. WUFI® is a validated simulation software for dynamic simulations that simultaneously calculate the heat

and moisture transport through the enclosure. WUFI® can simulate 1-D and 3-D spaces. The 1-D (WUFI®) Pro software focuses on building component cross-sections that allows for a more complex analyses than the only evaluation of winter condensation, as the traditional Glaser method does (Cascione et al., 2017). WUFI® Pro analyses the hygrothermal response of walls to indoor and outdoor environmental variations, but it does not look at the interaction between walls and the indoor environment. The 3-D software (WUFI® Plus) simulates the indoor environment, thermal comfort and energy consumption of a 3-D building, in addition to simulating the 1-D heat and moisture transport in enclosures.

At the beginning of this study, 1-D pre-experimental simulations were performed on the East facing wall of the three rooms to define the research plan at the BRP. This analysis was followed by 3-D simulations of the cells to help with the design of the humidification system (Section 4.2.1). After the field testing, experimentally based simulations were run on the whole rooms using WUFI® Plus. Results were compared with the full-scale testing, to reproduce accurately the experimental testing into simulations. The capacity of the the wall assembly to buffer moisture was investigated, to understand the influence of the overall hygroscopicity of the wall assembly on the dynamic sorption capacity. Investigatory simulations were run on WUFI® Plus to perform a sensitivity analysis of ventilation and moisture load, and to investigate the correlation between ventilation, moisture load and moisture buffering. Investigatory simulations in the whole cells (3-D) were also performed with clay, lime and gypsum as interior surface, instead of plasterboard, to compare the behaviour of three different coatings in the moderation of the indoor environment, and to investigate variations in the correlation between ventilation and moisture buffering.

5.1.1 Characteristics of the Software

For thermo-hygrometric simulations of the walls and buildings, WUFI®Pro V6.2 and WUFI®Plus V3.0.3 were chosen, as it was demonstrated they are the most accurate commercially available software for moisture buffering analysis (Holm, Kuenzel and Sedlbauer, 2003) and it is still widely used (Kordziel, 2018; Gholami et al., 2020; Libralato et al., 2019). The two software are based on the same heat and moisture transport mechanisms, which are described with the following equations Künzel (1995):

$$\frac{dH}{dT} \cdot \frac{dT}{dt} = \bigtriangledown \cdot (\lambda \cdot \bigtriangledown T) + h_v \cdot \bigtriangledown(\delta_p \cdot \bigtriangledown(\phi p_{sat})) \tag{5.1.1}$$

$$\frac{dw}{d\phi} \cdot \frac{d\phi}{dt} = \bigtriangledown \cdot (D_\phi \cdot \bigtriangledown \phi) + \delta_p \cdot (\delta_p \cdot \bigtriangledown(\phi p_{sat})) \tag{5.1.2}$$

where: ϕ is the relative humidity (-), t is time, T is the temperature ($°C$), w is the moisture content (kg/m^3), p_{sat} is the saturation vapour pressure (Pa), λ is the thermal conductivity (W/mK), H is the total enthalpy (J/m^3), D_ϕ is the liquid conduction

coefficient ($kg/m \cdot s$), δ_p is the vapour permeability ($kg/m \cdot sPa$), h_v is the latent heat of phase change (J/kg).

WUFI®Plus simulates, in addition, the moisture content in the indoor air by applying a moisture balance equation. The indoor absolute moisture ratio (c_i $[kg/m^3]$) is calculated from the following water vapour mass balance equation:

$$V\frac{dc_i}{dt} = \sum_f A \cdot \dot{g}_{wj} + nV(c_a - c_i) + \dot{w}_{Imp} + \dot{w}_{Vent} + \dot{w}_{HVAC} \tag{5.1.3}$$

where: c_a and c_i are respectively the absolute moisture ratio of the exterior and interior air, $\dot{g}_{wj}$ is the moisture flux from the interior surface into the room, $\dot{w}_{Imp}$ is the moisture production, $\dot{w}_{Vent}$ and $\dot{w}_{HVAC}$ are respectively the moisture gains or losses due to ventilation and HVAC systems. Moisture buffering is represented by $\dot{M}_{diff}$ in Eq. 5.1.3, and it is also indirectly included in Eq. 5.1.2, as the equation consider several moisture transport mechanisms, as moisture adsorption, moisture distribution and surface diffusion.

5.1.2 Material Properties

The key thermo-physical and hygric material properties necessary to heat and mass transfer evaluations are presented in Table 5.1. The moisture storage function refers to the absorption curve, as the software ignores the impact of the desoprtion and hysteresis. The software requires some other properties, which were not measured for this study (such as liquid transport and enthalpy). In general, it can be stated that thermal properties are not predominate factors in WUFI®'s moisture transport equation. Before running simulations in this chapter a sensitivity analysis was performed, as also mentioned in Section 3.2.3, that confirmed this statement. Regarding the liquid transport coefficients, WUFI® guidelines suggest to calculate this value only for capillary active materials. Due to the complexity of the testing procedure to measure the liquid transport coefficients, WUFI® can estimate the values. Simulations were run with and without the use of the liquid transport mechanism, showing negligible differences, when estimated coefficients were used. The basic properties of plasterboard, clay, gypsum and lime were measured and reported in Chapter 3, whilst the other elements properties were taken from WUFI® database. The summary of the walls components properties is shown in Table 5.2.

Table 5.1. Basic material properties for WUFI®.

Properties	Symbol	Unit
Bulk Density	ρ_{dry}	(kg/m^3)
Porosity	Φ	(m^3/m^3)
Specific Heat Capacity	c_h	(J/kgK)
Thermal Conductivity	λ	(W/mK)
Water Vapour Resistance Factor	μ	$(-)$
Moisture Storage Function	ξ_w	(kg/kg)

Table 5.2. Element properties

Components	ρ_{dry} (kg/m^3)	Φ (%)	c_h (J/kgK)	λ (W/mK)	μ $(-)$	ξ_w (kg/kg)
AAC	600	0.72	850	0.16	8.3	0.18
PIR Insulation	40	0.95	1500	0.02	50	0.04
Concrete Brick	2315	0.13	800	1.13	182.5	0.45
OSB	595	0.85	1700	9	165	1.2
Air Gap	1.3	0.99	1000	0.14	0.51	0.017
Wood Fibre 1	155	0.98	2000	0.03	3	0.38
Wood Fibre 2	168	0.88	1700	0.15	3.3	0.31
Hard Wood	650	0.47	1500	0.12	200	1.50

5.1.3 Weather Data and Indoor Climate

For the pre-experimental simulations the outdoor weather data from Lyneham were used, as described in Section 4.2.1. Otherwise, the outdoor climatic data were taken from the BRP weather station. Fig. 5-1 shows the monitored weather data for 2019-2020. The west of England weather presents high temperatures and RH variations across the seasons, but also strong daily fluctuation. Winters are cold and wet, while summers are mild, except for short heat waves (Perry et al., 2014). However, rains are frequent, which considerably increase the moisture content in the air. The reference weather year (Fig. 5-1) showed consistent high RH levels, whit minimum RH below 60% recorded in few days in April and August. The main wind direction is South-West, as shown in Fig. 5-2. Temperature, RH, wind speed and direction, barometric pressure, diffuse and global solar radiation data were used in the software. In the experimental based and investigatory simulations, the simulated moisture buffering testing were run in the same weeks and months in which the experimental testing was carried on (February-March) (Section 4.4).

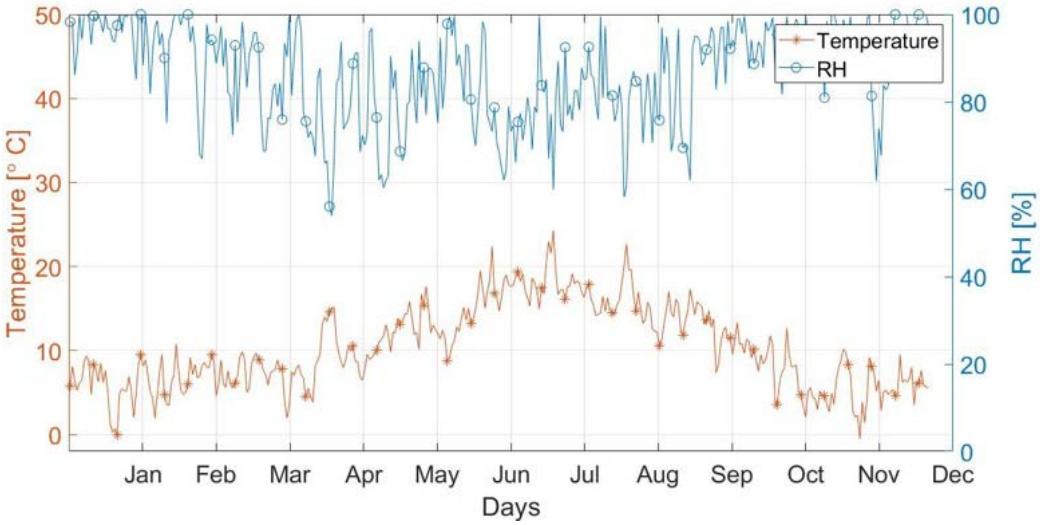

Fig. 5-1. Outdoor Temperature and RH data from the site weather station used for simulations.

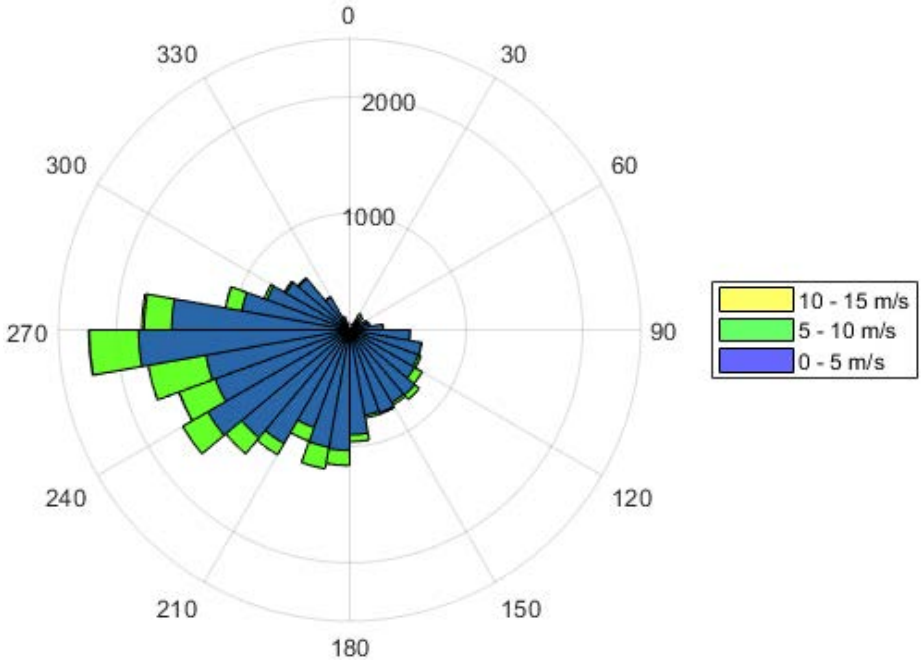

Fig. 5-2. Wind speed and direction in the reference year

In the pre-experimental 1-D simulations the indoor temperature was kept constant at 23^oC, while RH followed the NORDTEST square wave fluctuations, cycling between 75%RH and 33%RH, as discussed in Section 3.3 and Section 4.2.1. The outdoor weather did not influence the indoor environment and no ventilation and infiltration were considered. In the 3-D simulations (pre-experimental, experimental based and investigatory), the indoor climate was simulated together with the moisture transport in the walls. The effect of ventilation, infiltration and moisture load were considered in the calculation of the indoor moisture content. The temperature was kept constant at 23^oC. In the 3-D pre-experimental simulations the natural ventilation rate was set

to a constant $0.5ACH$. The reason of such a small ventilation rate was to minimise the risk of condensation in the room, without reducing the moisture buffering potential of the walls. The infiltration rate applied to the model was measured on-site through a gas decay test in the test cell, which measured a value equating to 0.06 ACH (Section 4.3.2.1). The experimental based simulation model reproduced the in-situ tests, in which ventilation and infiltration experimental data were used in the model.

As the moisture load was the only data not available for all cycles from the experimental testing, moisture load was estimated in the experimental based simulations. The moisture load was varied until the simulated indoor moisture content matched the values obtained in the experimental test. This process was possible because the ventilation/infiltration (Section 4.4) together with the plasterboard properties (Section 3.1) were experimentally determined. By running simulations without the moisture load the indoor RH fluctuations were significantly lower in the model than in the experimental testing. By increasing the moisture load, it was possible to obtain the same RH fluctuations than in the experimental testing. This process can be considered realistic, as it was also observed in the experimental testing that the non activation of the humidifier did not generate square wave variations in the cells, as also simulations suggested. This method is however an approximation as it cannot be stated that the moisture load selected in the simulations is exactly the one used in the experimental testing, but it is a good reference point to understand the correlation between ventilation and moisture buffering in buildings.

5.1.4 Boundary Conditions

The boundary conditions refer to the wall surface thermal and moisture characteristic, and initial temperature and RH conditions in the room and in the walls. The heat transfer resistance of the outdoor surface (R_{Se}) was considered as variable and wind dependent factor, while the indoor surface resistance (R_{Si}) was constant and defined following the *BS EN ISO 13788* (2002). To investigate the impact of the thermal surface resistance on the moisture buffering capacity of walls, simulations were initially run to verify the variability of the indoor absolute humidify and walls sorption capacity when the R_{Si} increases/decreases. Negligible variations were observed and, therefore, the prescribed R_{Si} in *BS EN ISO 13788* (2002) was applied in all simulations in this chapter. The summary of the surface resistance and surface coating values assigned to the indoor and outdoor surface are shown in Table 5.3. The internal coating represents the impermeable sheet, to which the S_d value specified by the vapour barrier producer (the one used in the full-scale testing) was assigned. As the test cells at the BRP were built few years before the moisture buffering test was carried out, two years

simulations were run, to simulate realistic variations of the moisture content in the enclosure elements after being exposed to the environmental conditions. The infiltration and ventilation rate were considered constant across the tests, as the software requires detailed information from experimental testing, such as the blower door test after the installation of the ventilation system, to consider the ventilation rate as a variable factor.

Table 5.3. Boundary conditions

	R_{si} $[m^2K/W]$	Inner Sd	Outer Sd
Walls	0.13	0	0
Ceiling	0.10	1500	50
Floor	0.17	1500	0
Door	0.13	1500	0

5.2 Results, Analyses and discussions

5.2.1 Pre-experimental simulations on WUFI® Pro

In the pre-experimental simulations the moisture transport and storage capacity of the walls were investigated. The analysis was performed on the average yearly data. However, six days at the end of April are presented in this section, to show typical daily moisture changes into the assemblies. It is clear there is a significant difference between the reference room, and the concrete and wood fibre cells (Fig. 5-3). The application of the impermeable sheet on the PIR room stopped any interaction between the room and the walls, generating condensation on the indoor surface (Fig. 5-3a). The indoor surface RH did not reach 100%, because walls were slightly influenced by the outdoor environment generating small fluctuations on the surface RH. In the time framed shown in (Fig. 5-3a) there was a slight increase of the outdoor temperature and a reduction of the outdoor absolute humidity, which justifies the lower RH on the indoor surface. This variation in the weather influenced the indoor surface RH that dropped from 100%RH to 95%RH. The indoor surface of the other two cells presented similar RH fluctuations of the ones in the indoor. The surface RH fluctuations for concrete and wood fibre were 38% and 37.7%, respectively, which indicated that the walls were actively exchanging moisture with the indoor by adsorbing moisture from the rooms and reducing the RH variations. Consequently, plasterboard stored water from the indoor until it reached its maximum moisture buffering capacity in the 33%-75% interval. Concrete and wood fibre plasterboard adsorbed 58 and 63 g/m^2, respectively, which are similar to the moisture buffering values obtained in the laboratory test (Section 3.3). The good agreement between simulations and laboratory experimental testing assured the reliability of the simulation model to predict moisture buffering capacity of the

materials. In the wood fibre the total water content in the plasterboard is higher than in concrete room, because the air layer behaved as a barrier that prevent moisture to move into the next layer. Consequently, plasterboard accumulate more moisture from the indoor. In the PIR room plasterboard did not show moisture content fluctuations, due to the moisture barrier. However, the total moisture content was significantly higher than in the hygroscopic cells, due to the moisture transport and accumulation into that plasters that could not be expelled into the room due to impermeable membrane.

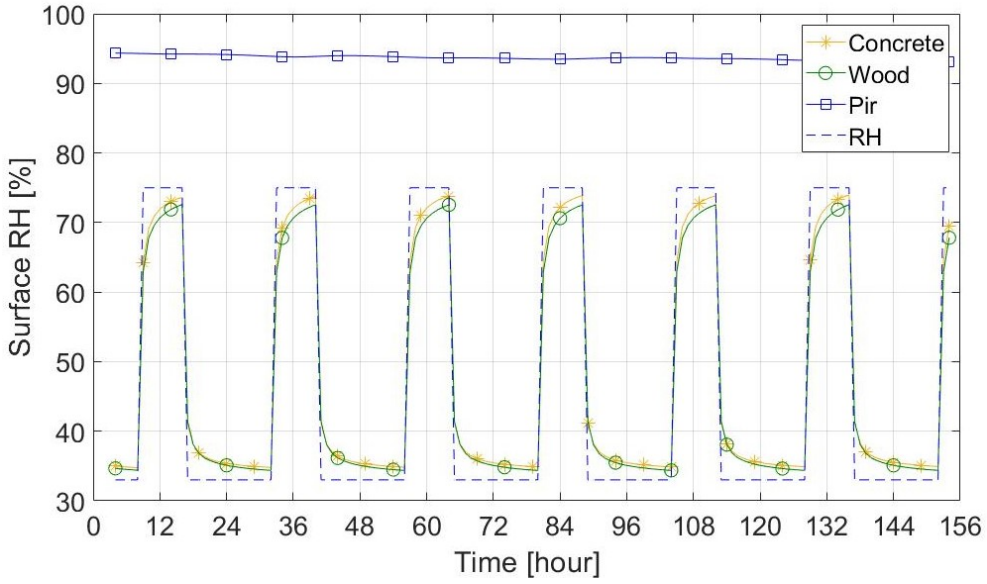

(a) Surface RH

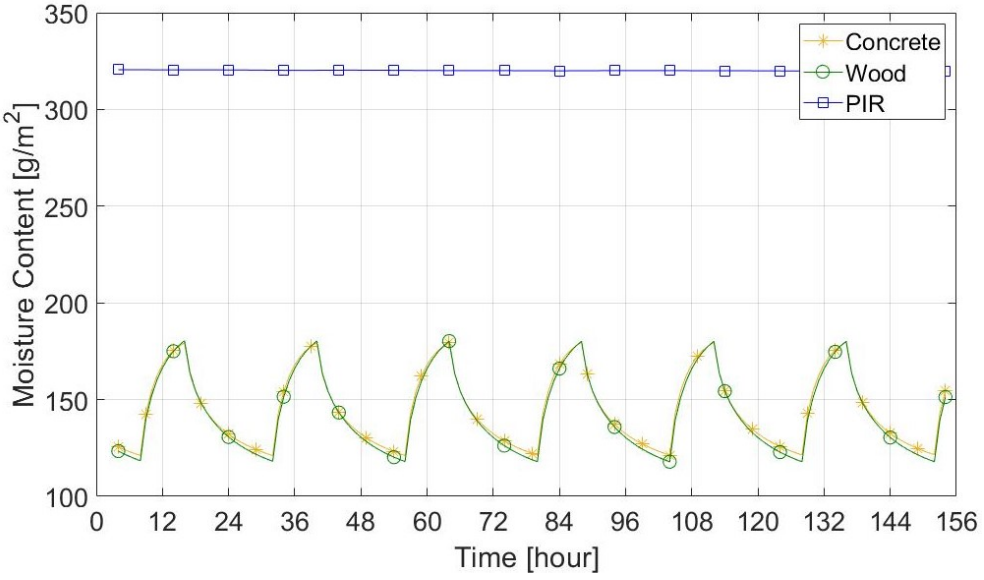

(b) Plasterboard

Fig. 5-3. Simulated variations of the surface RH and plasterboard moisture content in the three rooms

The main difference between simulations and the laboratory experimental results in

Section 3.3 is in the capacity of the material to transfer moisture to the next layer. Due to the vapour permeability of plasterboard, the coating transferred the moisture that the material cannot adsorb itself to its under-layer, which also presented daily moisture variations in Fig. 5-4. This increased the capacity of the walls to store water from the room. This first observation suggests the participation of the whole wall assembly to moderate the indoor moisture. Even though plasterboard behaved similarly in the concrete and wood fibre cells, the main difference between the two rooms is in the moisture distribution in the under-layers (Fig. 5-4). Observing the wall assembly in Section 4.4 and in Fig. 4-1, in the concrete room the AAC adsorbed 10.4 g/m^2 (peak to peak), while the PIR insulation board that is not an hygroscopic material did not participate to the room daily moisture moderation, but it stored 0.8 g/m^2 of moisture for each cycle. In the wood fibre room, the air gap transferred moisture to the OSB layer, which adsorbed 8.7 g/m^2. It was also observed that there was a lag in the adsorption of the OSB compared to the plasterboard, due to the water vapour resistance of the plasterboard and the air gap that slowed down and delayed the moisture transport through the wall. The wood fibre insulation did not significantly participate to the indoor daily moisture adsorption, as it presented daily fluctuations of 0.3 g/m^2, but the observation of wood fibre insulation across the year showed materials responded to the outdoor weather variation rather than to the indoor. In the particular time frame chosen (spring), the wood fibre insulation was drying, due to the outdoor higher temperatures and lower RH that reduced the outdoor partial pressure and generated the vapour flow crossing the walls moving from the indoor to the outdoor.

Overall, concrete's under-layers adsorbed and released around 10 g/m^2 for each daily cycle, while in the wood fibre the moisture adsorbed by the under-layer was halved. This indicates plasterboard regulates the amount of moisture to transfer to the under-layers, when in contact with another material and depending on the permeability, moisture capacity and thickness of the under-layers, the moisture propagates in the assembly from the indoor. When an air gap is present, the moisture transfer mechanisms may change, but experimental testing is necessary to better understand the dynamics. This first analysis prompted further investigation of the differences of the three rooms either in the full-scale testing and through simulations, as the reference room showed significant differences with the other two cells and the different moisture propagation into the wall in the concrete and wood fibre was of interest.

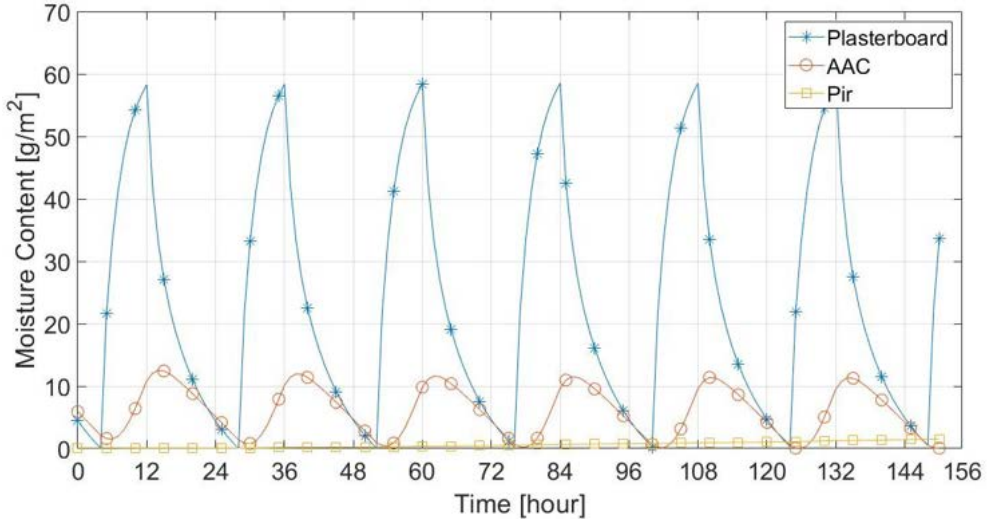

(a) Concrete

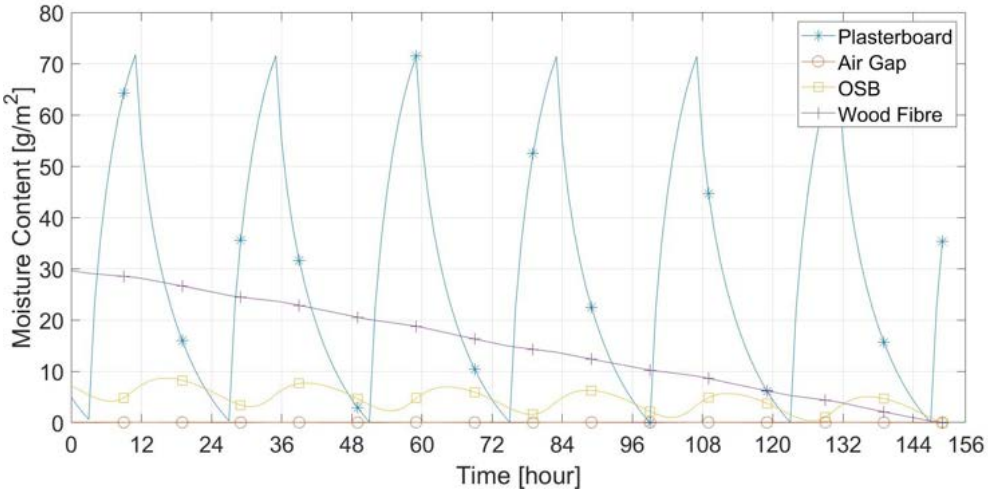

(b) Wood

Fig. 5-4. Simulated relative moisture content variations in the walls' layers in the concrete and wood fibre

5.2.2 Experimental Based Simulations: Modelling the Full-Scale Testing

Simulations of all internal walls were carried out incorporating the effects of ventilation, infiltration and moisture load on the moisture buffering capacity of the walls. The simulations were set to reproduce the same experimental set-up of the full-scale testing. Fig. 5-5 compares the experimental and RH fluctuations in the three rooms. Concrete and wood fibre showed a good match with the experimental (less than 0.5 g/m^3 difference that corresponds to around 2.7%RH difference), while the PIR room showed higher variations up to 3 g/m^3 (11%RH) during the de-humidification period. The reason of the higher differences in the reference room was due to the simulation assumption that the walls were perfectly non-hygroscopic

and the application of the impermeable sheet on the walls did not allow any moisture to pass through it. In the experimental testing the moisture could have managed to move behind the impermeable sheet through the walls' joints and the sealant that over time may have lost their tackiness. Moreover, moisture could have condensed and evaporated on the sheet surface. Therefore, the simulated RH variations assumed that infiltration and ventilation pushed out more moisture than in the experimental reference room.

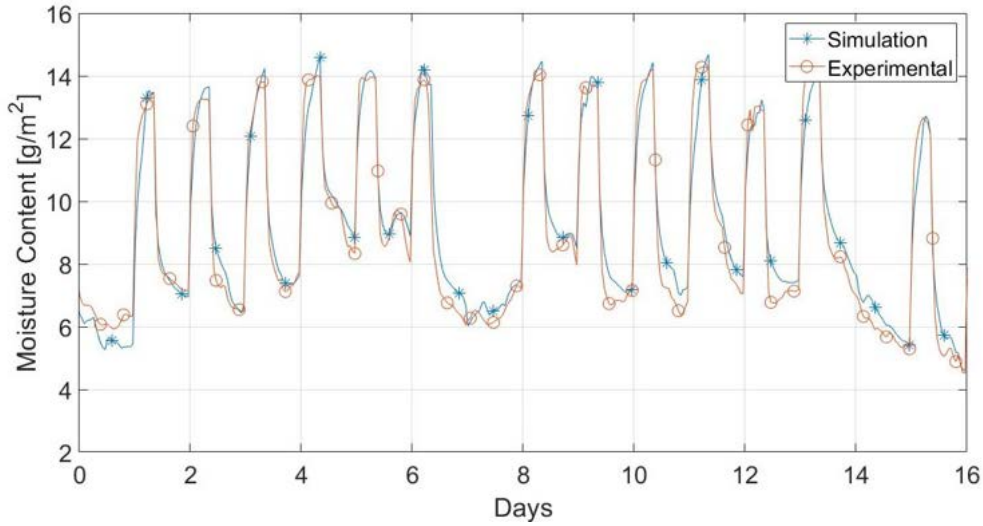

(a) Concrete

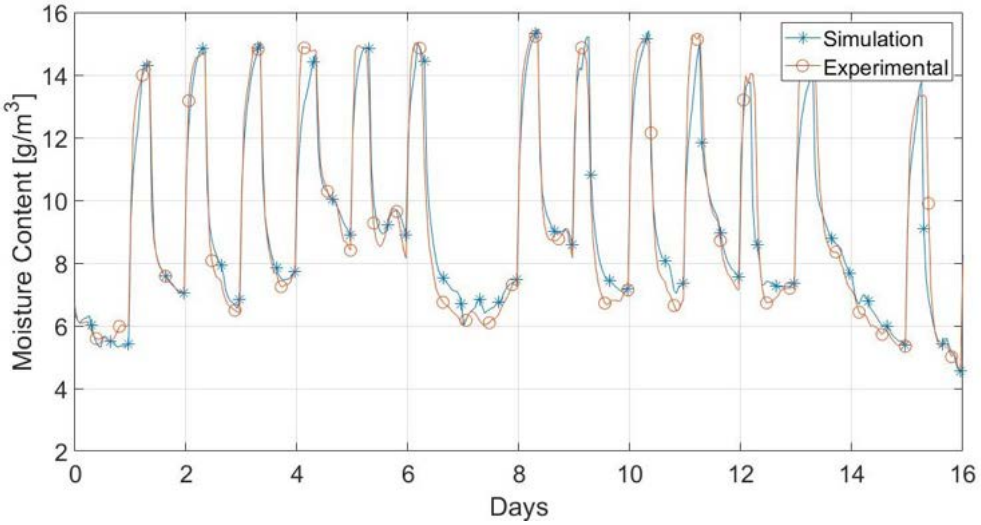

(b) Wood

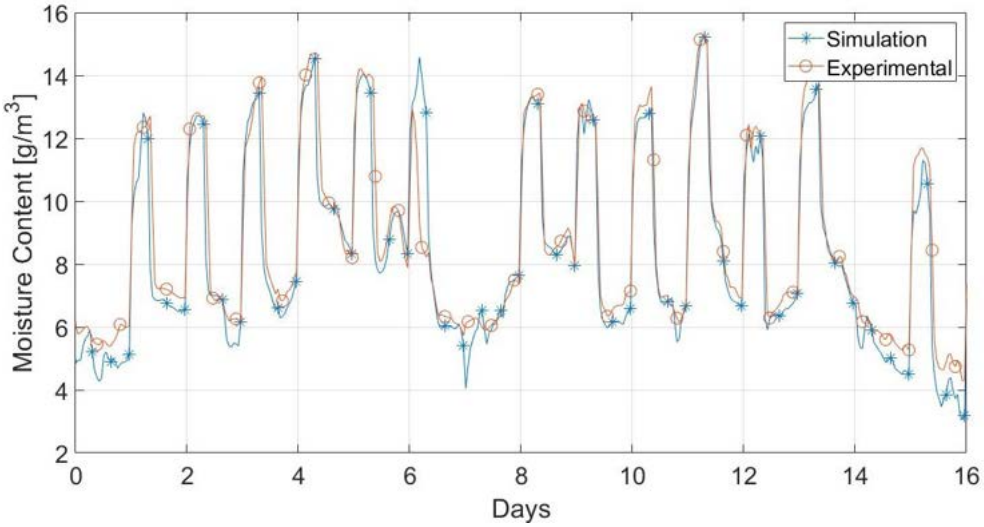

(c) PIR

Fig. 5-5. Comparison of the RH variations between simulation and experimental test in the three rooms

The moisture load applied for each cycle in each room is shown in Table 5.4, Table 5.5 and Table 5.6. Similarly to Section 4.3.2.4, the concrete and wood fibre room used more water to maintain high RH level during the humidification. Wood fibre used an average 150 g/h more water than the concrete room in most of the cycles, whilst PIR needed around 160 g/h less water than concrete. However, the rooms are subjected to different daily RH fluctuations, due to the weather influence, which did not allow to further comparison of the moisture load in the three rooms. In case all the rooms presented the same indoor RH variations, it was possible to compare the moisture load necessary to keep the RH at 75%.

Table 5.4. Concrete moisture load (g/h)

Concrete	Cycle 1	Cycle 2	Cycle 3	Cycle 4	Cycle 5	Cycle 6
Test 1	1080	970	970	800	800	800
Test 2	920	900	960	750	880	880
Test 3	1020	1020	1020	1020	-	-
Test 4	1070	1050	1000	980	850	850
Test 5	850	960	780	930	1100	1100

Table 5.5. Wood moisture load (g/h)

Wood	Cycle 1	Cycle 2	Cycle 3	Cycle 4	Cycle 5	Cycle 6
Test 1	1220	1140	1080	810	900	900
Test 2	1070	1080	1100	850	1100	900
Test 3	1100	1100	1100	1100	1200	1200
Test 4	1140	1140	980	1140	1150	1150
Test 5	850	1100	850	950	1200	1200

Table 5.6. PIR moisture load (g/h)

PIR	Cycle 1	Cycle 2	Cycle 3	Cycle 4	Cycle 5	Cycle 6
Test 1	700	720	720	690	700	700
Test 2	630	720	700	700	700	700
Test 3	660	630	630	630	780	780
Test 4	750	820	750	700	760	730
Test 5	730	800	660	700	880	840

To understand the capacity of simulation to realistically represent the rooms, the available experimental data were compared with the simulated ones. The effect of infiltration was investigated in the three rooms (Fig. 5-6), by calculating through the indoor moisture balance equation in each room the moisture exchanged by

ventilation, infiltration and walls in the simulated model. The comparison presented in general good agreement during the humidification phase. However, the simulated results showed that during the de-humidification phase, infiltration always removed moist air from the rooms, while experimental data suggested infiltration also transported moisture into the room. The difference between simulated and experimental data corresponded in the concrete and wood fibre to around 30 g/h. The difference was generated by the discrepancy in the indoor absolute humidity (Fig. 5-5). The experimental and simulated indoor absolute humidity presented 0.5 to 1 g/m^3 difference in the humidification or de-humidification, which correspond to 20 to 30 g/h variations between the two tests. The consequence of slightly higher absolute humidity variations in the simulation generated 30 g/h more moisture than in the experimental case that was removed through infiltration. It is of interest that the good fit of the absolute humidity in the first six days in Fig. 5-5c generated a less discrepancy between the simulated and experimental infiltration moisture exchange in Fig. 5-6c, which confirmed that the 30 g/h variation is related to small differences between the simulated and experimental indoor absolute humidity. In the PIR room a better fit was observed during the humidification, but during the de-humidification moist air was transported into the room.

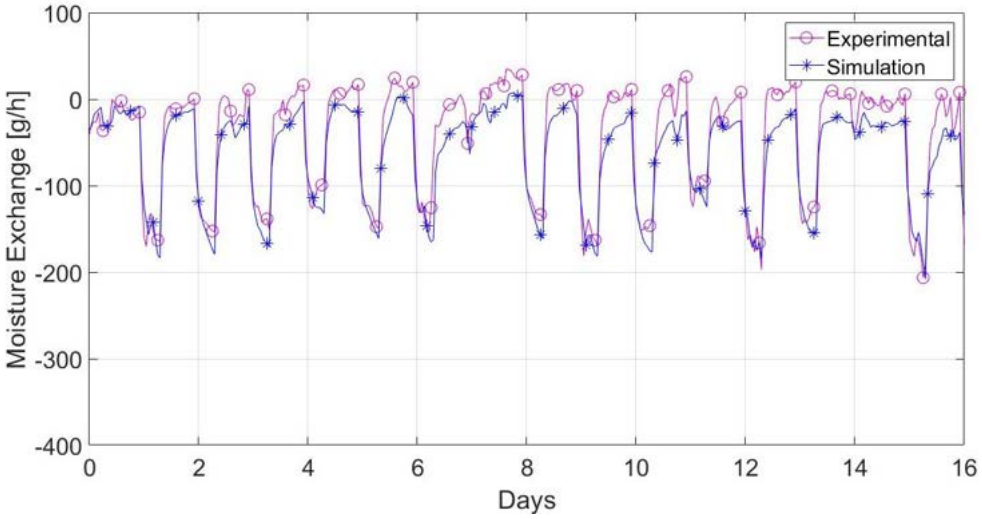

(a) Concrete

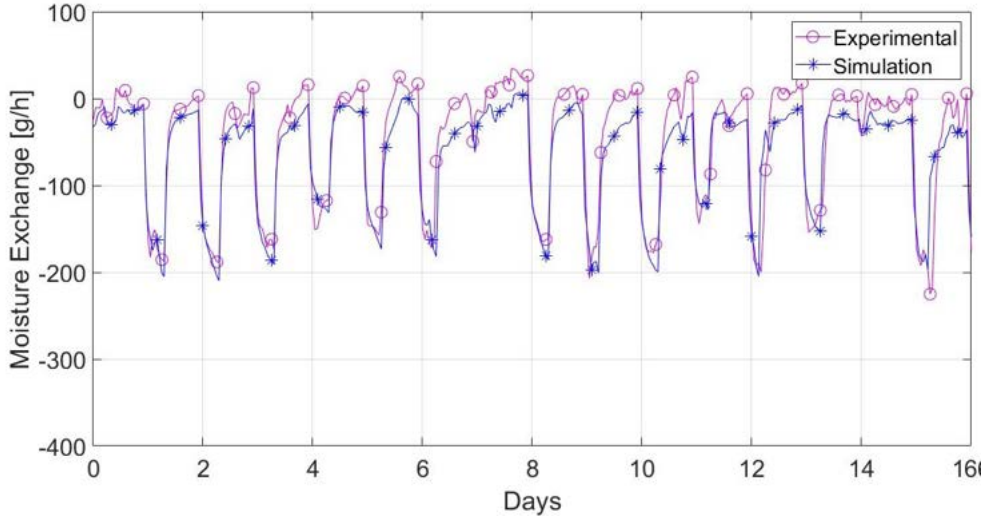

(b) Wood

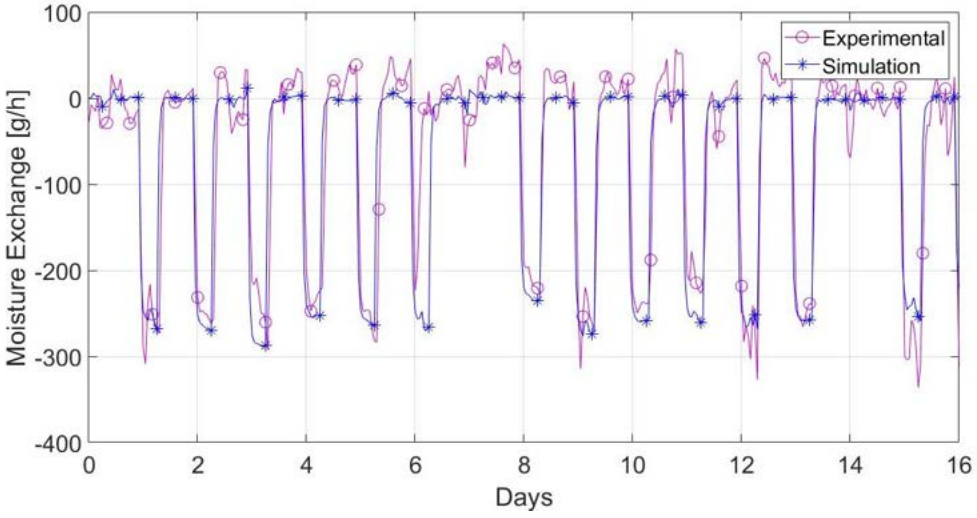

(c) PIR

Fig. 5-6. Comparison of infiltration Moisture exchange in the three rooms

The comparison between the experimental and simulated mechanical ventilation data also suggested a similar trend in the wood fibre, where 80 g/h shift was reported (Fig. 5-7). The reasons of the difference between experimental and simulations can be related to the model that assumed that the ventilation system was perfectly functioning, always pushing moist air outside.

It can be also observed in simulations the three rooms needed a higher moisture load to reach similar RH fluctuations than in the experimental test. The experimental case needed half of the amount of water than in the simulations to reach 75%RH (Fig. 5-8a). It can be assumed that the moisture load recorded in the experimental testing did not represent the real water usage during the test, due to a possible inaccuracy of the humidification system to monitor the water usage, or because simulations are not accurate. On the other side, simulations may overestimate the moisture buffering capacity of walls, as Kalamees et al. (2009a) study on in-situ testing stated. By increasing the moisture load in the experimental moisture balance equation, a good fit of the walls adsorption capacity between the experimental and simulation was observed (Fig. 5-8b), which suggests the experimental data might be erroneous or simulation overestimate the water usage. However, even though the magnitude of the moisture buffering participation differs, the overall good match of moisture exchange curves in Fig. 5-8b gave good confidence that simulations accurately represent the experimental trend.

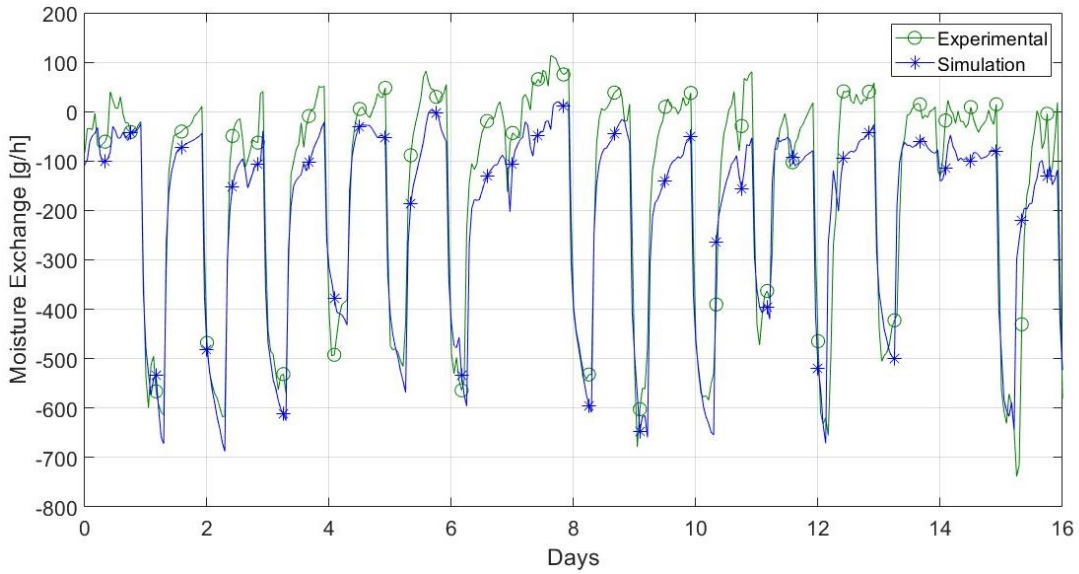

Fig. 5-7. Comparison of the mechanical ventilation in the wood fibre room

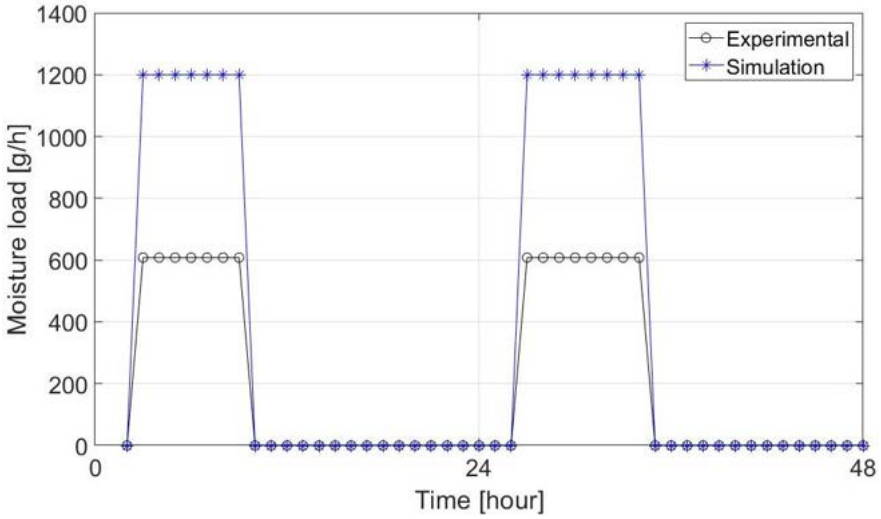

(a) Load

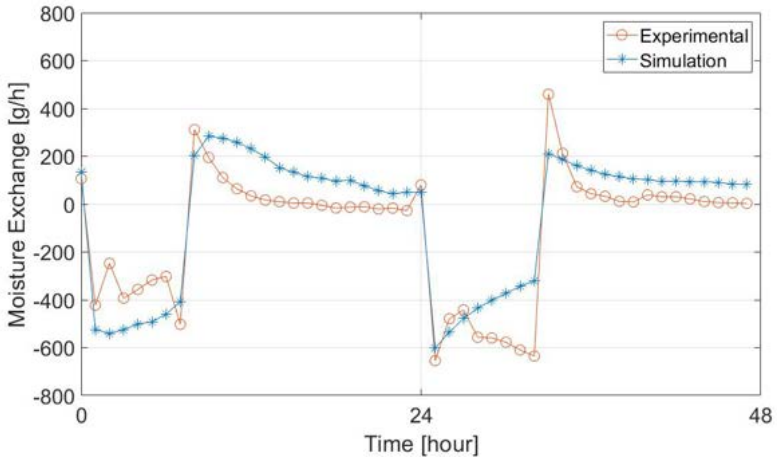

(b) Walls

Fig. 5-8. Comparison of moisture load and moisture exchange with the walls in the wood fibre room

5.2.3 Moisture balance analyses and comparison of the three rooms

Infiltration and ventilation participate together with the walls to modify the moisture concentration in the room. Fig. 5-9a and Fig. 5-9b illustrate that in the simulated concrete and wood fibre ventilation and infiltration removed moisture from the environment, together with plasterboard, in order to balance the moisture content in the room. The moisture removal reached the peak in correspondence of the humidification period, due to the significant increase of the water vapour pressure differential between the indoor and outdoor. In the dehumidifying phase ventilation and infiltration kept removing moisture at a lower rate, while walls compensated the moisture losses through ventilation in the room, releasing moisture. In the PIR room all the moisture is expelled through ventilation and infiltration (Fig. 5-9c). Section A.1 summarises the simulated moisture exchange during humidification and

de-humidification in the three rooms. Table 5.7 shows the average percentage of the indoor moisture increase produced by the humidifier that walls, infiltration and ventilation removed from the indoor during humidification. 3% of moisture produced by the humidifier was retained in the room, while walls buffered between 34% to 39% of the moisture load, and the resting 72% of moisture content was removed by ventilation and infiltration. Across all the cycles the proportion of moisture exchanged by walls was unvaried regardless of the amount of water released by the humidifier, suggesting there is a strong correlation between ventilation and moisture buffering. In the de-humidification (Table 5.8) the proportion changed. Infiltration and ventilation kept removing moisture from the room, whilst walls released moisture to balance the moisture content eliminated by ventilation. This correlation, however, varies, when the ventilation rate changes, or when there are significant variations of the moisture load. The sensibility of moisture buffering to these factors was analysed in the following section (Section 5.2.4). In the PIR room walls did not participate to the moisture exchange, which significantly increased the moisture removed by infiltration and increased of more than 12% the ventilation impact on the moisture balance.

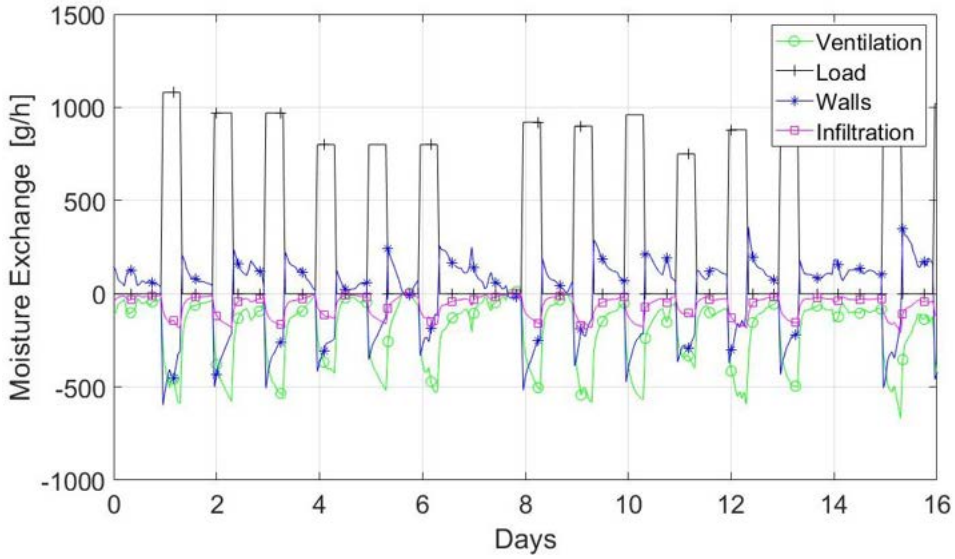

(a) Concrete

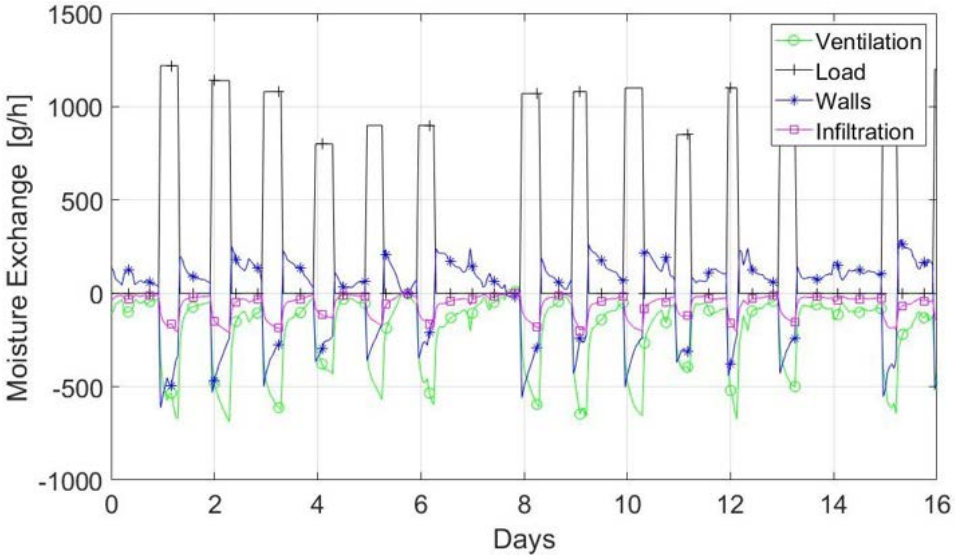

(b) Wood

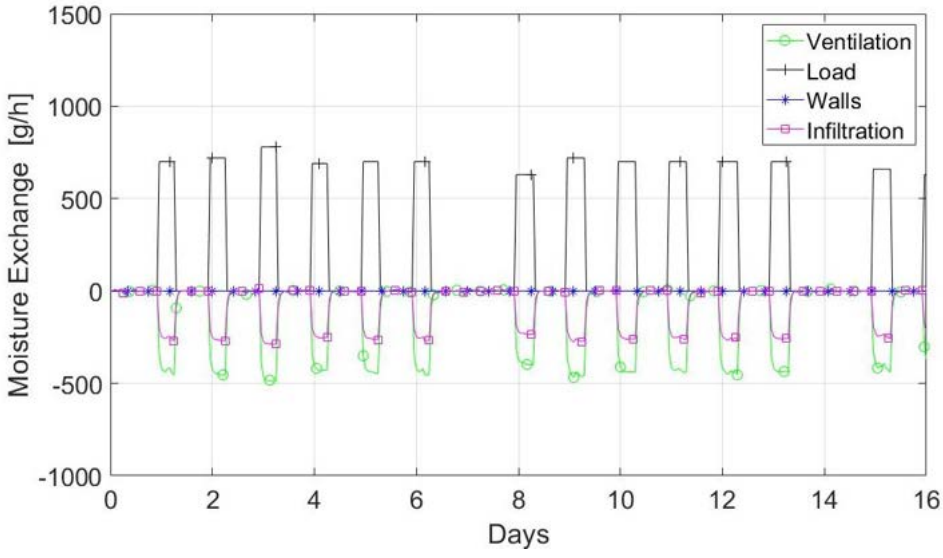

(c) PIR

Fig. 5-9. Moisture balance in the three rooms

Table 5.7. Moisture load distribution in the cells in percentage (%)

	Walls	Infiltration	Ventilation	Room
Concrete	39.13 ±1.9	13.66 ±0.5	43.88±1.5	3.33±0.2
Wood	34.58±1.8	14.48±0.5	47.47±1.5	3.47±0.2
PIR	0.00±0	35.21±0.2	59.63±0.2	5.16±0.4

Table 5.8. Moisture load distribution during de-humidification (%)

	Walls	Infiltration	Ventilation
Concrete	86.42 ± 2.5	-26.95 ± 0.5	-86.57 ± 2
Wood	89.67 ± 2.8	-25.78 ± 0.5	-84.52 ± 2
PIR	0.00 ± 0	-37.12 ± 7	-62.88 ± 12

By comparing the contribution of the walls in the concrete and wood fibre room, wood fibre buffered 5% more moisture in the humidification and 3% more during de-humidification. This is due to the higher moisture load in the wood fibre or due to the different sorption capacity of the walls. For this reason the moisture uptake of the walls was investigated.

The variations of the moisture buffering capacity of plasterboard between the East, West, South and North walls were less than 2%, as shown in Section A.2. However, solar radiations indirectly influenced some components of the south facing walls. To investigate the moisture propagation from the indoor into the walls without the interference of solar radiations, simulations were run by eliminating the solar radiation effect in the simulated hygroscopic rooms (Section A.2). The sole effect of temperature, RH, wind and barometric pressure were considered for the moisture transport into the assemblies. By observing that only the first three to four components from the indoor participate to buffer the indoor moisture (Fig. 5-10), the impact of solar radiations on these elements was investigated. The elimination of solar radiations generated less than 0.6% variations on plasterboard and AAC sorption capacity in the concrete room, whilst their influence on the indoor were negligible. The PIR insulation variations were more significant (30% increase of moisture), but the PIR contribution to buffer moisture was, anyway, negligible and did not significantly influence the overall moisture storage capacity of the South facing wall. Similar observation could be done for the wood fibre room for plasterboard and the air gap. In the south wall the OSB presented less than 1% variation between simulations with and without solar radiations, while the wood fibre insulation was strongly influenced by solar radiation after the 14^{th} day of simulations (Fig. A-4b), where a significant increase of radiations and increase of the outdoor surface temperature was observed. However, in the wood fibre insulation panel the daily moisture fluctuations are still small. As the overall impact on the main

component without solar radiations was negligible, the average moisture content of the four walls without the impact of solar radiations was analysed.

In Fig. 5-10 it can be observed the moisture content of each wall element for the concrete and wood fibre room. It is evident plasterboard is the main responsible of the daily moisture regulation of the room. In Fig. 5-10a the AAC did also present daily fluctuation of a smaller magnitude than plasterboard, and it also stored moisture, which increased the overall moisture content of the AAC. The average moisture increase was around 2%. The PIR insulation panel also stored a small amount of water across the five weeks testing, but it did not present daily fluctuation. Both the considerable size of the AAC (0.1 m) and the non-hygroscopicity of the insulation reduced the moisture participation of PIR insulation to buffer moisture. In the wood fibre room (Fig. 5-10b), the air gap did not present daily fluctuation, but the moisture was then transmitted to the OSB, which showed daily fluctuations and a total increase of moisture. The wood fibre insulation did not show daily fluctuations, but it presented an increase of the total moisture content, due to the outdoor environmental influence. By comparing the moisture content in the wood fibre insulation panel in this section with the one in the pre-experimental simulations (Sect. 5.2.1), the small variations of the weather data and the different time of the year in the two tests generated in the 3-D simulations an increase of the total moisture content in the insulation, while in the 1-D simulation the insulation panel was drying.

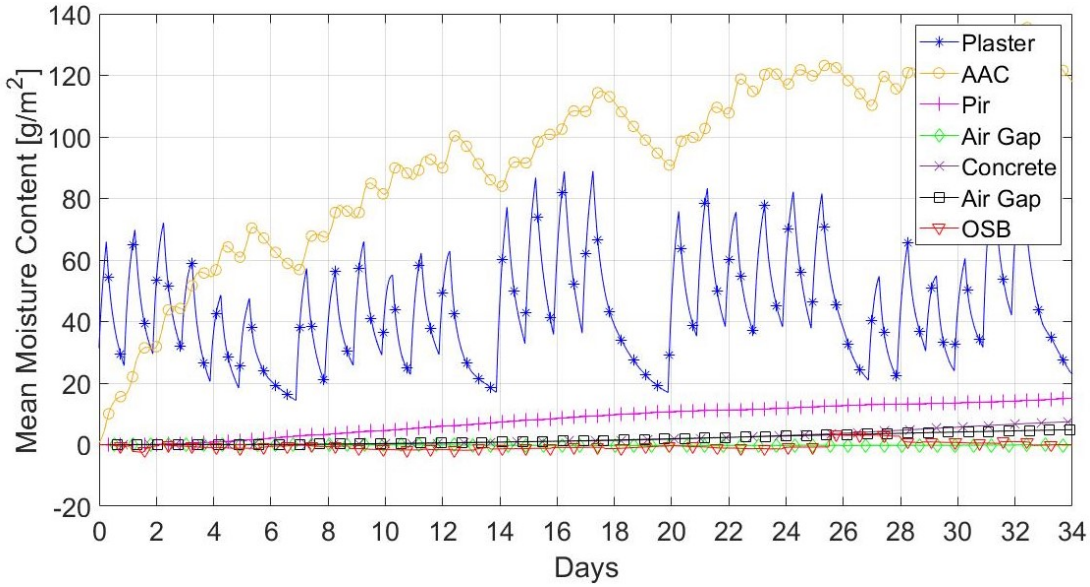

(a) Concrete

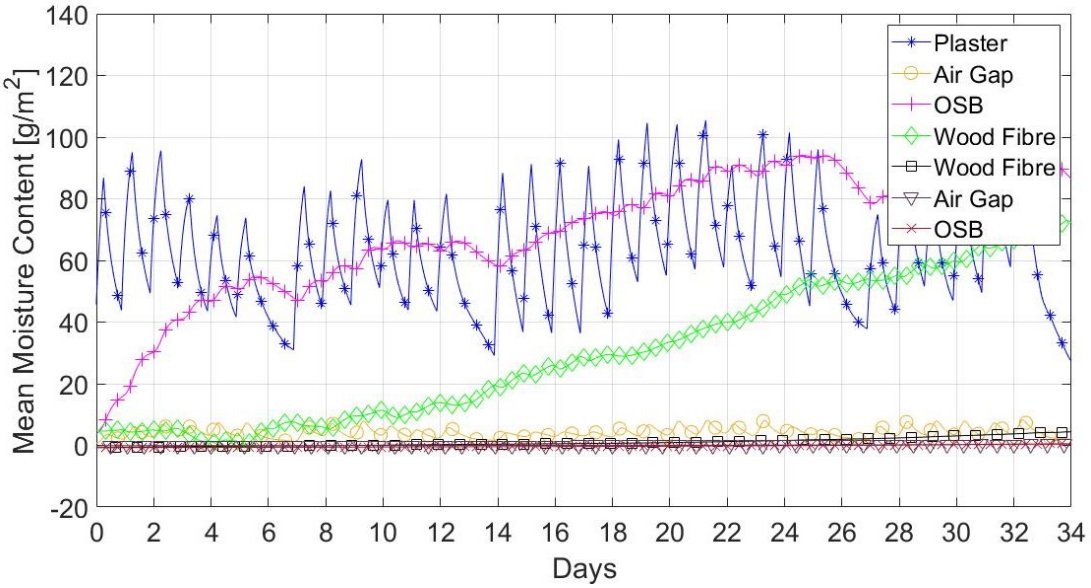

(b) Wood

Fig. 5-10. Simulated moisture uptake of the walls

The moisture buffering capacity of plasterboard can be seen in Table 5.9 and Table 5.10. The differences between the concrete and wood fibre rooms were small except in the third test, where plasterboard in the concrete room adsorbed more water (Fig. 5-11a), even though the daily fluctuations amplitude was preserved. The difference between the two rooms were around $3 \pm 1 g/m^2$ that can be related to the different moisture loads in the rooms. By comparing the simulated results with the experimental weight variations of the plasterboard specimen placed in the concrete room (Section 4.5), the simulated plasterboard adsorbed less water than the experimental specimen (Fig. 5-11b). The specimen adsorbed 13 g/m^2 more as average, which corresponded to 21% more moisture than in simulations, as shown in Table 5.11. The discrepancy may be

due to experimental measurements uncertainty and simulation simplification in the moisture transport estimation, as it is later discussed in Section 5.2.6.

Table 5.9. Plasterboard moisture uptake in the concrete room (g/m^2)

Plasterboard	Test 1	Test 2	Test 3	Test 4	Test 5
Cycle 1	61.36	44.62	61.77	52.34	35.89
Cycle 2	48.50	46.42	60.03	40.69	35.78
Cycle 3	41.99	45.09	67.04	46.01	34.51
Cycle 4	36.92	38.06	57.44	58.06	61.20
Cycle 5	27.30	39.31	-	56.25	44.49
Cycle 6	49.64	35.38	-	46.23	68.16

Table 5.10. Plasterboard moisture uptake in the wood fibre room (g/m^2)

Plasterboard	Test 1	Test 2	Test 3	Test 4	Test 5
Cycle 1	68.62	52.91	62.53	50.64	38.20
Cycle 2	53.32	53.25	58.35	42.44	40.46
Cycle 3	44.59	48.61	64.88	45.32	37.31
Cycle 4	36.74	36.63	55.80	62.48	64.06
Cycle 5	31.51	43.73	54.61	65.29	47.06
Cycle 6	54.09	37.62	47.82	47.69	72.12

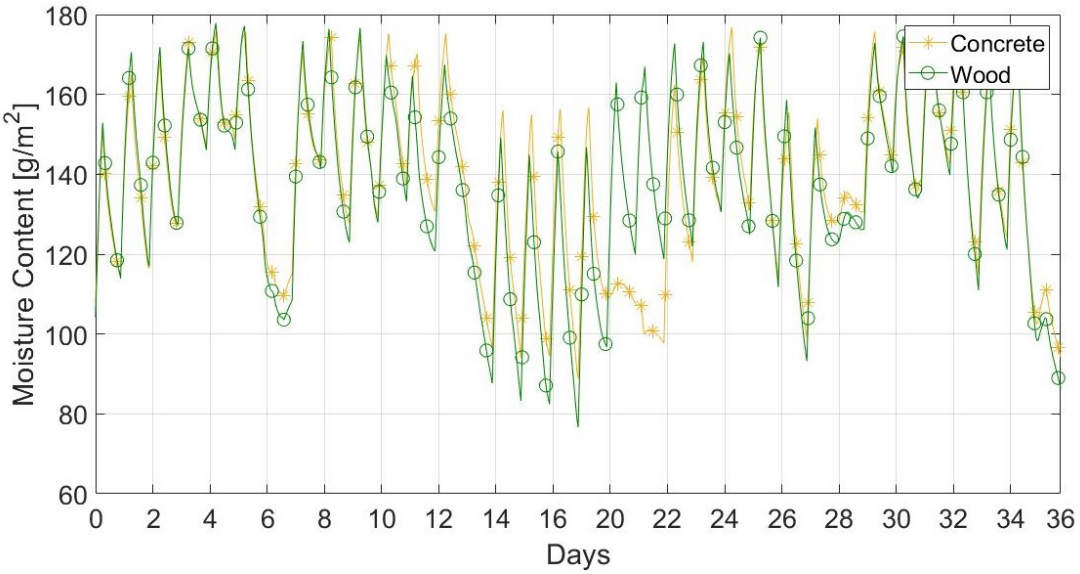

(a) Concrete and Wood fibre

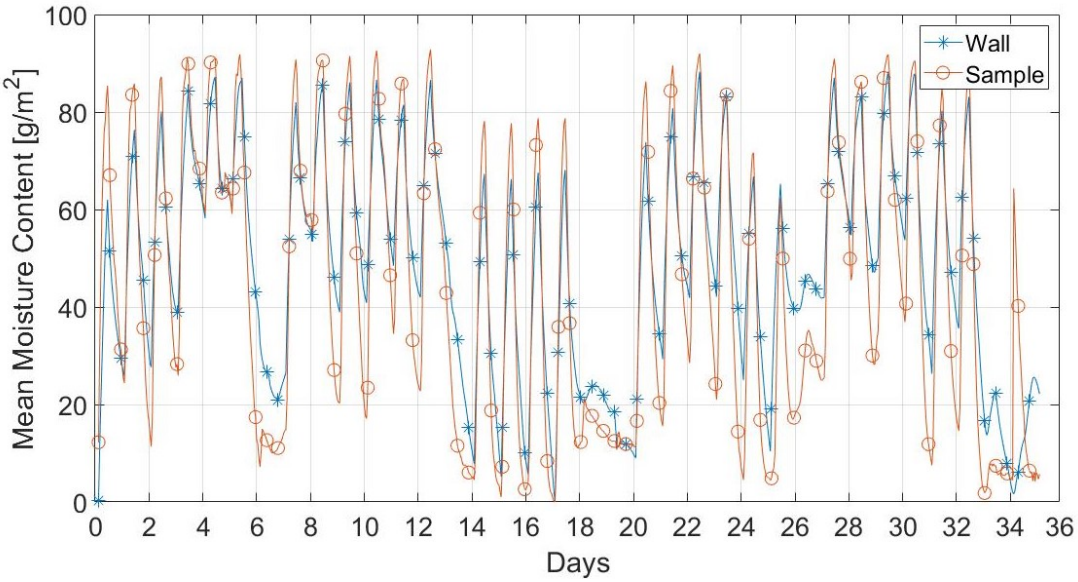

(b) Wall and sample

Fig. 5-11. Comparison of the plasterboard moisture uptake between the simulated rooms and between the simulated concrete room and the experimental plasterboard sample

Table 5.11. Experimental moisture buffering capacity of the plasterboard specimen (g/m^2)

Sample	Test 1	Test 2	Test 3	Test 4	Test 5
Cycle 1	73.11	70.13	77.17	70.73	59.29
Cycle 2	74.41	70.39	75.25	69.84	58.05
Cycle 3	69.77	74.40	78.73	70.99	54.92
Cycle 4	56.81	69.13	72.84	79.13	82.95
Cycle 5	31.80	64.06	-	67.22	73.47
Cycle 6	82.81	64.27	-	57.55	85.88

Observing the simulated moisture content in the under-layers, plasterboard adsorbed 78% of the total moisture adsorbed by the walls, while 22% by mass was transferred and distributed in the other materials in both rooms. This results suggest that plasterboard regulated the amount of water transferred to the under-layer. The under-layers then stored and transported moisture in the next layer depending on their hygroscopicity. As an example, in the concrete room the AAC adsorbed more moisture than the PIR insulation (Table 5.12 and Table 5.13), either for the proximity to the AAC to the plasterboard and for the hygroscopicity of the material. The PIR insulation did not adsorb and did not transfer moisture, as it is not an hygroscopic materials. For this reason, the moisture was not transferred to the other layers and the insulation worked as a moisture barrier, which generated a 2 mass% increase of the moisture content in the AAC. In the wood fibre room, the air gap was the first layer to store moisture from the plasterboard that transported moisture into the OSB. The OSB (Table 5.14) is the material that adsorbed most of the moisture transferred by the plasterboard, but due to its small thickness and high permeability the moisture moved into the wood fibre insulation (Table 5.15). The moisture was not then transferred in the following layers, which suggested that the maximum moisture penetration depth of the wall was reached in the wood fibre insulation panel.

Table 5.12. Moisture uptake of AAC (g/m^2)

AAC	Test 1	Test 2	Test 3	Test 4	Test 5
Cycle 1	13.03	15.10	6.18	10.74	4.00
Cycle 2	16.16	12.57	5.77	11.32	9.62
Cycle 3	14.23	11.36	5.75	14.07	13.33
Cycle 4	19.54	12.34	5.10	9.42	10.91
Cycle 5	15.70	7.24	-	7.16	5.26
Cycle 6	13.62	11.60	-		8.91

Table 5.13. Moisture uptake of PIR (g/m^2)

PIR	Test 1	Test 2	Test 3	Test 4	Test 5
Cycle 1	0.14	1.11	0.65	0.07	0.40
Cycle 2	0.21	0.75	0.63	0.06	0.18
Cycle 3	0.35	0.86	0.53	0.13	0.48
Cycle 4	0.86	1.09	0.53	0.07	0.24
Cycle 5	0.86	0.81	-	0.23	0.48
Cycle 6	0.71	1.05	-	0.51	0.37

Table 5.14. Moisture uptake of the OSB (g/m^2)

OSB	Test 1	Test 2	Test 3	Test 4	Test 5
Cycle 1	8.90	8.89	7.33	6.92	10.66
Cycle 2	14.06	7.37	7.46	6.29	7.90
Cycle 3	11.20	6.47	6.33	4.55	8.10
Cycle 4	12.61	4.68	5.06	5.62	5.36
Cycle 5	12.46	3.16	4.92	5.01	1.95
Cycle 6	8.70	3.99	6.24	3.73	3.30

Table 5.15. Moisture uptake of the wood fibre insulation (g/m^2)

Wood Fibre	Test 1	Test 2	Test 3	Test 4	Test 5
Cycle 1	1.18	5.56	2.84	0.90	4.84
Cycle 2	1.21	2.53	1.53	1.42	1.39
Cycle 3	1.19	1.54	2.32	1.89	3.74
Cycle 4	5.73	5.55	2.48	2.84	3.55
Cycle 5	1.52	1.00	4.45	1.38	1.61
Cycle 6	4.25	4.58	1.02	5.17	4.16

5.2.4 Investigatory Simulations: Sensitivity Analysis

In this section, load and ventilation rate were varied to analyse the impact of these factors on the sorption capacity of the walls in the concrete room. Wood fibre was also analysed, but results were not reported, as differences between the two hygroscopic rooms were negligible. The PIR cell was not analysed, because was not of interest in the investigation of the correlation between moisture buffering and environmental conditions, due to the non-hygroscopicity of the walls. Ventilation and moisture load were individually either increased or decreased by 20%, 50% and 80% by mass, to understand their role in the moisture balance of the rooms. Furthermore, the load and ventilation rate were simultaneously varied to investigate the response of the walls to these two factors, when the indoor RH was kept unvaried.

5.2.4.1 Load Variations

In the hygroscopic rooms the load was varied, while all the other inputs were maintained unvaried. The increase and decrease of the humidifier water consumption produced variations to the RH of the rooms (Fig. 5-12a), which consequently, generated different response of the walls. By increasing the RH fluctuations, the walls uptake increased (Fig. 5-12b). As shown in Table 5.16, the moisture uptake of the walls did not increased at the same rate of ventilation. When the load increased by 20% by mass, moisture buffering increased by 15%, at 50% it increased by 36% and when the load jumped to 80% by mass, the wall moisture uptake increased by 60%. In response to the slower moisture exchange of walls ventilation and infiltration moisture removal increased by 23%, 57% and 91% at 20%, 50% and 80% load increase, respectively (Fig. 5-13). During de-humidification walls, ventilation and infiltration presented smaller variations (Table 5.17). The increase or decrease of moisture removed through ventilation is in line with variations of the load. When the load was increased by 80%, the ventilation's moisture removal increased by 80%. To compensate the moisture removal by infiltration and ventilation, walls released a similar amount of moisture into the room.

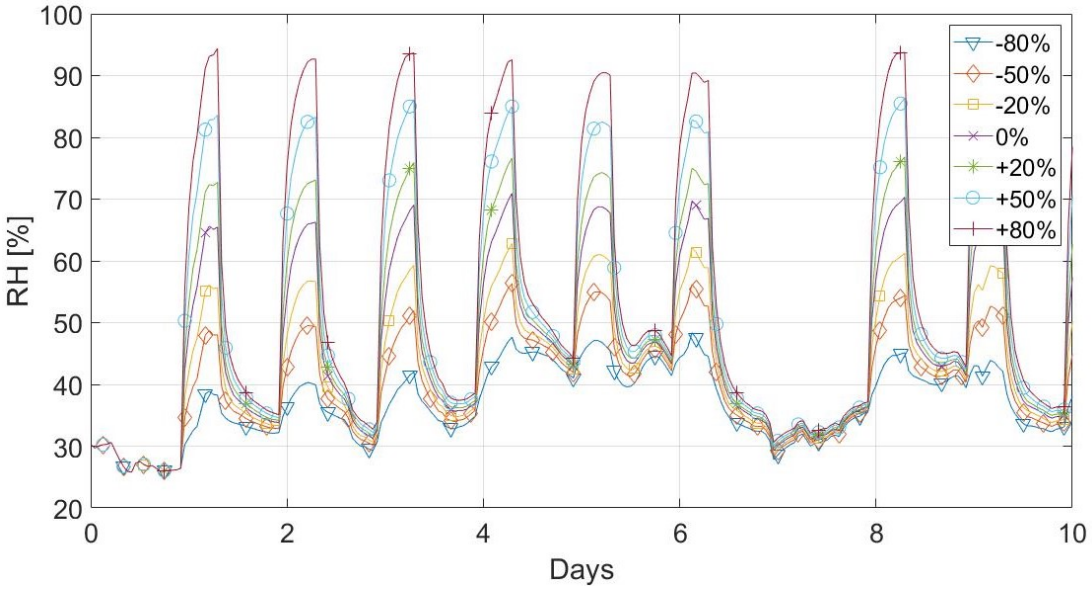

(a) RH

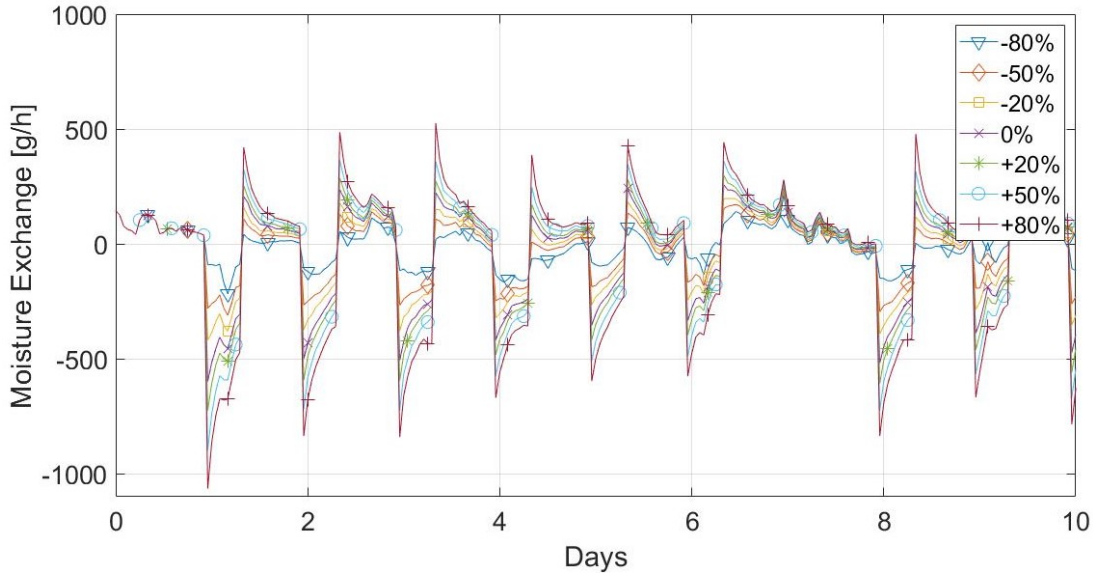

(b) Walls

Fig. 5-12. RH and moisture exchange variation when the load is varied

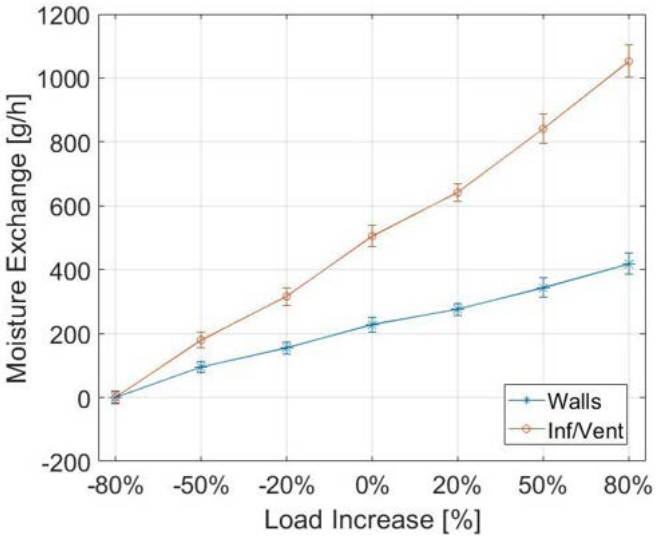

Fig. 5-13. Moisture exchange and confidence intervals when the load is varied from -80% to +80% mass increase during the de-humidification

Table 5.16. Moisture exchange (g/h) during the humidification

	Walls	Infiltration	Ventilation
-80%	-100.08 ±19	-19.40±6	-62.32 ±21
-50%	-195.47±17	-62.11 ±6	-199.54±18
-20%	-255.00±17	-94.48±5	-303.51±16
0%	-329.00±23	-139.42±8	-447.88 ±25
20%	-376.31±26	-171.77 ±9	-551.79 ±28
50%	-444.19±31	-219.12±11	-703.89 ±34
80%	-518.12±33	-269.27±12	-864.99 ±39

Table 5.17. Moisture exchange (g/h) during the de-humidification

	Walls	Infiltration	Ventilation
-80%	50.29±22	-13.07 ±5	-42.00±17
-50%	93.99±26	-24.61 ±6	-79.07±21
-20%	121.01±28	-31.94 ±7	-102.62±23
0%	154.56±31	-41.13 ±8	-132.14 ±26
20%	176.54±34	-47.25 ±9	-151.78±29
50%	208.±31	-56.17±10	-180.45±32
80%	256.66±45	-68.72 ±12	-220.75±39

The amount of water (in percentage) adsorbed by walls, ventilation and infiltration to reduce the moisture level in the rooms during the humidification is shown in Table 5.18. The "room" represents the moisture retained in the room to increase the RH level. The negative values indicate the percentage of water adsorbed or removed from the

room, while the positive numbers indicate the moisture gained by the room. It can be observed that when the load is low, the wall is the element, which predominately moderated the moisture content. However, higher is the load, stronger is the impact of ventilation to balance the moisture in the room (Table 5.18). It can be observed that the percentage of water adsorbed by the walls did not substantially vary, as there were less than 5% variations in the moisture buffering performances of the wall between the tests (Table 5.18). This is probably due to the reduction of the moisture buffering capacity of the walls was reduced above 0% load increase, which corresponded to RH fluctuations higher than 70%RH, due to the materials saturation or condensation. Overall, an average of 33% of the moisture load was adsorbed by walls, 63% was eliminated through ventilation and the remaining 4% was retained into the room.

Table 5.18. Moisture distribution proportion between walls, infiltration, ventilation and room (%) during humidification in the concrete room

Concrete	Walls	Infiltration	Ventilation	Room
-80%	-52.76±10	-10.12±3	-32.51±8	4.62±1
-50%	-41.99±4	-12.91 ±1	-41.49±3	3.61±1
-20%	-38.79±3	-13.70 ±1	-44.02±2	3.49±0
0%	-35.99±2	-14.39 ±1	-46.22±2	3.41±0
20%	-34.54±2	-14.73 ±0	-47.33±1	3.40±0
50%	-32.99±1	-15.11 ±0	-48.52±1	3.39±0
80%	-32.02±1	-15.35 ±0	-49.30±1	3.34±0

Observing the plasterboard response to the load variations, it is evident plasterboard buffered a higher amount of moisture compared to other wall components, as shown in Fig. 5-14. In the mean time, a portion of the moisture was transported into the under-layers. The increase of RH produced an increase of moisture transported through plasterboard, due to the action of simultaneous liquid and vapour moisture transport (Table 5.19). The increase of RH into the under-layer proportionally grows with the increase of relative humidity in the room.

Table 5.19. Percentage of moisture adsorbed by plasterboard (%)

	-80%	-50%	-20%	0%	20%	50%	80%
Concrete	79.68±2	82.30±3	81.34±2	80.78±3	78.77±3	75.79±3	74.24±2

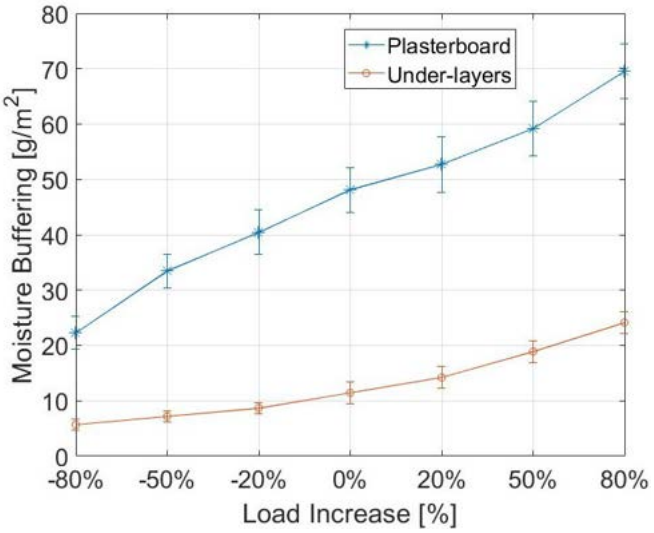

Fig. 5-14. Moisture buffering variations and confidence intervals when the load is varied

5.2.4.2 Ventilation Variations

Infiltration and ventilation rate were increased/decreased by 20%, 50%, 80%, while load was unvaried. Results showed that when the mechanical ventilation increased, the RH in the indoor decreased, whilst when ventilation is too low, the cells cannot remove the moisture load, reaching 100% RH (Fig. 5-15a). This last case was excluded from the observations, because high RH level might also generate condensation in the rooms that adds an higher level of complexity to the moisture balance calculation. Moreover, above 90%RH materials' sorption capacity significantly changes, due to possible pores and capillary saturation. As Künzel (1995) explained, in this region moisture transport mechanisms significantly vary and information about materials liquid transport property needs to be provided in the simulation. Excluding this case, it could be observed that when ventilation varied, lower variations of the walls contribution to balance the moisture were observed (Fig. 5-15b and Fig. 5-16) compared to the previous section (Section 5.2.4.1).

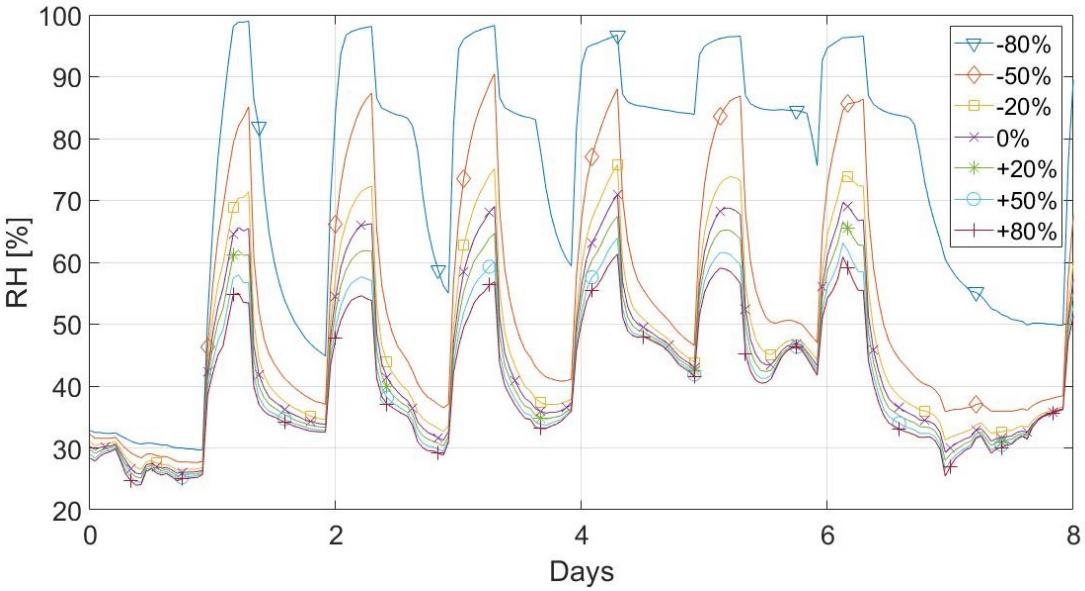

(a) RH

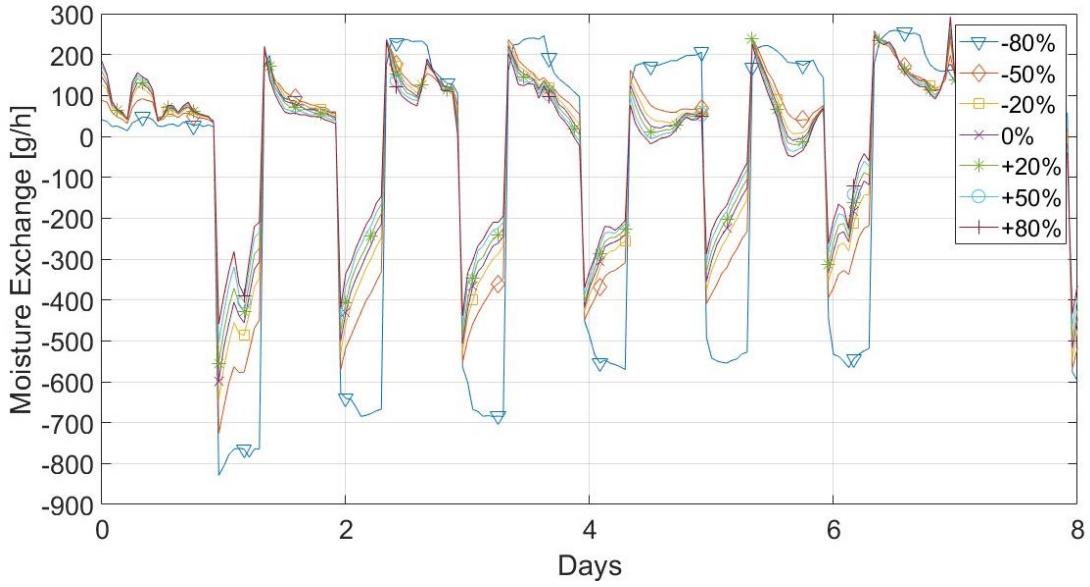

(b) Walls

Fig. 5-15. RH and moisture exchange variation when the ventilation rate is varied

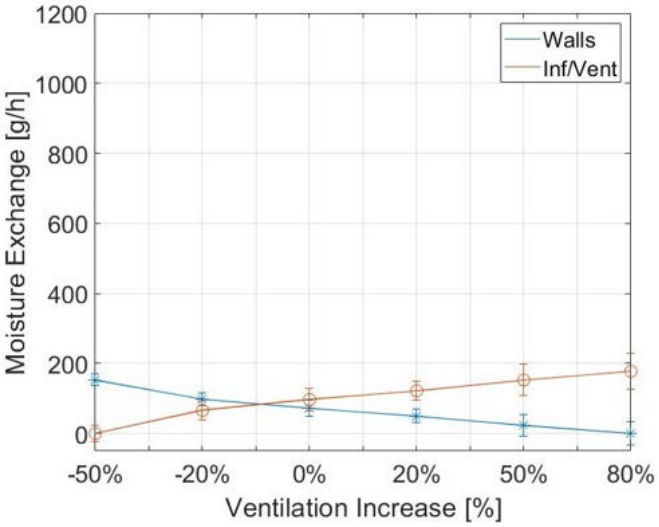

Fig. 5-16. Moisture exchange and confidence intervals when the ventilation is varied

By increasing ventilation by 20%, walls participation decreased by 6%, whilst it decreased by 15% and 22% at 50% and 80% ventilation increase, respectively (Table 5.20). On the contrary, when ventilation was reduced, walls participation was slightly higher due to the moisture increase in the room, by increasing the moisture adsorption by 8% and 24% at 20% and 50% ventilation reduction, respectively. During the de-humidification, smaller variations between each test were observed (Table 5.21). The ventilation moisture removal and the wall participation to buffer moisture as shown in Table 5.22. Overall, the analysis showed that ventilation had a lower impact than load variations on the sorption capacity of the walls.

Table 5.20. Moisture exchange in the room (g/h) during the humidification

	Walls	Infiltration	Ventilation
-80%	-626.84±31	-65.00±3	-218.62±10
-50%	-419.52±26	-111.29±6	-361.58±20
-20%	-364.32±25	-127.62±7	-411.13±22
0%	-338.23±24	-135.20±7	-434.31±24
20%	-316.33±23	-141.35±8	-453.21±25
50%	-289.02±24	-148.01±7	-477.26±24
80%	-266.69±24	-154.20±9	-495.98±28

Table 5.21. Moisture exchange in the room (g/h) during the de-humidification

	Walls	Infiltration	Ventilation
-80%	210.06±23	-50.58±5	-170.14±18
-50%	173.82±28	-47.48±8	-154.27±25
-20%	160.99±30	-43.26±8	-139.37±26
0%	154.56±26	-41.13±6	-132.14±20
20%	148.33±32	-39.23±8	-125.78±26
50%	139.66±32	-36.49±8	-117.67±26
80%	131.88±32	-34.31±8	-110.36±26

Table 5.22. Moisture distribution proportion between walls, infiltration, ventilation and room (%) during humidification in the concrete room

Concrete	Walls	Infiltration	Ventilation	Room
-80%	-66.62±1	-6.95±0	-23.37±1	3.06±0
-50%	-44.60±2	-11.85±0	-38.51±1	5.04±0
-20%	-38.75±2	-13.59±0	-43.76±2	3.90±0
0%	-35.99±2	-14.39±0	-46.22±2	3.41±0
20%	-33.68±2	-15.04±1	-48.21±2	3.07±0
50%	-30.80±2	-15.74±1	-50.76±2	2.71±1
80%	-28.44±2	-16.39±1	-52.73±2	2.43±1

Table 5.23. Moisture distribution proportion between walls, infiltration, ventilation and room (%) during humidification in the wood fibre room

Wood	Walls	Infiltration	Ventilation	Room
-80%	-64.04	-7.10	-23.27	5.59
-50%	-43.32	-11.92	-39.55	5.21
-20%	-37.54	-13.60	-44.87	3.98
0%	-34.69	-14.45	-47.38	3.48
20%	-32.37	-15.01	-49.52	3.10
50%	-29.46	-15.81	-52.03	2.70
80%	-27.09	-16.53	-53.97	2.41

As the walls participation to the room moisture regulations was less significant than in Section 5.2.4.1, also plasterboard presented smaller variations, except in the -80% test, where the RH reached 100% RH (Fig. 5-17). However, similarly to Section 5.2.4.1, when the moisture content in the room was high, more moisture was transported and stored in the under-layers, whilst, when ventilation is high and RH is low, plasterboard adsorbed most of the total moisture stored in the walls (Table 5.24).

Table 5.24. Percentage of moisture adsorbed by plasterboard (%)

	-80%	-50%	-20%	0%	20%	50%	80%
Concrete	73.60±4	70.84±3	78.04±4	80.78±3	82.42±4	83.32±4	83.46±4

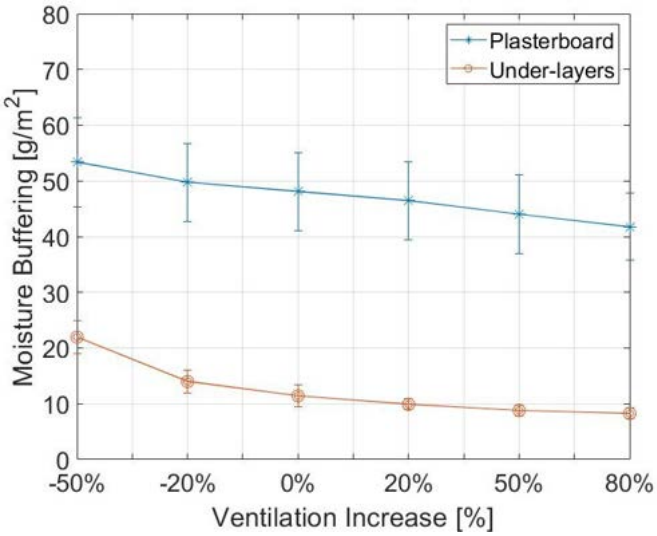

Fig. 5-17. Moisture buffering variations and confidence intervals when the ventilation is varied

5.2.4.3 Simultaneous load and ventilation rate variation

When the moisture load and ventilation rate are varied individually, the RH significantly increased or decreased, and, therefore, the variations of these parameters modified the moisture balance mechanisms in the cells. Therefore, when the indoor RH varies, a relationship between ventilation, plasterboard and the under-layers cannot be found, as different environmental conditions produce different material's responses. For this reasons, load and ventilation were varied simultaneously in order to have similar RH fluctuations in all tests. In the range between -20% and +50%, where similar RH were generated (Fig. 5-18a), similar results were observed (Fig. 5-18b). When ventilation and load increased, walls did not significantly increase their moisture exchange capacity. At 50% increase, the moisture removed by ventilation increased by 7%, which corresponds to approximately 26 g/h more to add to the 330 g/h of the "zero" case (Table 5.25). The increase or decrease of the walls moisture exchange was produced by small RH variations between the tests, which still influenced the sorption capacity of the materials. Outside this range, the impact of load/ventilation variation was higher, especially when the factors were reduced. At -80% the walls moisture exchange dropped to less than 64% than at the reference test, as the RH significantly varied. In the de-humidification (Table 5.26), similar trend to Section 5.2.4.2 were observed, but variations were significantly smaller. Observing the proportion in Table 5.27, at low ventilation walls' participation to moderate the

moisture content was significant, but when ventilation rate was increased, more moisture was removed by ventilation. This analysis suggests that walls stored a fixed amount of moisture, which did not significantly vary when the RH is kept constant. Consequently, when the walls reached their maximum "storage" capacity in a specific environmental condition, materials did not participate anymore to the moisture exchange and all the rest of moisture was then removed by ventilation (Fig. 5-19).

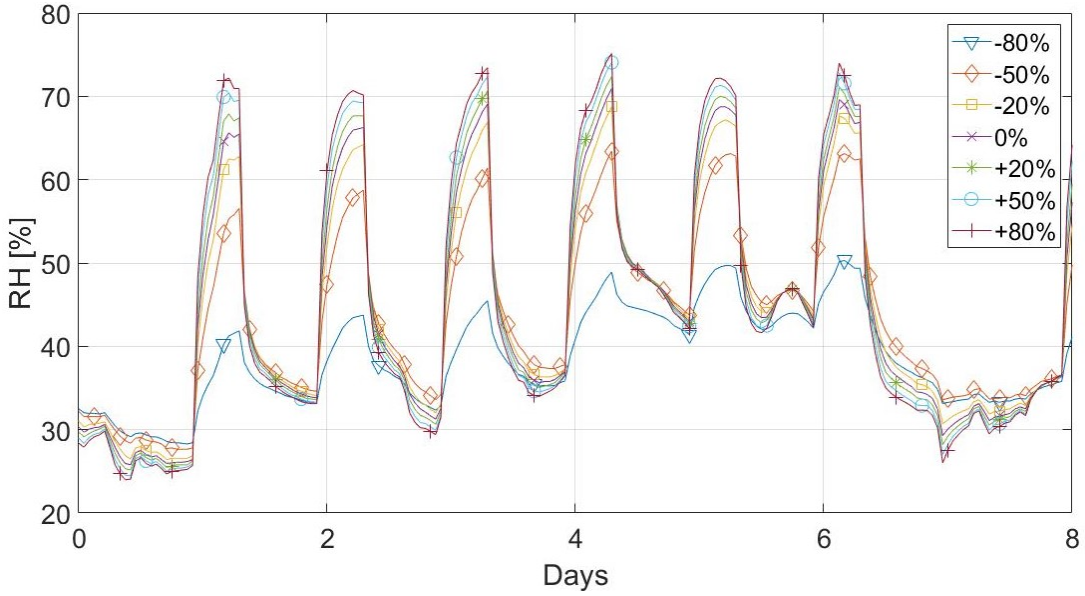

(a) RH

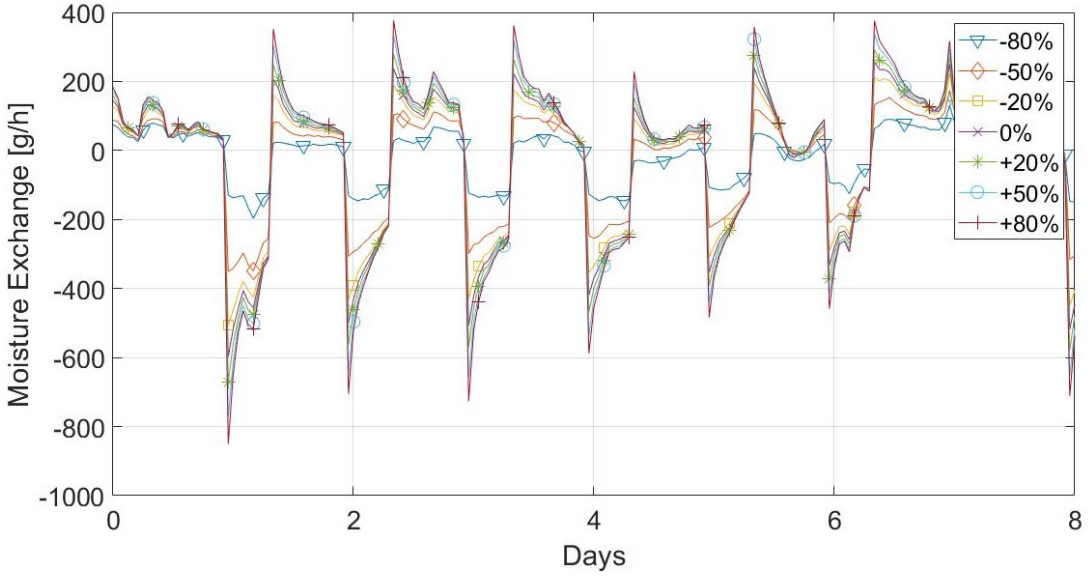

(b) Walls

Fig. 5-18. RH and moisture exchange variation when the thermal surface resistance is varied

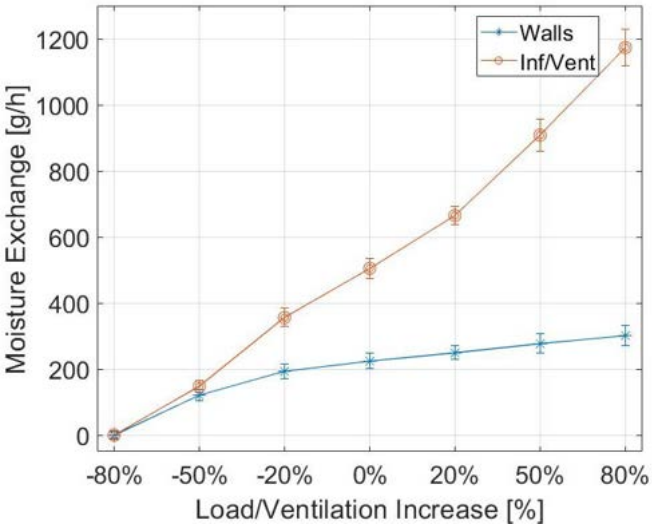

Fig. 5-19. Moisture exchange and confidence intervals when the load and ventilation rate are varied

Table 5.25. Moisture exchange in the room (g/h) during the humidification

	Walls	Infiltration	Ventilation
-80%	-114.19±11	-39.58±8	-25.26±5
-50%	-234.79±16	-50.37±4	-161.81±13
-20%	-307.39±21	-99.87±7	-320.83±22
0%	-338.23±24	-135.20±7	-434.31±24
20%	-363.82±26	-173.47±9	-556.20±28
50%	-391.50±29	-230.39±11	-742.88±36
80%	-414.90±30	-293.72±13	-944.72±43

Table 5.26. Moisture exchange in the room (g/h) during de-humidification

	Walls	Infiltration	Ventilation
-80%	47.86±14	-32.74±9	-20.89±6
-50%	98.30±18	-26.54±5	-85.26±15
-20%	136.90±24	-36.60±6	-117.59±20
0%	154.56±24	-41.13±6	-132.14±20
20%	168.83±29	-44.89±7	-143.94±24
50%	184.56±35	-48.69±8	-157.01±26
80%	197.67±33	-52.12±9	-167.65±28

Table 5.27. Moisture distribution proportion between walls, infiltration, ventilation and room (%) during humidification in the concrete room

Concrete	Walls	Infiltration	Ventilation	Room
-80%	-60.80±6	-20.63±8	-13.17±2	5.40±0
-50%	-50.06±3	-10.70±3	-34.36±2	4.88±0
-20%	-40.64±2	-13.17±3	-42.30±2	3.89±0
0%	-35.99±2	-14.39±2	-46.22±2	3.41±0
20%	-32.25±2	-15.39±2	-49.33±1	3.03±0
50%	-27.91±2	-16.45±1	-53.06±1	2.58±0
80%	-25.71±1	-17.13±1	-55.87±1	2.41±1

In the range -20% and 20%, moisture buffering variations of plasterboard were up to 8 g/m^2 and were smaller in the under-layers (Fig. 5-20), which gave confidence that variations of the ventilation/load up to 20% in the results in Section 5.2.2 generated negligible alteration in the moisture buffering capacity of the walls. Also in this case, plasterboard had a stronger impact on the indoor moisture regulation than the under-layers (Fig. 5-20).

Table 5.28. Percentage of moisture adsorbed by plasterboard (%)

	-80%	-50%	-20%	0%	20%	50%	80%
Concrete	79.06±1	79.73±1	80.50±2	80.78±2	80.90±3	81.08±3	79.90±3

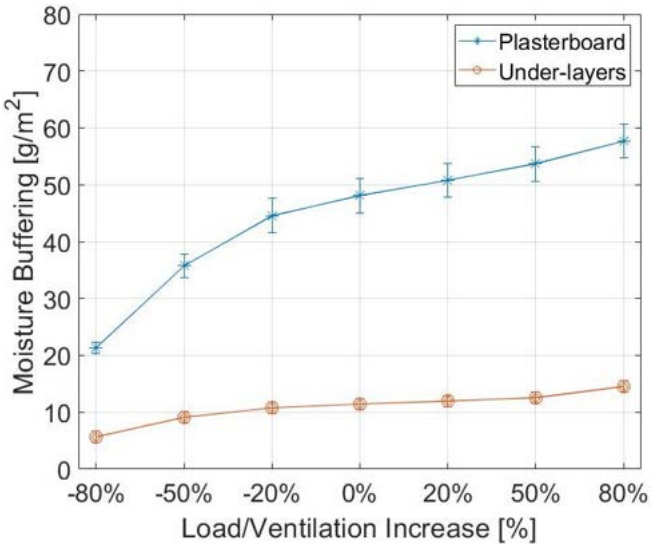

Fig. 5-20. Moisture buffering variations and confidence intervals when the load and ventilation rate are varied

The results of the sensibility analyses were summarised in Fig. 5-21 and Fig. 5-22. The load variations generated higher RH fluctuations in the rooms that, consequently,

produced higher variations in the walls moisture exchange (Fig. 5-21). The simultaneous load and ventilation variations presented smaller RH fluctuations between each test that explained the smaller increase of the walls moisture exchange. The observation of the overlapping area between the three sensitivity analyses indicates that similar results were achieved, when the RH interval was unvaried. This confirms materials respond to RH fluctuations rather than load/ventilation variations. In support of this statement Yoshino, Mitamura and Hasegawa (2009) also found out that the increase of ventilation rate does not impact significantly the moisture buffering capacity of materials, when the indoor RH levels are unvaried. Similar observation can be done with the moisture buffering variations of plasterboard (Fig. 5-22a). Under-layers did not present a linear increase of their moisture buffering capacity, but it showed significant differences above 40%RH fluctuations between load and ventilation variations. The reason is not clear, but the under-layers may be more sensitive to ventilation variations than to the load increase, due to variations of the moisture transport mechanisms.

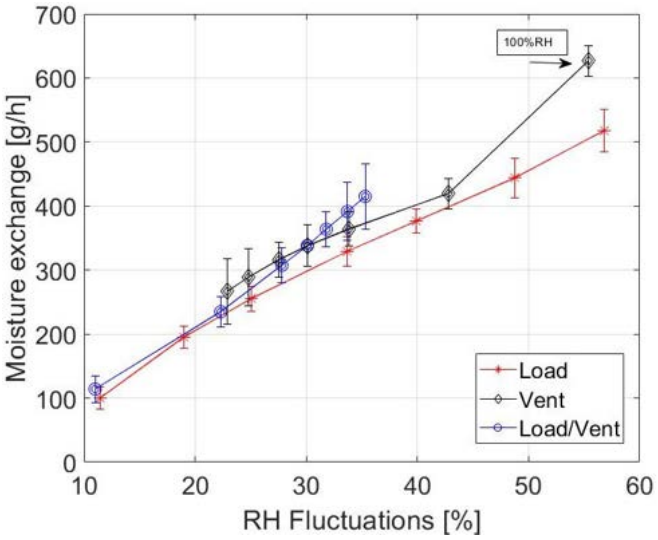

Fig. 5-21. Moisture exchange at different RH intervals

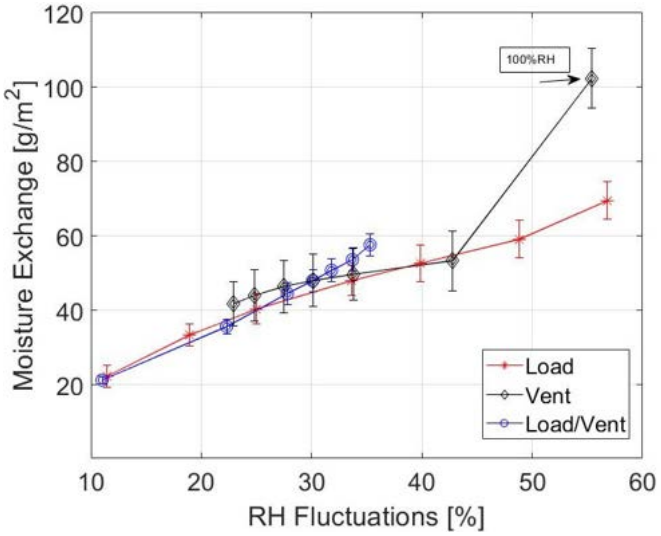

(a) Plasterboard

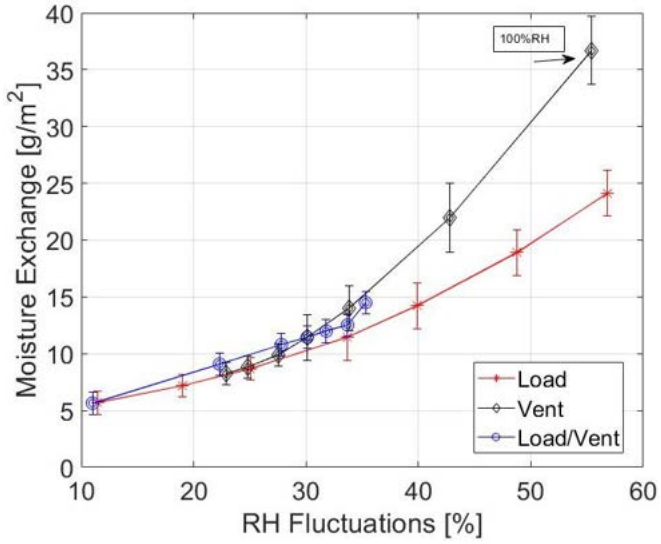

(b) Under-layers

Fig. 5-22. Moisture buffering variations at different RH intervals

5.2.5 Investigative Simulations: Moisture Buffering Performances of other Plasters

In this section simulations were repeated by coating the internal aerated concrete block surface in the concrete room alternatively with 20 mm thickness clay, lime and gypsum plaster. The materials properties used in the model were taken from Chapter 3, while all the other parameters were the same as in Section 5.1. As the discrepancies of the results between the concrete and wood fibre room were negligible, therefore, only the concrete room is shown. The impact of the coatings to regulate the indoor relative humidity was investigated. As Fig. 5-23a illustrates, all materials, included plasterboard, moderate the RH similarly, presenting some minor variations (up to 7%RH). Gypsum demonstrated the highest humidity moderation capacity, while lime

performed the least effectively. Fig. 5-23a indicates that for clay the average indoor relative humidity peak-to-peak amplitude was reduced to 36% RH in the indoor environment, whilst lime had a lower impact in the room (40% RH). Gypsum and plasterboard adsorbed a greater proportion of the generated moisture, as humidity fluctuations were reduced to 33% and 35%, respectively. By analysing the moisture buffering performances of the coatings (Fig. 5-23b), the difference between the materials was significant. Gypsum and lime adsorbed and desorbed, $61.40\,g/m^2$ and $32.10\,g/m^2$, respectively, while plasterboard and clay stored and released 47.90 and 48.60 g/m^2, respectively. The reason of the similarity between clay and plasterboard is linked to the thickness of plasterboard. Even though plasterboard had an higher sorption potential, the small thickness reduced the moisture buffering performances of the material, which in this case became similar to clay in terms of moisture buffering ability. Overall, results indicate that even though materials presented different moisture buffering performancesc, the impact on the environment is similar. In Section A.3 the moisture buffering ability for each cycle and materials is shown.

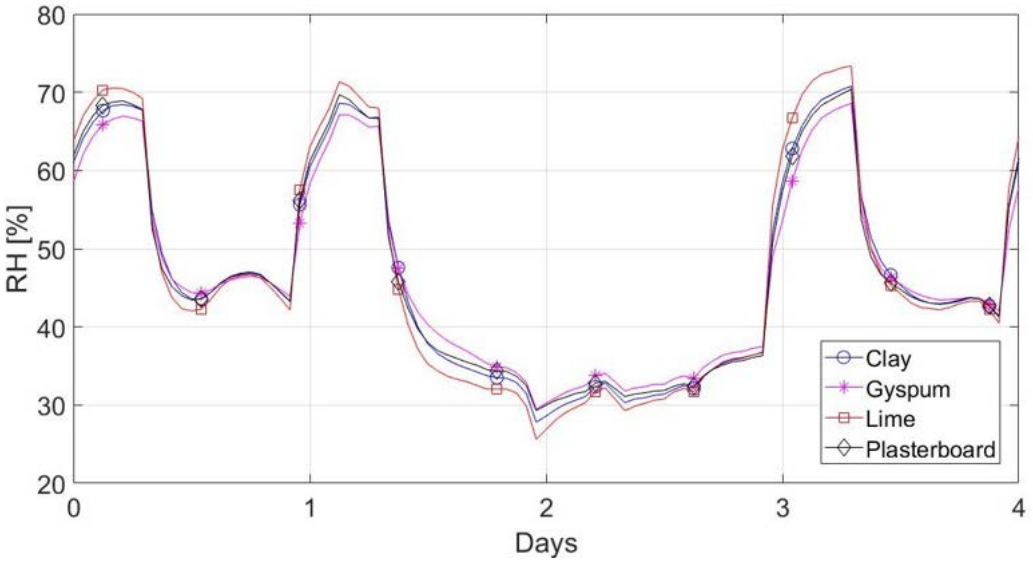

(a) RH

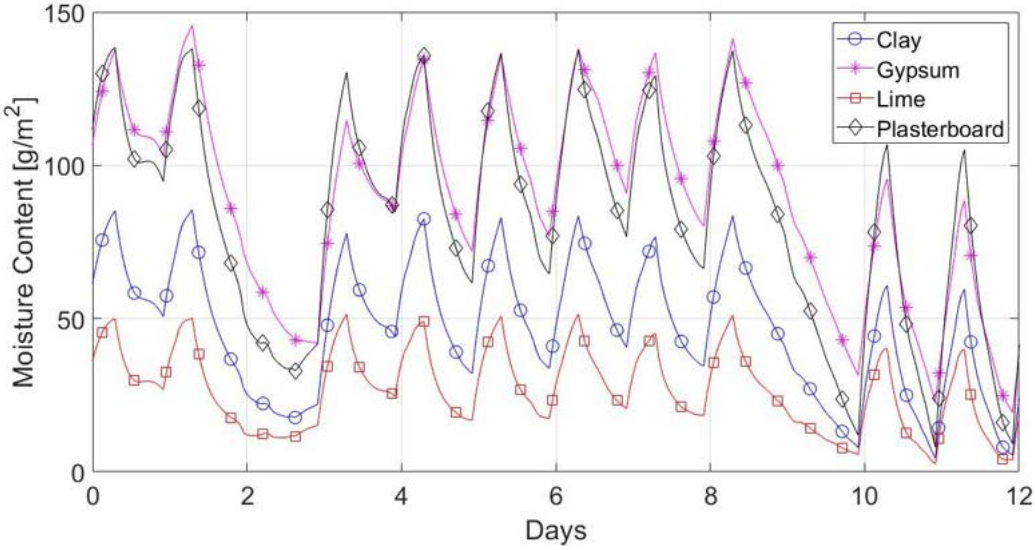

(b) Plasters

Fig. 5-23. RH and moisture content in the plasters in the concrete room

Table 5.29 summarises the simulated moisture exchanged by walls and ventilation during the humidification. When gypsum was applied, walls presented an higher involvement in the indoor moisture balance compared to the other materials, as gypsum was able to gain more vapour from the environment. At the same time, gypsum reduced by 9.70% the amount of moisture expelled through ventilation, when compared to plasterboard. In general, Table 5.30 clearly shows walls played an important role in the moisture regulation of the indoor, as they buffered between 26.17% to 41.93% of the moisture in the building. During the de-humidification gypsum released less moisture than the other coatings into the environment (Table 5.31). Due to the higher participation of gypsum to regulate the humidity in the humidification, during the humidification, less moisture was removed through

ventilation/infiltration than in the other cases. Therefore, gypsum did not need to release as much moisture as the other materials to increase the humidity level indoor.

Fig. 5-24 represents the moisture exchange through the walls, which indicates that the differences between materials varied for every cycle. However, variations during the de-humidification were negligible, except in day 2 in Fig. 5-24, in which significant differences between the plasters were noticed. In this case lime participated less than gypsum to release moisture, whilst plasterboard and clay still presented similar results. This is due to the particularly dry environment in that cycle (Fig. 5-23), which required all materials to release more moisture accordingly to their moisture buffering potential. Similarly during the humidification in day 3, the higher moisture load required walls to adsorb more moisture from the room. This generated significant discrepancies between the materials, due to their different moisture buffering capacity. This indicates that when the humidity variations in a room are significant, a material with an higher moisture buffering potential is essential to have a better regulation of the indoor environment.

Table 5.29. Average moisture exchange between the indoor space, walls and ventilation (g/h) during the humidification

	Walls	Infiltration	Ventilation	Room
Clay	323.84±18	139.45±8	447.97±27	11.77±0
Gypsum	394.86±22	123.36±8	396.28±26	9.69±0
Lime	246.41±13	156.95±9	504.18±27	17.26±0
Plasterboard	336.70±24	136.67±8	439.04±26	12.48±0

Table 5.30. Percentage of the moisture load exchanged by walls and ventilation (%) during the humidification

Concrete	Walls	Infiltration	Ventilation	Room
Clay	-34.38±2	-14.74±0	-47.34±1	3.54±0
Gypsum	-41.93±2	-13.03±1	-41.85±2	3.19±0
Lime	-26.17±1	-16.59±0	-53.30±2	3.93±0
Plasterboard	-35.62±2	-14.47±1	-46.49±1	3.42±0

Table 5.31. Average moisture exchange between the indoor space, walls and ventilation (g/h) during the de-humidification

	Walls	Infiltration	Ventilation	Room
Clay	133.58±23	-34.20±6	-109.86±19	10.47±1
Gypsum	96.71±30	-25.43±7	-81.70±24	10.42±1
Lime	164.20±17	-41.10±4	-132.01±14	8.91±2
Plasterboard	135.03±26	-33.98±7	-109.16±21	8.11±1

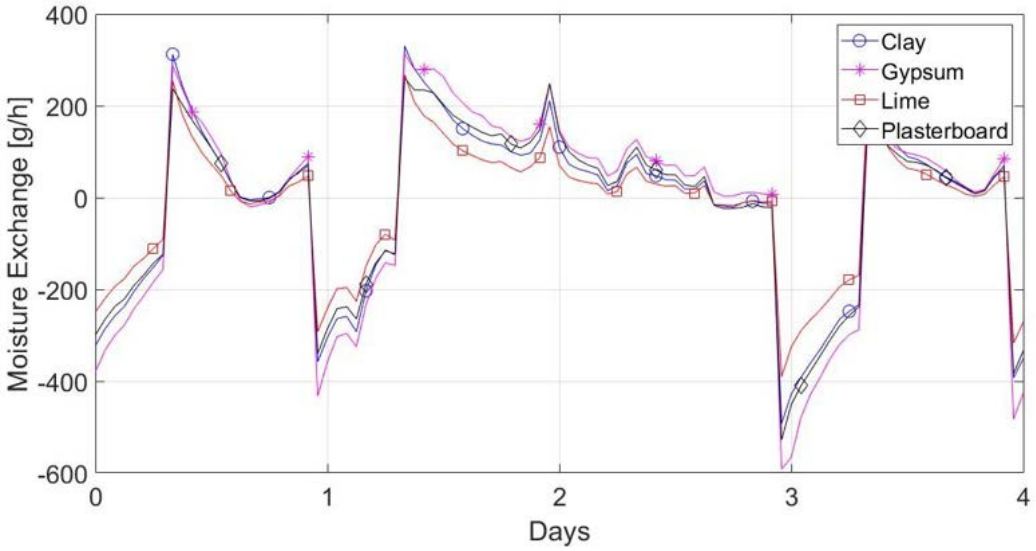

Fig. 5-24. Moisture exchange of walls in the concrete room

As already mentioned in Section 5.2.5, simulations showed that the AAC, underneath the plaster, actively participated in the moisture buffering process. Fig. 5-25a shows the daily moisture content fluctuations in the AAC. AAC with clay, plasterboard and lime presents 8.82, 10.95 and 11.10 g/m^2 daily fluctuations, respectively, whilst fluctuations were less marked with gypsum plaster (0.50 g/m^2), probably due to the higher moisture sorption ability of gypsum. The PIR insulation panel presented negligible moisture buffering fluctuation of less than 0.48 g/m^2 in all cases. (Fig. 5-25b).

Both AAC and PIR also showed an overall increase of their moisture content. The moisture storage capacity of those layers is related to the seasonal moisture buffering capacity of walls. The high absolute humidity during the moisture buffering test in the room participated to the overall increase in the moisture content of the layers closest to the indoor environment, together with seasonal variations that also influence most of the wall elements. However, the two moisture transport mechanisms should be considered as independent phenomenon that do not strictly interfere with each other in simulations, as demonstrated by the author in Cascione et al. (2020b). The influence of the outdoor weather on the daily moisture variations can be demonstrated by eliminating the influence of the outdoor. This can be done by observing the differences between simulation performed with and without the indoor RH variations, as Cascione et al. (2020b) explained. The result of this analysis assured that daily fluctuations are not significantly effected by the wall moisture variation across the year. For these reasons, the overall increase of the moisture content in the layers was not considered in the anlysis of the daily moisture buffering capacity of walls.

In conclusion, it can be stated that depending on the plaster, a fixed amount of water moves to the under-layers. When clay, plasterboard and lime were applied on the

wall, the AAC is responsible of the 21.26% , 24.48% and 32.44%, respectively, of the total moisture buffering capacity of wall, whilst with gypsum AAC buffered 1.40% of moisture (Table 5.32). The daily amount of moisture buffered by the under-layers depends on the moisture buffering capacity of the indoor coatings. Overall, it can be stated that after plasters reached their maximum moisture buffering capacity in that particular RH interval, moisture moved into the adjacent material (in this case AAC). However, due to gypsum's higher performances, the materials did not reached its maximum moisture buffering capacity, therefore, gypsum adsorb most of the indoor moisture without transferring moisture into the AAC.

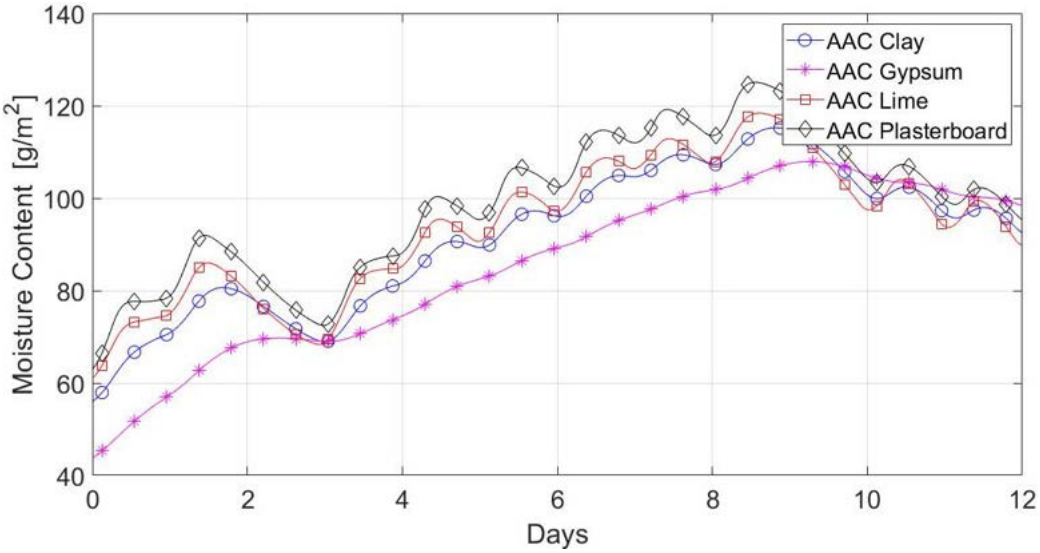

(a) RH

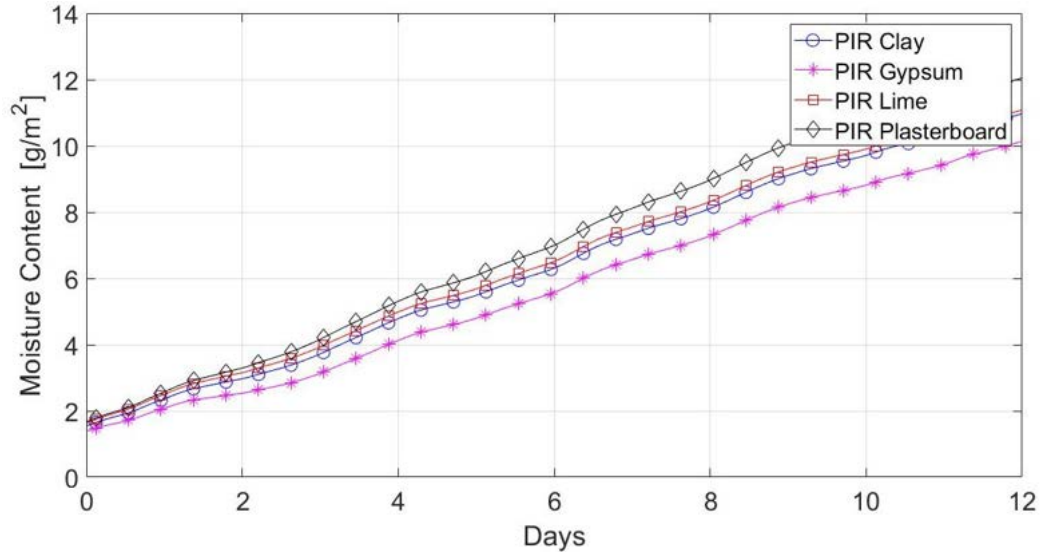

(b) Plasters

Fig. 5-25. Moisture content in the AAC and Pir in the concrete room

Table 5.32. Distribution of the total moisture buffered by walls (%)

	Plaster	Under-Layer
Clay	78.74±3	21.26±2
Gypsum	98.66±4	1.34±3
Lime	67.56±3	32.44±3
Plasterboard	75.52±5	24.48±4

5.2.6 Comparison between Full-Scale Simulations and Experimental in-situ Specimen

The simulated moisture buffering performance of the plasters was compared with the experimental change in weight of the specimens of the same materials under the same environmental conditions in the test room (Section 4.4). In general, a good agreement was observed (Table 5.33), as the average moisture buffering capacity of the materials is similar in both investigations. However, in some cycles some variations were noticed (Fig. 5-26 and Fig. 5-27). The differences were not significant in the daily fluctuations, but in the total moisture content of the materials. As demonstrated in Cascione et al. (2020b), gypsum presented a more irregular behaviour than the other materials (Fig. 5-26b). In the first two weeks of testing (days 0 to 13) the gypsum specimen accumulated moisture because it took longer for the plaster to balance its moisture content with the environment. This behaviour was not observed in the laboratory testing because of the materials preconditioning (Section 3.3). Even though the amplitude of the moisture fluctuations was preserved, the total moisture increase is higher in the specimen rather than in simulations, probably because the specimen cannot transfer moisture to the under-layers, and, therefore, it accumulated more water than the simulated walls. Moreover, the experimental specimens were exposed for a shorter time to the room environmental conditions, as the materials were not previously preconditioned and directly placed in the room to test their response. However, after the 14^{th} day, gypsum reached its moisture balance by presenting only daily fluctuations. Lime and plasterboard (Fig. 5-27a and Fig. 5-27b) did not present this behaviour due to the low sorption capacity of lime and the longest exposure of plasterboard to the test room environment (the plasterboard specimen was placed one month before the others in the room). Clay also presented similar water accumulation capacity as gypsum, but to a lower rate and the total moisture increase is in line with simulations (Fig. 5-26a).

Overall, it can be stated that simulations can reproduce the the dynamic sorption capacity of materials, when compared with the experimental sorption capacity of the specimens, even though simulations applied steady-state hygric properties. However, it cannot be confirmed that simulations represent the real behaviour of plasters, when applied on walls. The simulated sorption capacity and the standard moisture buffering

testing may be higher than in real buildings, as already mentioned in Section 4.4.

Table 5.33. Comparison of the moisture buffering capacity of plasters (g/m^2)

	Clay	Gypsum	Lime	Plasterboard
In-situ	46.79±3	88.63±8	35.37±3	76.00±7
Simulation	59.97±3	80.84 ±4	34.60±2	62.94±4

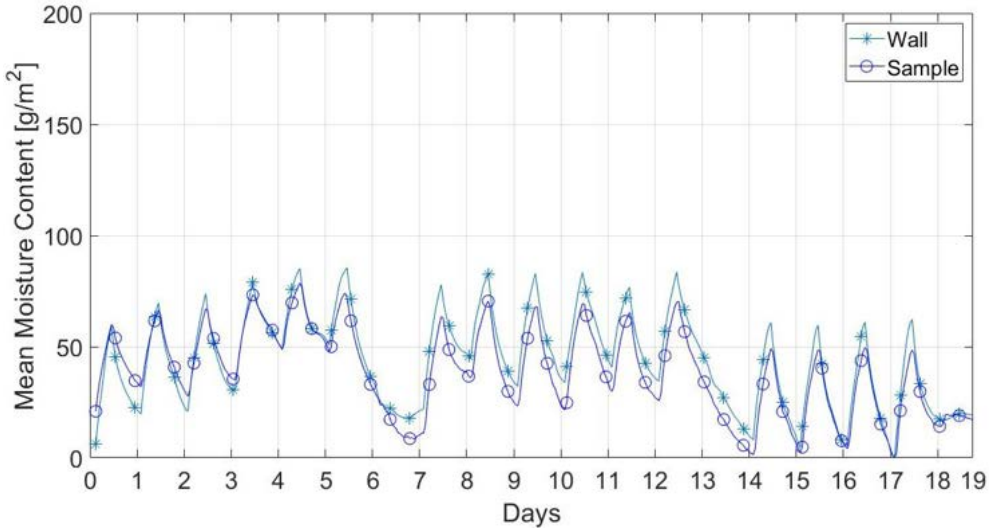

(a) Clay

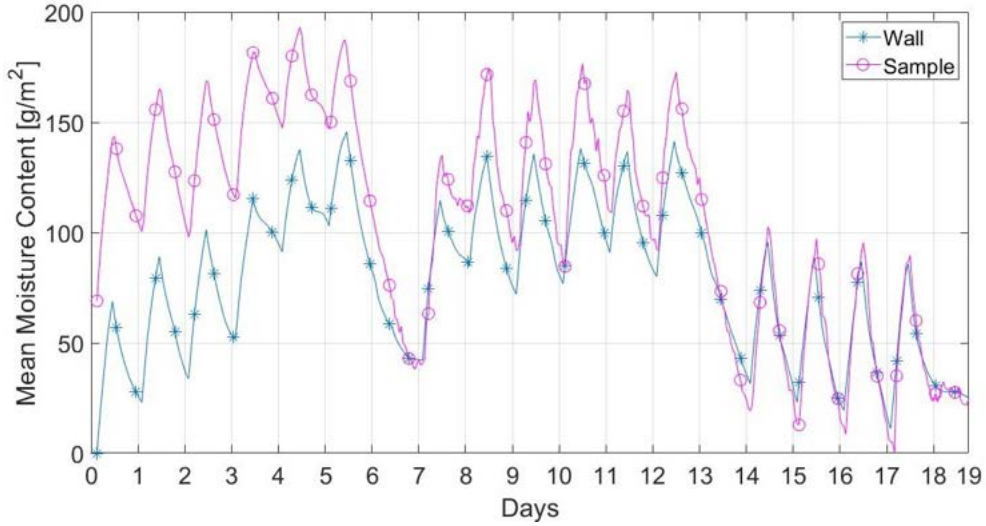

(b) Gypsum

Fig. 5-26. Simulated and experimental Moisture buffering of clay and gypsum in the concrete room

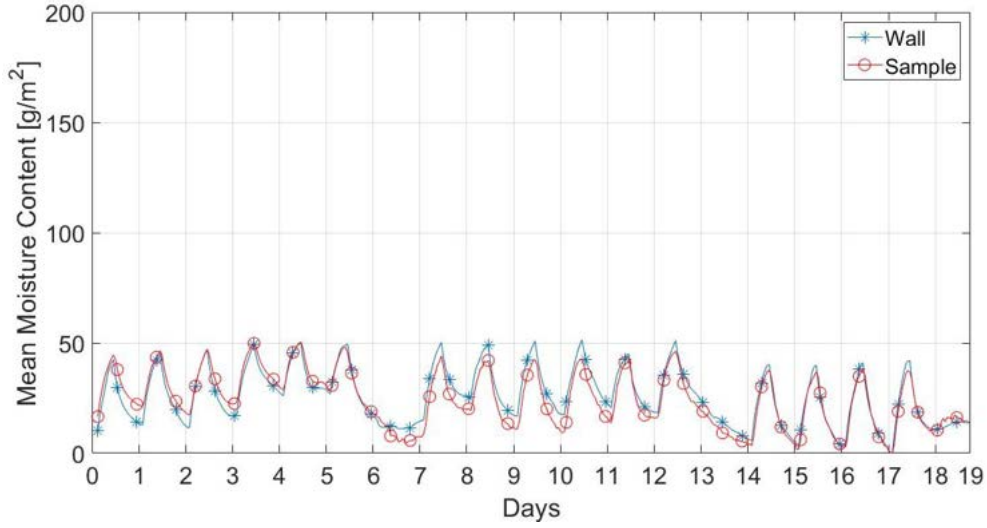

(a) Lime

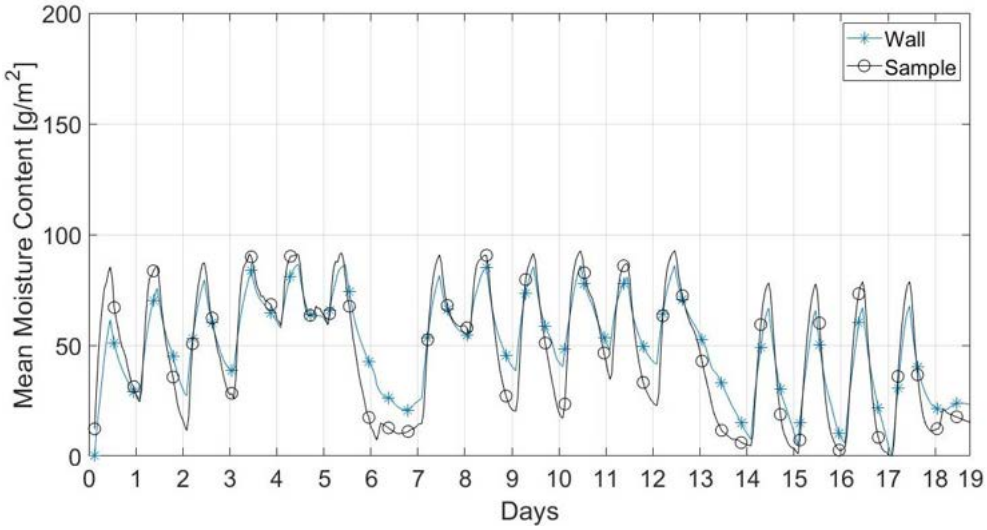

(b) Plasterboard

Fig. 5-27. Simulated and experimental moisture buffering of lime and plasterboard in the concrete room

5.3 Summary

In this chapter the test rooms were modelled and the moisture buffering test performed at the BRP was simulated to integrate and further analyse the response of walls to humidity fluctuations. Data of ventilation and infiltration rate, and plaster properties obtained from the laboratory testing and the full-scale experimentation were applied in the simulation software. Due to the limited data on the humidifier moisture load from the experimental testing, in simulations the load was modified until the indoor absolute humidity matched the results obtained in the field testing. Simulations demonstrated that the moisture load in the field testing was consistently lower than (600g) in simulation due to the inaccuracy of the water tank monitoring

system or due to the simulation overestimation of the moisture buffering capacity of walls.

The moisture balance analysis with plasterboard highlighted that the impact of walls is significant in the moisture regulation, even though ventilation, combined with building infiltration, also participated to the moisture regulation of the room. However, the contribution of walls to buffer moisture is related to ventilation variations. Low ventilation rate increased the involvement of materials to buffer moisture, which is typical in an air tight building with low ventilation strategies (like in cold environments). When the ventilation rate was increased the walls contributions was lower. Nevertheless, the capacity of walls to buffer moisture is not directly influenced by the ventilation rate, but it is influenced by the change in the RH in the rooms, as consequence of the variations of the ventilation. When the ventilation rate increased, the indoor RH is reduced, due to the higher volume of moist air eliminated through ventilation. Consequently, as the indoor absolute humidity is reduced, the response of walls to buffer moisture is receded. On the contrary, when the ventilation is reduced, the RH increases, increasing the ability of materials to buffer the moisture. When the RH intervals is kept unvaried, even though the ventilation rate is varied, walls performances do not vary, as they reach their maximum moisture buffering performances in that particular RH fluctuation interval. When the walls reached that threshold, ventilation removed the rest of moisture that walls do not adsorb. However, in reality the increase of ventilation rate can generate variation on the air velocities in the room and, therefore, change the moisture surface resistance of walls. WUFI® does not directly include the moisture surface resistance in the simulations, but it is a factor that should be included in simulations. Overall, as walls significantly influence the moisture moderation, potentially lower ventilation rate may be allowed in buildings to moderate humidity in the room.

The computational model also revealed the deeper penetration of water vapour into the wall from the room that cross the surface material to be stored in the under-layers. It was estimated 24% of total moisture buffered by the walls moved into the under-layers. This mechanism may be partially attributed to the water vapour permeability of the finishing materials and the vapour pressure and temperature differential between the indoor and outdoor environment, as well as the water transport mechanism of different materials.

It was found that there were not significant differences between the concrete and wood fibre rooms, because in both rooms plasterboard regulated the amount of moisture that can move into the under-layers. Depending on the moisture level and RH fluctuation amplitudes in the rooms, plasters allow the moisture propagation into the walls. The only main difference between the hygroscopic rooms was that wood fibre room needed slightly higher moisture load, due to the higher overall hygroscopicity of the walls.

Compared to the concrete room, in the wood fibre the moisture is free to cross the wall and exchange moisture with the outdoor, due to the hygroscopicity of the wall elements. In the concrete room a PIR insulation panel acted as a moisture barrier. Wood fibre can potentially transport more moisture outdoor than concrete, so the double capacity to buffer and expel moisture through moisture transport needs to be further investigated. However, the seasonal capacity of walls to store moisture in winter and release vapour in summer did not significantly impact the daily moisture fluctuations, as the daily moisture fluctuations of materials were similar for both rooms. Overall, it can be stated that the two rooms behave similarly because wood fibre had an higher penetration depth, whilst concrete under-layers material (AAC) had significant sorption capacity. Nevertheless, the overall penetration depth of the walls needs to be better understood, because daily and seasonal moisture variations in the materials may interfere with each other, which make more complex the calculation of the penetration depth necessary to buffer the sole indoor moisture. The moisture penetration needs to be verified, as simulations were based on the static material properties, which means the results are based on the average adsorption curve of plasters and steady-state water vapour permeability. Further analysis, outside the scope of this research, will assure the causes of the water transport, and verify if hygrothermal simulations magnify this process, as based on simplified models and laboratory tested materials properties. Nevertheless, it is, overall, possible to accurately predict through simulation the response of materials to control the environment.

The moisture buffering capacity of clay, lime and gypsum coatings was also determined through hygrothermal simulations on the concrete room. Materials responded quite differently to moisture variations. Gypsum buffered more water and, consequently, transported less moisture to the under-layers, whilst lime adsorbed the least moisture from the indoor, but more vapour was transported into the under-layers. Clay and plasterboard behaved similarly due to the thickness difference between the two materials, which indicates that even though plasterboard had higher sorption potential than clay, the small thickness of the material reduces the moisture buffering perfomances of plasterboard. It can be so confirmed plasters applied on the indoor control the overall moisture regulation and transport into the walls. The quantity of vapour that is stored by under-layers strongly depends on the plasters sorption capacity potential and vapour permeability. By calculating the total moisture buffered by the whole assembly, it was also observed that the overall moisture adsorbed in the room varied for each plasters. When lime was applied, the wall adsorbed 37% less moisture than plasterboard, whilst clay only 16% less. Gypsum and plasterboard showed similar results. These differences also indicate that the slower capacity of some materials to store moisture reduce the overall performances of the wall, and consequently, more moisture is removed through ventilation.

In conclusion, even though materials behaved differently, their impact on the indoor moisture moderation was similar. Plasters all participated in the reduction of the humidity levels showing up to 7% differences on the RH fluctuations in the rooms. It appears that even though materials presented significantly different moisture buffering results from the experimental testing, similar results in the moisture regulation were achieved. This demonstrate that comparing the materials for their moisture buffering capacity, rather than by their capacity to regulate the environment, is not the right approach. The simulated four materials were also compared with the laboratory test and the experimental change in weight monitoring of the specimens in the full-scale rooms. Materials analysed in the full-testing (especially gypsum) presented different results from those obtained from the laboratory testing. The laboratory testing showed a regular and steady moisture buffering capacity of gypsum, while simulations and in-situ specimens presented an increase of its total moisture content, due to its higher sensitivity to moisture changes. As the amplitude of daily fluctuations were not affected by the total increase of moisture in the materials, it is necessary to consider the double capacity of the materials to buffer moisture daily but also store moisture for longer term fluctuations. Moreover, moisture transport and material vapour permeability also play a role to buffer moisture. These factors diffuse moisture in the under-layers and reduce the total moisture content in the plasters, differently from the single layer specimen that gained more moisture than in simulations. Multiple processes can happen in the materials and would be of interest to observe the moisture distribution in the walls and how different processes work simultaneously. In terms of daily fluctuations simulations and in-situ specimens change in weight overall showed a good agreement, which indicates simulations can be used as reference for the square wave protocols. However, it cannot be confirmed either simulations and square wave testing give real indications of the materials behaviour directly applied on walls, as they may overestimate the materials moisture buffering capacity, as the full-scale testing suggested (Section 4.4).

6. *Discussion and Conclusions*

6.1 Discussion

The overall aim of the study is to investigate a method to quantify the impact of moisture buffering on the environment. To achieve this objective, it is necessary to understand the moisture buffering mechanism both in laboratory and full-scale testing. In this thesis, the analysis at the laboratory level provided insights on the materials properties role in the moisture buffering process. The influence of testing protocol and boundary conditions on materials were also investigated for a correlation between materials properties, environmental conditions and moisture buffering. The full-scale testing explored the impact of materials on the indoor moisture regulation through field testing and hygrothermal simulations.

6.1.1 Laboratory Testing

This study initially consisted of understanding the experimental process of moisture buffering when specimens of materials are tested in the laboratory. Porosity and porous structure are the properties that mostly influence the moisture buffering capacity. The focus on the porous structure can be the key to develop materials with higher moisture buffering performance.

The suitability of standard protocols that estimate the moisture buffering capacity of materials through the monitoring of the change in weight of samples subjected to constant temperature, low air velocities and square wave RH variations, was investigated. One of the most used protocol is the NORDTEST that exposes materials to daily cycles, where humidity varies from 75% for 8 hours to 33% for 16 hours. This protocol is easy to perform for materials comparison, but it is not clear whether this method can be used for practical applications and building design. For this reason, the test was modified, by varying temperature, air velocity and RH signal, to evaluate the response of materials to different environmental conditions. Environmental conditions strongly impact the materials response. In particular air speed is a factor that can significantly change the dynamic sorption capacity of

materials. Testing facilities and climatic chambers, as well as real buildings, may present a non-homogeneous air velocity distributions and may not have control on the air speed. Consequently, the mass surface resistance of materials may vary and influence the moisture buffering results. The sensitivity of moisture buffering to air velocity was monitored in a climatic chamber. It can be stated that within the same chamber a range of air velocities between 0.4 and 0.9 m/s (higher than 0.1 m/s prescribed by the protocols) were observed. However, air velocities in this range do not significantly influence the moisture buffering results and no correlation between air speed and dynamic sorption capacity was found. This gave confidence on the climatic chamber accuracy and the repeatability of any applied testing procedure.

In moisture buffering test protocols materials are normally subjected to square wave RH signals, but in reality the indoor environment follows more complex functions. Depending on the signal, the moisture buffering response of materials differs. When applied sinusoidal variations, materials presented different results than with square wave signals. The comparison of square and sinusoidal RH variations showed that sinusoidal RH fluctuations reduce the moisture buffering ability of materials. In the square wave testing humidity immediately jumps to 75%RH and stay constant for few hours, while in the sinusoidal test there is a smooth transition between high and low humidity levels that reduces the performance of the materials to balance the moisture content with the environment. As examples, in the sinusoidal variations humidity reaches the maximum RH in 4 hours maintaining the RH for approximately 1 hour at 75%RH before it starts decreasing. The shorter and quicker humidity variations explain the lower moisture buffering ability, due to the incapacity materials to balance moisture. Moreover, when sinusoidal variations were applied, materials also presented a delayed response to RH variations. Materials reached the maximum dynamic sorption capacity with a lag that varies depending on the materials and it is generated by the moisture unbalance between materials and the environment. This behaviour was not highlighted by the NORDTEST and questioned the principle of the immediate response of materials to moisture variations (applied by some simulation models).

Temperature, which is not typically considered in the moisture buffering evaluation, has been shown to impact the moisture buffering performance of materials. When both square wave and sinusoidal RH variations tests are performed at different temperatures, the dynamic sorption capacity of materials varied. Regardless of the shape of the RH signal, the temperature influences the moisture transport mechanisms, depending on the material porous structure. Overall, it can be stated that higher is the temperature the highest is the impact on moisture buffering. To isolate the impact of temperature on the dynamic sorption capacity, the change in mass of specimens was monitored, when RH is constant but temperature varied. In the square wave test, temperature did not significantly impact the materials, as no significant changes in weight were observed. Only during the transaction between low

and high temperature (or high to low) a mass increase (or decrease) was recorded. This temporary increase in mass reduced after the temperature stabilised. This phenomena is due to the sudden temperature change that causes the climatic chamber to generate more or less moist air. Even though temperature does not impact the sorption performance when unvaried, it is of interest to determine the response of walls when turning on and off heating systems, as materials may impact the energy requirements for air conditioning systems during this transition. When sinusoidal temperature variations are applied small mass fluctuations were observed, which indicates that the material drying and cooling did impact the dynamic sorption performance of materials. The response of materials to sinusoidal temperature variations is, however, low compared to when subjected to only RH fluctuations, but temperature significantly delays materials dynamic sorption capacity.

When temperature and RH were simultaneously varied and square waves were applied, the results were similar to the NORDTEST results. The reason can be related to the joint effect of temperature and RH on materials. By comparing the vapour pressure variations in the chamber when only RH is varied, in the simultaneous testing the partial pressure variations are significantly lower. However, due to the combination of low RH and high temperature, pores dry quicker as the high temperature increases the desorption capacity of materials. When sinusoidal variations are applied, some differences with sinusoidal tests at constant temperature were found. When materials have micro-pores, they adsorb more water at variable temperature than at constant temperature. The sinusoidal and simultaneous temperature and RH variations also generated a significant lag due to the effect of temperature. A four hour delay was found rather than the two hours lag in the test at constant temperature. Overall, it can be stated that temperature did impact the materials, but a correlation between temperature and porosity needs to be verified as the two factors might be independently influencing the moisture buffering capacity of materials. This study was the first step to bring real building indoor conditions into a laboratory. The laboratory testing showed the potential to reproduce more realistic environmental conditions that allows for a wider analysis on the correlation between dynamic storage capacity and the environment. The investigation of air velocity, RH and temperature impact on moisture buffering in a controlled environment led to a better understanding of the complexity of the moisture exchange in buildings, by reproducing a range of environmental conditions that can be observed indoors.

6.1.2 Full-scale testing

The second stage of the work involved the design and testing of full-scale cells. The objective was to design a full-scale test protocol to quantify the impact of walls to buffer the indoor moisture. The ambition of the experimental testing is to bring full-

size buildings' moisture buffering into the laboratory to develop a new laboratory scale protocol. Three test rooms at the Building Research Park of the University of Bath were tested to identify the main factors that contribute to the moisture balance indoors and investigate the involvement of walls, to regulate the indoor humidity. The three cells presented different wall structures (timber frame with PIR insulation, timber frame with wooden fibre insulation and PIR insulated AAC concrete cavity wall), but they all had plasterboard in the indoor surface. The PIR timber frame cell (PIR room) was used as the reference room as all indoor surfaces were covered with a water vapour resistant membrane. The test set-up was an affordable and effective solution to investigate moisture buffering and to have a realistic representation of what happens in real buildings, in which there is the potential to use the enclosure for passive regulation.

In each cell an instantaneous moisture injection, moisture decay and moisture buffering tests were performed. The three tests were designed to study the response of the cells to different boundary conditions and sources of moisture, whilst exposed to the outdoor weather. The instantaneous injection test was performed to assess the suitability of the three rooms to perform the moisture buffering test. The comparison of the three cells highlighted significant differences between the reference room and the hygroscopic cells due to the capacity of the exposed walls to store moisture from the indoor and reduce the humidity peaks. The differences between the concrete (cavity wall) and wood fibre room were small, which suggested the walls behaved similarly because the same material (plasterboard) was applied on the indoor surfaces.

The decay test consisted of an humidification phase, where the RH was kept constant for 8 hours at 75%RH, followed by the de-humidification, where the reduction of the humidity was observed for 40 hours. The analysis of the humidification phase highlighted that the amount of moisture necessary to keep the RH constant in the room depends on the weather. Outdoor temperature, absolute humidity and wind speed are likely to be the main factors that influence the amount of moisture necessary to maintain the RH at 75%. However, the lack of data did not allow to establish a strong statistical correlation between the water usage and the outdoor environmental conditions. By comparing the three rooms, the PIR room needed less water to maintain the RH at a constant level (75%RH) because the non-hygroscopicity of the walls did not allow the moisture to be removed. In the other two rooms walls adsorbed the indoor moist air to reduce the humidity level and, consequently, the humidifier needed to produce more vapour to keep the RH high.

During the de-humidification the moisture reduction could be described as a logarithmic decay. The impact of the weather on the rooms moisture removal was statistically investigated to isolate and assess the differences between the rooms. By applying a repeated measurement mixed model to globally analyse all the tests performed in the rooms, it was observed that when the outdoor temperature and air velocity increased, the indoor absolute humidity level increased; when the outdoor absolute humidity

increased, the indoor absolute humidity level decreased. This is due to the moisture transport mechanism through the walls and the influence of the building infiltration. The wind pressure on the buildings and the increase of temperature and RH may change the moisture transport dynamics between the indoor and outdoor by changing either the vapour pressure and total pressure differential. The statistical model allowed to isolate the weather effect on the decay test, and to standardise the de-humidification curves to investigate the differences between the cells. The three cells presented similar absolute humidity reductions, which suggested that the rooms managed to remove a similar amount of moisture. This indicates that the rooms activated different mechanisms to reduce the moisture content indoors. However, the curvature of the decay was significantly different between the three rooms. The concrete and wood fibre rooms presented a smoother decay than the PIR room. The reference room eliminated moist air mainly through the door leakages, which explains the more irregular shape of the moisture decay. Concrete and wood fibre had a smother decay because walls helped to buffer and regulate moisture. Overall, the two humidification and de-humidification phases of the decay test gave indication of the influence of the outdoor environment indoors and confirmed the capacity of hygroscopic walls not only to store moisture, but also to mitigate and smooth the moisture transaction between high and low humidity.

In the moisture buffering test, a similar test set up to the laboratory NORDTEST protocol was arranged. Each room was subjected to six daily humidity cycles (8 hours of humidification at 75%RH and 16 of de-humidification). In addition, a ventilation system was installed to investigate the impact of ventilation on the indoor moisture regulation. The indoor change of humidity and the moisture exchange through the ventilation system were monitored. The test was performed either at constant temperature (23^oC) and at variable temperature (temperature free to vary). Results showed that ventilation had a strong impact on the indoor moisture balance in all cells. Ventilation removed moisture from the indoor during the humidification phase, to reduce significantly the vapour generated by the humidifier. However, during the de-humidification ventilation is neither removing or adding moisture to the hygroscopic rooms, whilst its participation was more significant in the PIR room, as it kept removing moisture from the room. The difference between the reference and the hygroscopic rooms indicates that walls still have an active role in the indoor moisture regulation. The calculation of the moisture balance equation indicated that during the humidification the hygroscopic walls adsorbed moisture from the indoor, reducing the load removed by ventilation, whilst during the decay walls release moisture into the room to compensate for the moisture removed by the ventilation system.

The test at variable temperatures was performed in winter, when the outdoor temperatures were relatively low. Therefore, the overall temperature in the indoor was significantly lower than in the test at constant temperature due to the strong impact of the outdoor indoors. The indoor humidity was strongly influenced by the

outdoor humidity level, by showing significant increase of humidity in correspondence of outdoor humidity peaks. Due to the high humidity level in the cells, the rooms presented a significant lower water usage for the humidification than at constant temperature. The combination of lower temperatures, high humidity levels and small water usages during the humidification demonstrated that the impact of the walls to moderate humidity is negligible. The small partial pressure differential between the indoor and outdoor, and the combination of high humidity levels and low temperature did not allow for the moisture to be released into the indoor environment and for the materials to dry. It can be stated that higher temperatures dry the indoor air allowing the materials to dry and releasing moisture, so that when humidity increases materials are able to store more moisture.

During the moisture buffering test in the cells, a plasterboard specimen was placed on a mass balance to combine elements of the NORDTEST (square wave RH variations, constant temperature and low air velocities) in realistic environmental conditions (ventilation, size of the room and walls interaction). In this way it was possible to investigate the impact of plasters to moderate the humidity in a full-size room, where the NORDTEST test conditions were not strictly followed, as it would normally happen in a real building. While the results between the laboratory testing and the in-situ experimental testing were in agreement, there was a significant difference between the moisture buffering performances of the walls, calculated through the moisture balance equation, and the experimental performances of the coatings. The walls presented over 70% smaller values than the single plasterboard on the mass balance. The discrepancy may depend on the difference in air velocities above the specimen (less than 0.1 m/s) and on the walls position. Due to the fan and ventilation system the air velocity on the surface may be significantly higher on the walls than on the specimens. The position of the specimen can also play a role, as the specimen is placed horizontally, which means it can adsorb more water due to gravitation, while on walls plasters are placed vertically. Also the presence of under-layers below plasterboard can reduce the moisture stored by the plasterboard itself.

The full-scale testing did not provide conclusive results to be used as calibration of the laboratory scale protocol development. It has, however, highlighted the importance of moisture buffering in the moisture regulation. The capacity of the walls to release and store moisture maintains the RH into healthier and comfortable ranges, significantly reducing the risk of condensation and over-drying. The testing results are also strictly related to the location of the testing facility. Nevertheless, the moisture buffering impact may not be significant in location, where there are no daily and yearly moisture variations, and where natural ventilation is preferred. This is the case of tropical zones with perpetual hot and humid environments.

6.1.3 Hygrothermal simulations of buildings

The three rooms were modelled using WUFI® Plus to further investigate the impact of walls on the indoor moisture regulation, by analysing the relationship between ventilation and moisture buffering. This allowed for the study of the participation of the wall assembly and its elements to moderate the humidity. The hygrothermal simulations were run by reproducing the experimental cells and replicating the test set-up to have results in line with the in-situ tests.

Overall, the comparison between simulation and experimental testing showed an agreement in the moisture exchange through ventilation and infiltration, while significant differences were found in the moisture load produced by the humidifier in simulations to reach the same RH fluctuation than in the experimental cells. In simulations the amount of moisture necessary to reach 75%RH was double the amount used in the experimental test to reach the same humidity level. This can be due to issues with the experimental water usage monitoring or due to the overestimation of the vapour adsorbed by the walls in WUFI®. The use of steady-state hygric properties might significantly magnify the impact of the walls on the moisture regulation by adsorbing more than 70% more moisture than the value calculated in the moisture balance equation in the experimental testing. Even though the moisture buffering capacity is overestimated, the moisture content variation of the walls components gave a good indication of the moisture buffering dynamics, when the indoor is subjected to daily variations, due to the overall good agreement between simulations and experimental data. The analysis showed that the material applied on the indoor surface is mainly responsible of the regulation of the total moisture adsorbed by the whole assembly. Only when the surface coating reaches its maximum storage capacity, the material transfers moisture in the under-layers. This behaviour was confirmed by the daily moisture fluctuations that the under-layers presented.

During the humidification phase both ventilation and walls participated to the reduction of the moisture in the cells. Ventilation had a significantly higher impact due to the high amount of moisture produced by the humidifier that could not be adsorbed by the walls. A sensitivity analysis was performed to investigate variations on the sortpion capacity of walls, when the ventilation rate and moisture load were varied. The analysis highlighted that the two factors did not impact the walls participation to buffer moisture, as the enclosure capacity to adsorb moisture depends mainly by the environmental conditions (temperature, RH and RH signal) and the walls properties. Even though ventilation rate and moisture load increased or decreased, the amount of moisture adsorbed by the walls did not vary significantly, when the environmental conditions are preserved.

Overall, this chapter investigated aspects that the full-scale testing did not explore. However, due to several uncertainty around the accuracy of the model, the results were

not used to pursue the aim to develop a new laboratory protocol. However, simulations highlighted the strong correlation between ventilation and moisture buffering. This can potentially reduce the need of ventilation in buildings where mechanical ventilation is used, or in location where natural ventilation is not preferred due to the environmental conditions.

6.1.4 Summary

This thesis provides guidelines to perform the three investigation methods and to help designers and researchers to give an overall judgement of the materials participation to passively regulate the indoor environment. For the laboratory testing the introduction of a new approach for the evaluation of moisture buffering was established for further materials development and further understanding of possible improvements of the material moisture buffering potential. An affordable and easily reproducible in-situ testing set-up was proposed, and an accurate evaluation of the impact of enclosures on the indoor moisture balance was presented. A method to establish the impact of different environmental and boundary conditions through simulations was also introduced, together with the procedure to assess the participation of the assembly stratigraphy to moderate the indoor humidity.

Overall, this thesis presents three different approaches to investigate the moisture buffering capacity of materials. The laboratory testing focuses on the understanding of the materials response to the environment by analysing the moisture transport and storage mechanisms into the materials. The full-scale testing gives information on the interaction between walls and the indoor environment, focusing on the capacity of the whole building system to moderate humidity. The main target of this testing is to investigate the real impact of enclosure on the environment by exposing the building to other factors responsible to moderate the indoor RH. Simulations unite the laboratory and full-scale testing by giving an insight on the possible improvements of the enclosure cross section to increase the building capacity to regulate humidity at the building design level. Even though each of this category needs further development, each investigation method gives different information at different stages of the building design on the the moisture buffering capacity of a single material from its production until its application on a building. The three levels are complementary investigation that should all be performed to have a full picture of the moisture buffering capacity of materials to moderate the RH, even though each method has different benefits and limitations. The full understanding of the role of moisture buffering on the RH at different levels and stages will lead to the development of a global method or methodology to assess materials' potential to regulate the RH.

6.2 Conclusions

The combination of laboratories and full scale testing highlighted limitations of laboratory testing to estimate the moisture buffering potential to moderate the indoor RH, because existing protocols are simplified methods and do not provide any information on the capacity of materials to control the relative humidity level. For these reasons, this work analysed the impact of moisture buffering in real buildings, to, successively, improve the laboratory protocols, in order to evaluate materials not solely from their dynamic storage capacity, but also from their capacity to regulate the environment. This thesis provided the basis to develop in future research test protocols that can achieve this objective, so that designers can obtain the desired indoor RH, by choosing the most suitable hygriscopic materials.

The specific objectives and main conclusions were to:

- *Analyse the moisture buffering response of materials in a controlled laboratory to the variations of parameters that are usually variable in buildings, such as air velocity, temperature and humidity functions.* The testing results demonstrated that realistic environmental conditions can be simulated in laboratory testing, which give confidence in pursuing the aim of this research. Overall, it can be stated temperature and RH signal are essential factors that need to be included in the moisture buffering analysis, while pore structure can be the key property that determines the moisture buffering potential of materials.

- *Devise and conduct experimental testing to define a method to quantify moisture buffering in real-scale buildings. An affordable and easily reproducible testing set-up was designed, showing a good potential for the definition of a global full-scale testing methodology for moisture buffering.* Results indicated moisture buffering has a significant impact in the indoor moisture regulation, but it is also strongly influenced by the weather and location, indoor temperature regulation and building components.

- *Analyse the sensitivity of the moisture buffering capacity of walls to boundary conditions and environmental factors by using a hygrothermal simulation model.* Depending on the amount of moisture exchanged though ventilation, the enclosure stores and releases more or less moisture. This gives confidence in the possibility to reduce the use of energy-consuming ventilation/air-conditioning systems, as well as reduce natural ventilation strategies, when necessary.

- *Analyse through simulations the behaviour of different coatings and the involvement of sub-layers in the walls to moderate the indoor humidity.* The internal coating is the material that is mostly involved in moisture buffering, but the design of a vapour permeable enclosure can increase the capacity to

buffer humidity, by distributing the indoor moisture on different wall's layer. It is, however, necessary to understand the role of materials to reduce the indoor humidity, rather than investigate how much moisture walls can store.

- *Investigate and compare full-scale and existing laboratory scale testing.* The use of full-scale testing as input for the laboratory testing could not be pursued due to various uncertainty in each stage of this study. Analysis of discrepancy between the three levels highlighted the importance to further understand the moisture exchange between the enclosure and the environment in real buildings.

6.3 Future Work

Further research is recommended to develop a laboratory testing from the full-scale investigation. It is also recommended to further investigate some aspects of the moisture buffering mechanism to better understand the moisture exchange between the environment and the enclosure.

6.3.1 Laboratory testing

Moisture buffering is a tangible property, which influences the hygric balance of indoor environments and improves hygrothermal comfort. Laboratory testing is essential to improve the materials potential to regulate the indoor humidity. Therefore, further investigations are necessary, as listed below:

- The role of pores and pore structure is vital to improve the moisture buffering capacity of materials should be analysed. A better understanding of the range of pores that mainly influence the material dynamic sorption capacity, and an investigation of the transport mechanisms that activate in the pores can bring to a significant improvement of the development of materials. Either the use of NMR spectroscopy to observe the moisture distribution together with the comparison of materials with different pore structures would improve the knowledge on the moisture buffering potential.
- Investigate the effect of temperature on a wider range of materials to better identify the role of temperature on the dynamic sorption capacity. A broad range will help find patterns in the moisture transfer mechanisms due to temperature variations. The temperature impact on materials should be explored to examine variations on the dynamic moisture storage and transport mechanism at different and variable temperatures. Moreover, a possible correlation between pore structure and temperature should be investigated, to understand the possible implication of the variations of temperature on different

materials.

- Further analyse the impact of air velocities on the moisture buffering performance of materials. Even though it was demonstrated moisture buffering is not sensitive to small air speed variations, when materials with good dynamic sorption capacity are tested, it is important to have full control of air movements during testing. This is necessary for more accurate testing and because there may be materials more sensitive to air speed variations. As it is not always possible to control the air velocity, this study highlights the necessity to further analyses on this field, to facilitate laboratories, which do not have the equipment to perform a moisture buffering test in a homogeneous environment.

- As the step response method is not representative of real indoor RH variation, it is necessary to apply other RH profiles other than the sinusoidal signal (e.g triangular fluctuations) and different time intervals for high and low humidity (e.g. 12/12h cycles). The investigation of different environmental signals is important to better understand the influence of temperature and humidity on the moisture uptake of construction materials.

- Improve or develop a new protocol to quantify moisture buffering in laboratory scale testing, by looking into a method to make comparable in-situ experimentation results and material testing analysis. This will lead to perfect or introduce a new protocol for moisture buffering measurement, which gives a realistic quantification of the dynamic sorption capacity of finishing materials.

6.3.2 Full-Scale Testing

It is necessary to further improve the full scale testing and develop a standard procedure to evaluate moisture buffering performance of a building, to allow systematic and replicable verification methods. This would include:

- The moisture content of the walls should be measured to monitor the moisture content variation into the wall assembly. Sensors could be placed across the wall section to verify the moisture variations between each layer to determine the daily moisture fluctuation and moisture propagation in the walls. Sensors should be applied during the construction of walls, which was not possible in this study as the test cells were built for a previous project.

- To better understand the moisture buffering mechanisms of a wall, tests should be performed by applying initially an impermeable membrane behind the indoor surface coating and than compare the rooms behaviour when the membrane is removed to have a better understanding of the participation of under-layers and moisture transport mechanism on the dynamic sorption capacity of walls.

- The effect of the weather on the indoor moisture regulation should be further explored, because regardless of the air tightness of buildings, there is still a strong correlation between the indoor and outdoor environmental conditions. The environmental factors that mostly influence the most the indoor environment should be identified.
- Analyse the impact of moisture buffering on energy usage of the rooms, by analysing the data of the energy meter through which the fan and heaters were monitored. The energy meters were initially used to control when fan and heaters were turned on and off by the thermostat. As the pulse was monitored throughout all the testing campaign, the data will be in future elaborated to investigate differences between the reference room and the other two cells
- Analyse the impact of moisture fluctuation on the thermal transmittance of the walls. Similarly to the energy monitoring, the heat flux was constantly monitored to have a true measure of the thermal transmittance of the three cells to better understand the rooms differences. However, the data can be used to investigate the impact of moisture on the heat flux.
- Perform a full-scale testing in a controlled environment. A test cell can be build inside an environmental chamber to control the environmental conditions. In this way, a better understating of the impact of the outdoor weather is possible. The risk is, however, to exclude or wrongly estimate the impact of some environmental factors that in reality may or my not influence the indoor.
- In the simulation different coatings produced similar RH fluctuations regardless of their moisture buffering performance. This behaviour should be verified experimentally by testing the impact of different coatings on the indoor environment.

6.3.3 Simulations

Simulations proved to have a good agreement with laboratory results. However, discrepancy with the in-situ experimental testing should be investigated:

- In the simulation model the overestimation of the moisture buffering capacity of the walls should be verified. This can be due to the use of steady-state hygric properties, to the mathematical simplification of physical phenomenon, such as capillary transport, or to the lack of some factor.
- Simulations consider the sortpion capacity of the walls as a fixed values that does not change when ventilation and moisture load are varied. This may be not true in real buildings as ventilation may have a double impact on the walls: as contribution to indoors moisture balance and as air movement on the wall

surface. The combination of these two factors may increase or decrease the wall capacity to buffer moisture.

- Another consideration is related to moisture transport mechanism in walls. Moisture moves through the enclosure, due to water vapour pressure or RH differential between the indoor and the outdoor. It is not yet clear if moisture buffering is an independent property or it is part of the general moisture transport mechanism in a wall. A better understanding on this would enhance a more accurate design of the whole enclosure that could amplified moisture buffering effect indoors.
- Better understating of the role of air gaps in walls. It is necessary to investigate the capacity of the air gap to transfer moisture, or to create a barrier to the surface material.

6.3.4 General recommendations

Moisture buffering should be explored for a wider implementation of this property in the building design by involving industry and professionals. Moisture buffering can have beneficial impact in other aspects of the building design and management:

- Combine the design of HVAC units with moisture buffering to reduce the usage of a mechanical system to moderate humidity. By considering the participation of moisture buffering, HVAC systems can be downsized, reducing its energy usage.
- Explore the impact of moisture buffering on energy savings and on temperature regulation. Moisture buffering can have a direct impact on the temperature regulation by releasing sensible heat during the moisture exchange between the environment and the walls, increasing the overall temperature in the room. At the same time, the passive RH moderation increases the hygrothermal comfort of the users, which indirectly reduces the necessity for the users to adjust the indoor temperature.
- Investigate the impact of moisture buffering on the reduction of indoor pollutants and its impact on the improvement of health conditions in buildings.
- Improve the design of enclosures to reduce thermal losses and increase air tightness, but still guarantee the vapour and moisture permeability of walls, together with the reduction of the condensation risks.
- Promote the use of bio materials, which demonstrated an excellent suitability to buffer moisture.
- Better understand the impact of paints and wall paper on moisture buffering, and promote the development of finishing materials that allow or increase the

moisture exchange between hygroscopic materials and the environment.

6.4 Concluding Comments

The impact of this research is to move a step forward into the understanding of moisture buffering on buildings, by resolving some of the uncertainty in the use of hygroscopic materials. The aim is to help professionals to design healthy and durable buildings, by providing an insights on the moisture buffering role in the moisture moderation, and by suggesting new testing methods to asses moisture buffering. Analysing moisture buffering from a material scale up to its impact on a building system can lead to a more realistic understanding of hygroscopic materials' capacity to passively regulate humidity.

This will stimulate development and improvement of new moisture control materials and promote their use. The use of hygroscopic materials will improve the indoor hygrothermal comfort, and reduce health risk indoors by maintaining the indoor humidity in the optimal humidity range. It will reduce the risk of condensation and increase the durability of materials by reducing the humidity peaks. At the same time, it can potentially reduce buildings' energy use for air conditioning and heating systems. Moisture buffering is a key point into the development of sustainable and healthy buildings.

Bibliography

Abadie, M.O. and Mendonça, K.C., 2009. Moisture performance of building materials: From material characterization to building simulation using the moisture buffer value concept. *Building and Environment*, 44(2), pp.388–401. Available from: `https://doi.org/10.1016/j.buildenv.2008.03.015`.

Allinson, D. and Hall, M., 2010. Hygrothermal analysis of a stabilised rammed earth test building in the uk. *Energy and Buildings*, 42(6), pp.845–852. Available from: `https://doi.org/10.1016/j.enbuild.2009.12.005`.

Allinson, D. and Hall, M., 2012. Humidity buffering using stabilised rammed earth materials. *Proceedings of the ICE: Construction materials*, 165 (CM6), pp.335 – 344. Available from: `https://doi.org/10.1680/coma.11.00023`.

Alvarez, J.C., 1998. *Evaluation of moisture diffusion theories in porous materials*. Ph.D. thesis. Virginia Tech.

Antretter, F., Fink, M., Pazold, M., Radon, J. and Winkler, M., 2015. Wufi® pro–manual. *Fraunhofer Institute (2015)*.

Arfvidsson, J., 1999. A new algorithm to calculate the isothermal moisture penetration for periodically varying relative humidity at the boundary. *Nordic Journal of Building Physics*, 2.

Arundel, A.V., Sterling, E.M., Biggin, J.H. and Sterling, T.D., 1986. Indirect health effects of relative humidity in indoor environments. *Environmental Health Perspectives*, 65, p.351. Available from: `https://doi.org/10.1289/ehp.8665351`.

ASHRAE-55, 2017. Standard 55–2017 thermal environmental conditions for human occupancy. *Ashrae: Atlanta, GA, USA*.

Barclay, M., Holcroft, N. and Shea, A.D., 2014. Methods to determine whole building hygrothermal performance of hemp–lime buildings. *Building and environment*, 80, pp.204–212. Available from: `https://doi.org/10.1016/j.buildenv.2014.06.003`.

Bennai, F., Abahri, K., Belarbi, R. and Tahakourt, A., 2016. Periodic homogenization

for heat, air, and moisture transfer of porous building materials. *Numerical Heat Transfer, Part B: Fundamentals*, 70(5), pp.420–440. Available from: https://doi.org/10.1080/10407790.2016.1230393.

Besant, R.W. and Simonson, C.J., 2000. Air-to-air energy recovery. *ASHRAE journal*, 42(5), p.31.

Bn en iso 6946, 2007. British Standards Institution, (Building components and building elements-thermal resistance and thermal transmittance-calculation method).

Bs en iso 12569, 2017. International Organization for Standards, (Thermal performance of buildings and materials. determination of specific airflow rate in buildings. tracer gas dilution method).

Bs en iso 13788, 2002. British Standard, (Hygrothermal performance of building components and building elements-internal surface temperature to avoid critical surface humidity and interstitial condensation-calculation methods).

Bs en iso 9972, 2015. International Organization for Standards, (Thermal performance of buildings. determination of air permeability of buildings. fan pressurization method).

Budaiwi, I. and Abdou, A., 2013. The impact of thermal conductivity change of moist fibrous insulation on energy performance of buildings under hot–humid conditions. *Energy and Buildings*, 60, pp.388–399. Available from: https://doi.org/10.1016/j.enbuild.2013.01.035.

Bylund Melin, C., Gebäck, T., Heintz, A. and Bjurman, J., 2016. Monitoring dynamic moisture gradients in wood using inserted relative humidity and temperature sensors. *E-Preserv. Sci*, 13, pp.7–14.

Cascione, V., Hagentoft, C.E., Maskell, D., Shea, A. and Walker, P., 2020a. Moisture buffering in surface materials due to simultaneous varying relative humidity and temperatures: Experimental validation of new analytical formulas. *Applied Sciences*, 10(21), p.7665.

Cascione, V., Marra, E., Zirkelbach, D., Liuzzi, S. and Stefanizzi, P., 2017. Hygrothermal analysis of technical solutions for insulating the opaque building envelope. *Energy Procedia*, 126, pp.203–210. Available from: https://doi.org/10.1016/j.egypro.2017.08.141.

Cascione, V., Maskell, D., Shea, A., Walker, P. and Mani, M., 2020b. Comparison of moisture buffering properties of plasters in full scale simulations and laboratory testing. *Construction and Building Materials*, 252, p.119033. Available from: https://doi.org/10.1016/j.conbuildmat.2020.119033.

Climate Change, I.P. on, 2015. *Climate change 2014: mitigation of climate change*, vol. 3. Cambridge University Press.

Crump, D., Dengel, A. and Swainson, M., 2009. Indoor air quality in highly energy efficient homes–a review. *United Kingdom: NHBC Foundation*.

Cunningham, M.J., 1992. Effective penetration depth and effective resistance in moisture transfer. *Building and Environment*, 27(3), pp.379–386. Available from: https://doi.org/10.1016/0360-1323(92)90037-p.

Delgado, J., Ramos, N.M., Barreira, E. and De Freitas, V.P., 2010. A critical review of hygrothermal models used in porous building materials. *Journal of Porous Media*, 13(3). Available from: https://doi.org/10.1615/JPorMedia.v13.i3.30.

Di Giuseppe, E. and D'Orazio, M., 2014. Moisture buffering "active" devices for indoor humidity control: preliminary experimental evaluations. *Energy Procedia*, 62, p.42 – 51. Available from: https://doi.org/10.1016/j.egypro.2014.12.365.

Din 18947, 2013. Deutsches Institut fur Normung E.V., (Earth plasters-terms and definitions, requirements, test methods (in german).).

Dongdong, Z. and Kefei, L., 2016. Prediction of permeability from water vapor sorption isotherm of cement-based materials. *RILEM Conference on Materials, Systems and Structures in Civil Engineering (MSSCE2016), Lyngby, Denmark*.

Dubois, S., McGregor, F., Evrard, A., Heath, A. and Lebeau, F., 2014. An inverse modelling approach to estimate the hygric parameters of clay-based masonry during a moisture buffer value test. *Building and Environment*, 81, pp.192–203.

Eurostat and Commission européenne, U. européenne., 2016. *Energy, transport and environment indicators*. Office for Official Publications of the European Communities.

Fanger, P.O. et al., 1970. Thermal comfort. analysis and applications in environmental engineering. *Thermal comfort. Analysis and applications in environmental engineering.*

Feng, C. and Janssen, H., 2016. Hygric properties of porous building materials (ii): Analysis of temperature influence. *Building and Environment*, 99, pp.107–118. Available from: https://doi.org/10.1016/j.buildenv.2016.01.016.

Field, A., 2013. *Discovering statistics using ibm spss statistics*. sage.

Galbraith, G., Guo, J., McLean, R., Lee, C. and Kelly, D., 2000. The temperature dependence of moisture permeability. *CIB REPORT*, pp.105–110.

Gholami, M., Barbaresi, A., Tassinari, P., Bovo, M. and Torreggiani, D., 2020. A comparison of energy and thermal performance of rooftop greenhouses and green

roofs in mediterranean climate: A hygrothermal assessment in wufi. *Energies*, 13(8), p.2030.

Gómez, I., Guths, S., Souza, R., Millan, J.A., Martína, K. and Sala, J.M., 2011. Moisture buffering performance of a new pozolanic ceramic material: influence of the film layer resistance. *Energy and Buildings*, 43(4), pp.873–878. Available from: https://doi.org/10.1016/j.enbuild.2010.12.007.

Hagentoft, C.E., 2002. Hamstad–final report: Methodology of ham-modeling. *Report R-02*, 8, pp.19–23.

Hameury, S., 2005. The buffering effect of heavy timber constructions on the indoor moisture dynamic. *Nordic symposium on building physics, reykjavik*. pp.1–8.

Hameury, S. and Sterley, M., 2006. Magnetic resonance imaging of moisture distribution in pinus sylvestris l. exposed to daily indoor relative humidity fluctuations. *Wood Material Science and Engineering*, 1(3-4), pp.116–126. Available from: https://doi.org/10.1080/17480270601150578.

HEMPSEC, 2014. Market development of a bio based pre fabricated construction system which significantly reduces both embodied carbon and in use energy consumption. https://ec.europa.eu/environment/eco-innovation/projects/en/projects/hempsec. [2019.11.04].

Holcroft, N., 2016a. Natural fibre insulation materials for retrofit applications. *University of Bath*.

Holcroft, N., 2016b. *Natural fibre insulation materials for retrot applications*. Ph.D. thesis. University of Bath.

Holm, A., Kuenzel, H.M. and Sedlbauer, K., 2003. The hygrothermal behaviour of rooms: combining thermal building simulation and hygrothermal envelope calculation. *Eighth international ibpsa conference*. Eindhoven Netherlands, vol. 1, pp.499–505.

Isetti, C., Laurenti, L. and Ponticiello, A., 1988. Predicting vapour content of the indoor air and latent loads for air-conditioned environments: effect of moisture storage capacity of the walls. *Energy and Buildings*, 12(2), pp.141–148. Available from: https://doi.org/10.1016/0378-7788(88)90076-x.

Iso 12572, 2016. British Standards Institution, (Hygrothermal performance of building materials and products: Determination of water vapour transmission properties).

Iso-24353, 2008. Internationl Standard, (Hygrothermal performance of building materials and products — determination of moisture adsorption/desorption properties in response to humidity variation).

Janssen, H. and Roels, S., 2007. The hygric inertia of building zones: characterisation and application. *IEA Annex*, 41.

Janssen, H. and Roels, S., 2009. Qualitative and quantitative assessment of interior moisture buffering by enclosures. *Energy and Buildings*, 41(4), pp.382–394. Available from: https://doi.org/10.1016/j.enbuild.2008.11.007.

Jis a 1470-1, 2002. Japanese Standards Association, (Test method of adsorption/desorption efficiency for building materials to regulate an indoor humidity part 1: Response method of humidity).

Kaczorek, D., 2019. Moisture buffering of multilayer internal wall assemblies at the micro scale: Experimental study and numerical modelling. *Applied Sciences*, 9(16), p.3438. Available from: https://doi.org/10.3390/app9163438.

Kalamees, T., Korpi, M., Vinha, J. and Kurnitski, J., 2009a. The effects of ventilation systems and building fabric on the stability of indoor temperature and humidity in finnish detached houses. *Building and Environment*, 44(8), pp.1643–1650. Available from: https://doi.org/10.1016/j.buildenv.2008.10.010.

Kalamees, T., Korpi, M., Vinha, J. and Kurnitski, J., 2009b. The effects of ventilation systems and building fabric on the stability of indoor temperature and humidity in finnish detached houses. *Building and Environment*, 44(8), pp.1643–1650. Available from: https://doi.org/10.1016/j.buildenv.2008.10.010.

Keefe, D., 2010. Blower door testing. *Journal of Light Construction*, pp.1–7.

Kordziel, S., 2018. *Study of moisture conditions in a multi-story mass timber building through the use of sensors and wufi hygrothermal modeling.* Ph.D. thesis. Colorado School of Mines. Arthur Lakes Library.

Kraniotis, D., Aurlien, T., Brückner, C. and Nore, K., 2015. Impact of air infiltration rates on moisture buffering effect of wooden surfaces. *Proceedings: 36th air infiltration ventilation conference–5th tightvent–3rd venticool, madrid, spain.* pp.23–24.

Kraniotis, D., Langouet, N., Orskaug, T., Nore, K. and Glasø, G., 2016. Moisture buffering and latent heat sorption phenomena of a wood-based insulating sandwich panel. *Proceedings: World conference on timber engineering.* pp.22–26.

Kreiger, B.K. and Srubar III, W.V., 2019. Moisture buffering in buildings: A review of experimental and numerical methods. *Energy and Buildings*, p.109394. Available from: https://doi.org/10.1016/j.enbuild.2019.109394.

Kruk, M. and Jaroniec, M., 2001. Gas adsorption characterization of ordered organic-inorganic nanocomposite materials. *Chemistry of materials*, 13(10), pp.3169–3183. Available from: https://doi.org/10.1021/cm0101069.

Künzel, H., 1960. The "climate-regulating effect" of interior plasters". *Health Engineering*, 81(7), pp.196–201.

Künzel, H., 1965. Die feuchtigkeitsabsorption von innenoberflä chen und inneneinrichtungen. *Rep Build Res*, 42, pp.102–116.

Künzel, H., Holm, A., Sedlbauer, K., Antretter, F. and Ellinger, M., 2004. Moisture buffering effects of interior linings made from wood or wood based products. *IBP-Report HTB-04*.

Künzel, H.M., 1995. *Simultaneous heat and moisture transport in building components*.

Künzel, H.M., Zirkelbach, D. and Sedlbauer, K., 2003. Predicting indoor temperature and humidity conditions including hygrothermal interactions with the building envelope. *Proceedings of 1st international conference on sustainable energy and green architecture*.

Lagouin, M., Magniont, C., Sénéchal, P., Moonen, P., Aubert, J.E. and Laborel-Préneron, A., 2019. Influence of types of binder and plant aggregates on hygrothermal and mechanical properties of vegetal concretes. *Construction and Building Materials*, 222, pp.852–871. Available from: `https://doi.org/10.1016/j.conbuildmat.2019.06.004`.

Latif, E., Lawrence, M., Shea, A. and Walker, P., 2015. Moisture buffer potential of experimental wall assemblies incorporating formulated hemp-lime. *Building and Environment*, 93, pp.199–209. Available from: `https://doi.org/10.1016/j.buildenv.2015.07.011`.

Latif, E., Lawrence, M., Shea, A. and Walker, P., 2016. In situ assessment of the fabric and energy performance of five conventional and non-conventional wall systems using comparative coheating tests. *Building and Environment*, 109, pp.68–81. Available from: `https://doi.org/10.1016/j.buildenv.2016.09.017`.

Li, Y., Fazio, P. and Rao, J., 2012. An investigation of moisture buffering performance of wood paneling at room level and its buffering effect on a test room. *Building and Environment*, 47, pp.205–216. Available from: `https://doi.org/10.1016/j.buildenv.2011.07.021`.

Libralato, M., Saro, O., De Angelis, A. and Spinazzè, S., 2019. Comparison between glaser method and heat, air and moisture transient model for moisture migration in building envelopes. *Applied mechanics and materials*. Trans Tech Publ, vol. 887, pp.385–392.

Lombardi, S., 2005. *Umidità nelle murature: diagnosi e recupero*. Ph.D. thesis. Doctoral Thesis, Università degli Studi di Napoli.

Mahdavi, A. and Kumar, S., 1996. Implications of indoor climate control for comfort,

energy and environment. *Energy and Buildings*, 24(3), pp.167–177. Available from: https://doi.org/10.1016/S0378-7788(96)00975-9.

Maskell, D., Thomson, A., Walker, P. and Lemke, M., 2016. Direct measurement of effective moisture buffering penetration depths in clay plasters. *LEHM 2016*.

Maskell, D., Thomson, A., Walker, P. and Lemke, M., 2018. Determination of optimal plaster thickness for moisture buffering of indoor air. *Building and Environment*, 130, pp.143–150. Available from: https://doi.org/10.1016/j.buildenv.2017.11.045.

McGregor, F., Heath, A., Fodde, E. and Shea, A., 2014a. Conditions affecting the moisture buffering measurement performed on compressed earth blocks. *Building and Environment*, 75, pp.11–18. Available from: https://doi.org/10.1016/j.buildenv.2014.01.009.

McGregor, F., Heath, A., Maskell, D., Fabbri, A. and Morel, J.C., 2016. A review on the buffering capacity of earth building materials. *Proceedings of the Institution of Civil Engineers - Construction Materials*, 169(5), pp.241–251. Available from: https://doi.org/10.1680/jcoma.15.00035.

McGregor, F., Heath, A., Shea, A. and Lawrence, M., 2014b. The moisture buffering capacity of unfired clay masonry. *Building and Environment*, 82, pp.599–607.

Meissner, J.W., Mendes, N., Mendonça, K.C. and Moura, L.M., 2007. An experimental set-up for evaluating moisture buffering effects of porous material. *Proceedings of COBEM 2007*.

Meissner, J.W., Mendes, N., Mendonça, K.C. and Moura, L.M., 2010. A full-scale experimental set-up for evaluating the moisture buffer effects of porous material. *International Communications in Heat and Mass Transfer*, 37(9), pp.1197–1202. Available from: https://doi.org/10.1016/j.icheatmasstransfer.2010.07.022.

Mitamura, T., Hasegawa, K., Yoshino, H., Mastumoto, S. and Takshashi, N., 2004. Experiment for moisture buffering and effects of ventilation rate, volume rate of the hygrothermal materials. *5th international conference of indoor air quality, ventilation and energy conservation, toronto*.

Morlot, J.C. et al., 1999. *National climate policies and the kyoto protocol*. Organization for Economic.

Murat, M. and Attari, A., 1991. Modification of some physical properties of gypsum plaster by addition of clay minerals. *Cement and concrete research*, 21(2-3), pp.378–387.

Nghana, B. and Tariku, F., 2018. Field investigation of moisture buffering potential of american clay and magnesium oxide board in a mild climate. *Journal of Architectural*

Engineering, 24(4), p.04018023. Available from: https://doi.org/10.1061/(ASCE)AE.1943-5568.0000325.

Nguyen, J.L., Schwartz, J. and Dockery, D.W., 2014. The relationship between indoor and outdoor temperature, apparent temperature, relative humidity, and absolute humidity. *Indoor air*, 24(1), pp.103–112. Available from: https://doi.org/10.1111/ina.12052.

Nicolai, A., 2017. New features and optimizations in the hygrothermal transport model delphin 6. Software Presentation.

Nore, K., Nyrud, A.Q., Kraniotis, D., Skulberg, K.R., Englund, F. and Aurlien, T., 2017. Moisture buffering, energy potential, and volatile organic compound emissions of wood exposed to indoor environments. *Science and Technology for the Built Environment*, 23(3), pp.512–521. Available from: https://doi.org/10.1080/23744731.2017.1288503.

Ojanen, T., Kohonen, R. and Kumaran, M.K., 1994. Modeling heat, air, and moisture transport through building materials and components. *Moisture control in buildings*, pp.18–34.

Osanyintola, O.F. and Simonson, C.J., 2006. Moisture buffering capacity of hygroscopic building materials: experimental facilities and energy impact. *Energy and Buildings*, 38(10), pp.1270–1282. Available from: https://doi.org/10.1016/j.enbuild.2006.03.026.

Padfield, T., 1998. *The role of absorbent building materials in moderating changes of relative humidity*. Ph.D. thesis. The Technical University of Denmark.

Padfield, T. and Jensen, L.A., 2010. Humidity buffering by absorbent materials. *Conserv. Phys*, 1, pp.475–482.

Parliament, E., 2010. Directive 2010/31/eu of the european parliament and of the council of 19 may 2010 on the energy performance of buildings (recast). *Official Journal of the European Union*, 18(06), p.2010.

Patel, T., Mitsingas, C., Miller, J.P. and Newell, T.A., 2011. Comparison of blower door and tracer gas testing methods for determination of air infiltration rates through building envelopes at normal operating conditions. *Asme 2011 5th international conference on energy sustainability*. American Society of Mechanical Engineers Digital Collection, pp.1013–1019.

Perry, A.H. et al., 2014. Regional weather and climates of the british isles-part 8: South west england and the channel islands. *Weather*, 69(8), pp.208–212.

Peuhkuri, R., Rode, C. and Hansen, K.K., 2008. Non-isothermal moisture transport

through insulation materials. *Building and Environment*, 43(5), pp.811–822. Available from: https://doi.org/10.1016/j.buildenv.2007.01.021.

Peuhkuri, R.H. and Rode, C., 2005. Moisture buffer value: analytical determination and use of dynamic measurements. *IEA, ECBCS Annex*, 41.

Rahim, M., Douzane, O., Le, A.T., Promis, G. and Langlet, T., 2016. Characterization and comparison of hygric properties of rape straw concrete and hemp concrete. *Construction and Building Materials*, 102, pp.679–687. Available from: https://doi.org/10.1016/j.conbuildmat.2015.11.021.

Ramos, N. and Freitas, V.P. de, 2004. Hygroscopic inertia as a function of transient behavior of covering materials. *Proceedings of performance of exterior envelopes of whole buildings ix international conference*.

Ramos, N.M.M., Delgado, J.M.P.Q. and Freitas, V.P. de, 2010. Influence of finishing coatings on hygroscopic moisture buffering in building elements. *Construction and Building Materials*, 24(12), pp.2590–2597. Available from: https://doi.org/10.1016/j.conbuildmat.2010.05.017.

Reuge, N., Collet, F., Pretot, S., Moisette, S., Bart, M., Style, O., Shea, A. and Lanos, C., 2020. Hygrothermal effects and moisture kinetics in a bio-based multi-layered wall: Experimental and numerical studies. *Construction and Building Materials*, 240, p.117928. Available from: https://doi.org/10.1016/j.conbuildmat.2019.117928.

Rode, C., Mitamura, T., Schultz, J.M. and Padfield, T., 2002. Test cell measurements of moisture buffer effects. *Building Physics in the Nordic Countries*, 2, pp.619–626.

Rode, C., Peuhkuri, R., Time, B., Svennberg, K. and Ojanen, T., 2007. Moisture buffer value of building materials. *Journal of ASTM International*, 4(5).

Rode, C., Peuhkuri, R.H., Mortensen, L.H., Hansen, K.K., Time, B., Gustavsen, A., Ojanen, T., Ahonen, J., Svennberg, K., Arfvidsson, J. et al., 2005. *Moisture buffering of building materials*. Danmarks tekniske universitet, Technical University of Denmark, Department of Civil Engineering.

Rode, C., Sørensen, K.G. and Mitamura, T., 2001. Model and experiments for hygrothermal conditions of the envelope and indoor air of buildings. *Performance of exterior envelopes of whole buildings viii. integration of building envelopes 2*.

Roels, S. and Janssen, H., 2006. A comparison of the nordtest and japanese test methods for the moisture buffering performance of building materials. *Journal of Building Physics*, 30(2), pp.137–161. Available from: https://doi.org/10.1177/1744259106068101.

Sagae, A., Wami, H., Arai, Y., Kasai, H., Sato, T. and Matumoto, H., 1994. Study

on a new humidity controlling material using zeolite for building. *Zeolites and microporous crystals, proceedings of the international symposium on zeolites and microporous crystals*. Elsevier, pp.251–260. Available from: https://doi.org/10.1016/s0167-2991(08)63264-4.

Saito, H., n.d. Moisture resources to predict indoor humidity for whole building ham analyses in japan. *IEA Annex*, 41.

Salonvaara, M., T. Ojanen, A.H., Künzel, H.M. and Karagiozis, A.N., 2004. Moisture buffering effects on indoor air quality—experimental and simulation results. *Proceedings (CD) of the Performance of Exterior Envelopes of Whole Buildings IX International Conference*.

Scheffler, G.A. and Plagge, R., 2010. A whole range hygric material model: Modelling liquid and vapour transport properties in porous media. *International Journal of Heat and Mass Transfer*, 53(1-3), pp.286–296. Available from: https://doi.org/10.1016/j.ijheatmasstransfer.2009.09.0.

Simonson, C., Salonvaara, M. and Ojanen, T., 2004. Heat and mass transfer between indoor air and a permeable and hygroscopic building envelope: part one – field measurements. *Journal of Thermal Envelope and Building Science*, 28(1), pp.63–101. Available from: https://doi.org/10.1177/1097196304044395.

Simonson, C.J., Salaonvaara, M. and Ojanen, T., 2004. Heat and mass transfer between indoor air and a permeable and hygroscopic building envelope: part II – verification and numerical studies. *Journal of Thermal Envelope and Building Science*, 28(2), pp.161–185. Available from: https://doi.org/10.1177/1097196304044397.

Sing, K.S., 1985. Reporting physisorption data for gas/solid systems with special reference to the determination of surface area and porosity (recommendations 1984). *Pure and applied chemistry*, 57(4), pp.603–619. Available from: https://doi.org/10.1351/pac198557040603.

Stahl, T., Vonbank, R. and Holzer, M., 2013. Die entwicklung eines mineralischen feuchtespeicher-grundputzes. *Bauphysik*, 35(5), pp.346–355. Available from: https://doi.org/10.1002/bapi.201310077.

Steeman, H.J., Janssens, A., Carmeliet, J. and De Paepe, M., 2009. Modelling indoor air and hygrothermal wall interaction in building simulation: Comparison between cfd and a well-mixed zonal model. *Building and environment*, 44(3), pp.572–583.

Stehno, V., 1982. Praktische berechnung der instationären luftzustandsänderungen in aufenthaltsräumen zur beurteilung der feuchtigkeitsbelastung der raumbegrenzenden bauteile. *Bauphysik*, 4, pp.128–134.

Straube, J. and Burnett, E., 2001. Overview of hygrothermal (ham) analysis methods. *Moisture analysis and condensation control in building envelopes*, pp.81–89.

Svennberg, K., Lengsfeld, K., Harderup, L.E. and Holm, A., 2007. Previous experimental studies and field measurements on moisture buffering by indoor surface materials. *Journal of Building Physics*, 30(3), pp.261–274. Available from: https://doi.org/10.1177/1744259107073221.

Tijskens, A., Roels, S. and Janssen, H., 2019. Neural networks for metamodelling the hygrothermal behaviour of building components. *Building and Environment*, 162, p.106282. Available from: https://doi.org/10.1016/j.buildenv.2019.106282.

Tsuchiya, T., 1980. Infiltration and indoor air temperature and moisture variation in a detached residence. *Heating, Air-Conditioning and Sanitary Engineering of Japan*, 54(11), pp.13–19.

Tsutsumi, H., Tanabe, S.i., Harigaya, J., Iguchi, Y. and Nakamura, G., 2007. Effect of humidity on human comfort and productivity after step changes from warm and humid environment. *Building and Environment*, 42(12), pp.4034–4042. Available from: https://doi.org/10.1016/j.buildenv.2006.06.037.

Van Belleghem, M., Steeman, M., Janssen, H., Janssens, A. and De Paepe, M., 2014. Validation of a coupled heat, vapour and liquid moisture transport model for porous materials implemented in cfd. *Building and Environment*, 81, pp.340–353.

Veitch, J.A., 2008. Investigating and influencing how buildings affect health: Interdisciplinary endeavours. *Canadian Psychology/Psychologie canadienne*, 49(4), p.281. Available from: https://doi.org/10.1037/a0013567.

Vereecken, E., Roels, S. and Janssen, H., 2010. In situ determination of the moisture buffer potential of room enclosures. *Journal of Building Physics*, 34(3), pp.223–246. Available from: https://doi.org/10.1177/1744259109358268.

Wadsö, L., 1994. Describing non-fickian water-vapour sorption in wood. *Journal of Materials Science*, 29(9), pp.2367–2372. Available from: https://doi.org/10.1007/BF00363428.

Woloszyn, M., Kalamees, T., Abadie, M.O., Steeman, M. and Kalagasidis, A.S., 2009. The effect of combining a relative-humidity-sensitive ventilation system with the moisture-buffering capacity of materials on indoor climate and energy efficiency of buildings. *Building and Environment*, 44(3), pp.515–524. Available from: https://doi.org/10.1016/j.buildenv.2008.04.017.

Woloszyn, M. and Rode, C., 2007. Final report-modelling principles and common exercises, 2008. *IEA ECBCS Annex 41*.

Woods, J. and Winkler, J., 2016. Field measurement of moisture-buffering model

inputs for residential buildings. *Energy and Buildings*, 117, pp.91–98. Available from: https://doi.org/10.1016/j.enbuild.2016.02.008.

Woods, J. and Winkler, J., 2018. Effective moisture penetration depth model for residential buildings: Sensitivity analysis and guidance on model inputs. *Energy and Buildings*, 165, pp.216–232. Available from: https://doi.org/10.1016/j.enbuild.2018.01.040.

Woods, J., Winkler, J. and Christensen, D., 2013. Moisture modeling: effective moisture penetration depth versus effective capacitance. *Proceeding of thermal performance of the exterior envelopes of whole buildings xii international conference*.

Woods, J., Winkler, J., Christensen, D. and Hancock, E., 2014. *Using whole-house field tests to empirically derive moisture buffering model inputs*. National Renewable Energy Laboratory (NREL), Golden, CO.

Wu, Y., Gong, G., Yu, C.W. and Huang, Z., 2015. Proposing ultimate moisture buffering value (UMBV) for characterization of composite porous mortars. *Construction and Building Materials*, 82, pp.81–88. Available from: https://doi.org/10.1016/j.conbuildmat.2015.02.058.

Wyon, D.P., Fang, L., Lagercrantz, L. and Fanger, P.O., 2006. Experimental determination of the limiting criteria for human exposure to low winter humidity indoors (rp-1160). *Hvac&R Research*, 12(2), pp.201–213. Available from: https://doi.org/10.1080/10789669.2006.10391175.

Yang, X., Fazio, P., Rao, J., Vera, S. and Ge., H., 2009. Experimental evaluation of transient moisture buffering of interior surface materials in a full-scale one-room test setup. *Proceedings of 4th international conference on building physics (ibpc4), istanbul, turkey*. pp.15–18.

Yang, X., Ge, H., Fazio, P. and Rao, J., 2014. Evaluation of parameters influencing the moisture buffering potential of hygroscopic materials with BSim simulations. *Buildings*, 4(3), pp.375–393. Available from: https://doi.org/10.3390/buildings4030375.

Yang, X., Vera, S., Rao, J., Ge, H. and Fazio, P., 2007. Full-scale experimental investigation of moisture buffering effect and indoor moisture distribution. *Thermal Performance of Exterior Envelopes of Whole Buildings X. Florida, USA: ASHRAE*.

Yi, S.Y., Fan, L.W., Fu, J.H., Xu, X. and Yu, Z.T., 2016. Experimental determination of the water vapor diffusion coefficient of autoclaved aerated concrete (aac) via a transient method: Effects of the porosity and temperature. *International Journal of Heat and Mass Transfer*, 103, pp.607–610. Available from: https://doi.org/10.1016/j.ijheatmasstransfer.2016.07.111Get.

Yoshino, H., Mitamura, T. and Hasegawa, K., 2009. Moisture buffering and effect of ventilation rate and volume rate of hygrothermal materials in a single room under steady state exterior conditions. *Building and environment*, 44(7), pp.1418–1425. Available from: https://doi.org/10.1016/j.buildenv.2008.09.007.

Zhang, M., Qin, M., Rode, C. and Chen, Z., 2017. Moisture buffering phenomenon and its impact on building energy consumption. *Applied Thermal Engineering*, 124, pp.337–345. Available from: https://doi.org/10.1016/j.applthermaleng.2017.05.173.

Zu, K., Qin, M., Rode, C. and Libralato, M., 2020. Development of a moisture buffer value model (mbm) for indoor moisture prediction. *Applied Thermal Engineering*, p.115096. Available from: https://doi.org/10.1016/j.applthermaleng.2020.115096.

Appendices

A. *Simulations*

A.1 Moisture Balance Data

Table A.1. Moisture balance during humidification in the concrete room during humidification (g/h)

Tests	Cycles	Load	Walls	Infiltration	Ventilation	Room
Test 1	Cycle 1	1080.00	-473.73	-134.72	-432.78	38.77
	Cycle 2	970.00	-391.83	-129.89	-417.26	31.01
	Cycle 3	970.00	-383.49	-131.47	-422.34	32.69
	Cycle 4	800.00	-35327.29	-105.14	-337.71	30.31
	Cycle 5	800.00	-282.03	-117.03	-375.96	24.99
	Cycle 6	800.00	-254.76	-123.04	-395.31	26.88
Test 2	Cycle 1	950.00	-424.65	-116.87	-375.43	33.06
	Cycle 2	900.00	-291.03	-138.35	-444.42	26.20
	Cycle 3	960.00	-356.64	-135.72	-436.00	31.63
	Cycle 4	750.00	-321.82	-94.10	-302.28	31.80
	Cycle 5	880.00	-265.09	-140.02	-449.81	25.08
	Cycle 6	880.00	-335.26	-122.20	-392.55	29.99
Test 3	Cycle 1	1020.00	-379.30	-143.70	-461.62	35.38
	Cycle 2	1020.00	-360.25	-148.04	-475.57	36.14
	Cycle 3	1020.00	-377.40	-144.34	-463.67	34.60
	Cycle 4	1020.00	-442.34	-126.78	-407.28	43.59
Test 4	Cycle 1	1070.00	-447.10	-139.58	-448.40	34.91
	Cycle 2	1070.00	-390.18	-153.20	-492.15	34.47
	Cycle 3	1000.00	-379.07	-139.67	-448.68	32.57
	Cycle 4	980.00	-332.91	-146.23	-469.75	31.10
	Cycle 5	850.00	-261.35	-133.38	-428.48	26.79
	Cycle 6	850.00	-322.07	-117.97	-378.96	31.01
Test 5	Cycle 1	900.00	-392.59	-112.82	-362.43	32.16
	Cycle 2	960.00	-252.90	-162.61	-522.38	22.11
	Cycle 3	780.00	-323.33	-102.22	-328.37	26.08
	Cycle 4	930.00	-307.87	-140.97	-452.87	28.29
	Cycle 5	1100.00	-345.45	-170.79	-548.66	35.10
	Cycle 6	1100.00	-359.96	-168.22	-540.39	31.43

Table A.2. Moisture balance in the wood fibre room during humidification (g/h)

Tests	Cycles	Load	Walls	Infiltration	Ventilation	Room
Test 1	Cycle 1	1220.00	-516.26	-153.59	-503.61	46.54
	Cycle 2	1150.00	-419.00	-161.54	-529.68	39.78
	Cycle 3	1090.00	-387.27	-155.06	-508.45	39.22
	Cycle 4	800.00	-307.16	-107.18	-353.18	35.48
	Cycle 5	800.00	-251.51	-121.92	-399.08	32.49
	Cycle 6	800.00	-249.25	-121.42	-399.71	32.62
Test 2	Cycle 1	1070.00	-445.48	-136.69	-448.19	39.64
	Cycle 2	1100.00	-320.91	-173.78	-569.83	35.47
	Cycle 3	1000.00	-347.69	-144.33	-472.44	39.53
	Cycle 4	850.00	-327.67	-113.72	-370.11	39.50
	Cycle 5	833.00	-213.86	-142.97	-466.79	10.72
	Cycle 6	900.00	-339.31	-123.71	-404.83	36.16
Test 3	Cycle 1	1100.00	-406.28	-152.93	-501.46	39.33
	Cycle 2	1100.00	-394.42	-155.66	-510.41	39.51
	Cycle 3	1100.00	-414.23	-151.18	-495.71	38.88
	Cycle 4	1100.00	-475.24	-134.78	-441.95	48.02
	Cycle 5	1200.00	-477.44	-158.98	-521.27	42.32
	Cycle 6	1200.00	-379.32	-183.80	-602.66	34.22
Test 4	Cycle 1	1150.00	-390.40	-168.06	-551.04	40.50
	Cycle 2	1150.00	-366.78	-173.68	-569.49	40.06
	Cycle 3	980.00	-328.43	-144.06	-472.03	36.49
	Cycle 4	1150.00	-368.44	-173.66	-569.41	38.49
	Cycle 5	1150.00	-352.27	-177.26	-581.22	39.25
	Cycle 6	1150.00	-426.12	-159.08	-521.60	43.21
Test 5	Cycle 1	650.00	-255.64	-86.78	-284.39	32.19
	Cycle 2	1100.00	-276.67	-185.58	-608.51	29.23
	Cycle 3	650.00	-255.72	-86.25	-284.61	30.43
	Cycle 4	930.00	-288.57	-142.46	-468.75	32.22
	Cycle 5	1200.00	-370.71	-184.87	-604.62	39.80
	Cycle 6	1200.00	-369.83	-185.91	-608.75	36.52

Table A.3. Moisture balance in the PIR room during humidification (g/h)

Tests	Cycles	Load	Walls	Infiltration	Ventilation	Room
Test 1	Cycle 1	700.00	-0.02	-242.96	-411.49	45.53
	Cycle 2	720.00	-0.04	-254.01	-430.20	35.76
	Cycle 3	780.00	-0.04	-274.46	-464.82	40.68
	Cycle 4	690.00	-0.05	-241.92	-409.72	38.31
	Cycle 5	700.00	-0.05	-247.58	-419.31	33.06
	Cycle 6	700.00	-0.05	-247.58	-419.30	33.08
Test 2	Cycle 1	630.00	-0.04	-221.48	-375.11	33.37
	Cycle 2	720.00	-0.04	-255.69	-433.03	31.24
	Cycle 3	700.00	-0.04	-246.64	-417.72	35.60
	Cycle 4	700.00	-0.05	-242.07	-409.97	47.92
	Cycle 5	700.00	-0.03	-248.84	-421.44	29.69
	Cycle 6	700.00	-0.04	-246.56	-417.57	35.83
Test 3	Cycle 1	660.00	-0.01	-230.28	-390.00	39.71
	Cycle 2	630.00	-0.01	-218.74	-370.46	40.79
	Cycle 3	630.00	-0.01	-219.98	-372.57	37.43
	Cycle 4	630.00	-0.02	-213.90	-362.26	53.82
	Cycle 5	780.00	-0.04	-274.77	-465.36	39.83
	Cycle 6	780.00	-0.03	-280.74	-475.46	23.77
Test 4	Cycle 1	750.00	-0.04	-264.56	-448.07	37.33
	Cycle 2	820.00	-0.04	-289.43	-490.18	40.34
	Cycle 3	750.00	-0.05	-264.18	-447.42	38.36
	Cycle 4	700.00	-0.03	-246.92	-418.18	34.87
	Cycle 5	760.00	-0.02	-267.16	-452.47	40.35
	Cycle 6	730.00	-0.02	-254.60	-431.20	44.18
Test 5	Cycle 1	730.00	-0.06	-257.10	-435.43	37.40
	Cycle 2	800.00	-0.04	-288.48	-488.58	22.91
	Cycle 3	660.00	-0.05	-233.77	-395.92	30.26
	Cycle 4	700.00	-0.04	-249.33	-422.27	28.35
	Cycle 5	880.00	-0.03	-310.00	-525.02	44.96
	Cycle 6	840.00	-0.03	-299.38	-507.03	33.56

Table A.4. Moisture balance in the concrete room during de-humidification (g/h)

Tests	Cycles	Walls	Infiltration	Ventilation	Room
Test 1	Cycle 1	78.86	-18.90	-60.73	-0.77
	Cycle 2	118.76	-33.54	-107.75	-22.53
	Cycle 3	147.82	-40.55	-130.26	-22.99
	Cycle 4	159.32	-43.86	-140.89	-25.43
	Cycle 5	54.72	-17.36	-55.75	-18.39
	Cycle 6	120.74	-32.67	-104.93	-16.86
Test 2	Cycle 1	208.74	-55.37	-177.87	-24.50
	Cycle 2	56.27	-13.23	-42.51	0.53
	Cycle 3	103.12	-29.72	-95.48	-22.08
	Cycle 4	205.29	-54.42	-174.83	-23.96
	Cycle 5	169.62	-46.20	-148.40	-24.98
	Cycle 6	106.29	-30.69	-98.58	-22.98
Test 3	Cycle 1	192.12	-50.60	-162.56	-21.05
	Cycle 2	116.05	-32.68	-104.97	-21.60
	Cycle 3	123.81	-29.89	-96.03	-2.11
	Cycle 4	261.97	-67.98	-218.36	-24.37
Test 4	Cycle 1	231.86	-60.57	-194.58	-23.29
	Cycle 2	163.23	-44.65	-143.44	-24.87
	Cycle 3	160.19	-43.67	-140.28	-23.75
	Cycle 4	181.31	-49.13	-157.84	-25.66
	Cycle 5	216.31	-57.17	-183.65	-24.51
	Cycle 6	246.13	-63.57	-204.22	-21.66
Test 5	Cycle 1	125.99	-34.13	-109.65	-17.80
	Cycle 2	100.74	-29.08	-93.41	-21.75
	Cycle 3	188.31	-49.66	-159.52	-20.87
	Cycle 4	188.31	-49.66	-159.52	-20.87
	Cycle 5	127.67	-35.24	-113.21	-20.78
	Cycle 6	278.53	-72.71	-233.57	-27.75

Table A.5. Moisture balance in the wood fibre room during de-humidification (g/h)

Tests	Cycles	Walls	Infiltration	Ventilation	Room
Test 1	Cycle 1	80.13	-18.84	-61.78	-0.49
	Cycle 2	128.03	-36.41	-119.37	-27.74
	Cycle 3	168.64	-46.34	-151.93	-29.62
	Cycle 4	174.81	-47.75	-156.58	-29.52
	Cycle 5	71.27	-21.70	-71.16	-21.60
	Cycle 6	119.14	-29.41	-96.45	-6.73
Test 2	Cycle 1	199.10	-49.83	-163.39	-14.12
	Cycle 2	57.60	-13.39	-43.91	0.29
	Cycle 3	114.73	-32.94	-108.02	-26.24
	Cycle 4	180.95	-44.34	-145.40	-8.80
	Cycle 5	182.03	-49.46	-162.16	-29.59
	Cycle 6	82.31	-21.59	-70.79	-10.07
Test 3	Cycle 1	129.66	-30.97	-101.55	-2.86
	Cycle 2	95.40	-24.62	-80.74	-9.96
	Cycle 3	119.55	-28.48	-93.40	-2.34
	Cycle 4	208.97	-50.61	-165.95	-7.59
	Cycle 5	212.28	-51.82	-169.92	-9.46
	Cycle 6	174.69	-42.12	-138.12	-5.55
Test 4	Cycle 1	126.11	-31.86	-104.45	-10.20
	Cycle 2	158.77	-39.46	-129.40	-10.09
	Cycle 3	193.79	-52.12	-170.90	-29.24
	Cycle 4	176.44	-47.67	-156.31	-27.54
	Cycle 5	142.29	-35.12	-115.16	-7.99
	Cycle 6	227.87	-60.30	-197.73	-30.16
Test 5	Cycle 1	223.43	-54.26	-177.90	-8.73
	Cycle 2	101.85	-25.01	-82.01	-5.18
	Cycle 3	199.48	-52.41	-171.85	-24.78
	Cycle 4	132.56	-36.25	-118.86	-22.55
	Cycle 5	279.21	-72.47	-237.61	-30.87
	Cycle 6	196.62	-52.47	-172.06	-27.92

Table A.6. Moisture balance in the PIR room during de-humidification (g/h)

Tests	Cycles	Infiltration	Ventilation	Room
Test 1	Cycle 1	-1.73669	-2.94128	-4.68
	Cycle 2	-2.8479	-4.82324	-7.67
	Cycle 3	-4.53215	-7.67572	-12.21
	Cycle 4	-1.77549	-3.007	-4.78
	Cycle 5	0.197644	0.334732	0.53
	Cycle 6	-4.63049	-7.84226	-12.47
Test 2	Cycle 1	0.681085	1.153495	1.83
	Cycle 2	-7.59502	-12.863	-20.46
	Cycle 3	-9.94189	-16.8377	-26.78
	Cycle 4	-9.97687	-16.897	-26.87
	Cycle 5	-12.5323	-21.2249	-33.76
	Cycle 6	-8.34742	-14.1373	-22.48
Test 3	Cycle 1	-9.2333	-15.6376	-24.87
	Cycle 2	-1.08366	-1.8353	-2.92
	Cycle 3	-8.62187	-14.6021	-23.22
	Cycle 4	-9.3368	-15.813	-25.15
	Cycle 5	-10.479	-17.7474	-28.23
	Cycle 6	-7.29992	-12.3632	-19.66
Test 4	Cycle 1	-9.75635	-16.5235	-26.28
	Cycle 2	-9.39016	-15.9033	-25.29
	Cycle 3	-9.65847	-16.3577	-26.02
	Cycle 4	-9.07627	-15.3717	-24.45
	Cycle 5	-10.2692	-17.392	-27.66
	Cycle 6	-9.33152	-15.804	-25.14
Test 5	Cycle 1	-10.7597	-18.2228	-28.98
	Cycle 2	-8.68236	-14.7046	-23.39
	Cycle 3	-9.23173	-15.635	-24.87
	Cycle 4	-8.06062	-13.6516	-21.71
	Cycle 5	-9.21693	-15.6099	-24.83
	Cycle 6	-11.6443	-19.721	-31.37

A.2 Moisture uptake of the walls components in

In this section, the moisture variations between the North, South, East and West walls were observed due to the influence of the outdoor weather, especially in the south wall, due to the indirect effect of solar radiations. Variations of the moisture buffering capacity of plasterboard between the walls were less than 2% in both rooms, as shown in Fig. A-1a and Fig. A-3a. Similar statements could be done for the AAC and air gap

in the concrete and wood fibre room respectively, where $0.7\,g/m^2$ difference between the north and south walls was observed (Fig. A-1b and Fig. A-3b). The south PIR insulation panel in the concrete room presented up to $2\,g/m^2$ variations compared to the other walls, whilst the south OSB in the wood fibre room showed $3\,g/m^2$ difference (Fig. A-2a and Fig. A-4a). However, significant variations between the south wood fibre insulation panel in the wood fibre room and the other walls were observed.

Overall, it could be observed solar radiations indirectly reduced the moisture storage capacity of the components more exposed to the outdoor, by increasing the surface temperature of the south wall and constantly drying the materials. It is evident solar radiations increased around the 14^{th} day of testing, which significantly influenced the drying capacity of some materials, like wood fibre insulation. Wood fibre insulation was more influenced than the PIR panel in the concrete room due to the higher exposure and hygroscopicity of the wood fibre room's wall.

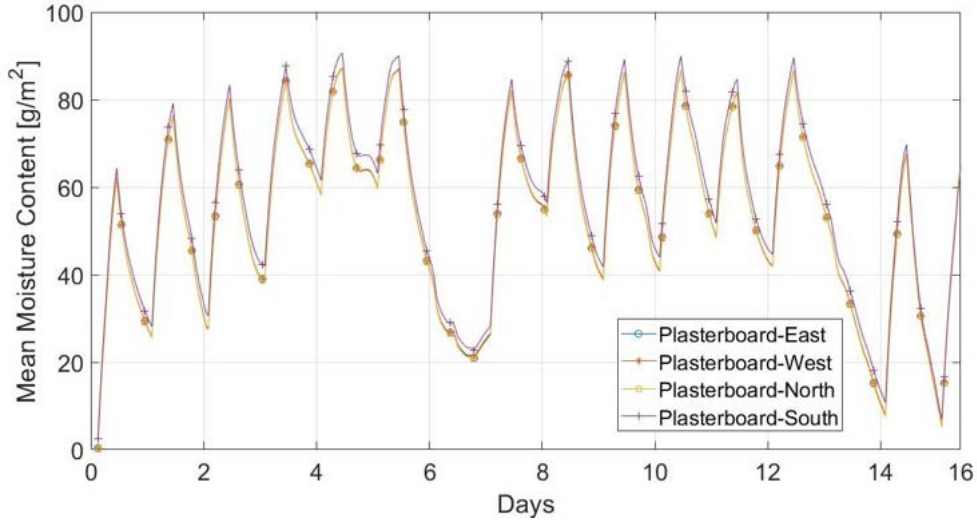

(a) Plasterboard

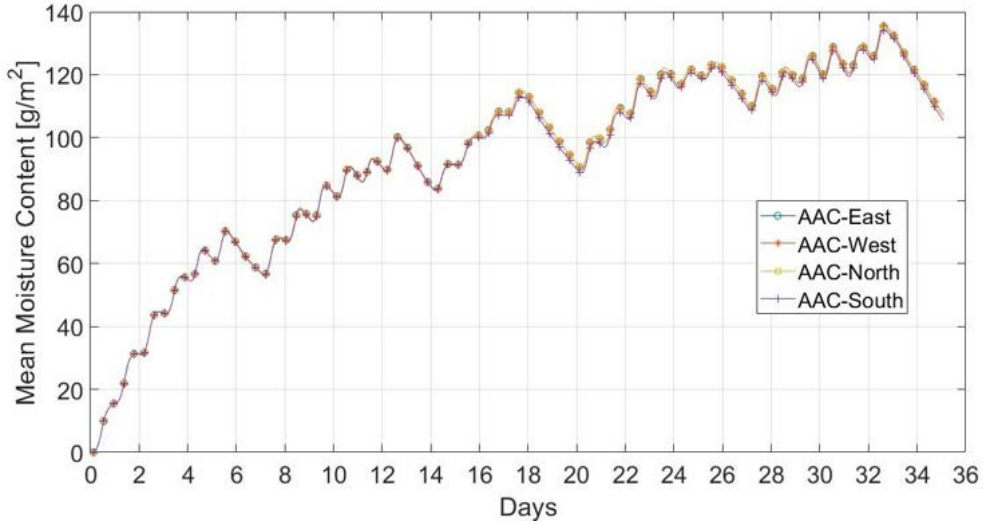

(b) AAc

Fig. A-1. Comparison of the moisture adsorption of the layers on the four walls in te concrete room

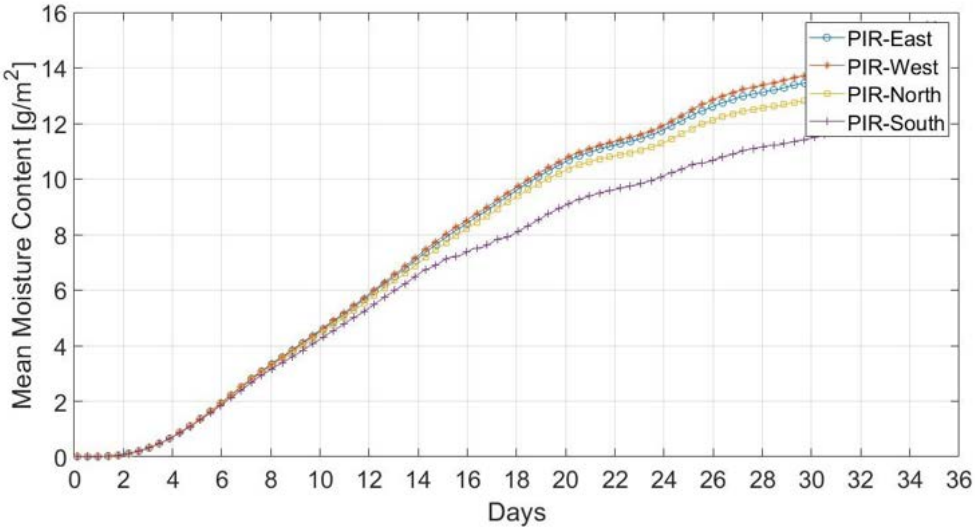

(a) Pir

Fig. A-2. Comparison of the moisture adsorption of the layers on the four walls in te concrete room

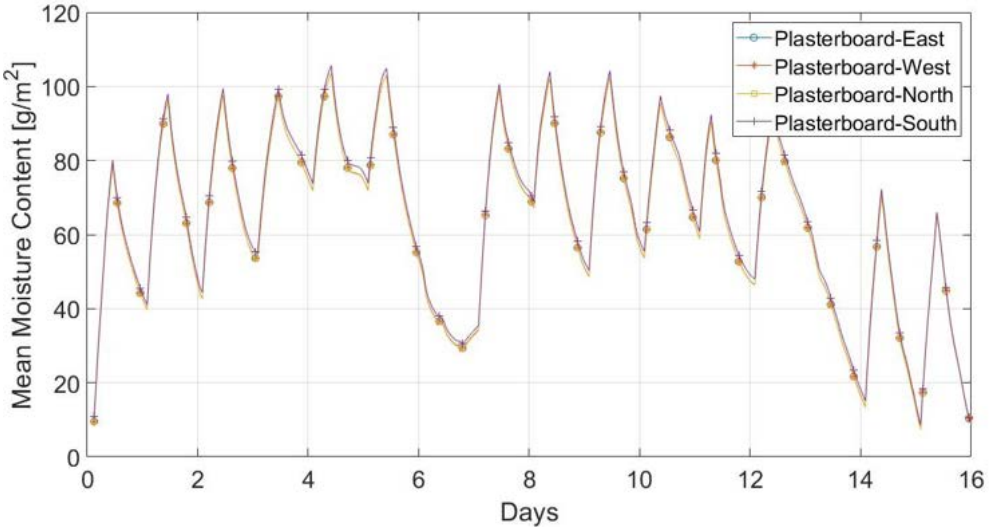

(a) Plasterboard

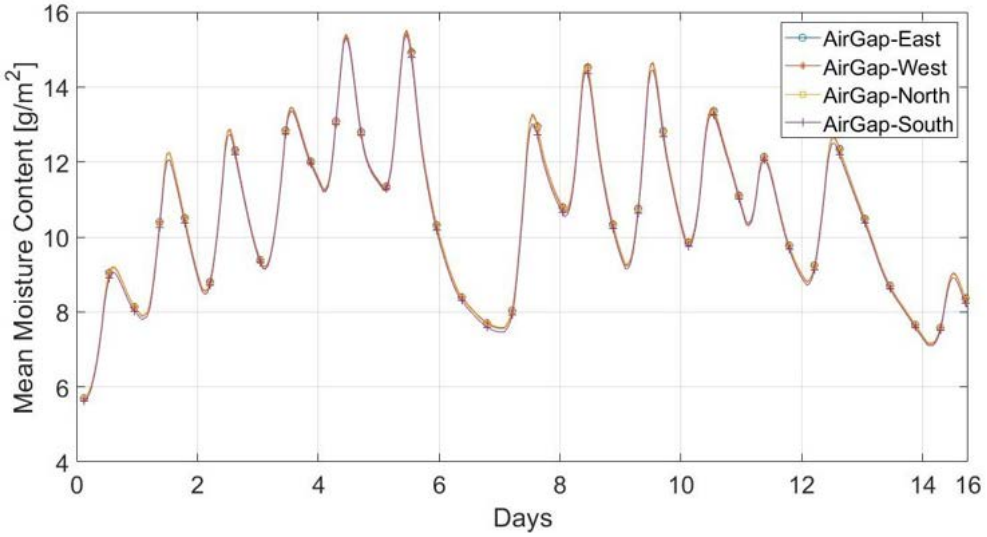

(b) Air gap fibre

Fig. A-3. Comparison of the moisture adsorption of the layers on the four walls in the wood fibre room

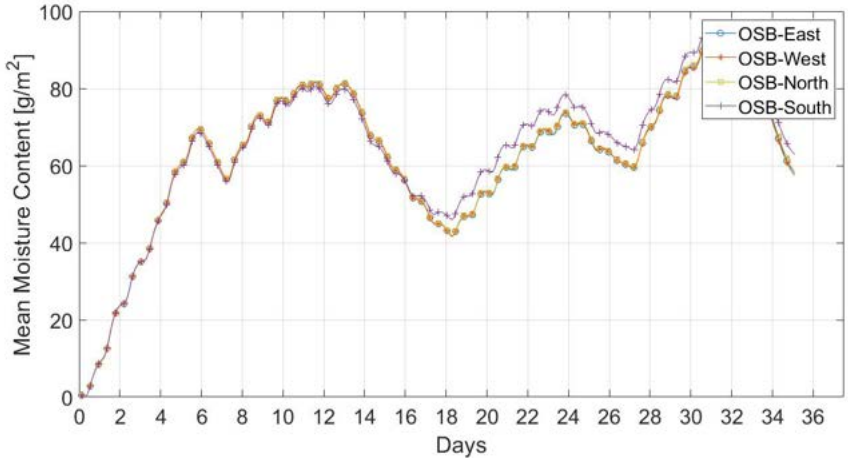

(a) OSB

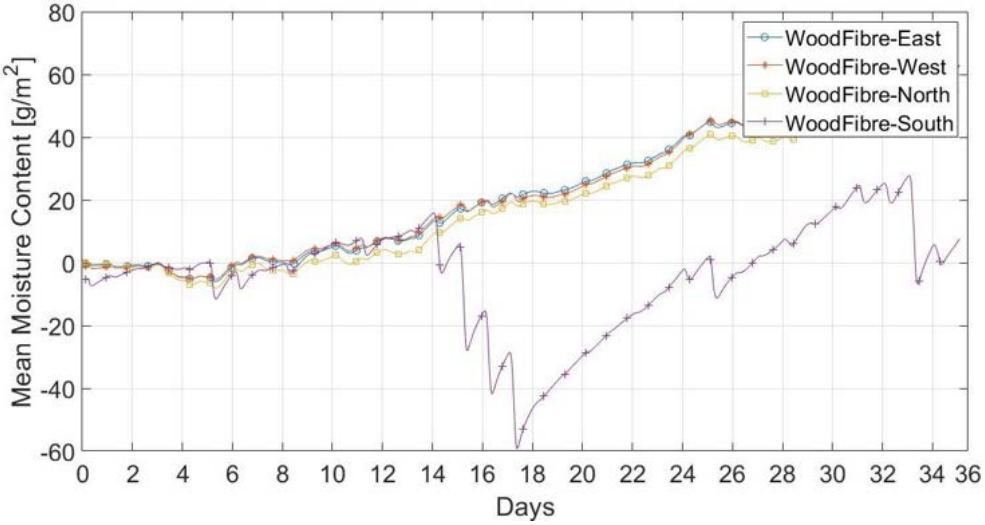

(b) Wood fibre fibre

Fig. A-4. Comparison of the moisture adsorption of the layers on the four walls in the wood fibre room

A.3 Moisture buffering capacity of plasters

Table A.7. Moisture buffering capacity of clay (g/m^2)

Clay	Test 1	Test 2	Test 3	Test 4	Test 5
Cycle 1	53.06	46.04	56.30	48.62	42.30
Cycle 2	48.63	50.43	54.03	42.41	39.77
Cycle 3	43.70	49.16	61.00	51.21	40.98
Cycle 4	40.97	42.81	51.92	58.29	64.11
Cycle 5	34.44	42.17	-	49.58	46.06
Cycle 6	54.47	40.54	-	41.12	66.12

Table A.8. Moisture buffering capacity of gypsum (g/m^2)

Gypsum	Test 1	Test 2	Test 3	Test 4	Test 5
Cycle 1	68.79	60.98	72.56	65.36	57.53
Cycle 2	55.57	62.40	69.17	57.45	48.95
Cycle 3	57.15	58.76	75.60	57.42	47.23
Cycle 4	54.16	53.13	64.94	72.26	82.43
Cycle 5	37.83	56.54	-	69.25	58.65
Cycle 6	69.02	51.20	-	51.02	84.48

Table A.9. Moisture buffering capacity of lime (g/m^2)

Lime	Test 1	Test 2	Test 3	Test 4	Test 5
Cycle 1	32.30	27.53	37.65	33.46	28.25
Cycle 2	33.44	32.27	35.98	29.22	26.12
Cycle 3	30.35	33.40	40.88	35.41	28.45
Cycle 4	26.05	30.89	33.24	37.75	40.29
Cycle 5	23.14	26.73	-	31.27	31.08
Cycle 6	34.37	29.09	-	26.63	42.65

Table A.10. Moisture buffering capacity of plasterboard (g/m^2)

Plasterboard	Test 1	Test 2	Test 3	Test 4	Test 5
Cycle 1	61.37	44.64	61.77	52.34	35.89
Cycle 2	48.51	46.43	60.02	40.69	35.79
Cycle 3	41.99	45.09	67.04	46.02	34.51
Cycle 4	36.93	38.05	57.45	58.07	61.23
Cycle 5	27.31	39.32	-	56.27	44.48
Cycle 6	49.66	35.39	-	46.25	68.16